Creep of aluminum alloys exposed to fire conditions

Soyal, Z.

Award date:
2016

UNIVERSITY OF TECHNOLOGY EINDHOVEN

Master thesis

"Creep of aluminum alloys exposed to fire conditions"

A-2016.169

Student: Zühal Soyal

Department of the Build Environment

Structural Design

Graduation committee: Prof. dr. ir. J. (Johan) Maljaars

Ir. B.W.E.M. (Dianne) van Hove

Drs. Ir. A. J. (Albert) Hogewoning

Academic year: 2015-2016

Master thesis of Z. Soyal for completing the Master phase at the Department of the Built Environment, University of Technology Eindhoven. Graduating as a Structural Engineer at the unit Structural Design.

AUTHOR

Name: *Zühal Soyal*

Address: *Reitse Hoevenstraat 11D*
5042 EB Tilburg

Phone nr: *+31 (0)620331585*

E-mail: *z.soyal@student.tue.nl*

ID-nr: 0741835

DATE *09-09-2016*
Version 1

NUMBER *A-2016.169*

EDUCATIONAL INSTITUION

Eindhoven University of Technology
Den Dolech 2
5612 AZ Eindhoven

FACULTY & MASTERTRACK

Architecture, Building and Planning
Structural Design

TUTORING MENTORS

Prof. dr. ir. J. (Johan) Maljaars
Ir. B.W.E.M. (Dianne) van Hove
Drs. Ir. A.J. (Albert) Hogewoning

Acknowledgements

I would like to express my gratitude to my supervisor Johan Maljaars for the useful comments and remarks through the learning process of this master thesis. Although it sometimes seemed like there was no end, I definitely learned a lot by performing this research. Furthermore I would like to thank Dianne van Hove and Albert Hogewoning for reviewing my report and supervising me in this project.

Finally, I must express my very profound gratitude to my parents and to my partner for providing me with unfailing support and continuous encouragement throughout my years of study and through the process of researching and writing this thesis. When I look back at the past time, I realize that it was a very busy and stressful year with two studies and my wedding, which was planned during this graduation research. Finally I'm glad that it is behind me and that I can proudly present my graduation thesis. This accomplishment would not have been possible without the support of my family and partner. Thank you.

Nahide Soyal

September 2016

Summary

Due to the low density, aluminum is a suitable material to be used in structures where the own weight plays a big role. Therefore, aluminum alloys are increasingly used in many load-bearing structures. Examples of these structures are helicopter decks, living quarters on drill platforms, buildings and ships. A lower own weight means that bigger (variable) loads can be allowed, or that the structure can be made lighter. One of the major concerns regarding the application of aluminum alloys is their mechanical performance in fire scenarios. The material strength may be degraded due to both thermal and mechanical damage during fire exposure.

Due to the constitutive properties of aluminum alloys, aluminum structures are usually relatively sensitive for fire exposure. During fire exposure, the material strength may be degraded and failure may occur. The constitutive behavior of aluminum alloys at elevated temperatures is dominated by creep. This makes aluminum structures relatively sensitive to fire. The strain as a function of time resulting from a creep test is usually divided into a primary stage with decreasing strain rate and slows with time, a secondary stage with constant, minimum strain rate, and a tertiary stage with accelerated creep and terminates when the material breaks or ruptures. Dorn-Harmathy creep model with the extension of Maljaars is a model to simulate this creep behavior. Their models is used in this thesis as a basis to determine the constitutive properties of fire-exposed aluminum alloys 6082-T6 both not welded and welded.

To determine the mechanical properties at elevated temperature of aluminum alloy 6082-T6 (welded and not welded), experimental data have been obtained and analyzed. Creep tests at a constant temperature and a constant force are performed to determine the parameters in the creep model. The model is validated with transient state tests with an increasing temperature and a constant or varying force in time. Stress-strain curves are plotted and comparisons with the data of Eurocode 9 and aluminum alloy 6060-T66 are made.

It is seen that the difference in strength of the not welded and welded aluminum alloys decrease with increasing temperature. It is examined whether there is a relation between the microstructural grain size and the behavior at elevated temperature.

Eurocode 9 gives design models to be used for load bearing structures of aluminum. Part 1-1 [EN 1999-1-1, 2007] gives general structural rules and part 1-2 [EN 1999-1-2, 2007] gives rules for structural fire design. Also a new model is developed by Maljaars [Maljaars, 2008] to determine flexural buckling of

aluminum alloys at elevated temperature. The determined stress-strain curves in this research are used in the calculation of the ultimate resistance for flexural buckling of a column, with the Eurocode and the new design models. A comparison of the different design models is made.

Symbols

The list below shows the frequently used symbols.

A	Cross-section (mm^2)
A	Material parameter in the equation for Z (/min)
A_1	Material parameter for primary creep in (/min)
D	Material parameter in the equation for ε_{t0} (-)
E	Young's modulus (N/mm^2)
$E_{T,\theta}$	Tangential stiffness (N/mm^2)
E_θ	Young's modulus at temperature θ (N/mm^2)
I	Moment of inertia (mm^4)
F_{cr}	Critical buckling load (N)
$F_{cr,inel,\theta}$	Inelastic critical buckling load at temperature θ (N)
F_{sd}	Applied design load (N)
F_u	Ultimate buckling resistance (N)
L	Section length (mm)
Q	Activation energy (J/mol)
Q_1	Activation energy for primary creep (J/mol)
R	universal gas contant (J/mol K)
T	temperature (K)
Z	Zener Holloman parameter (/min)
I_z	Radiative heat flux from a flame
I_t	Radiative heat flux from an opening
n	Material parameter in the equation for Z (-)
n	Material parameter in the Ramberg-Osgood relationship (-)

n_1	Material exponent for primary creep (-)
l	length (m)
Δl	expansion of the length caused by temperature (m)
l_{buc}	buckling length (m)
$\frac{l_{buc}}{i}$	Slenderness ratio of column (-)
b_{haz}	Width of the HAZ (mm)
$f_{0.2}$	0.2% proof stress (N/mm^2)
$f_{0.2,\theta}$	0.2% proof stress at temperature θ (N/mm^2)
t	Time (minutes)
k_{sh}	Correction factor for the shadow effect (-)
$\frac{A_m}{V}$	Profile factor for unprotected elements of aluminum (m^{-1})
$\frac{A_p}{V}$	Profile factor for protected elements of aluminum (m^{-1}).
σ_{cr}	Critical buckling strength (N/mm^2)
α	Material parameter in the equation for Z
θ	Temperature (°C)
ε	Strain (-)
ε_{el}	Elastic strain (-)
ε_t	Creep strain (-)
$\varepsilon_{t,I}$	Creep strain in the primary creep stages (-)
$\varepsilon_{t,I+II}$	Creep strain in the primary and secondary creep stages (-)
$\varepsilon_{t,I+II+III}$	Creep strain in the primary, secondary and tertiary creep stages (-)
$\dot{\varepsilon}_{III}$	Creep strain rate in the first part of the tertiary stage (/min
ε_{t0}	Projection back to zero time of the secondary creep curve (-)
ε_{lim}	Creep strain at which the tertiary creep stage starts (-)

ε_{th}	Thermal strain (-)
σ	Stress (N/mm^2)
θ_g	Gas temperature in compartment (°C)
$\chi_{20°C}$	Buckling resistance at 20°C (-)
χ_θ	Buckling resistance at temperature θ (-)
γ_{fi}	partial factor (-)
$\lambda_{rel,inel,\theta}$	Relative inelastic slenderness at temperature θ (-)
λ_{rel}	Relative slenderness (-)
$\theta_{al(t)}$	Aluminum temperature at time t (°C)
$\theta_{(t)}$	Temperature of the surrounding gases at time t (°C)
$\Delta\theta_{(t)}$	Increase of the temperature of the surrounding gases at time interval Δt (°C)
$\dot{h}_{net}$	Net heat flux density per unit area according to [EN1991-1-2]

Table of Contents

1. Introduction

This chapter gives a short introduction to the problem and underlines the relevancy of studying this problem. The research aims and limitations are also given.

1.1 Introduction to aluminum

It is 130 years (in 1886) since the discovery by Hall of a commercial relatively low cost method of extraction of aluminum from its oxide [Hall, 1889]. The new production technique of Hall is based on the reduction of aluminum oxide (Al_2O_3) to aluminum (Al) by means of electrolysis, see Figure 1.1. This electrolysis was made possible by the invention of the dynamo, allowing larger amounts of electricity become available. This extraction of the earth's most abundant metallic element led to gradual widespread commercial use of this metal, primarily because of its low density and useful strength. By this discovery, the price of aluminum products decreased significantly.

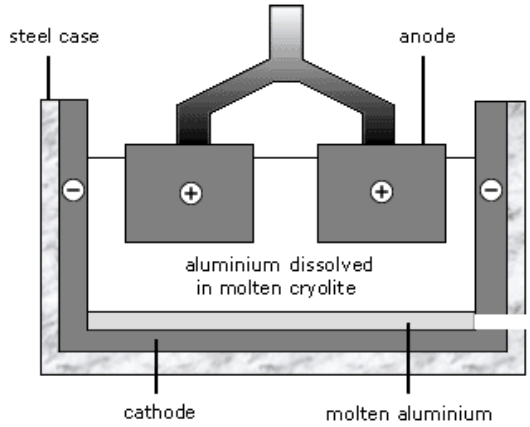

Figure 1.1 Reduction of aluminum oxide (Al_2O_3) to aluminum (Al) by means of electrolyse

Aluminum alloys are used in many load-bearing structures. Due to the low density, aluminum is a suitable material to be used in structures where the own weight plays a big role. Examples of these structures are helicopter decks, living quarters on drill platforms, buildings and ships. A lower own weight means that bigger (variable) loads can be allowed, or that the structure can be made lighter. One of the major concerns regarding the application of aluminum alloys is their mechanical performance in fire scenarios. The material strength may be degraded due to both thermal and mechanical damage during fire exposure.

As shown in Figure 1.2, the mechanical properties of aluminum alloys vary from low strength (pure aluminum 1050A), medium strength 5xxx and 6xxx series alloys (comparable to mild steel S235), to high strength 7xxx alloys (comparable to high strength steel S355).

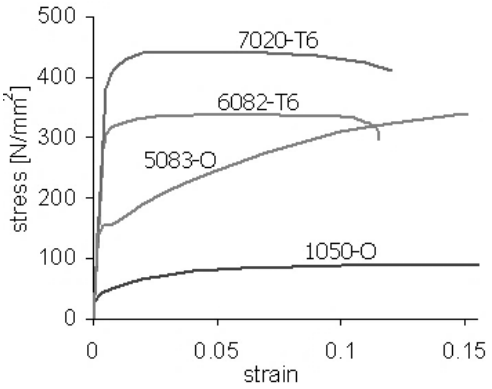

Figure 1.2 Stress-strain relation of aluminum and a few aluminum alloys [TALAT, 1994]

In building and civil engineering structural applications, mainly 5xxx and 6xxx series alloys are used. The stress-strain properties described above are representative for the temperature range −30 to 80 °C. At temperatures above 80 °C, the strength decreases (for aluminum faster than for steel) and the strain to failure increases [TALAT, 1994].

Due to the constitutive properties of aluminum alloys, aluminum structures are usually relatively sensitive for fire exposure. During fire exposure, the material strength may be degraded and failure may occur because of the accumulation of fire damage. This damage to aluminum is a complex combination of thermal exposure damage and stress-induced damage. For a number of structures, requirements are put forward in norms on the time that the structure has to remain its load-bearing or separating function when exposed to fire. In case of fire breaks out, people have to be able to safely escape before the structure collapses. This time is called the fire resistance and are typically specified as 30, 60, 90 or 120 minutes. Because of their relatively low melting temperature, low density, and high thermal conductivity [Soetens et. al, 2014], load-bearing structures composed of aluminum alloys need to be protected in almost all cases in order to fulfill these fire resistances. In many cases, the temperature of fire-exposed insulated aluminum members increases approximately linearly with time [Maljaars et. al, 2008].

In this thesis, where aluminum is mentioned, aluminum alloys are considered.

1.2 Aluminum exposed to fire conditions

Eurocode 9 gives design models to be used for load bearing structures of aluminum. Part 1-1 [EN 1999-1-1, 2007] gives general structural rules and part 1-2 [EN 1999-1-2, 2007] gives rules for structural fire design.

To be able to determine the amount of insulation required, knowledge on the constitutive properties of the applied alloys when exposed to fire is required. The influence of fire exposure on the structural behavior is mainly caused by the fact that the mechanical properties depend on the elevated temperature exposure. This will be the case when an aluminum construction is exposed to fire conditions. Aluminum heats relatively fast when exposed to fire conditions. The material strength and the stiffness already reduce significantly before the melting temperature is reached, which is approximately 660°C for pure aluminum and lower (approximately 600°C) for most aluminum alloys.

Aluminum alloys experience large reductions to their elastic stiffness, proof strength, ultimate strength and creep strength when heated over the range of 100–400 °C [Kaufmann, 1999], which is well below the temperature of many fires. As a result, aluminum structures can distort, buckle and collapse within a short time when exposed to a hot fire. The constitutive behavior of aluminum alloys at elevated temperatures is dominated by creep. This makes aluminum structures relatively sensitive to fire. The strain as a function of time resulting from a creep test is usually divided into a primary stage with decreasing strain rate and slows with time, a secondary stage with constant, minimum strain rate, and a tertiary stage with accelerated creep and terminates when the material breaks or ruptures, see figure 1.3.

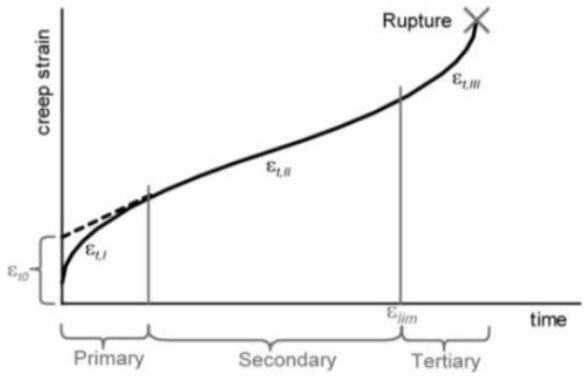

Figure 1.3 Creep curve with the different stages

Dorn proposed a model for secondary creep of metals [Dorn, 1954]. Harmathy extended Dorn's model, to account for primary creep and this model, which is called the Dorn-Harmathy creep model, has been

used to simulate the deflection of fire-exposed steel beams [Harmathy, 1967]. Their models will be used in the thesis as a basis to determine the constitutive properties of fire-exposed aluminum alloys. The model extension for primary creep is based on creep tests on steel specimens. It is not known whether these equations are also applicable to aluminum alloys.

The problems of the existing creep model are investigated on the basis of experiments on aluminum alloy 5083-H111 and 6060-T66. Due to the research of Maljaars [Maljaars, 2008] the creep behavior of aluminum alloys 5083-H111 and 6060-T66 is already known. However, test data of just two aluminum alloys are not enough in order to draw a proper conclusion about the constitutive properties of aluminum alloys at elevated temperatures. Maljaars [Maljaars, 2008] also proposed a model for tertiary creep of aluminum alloys. Creep modeling is very useful as it allows for prediction of creep behavior without performing long creep tests.

As previously mentioned, [EN 1999-1-2, 2007] provides simple calculation methods consisting of simple equations to check the resistance of the member to the governing failure mechanism. These models are based on steady state tests, which are tests with a constant, elevated temperature in time, while a certain strain rate is applied (i.e. a displacement-controlled test). Because of the few test data and the lack of fundamental studies on aluminum structures at elevated temperatures, the simple calculation models are partially based on research on steel structures, for which comprehensive testing and long-time experience are available. Due to expected differences in mechanical behavior at elevated temperature, a direct application of the models based on the steel research may be inappropriate for application in aluminum structures. Also the results of the steady state tests are not imitating the real temperature progression during fire. Transient state tests with a certain stress level and an increasing temperature in time will give more appropriate results, because these tests are imitating the real temperature progression during fire. It is expected that the fire design models in [EN 1999-1-2, 2007] are conservative design models.

1.3 Problem statement

While aluminum has several significant advantageous features as structural material, some of its properties could be detrimental if they are not considered properly. Fire is a special load where attention should be given in construction design. Because of its low melting point of circa 580 - 660°C, aluminum starts losing its mechanical and physical properties at rather low temperatures. As a result, in fire design, aluminum is less resistant compared to ambient temperatures.

In many structural applications aluminum's high ratio yield strength over density and good corrosion resistance is the most important reason for its use. For application in transport this is obvious (less energy needed), but also in civil engineering it can be important, i.e. for movable bridges (also less energy needed) and for long span bridges less dead weight means a higher live load (traffic) capacity. In building and civil engineering structural applications, mainly 5xxx and 6xxx series alloys are used. Most of those alloys have lost 50% of their original strength at temperatures between 180 - 250°C. The physical and mechanical properties of aluminum/aluminum alloys change when exposed to high temperatures [Soetens et. al, 2013]. The constitutive behavior of aluminum alloys at elevated temperatures is dominated by creep. The imperfections that are present in the structure, will be increased as the temperature will be increased. This makes aluminum structures relatively sensitive to fire. Below, some important points on aluminum structures at high temperatures can be read:

1) Welds are the most commonly used joints in aluminum structures. Not only when it is exposed to fire, but also when aluminum is welded, it is exposed to high temperatures. Welding causes an heat affected zone (HAZ), which reduces the strength of the material. Attention should be paid to both the weld and the heat affected zone adjacent to the weld. When welded aluminum is exposed to fire, it can have drastic consequences by changing constitutive properties. Welding and exposure to elevated temperatures leads to decreased mechanical properties with respect to the parent material.
2) There is insufficient knowledge about the grain structure of aluminum alloys exposed to fire conditions and what influence high temperature can have on the grain structure. The investigation of this phenomenon is important, because of the major influence of the grain structure on the strength of the material.
3) Also flexural buckling is an important aspect in structural engineering where sufficient attention should be paid on. Elevated temperatures have negative effects on the material properties of aluminum structures and so for the buckling of structural members.

1.4 Aim of the thesis

As mentioned before, a constitutive model has been proposed before to simulate the creep behavior of steel beams. Dorn proposed a model for secondary creep of metals [Dorn, 1954]. Harmathy extended Dorn's model, to account for primary creep and this model, which is called the Dorn-Harmathy creep model, has been used to simulate the deflection of fire-exposed steel beams [Harmathy, 1967]. Maljaars [Maljaars et. al, 2008] extended this model with the tertiary stage for aluminum alloys.

The main aim of this graduation thesis is to investigate the creep behavior of aluminum alloys exposed to fire conditions and find the constitutive properties of aluminum at elevated temperatures. There will be an experimental research which will continue the research of [Maljaars et. al, 2008]. In [Maljaars et. al, 2008] the constitutive properties at elevated temperatures of aluminum alloys 5083-H111 and 6060-T66 is investigasted. This thesis will extend the previous research with some additional research aspects. In addition to the alloys used in [Maljaars et. al, 2008], one additional aluminum alloy 6082-T6 will be used, with and without weld to investigate what influence welding has on the constitutive behavior at elevated temperatures. This regards in particular the negative impact of the heat affected zone. Also the influence of high temperature on the grain structure will be investigated. Aluminum alloy 6082-T6 is chosen for this study, because it is known with its substantially different properties in comparison with alloy 6060, which is investigated earlier. Due to a comparison between the creep behavior of these two aluminum alloys, a conclusion can be drawn on the creep behavior of aluminum alloys in the 6xxx series.

With the aid of this research, there will be find an answer for the main research question of this graduation project, which is:

- **What will be the effect of fire conditions on the constitutive properties of aluminum alloy 6082-T6, both with and without a heat affected zone (caused by welding)?**

Besides the main aim of the thesis, some sub aims are defined. These sub aims are as follows:

- *Determine whether the welding gives differences in the constitutive behavior with respect to parent material of aluminum alloy 6082-T6 exposed to fire conditions;*
- *Determine whether the creep behavior at elevated temperatures varies with the use of different aluminum alloys;*
- *Comparison of the steady state results in Eurocode 9 with transient state results in this research for both welded and not welded specimens;*
- *Determine if the decrease in strength with increasing temperature between not welded and welded specimens is also visible in the grain structure;*
- *Determine the results of ultimate loads of flexural buckling with the use of different calculation models, for both transient and steady state material properties,.*

In order to answer the research question, experiments will be carried out during the research project. On the basis of the measurements a conclusion will be drawn.

1.5 Research approach and structure of the thesis

Two methods will be used to find answers to the main question in section 1.4. These are the literature study and experimental research. The literature study will be a theoretical analysis, allowing to have a first insight into the material behavior of aluminum alloy 6082-T6 which will be used in this thesis. Publications about the influence of welding and grain structure at aluminum will be studied. Furthermore, research articles concerning creep of aluminum alloys will be studied to determine what kind of research has been conducted and what results have been found so far in this field. This thesis will contain the most important theoretical information. For more extensive literature study, reference is made to [Soyal, 2016].

By means of experimental analyses, results will be obtained of the creep behavior of aluminum alloy 6082-T6 exposed to fire conditions. After the experiments with high temperatures, the grain structure of the test pieces will be tested.

Chapter 2 gives theoretical background about the subjects which will be investigated in this research. The creep phenomena will be explained and mechanical properties at elevated temperatures will be discussed.

Chapter 3 explains the experimental work and gives the results of the creep and transient state experiments. The parameters of the creep model are provided and stress-strain diagrams are given based on the found results.

Chapter 4 contains the microstructural analyze. The results of the investigation of the grain structure of the specimens will be given in this chapter.

Chapter 5 contains a practical model, where hand calculations will be conducted. Flexural buckling calculation of several design models will be compared with each other.

2. Theoretical background

This chapter contains a theoretical analysis, allowing to have a first insight into the material behavior of aluminum alloy 6082-T6 which will be used in this thesis. Furthermore, research articles concerning creep of aluminum alloys and microstructure of aluminum are also studied. This thesis will contain the most important theoretical information. For more extensive literature study, reference is made to [Soyal, 2016].

2.1 Mechanical properties of aluminum

The mechanical properties of aluminum alloys differ with changing temperatures. The property degradation for aluminum alloys initiates at temperatures as low as 150°C and more than 50% strength reduction occurs after 380°C exposure [Matulich, 2011]. This paragraph gives an brief description of the mechanical properties of aluminum alloys. Most of the information in this chapter is from the following literature: [Mazzolani, 1995], [Kaufmann, 1999], [EN 1999-1-1, 2007] , [EN 1999-1-2, 2007], [EN 1991-1-2, 2002] , [Davis, 1993], [Aluminum Association, 2005], [Soetens et. al, 2013], [TALAT 1501, 1994]

2.1.1 Stress-strain relationship at ambient temperature

An important difference between aluminum and structural steel (S235 and S355) concerns the stress-strain behavior as shown in Figure 2.1. Structural steel exhibits a yield strength, a subsequent yield plateau and finally strain hardening to arrive at the maximum strength.

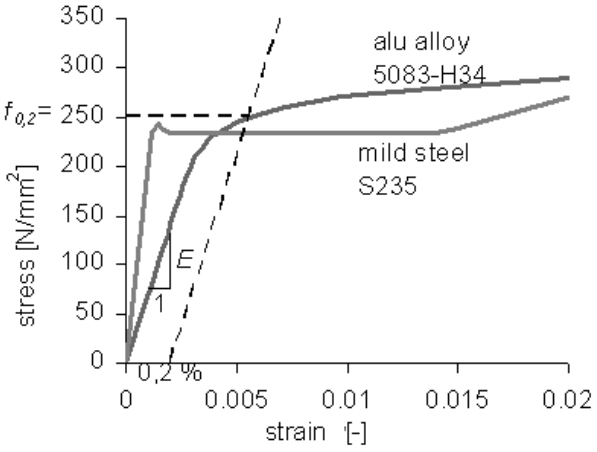

Figure 2.1 Stress-strain relation of aluminum and mild steel

Aluminum alloys show a highly non-linear stress-strain relationship up to the maximum strength. Yield strength is an important property to know because it defines the upper limit to which a load can be applied before permanent deformation occurs. For design purposes instead of the yield strength

conventionally the 0.2% proof stress $f_{0.2}$ is used. This is the border between linear-elastic behavior and plastic behavior for non-linear stress-strain relations. In addition to this 0.2% proof stress, also the following properties can be distinguished:

- The proportional limit f_p
- The engineering tensile strength f_u
- The strain at the engineering tensile strength ε_b
- The strain at rupture ε_x
- The modulus of elasticity E

These properties vary between alloys. It appears that the tensile strength is greatly influenced by the alloy components. The area under the stress-strain diagram till the point of rupture, is an indication for the amount of energy that can be absorbed by the material at loading under pure tension. [Mazzolani, 1995] also shows that the heat treatment process changes the behavior of the material by affecting either strength or ductility.

One of the most applied models to describe the stress-strain curve of aluminum for structural applications is the Ramberg and Osgood relation [Ramberg et. al, 1943], see equation (2.1).

$$\varepsilon = \frac{\sigma}{E} + 0.002\left(\frac{\sigma}{f_{0.2}}\right)^n \tag{2.1}$$

Parameter *n* in equation (2.1) describes the shape of the stress-strain curve (n>1). For alloys with a small ratio $f_p/f_{0.2}$, *n* is in the order of 5-8. For alloys with a high ratio $f_p/f_{0.2}$, *n* is in the order of 20-32.

2.1.2 Stress-strain relationship at elevated temperature

Different reports show that the mechanical properties and stress-strain relation changes at elevated temperatures as compared to ambient temperature.

[Langhelle et. al, 2001] reports that property degradation occurs at temperatures as low as 150 °C with a 50% yield strength reduction at approximately 275 °C.

[Ozturk et. al, 2008] performed tensile tests at various temperatures and varying strain rates, see Figure 2.2. Research revealed that the uniaxial tensile elongation increases with increasing the temperatures and decreases with increasing the strain rates. Necking has a greater influence on elevated temperatures with low strain rates. However the total elongation did not show very significant

difference at room temperature with increasing the strain rates. The total elongation is significantly enhanced above 200°C and low heating rates. Test results show that, at elevated temperatures, a higher strain rate results in higher values for $f_{0.2}$ and f_u.

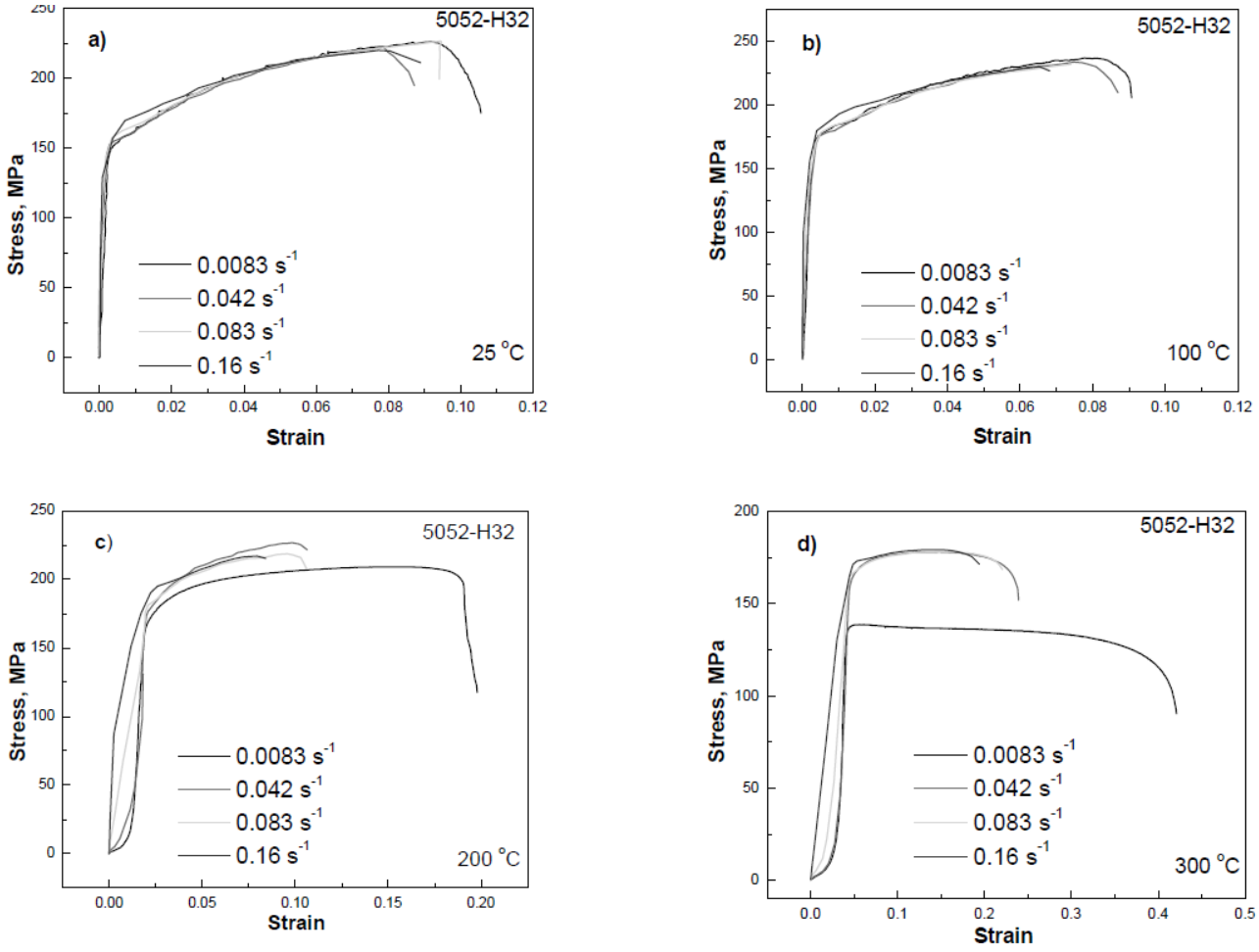

Sequel Figure 2.2 uniaxial tensile tests were performed at the temperatures of 25, 100, 200, and 300°C and with the strain rates of 0.0083, 0.042, 0.083, and 0.16s^{-1} at alloy 5052-H32. a) – d) True stress versus true strain curves at various temperatures and strain rates [Ozturk et. al, 2008]

Also [Mazzolani, 1995] reports that, starting from a temperature of about 80-100°C, the mechanical properties of aluminum alloys decrease in the way described in Figure 2.3, which refers to alloys fabricated in Switzerland.

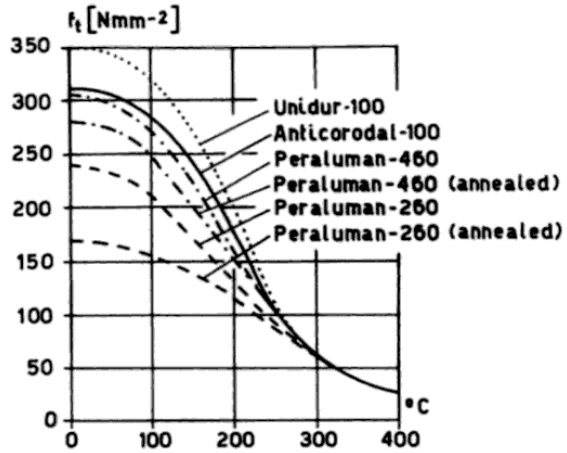

Figure 2.3 Decreasing mechanical properties of aluminum alloys [Mazzolani, 1995]

[El-Danaf et. al, 2008] examine in detail the high-temperature deformation of a 6082-T4 aluminum alloy over a wide range of stresses, strain rates, and temperatures. The results show the high strain rate sensitivity exhibited by the alloy at temperatures of 623, 673, 723 and 773K.

[Summers et. al., 2015] investigated elevated temperature 6061-T651 engineering stress-strain relations, which are shown in Figure 2.4. These graphs contain the high temperature mechanical behavior of 6061-T651 aluminum alloy. The presented data are performed regarding ASTM E21 (ASTM Standard E21 2009) and temperatures up to 500°C.

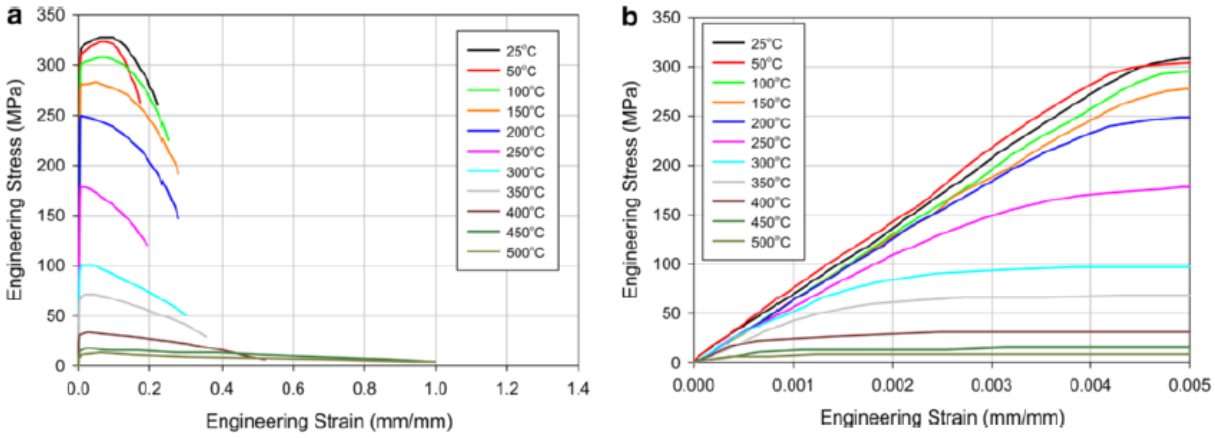

Figure 2.4 Engineering stress-strain relations of alloy 6061-T651 at elevated temperatures [Summers et. al., 2015]

The first thing that stands out is how each curve is lower than the previous, indicating a decrease in mechanical properties with increasing temperature. It should be noticed that the failure strain remains relatively constant from room-temperature to 400 °C. Above 400 °C the failure strain increases significantly. This is also confirmed by the increasing reduction in area at the necked region for temperatures above 400°C, see Figure 2.5. Ductile fracture is the dominant method of failure that

becomes more and more ductile with increasing temperature. Figure 2.5 shows agreement with Figure 2.4 in respect to elongation and strain at failure.

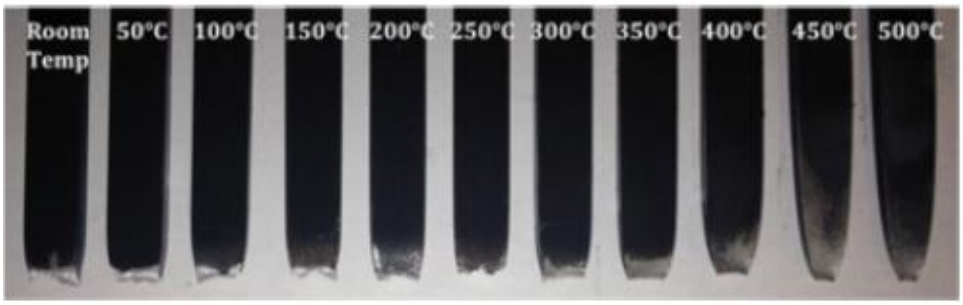

Figure 2.5 6061-T651 alloy tensile specimen fracture morphology [Summers et. al., 2015]

Figure 2.6 shows the development of the yield strength with increasing temperature. Also here the presented data are performed regarding ASTM E21 (ASTM Standard E21 2009) and temperatures up to 500°C. It could be noticed that the strength of the material decreases significantly with increasing temperature. For the 6061 alloy it could be noticed that in the region from room temperature to 150°C the strength steadily declines from 319 to 242MPa. While a noticeable drop-off in strength, it is minimal compared to the next region. Between 150 and 400°C, the yield strength of the material degrades at a much quicker rate with the largest drops occurring between 200 and 300°C where the yield strength drops from 242 to 101MPa. At this point it was already determined that the material is no longer stiff and now its observed that the yield strength is about 1/3 of its original strength. The final region from 400 to 500°C doesn't have any significant change in yield strength because it has essentially reached 0. A strength of 9MPa is all that remains at 500°C, approximately 3% of the room temperature strength.

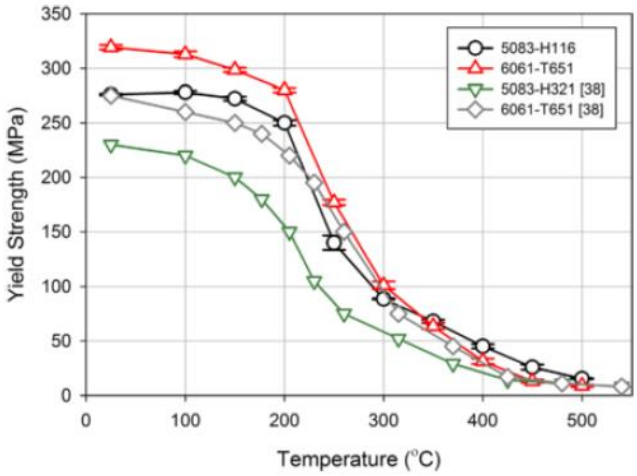

Figure 2.6 Yield strengths of alloy 5083-H116 and 6061-T651 alloy at elevated temperatures. Data reported in [Kaufmann, 1999] is shown for comparison. [Summers et. al., 2015]

2.2 Creep

Creep is defined as time-dependent deformation of a material. The rate of creep deformation is dependent on material behavior (i.e. creep constants), temperature, time, and stress. As temperature increases, the creep strain rate increases accordingly. Creep is a very important phenomenon which also determines the life of structures that are exposed to higher temperatures and stresses. The constitutive behavior of aluminum alloys at elevated temperatures is dominated by creep. This makes aluminum structures relatively sensitive to fire. The strain as a function of time resulting from a creep test is usually divided into a primary stage with decreasing strain rate and slows with time, a secondary stage with constant, minimum strain rate, and a tertiary stage with accelerated creep and terminates when the material breaks or ruptures, see Figure 2.7.

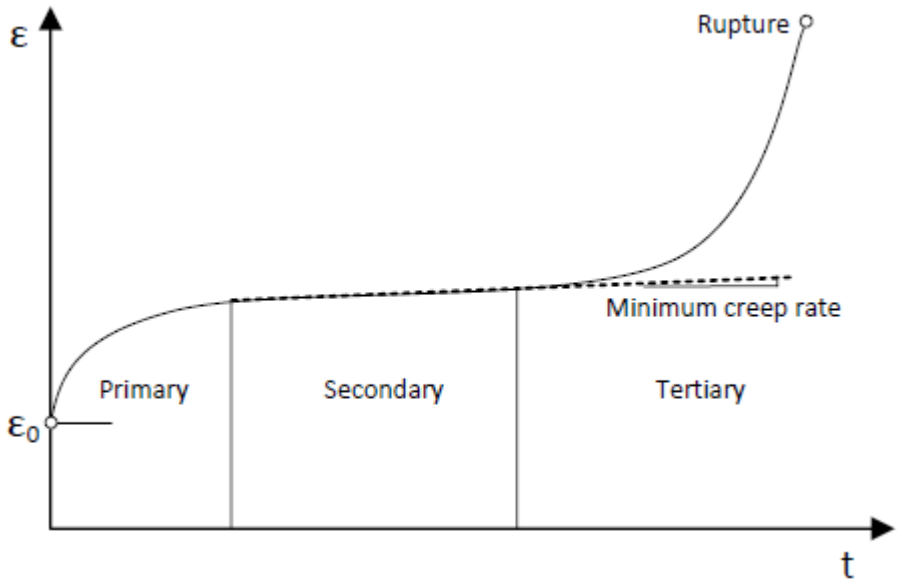

Figure 2.7 Description of creep deformation stages [Stewart, 2008]

When a material is subjected to constant stress for a certain period of time, three basic parts of strain response may typically be observed, see also Figure 2.8.

- Instantaneous elastic strain: immediately after applying a certain amount of stress.
- Delayed elastic strain: will completely recover after removing stress.
- Non-recoverable strain: strain caused by viscous flow leads to permanent deformation.

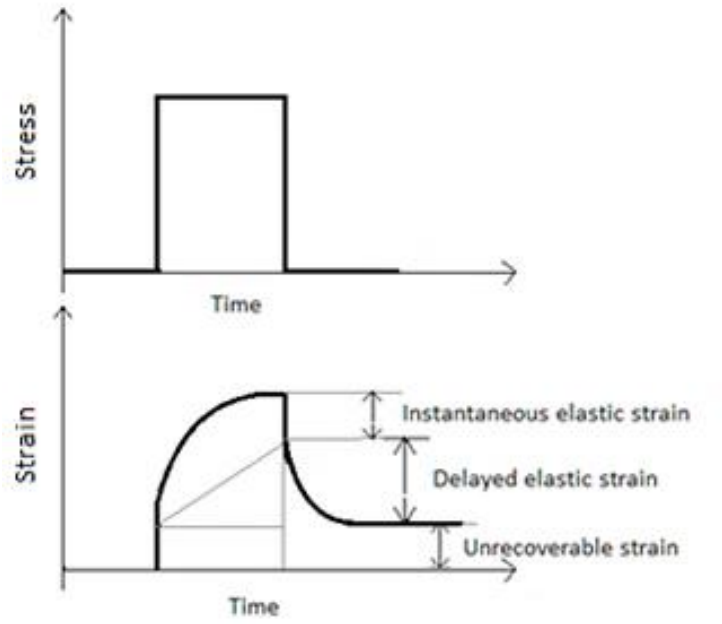

Figure 2.8 Strain as a function of the time during loading and unloading.

[Maljaars, 2008] refers to different creep databases. These literature give creep strains after various exposure periods and the time to rupture of various alloys and tempers. It is clear from the literature that creep has a major influence on the mechanical properties at temperatures exceeding 150°C. At elevated temperatures, creep strains develop in less than one hour. Therefore, creep is an important aspect to take into account in fire conditions. Also [Courtney, 2000] stated that creep strains are not considered significant at temperatures below ≈40 – 50% of the absolute melting temperature.

[Allen, 2012] has conducted creep tests at 6061-T651 and 5083-H116 alloy specimens. Figure 2.9 shows the creep behavior data of 6061-T651 alloy. Being a ductile material, the 6061 has a flat secondary region that quickly becomes tertiary and then fails. It can also be noticed that a small difference in stress can have a significant effect on the strain of the sample.

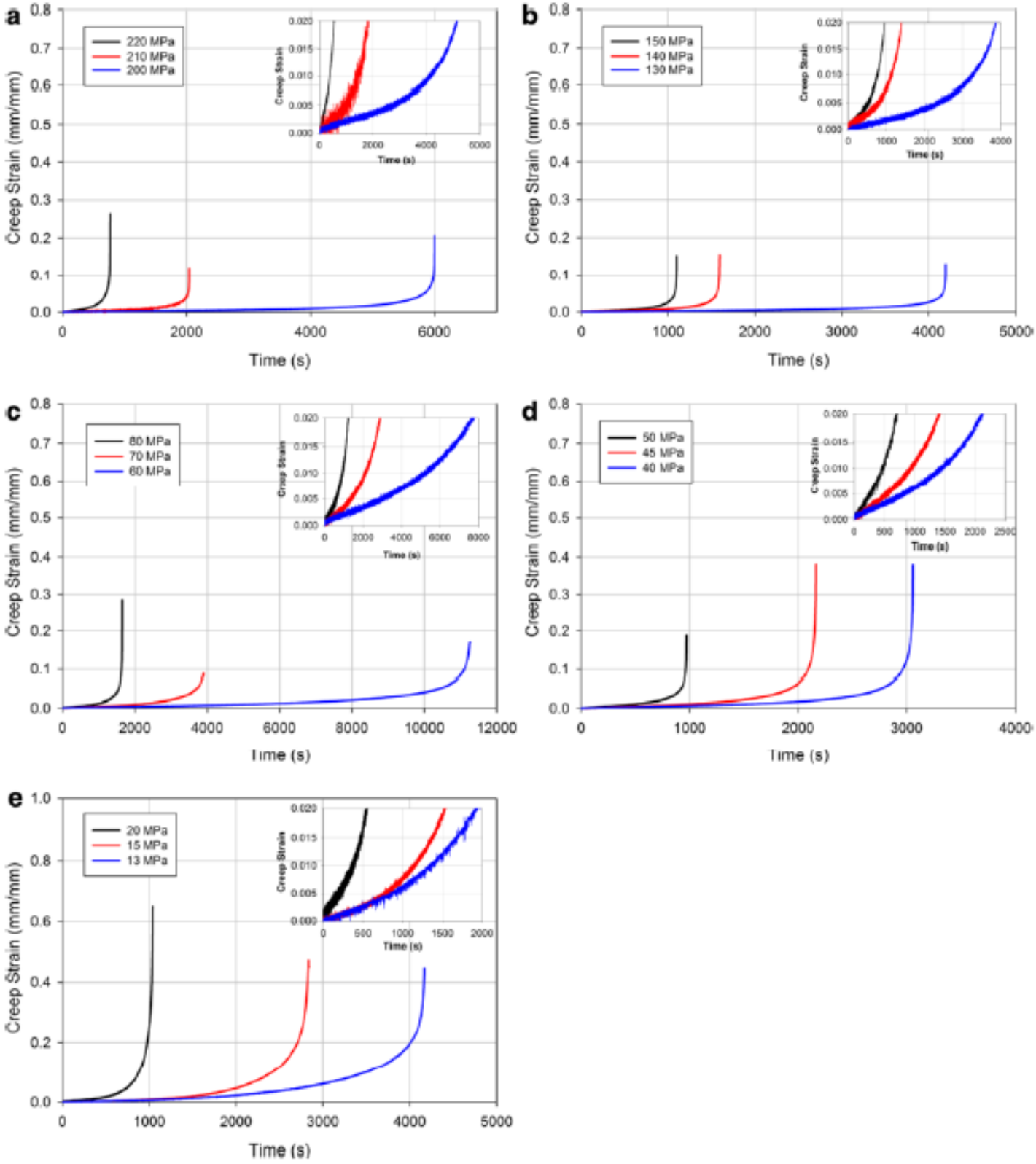

Figure 2.9 Creep behavior of 6061-T651 alloy at (a) 200°C (b) 250°C (c) 300°C (d) 350°C (e) 400°C. The inset figures detail the creep behavior at strains less than 2% [Allen, 2012].

2.2.1 Dorn-Harmathy creep model

The Dorn-Harmathy model provides an analytical model with which the primary and secondary creep strain $\dot{\varepsilon}_{t,I+II}$ can be determined as a function of time, temperature and stress. This equation will be used during the preparation of the test series in the further study. Dorn [Dom, 1954] has provided an equation for secondary creep strain rate $\dot{\varepsilon}_{t,II}$, see equation (2.2). This equation shows that the relation between the temperature and secondary creep stain rate can be described by the Arrhenius equation. Equation (2.2) leads to the secondary creep strain function, see Equation (2.3).

$$\dot{\varepsilon}_{t,II} = Z \cdot e^{-\frac{Q}{R \cdot T}} \tag{2.2}$$

$$\varepsilon_{t,II} = \int_0^t \left(Z \cdot e^{-\frac{Q}{R \cdot T}} \right) dt \tag{2.3}$$

Equation (2.4) is proposed for Z [Dorn, 1954] [McQueen et. al, 1971], in which A, α and n are material dependent parameters. These parameters are determined with curve fitting. Z is the Zener-Holloman parameter, describing the influence of stress on the secondary strain rate.

$$Z = A \cdot (\sinh \alpha\sigma)^n \tag{2.4}$$

[Harmathy, 1967] extended Equation (2.2) with the primary creep ε_{t0}, see Equation (2.5). ε_{t0} is a function of the stress level σ and is the projection back to zero time of the secondary creep curve, see Figure 2.7. Harmathy proposed Equation (2.6) for this parameter and noted that Equation (2.6) is based on a plot with badly scattered data.

$$\dot{\varepsilon}_{t,I+II} = A \cdot (\sinh \alpha\sigma)^n \cdot e^{-\frac{Q}{R \cdot T}} \cdot \coth^2 \left(\frac{\varepsilon_{t,I+II}}{\varepsilon_{t0}} \right) \tag{2.5}$$

$$\varepsilon_{t0} = D \cdot \sigma^m \tag{2.6}$$

Where D and m are material dependent parameters and also determined with curve fitting. The influence of temperature is incorporated by the so called Arrhenius equation, with Q the material dependent activation energy for creep in J/mol, R the universal gas constant (R=8.314 J/molK) and T the absolute temperature in Kelvin.

Equation (2.5) returns to infinity for σ=0 or $\varepsilon_{t_{I+II+III}} = 0$. This is easily solved by [Maljaars, 2008] by artificially increasing $\varepsilon_{t_{I+II+III}}$ and ε_{t0} with small numbers. The numbers which are chosen are so small that it have a negligible influence on the resulting strain rate, see Equation (2.7).

$$\dot{\varepsilon}_{t,I+II+III} = Z \cdot e^{-\frac{Q}{R \cdot T}} \cdot \coth^2\left(\frac{\varepsilon_{t,I+II+III} + 1 \cdot 10^{-7}}{\varepsilon_{t0} + 1 \cdot 10^{-7}}\right) \tag{2.7}$$

2.2.2 Tertiary creep

Tertiary creep is not incorporated in the Dorn-Harmathy model. [Maljaars, 2008] has made a modification on the existing constitutive model and extended the Dorn-Harmathy creep model for tertiary creep. Several experiments are performed on 5083-H111 and 6060-T66 alloys. In case of alloy 6060-T66, the tertiary creep stage with increasing strain rate started after a relatively short period and after a small creep strain. Creep tests on alloy 6060-T66 showed that creep deformation is dominated by tertiary creep. It is found that for strains up to 2%, a linear relation exists between the creep strain rate and the creep strain in the tertiary creep stage of alloy 6060-T66. It appeared that the tertiary creep stage (up to 2%) is (approximately) homogeneous.

Because of the first part of the creep strain rate in the tertiary creep stage $\dot{\varepsilon}_{t,III}$ is found to be linear proportional to the creep strain $\dot{\varepsilon}_{t,I+II+III}$, Equation (2.8) follows.

$$\dot{\varepsilon}_{t,III} = C \cdot \varepsilon_{t,I+II+III} \tag{2.8}$$

Where C is a constant. The creep strain at the start of the tertiary stage is denoted with symbol ε_{lim}. For reasons of continuity, the creep strain rate at the start of the tertiary stage should be equal to the secondary creep strain rate $\dot{\varepsilon}_{t,II}$, which allows Equation (2.9) for the elaboration of constant C.

$$C = \frac{\dot{\varepsilon}_{t,I+II}}{\varepsilon_{lim}} \tag{2.9}$$

With incorporation of this, the constitutive model including the first part of the tertiary creep is described with Equation (2.10) and (2.11).

$$\varepsilon_{t,I+II+III} \leq \varepsilon_{lim}: \quad \varepsilon = \frac{\sigma}{E} + \int_0^t \dot{\varepsilon}_{t,I+II}\ dt \tag{2.10}$$

$$\varepsilon_{t,I+II+III} > \varepsilon_{lim}: \quad \varepsilon = \frac{\sigma}{E} + \int_0^t \dot{\varepsilon}_{t,I+II} \cdot \frac{\varepsilon_{t,I+II+III}}{\varepsilon_{lim}} \, dt \tag{2.11}$$

Parameter ε_{lim} is stress and temperature dependent. Simulations with the model for transient state conditions in [Maljaars, 2008] showed that it is sufficiently accurate to use the average value of ε_{lim} of the creep tests.

2.2.3 Primary creep in [Kandare et. al, 2009]

Also [Kandare et. al, 2009] presents a creep-based modelling approach based on the analytical work by [Maljaars et. al, 2008]. [Kandare et. al, 2009] assumes that the creep strain at zero time, ε_{t0}, is considered by [Maljaars et al., 2008] to depend on stress only. However, ε_{t0} is actually a function of both stress and temperature, and the creep parameters must be calculated using a stress–temperature decoupling approach similar to that by defining for the secondary creep strain rate, see Equation (2.12).

$$\varepsilon_{t0} = A_1 \cdot \sigma_c^{nI} \cdot e^{-\frac{Q_I}{R \cdot T}} \tag{2.12}$$

Where A_1 is a material parameter for primary creep, n_I is the material exponent from primary creep, and Q_I is the activation energy for primary creep. The creep parameters of the material must be determined by creep testing. ε_{t0} is a function of both stress and temperature, and parameters describing this relationship are calculated using a stress–temperature decoupling procedure. A plot of ln ε_{t0} against ln σ_c yields a slope n_I. Also a plot of ln ε_{t0} against the reciprocal of absolute temperature will yield the apparent activation energy for primary creep. A curve fitting minimization algorithm can be used to calculate A_1.

2.3 Welds in load-bearing structures in aluminum

The most common connection elements for aluminum load-bearing structures are welds, bolts and rivets. Weight saving is an important advantage of welding compared to the use of bolts and rivets. In addition, the simple manufacturing and assembly, so that the construction costs will be reduced, are important advantages of welded structures. By these advantages, welds are the most commonly used joints in aluminum structures.

Welding can be defined as the joining of materials by means of heating, with or without a filler material. In addition to the many advantages welding also has some disadvantages. The welding of aluminum alloys is in general more critical than welding of structural steel. Although sometimes special welding

processes are used such as ultrasonic welding, friction welding etc., the MIG and TIG welding processes are the most commonly used techniques in construction. In this welding process, two members are joined by melting the parent metal, while adding a suitable filler metal. The MIG welding process results in two potentially weak parts of the connection, being:

- The weld metal itself, which is a mixture of parent metal and filler metal. This weld metal may have a lower strength than the parent metal.
- The zone that is affected by the heat input of the welding process (the heat affected zone, HAZ). Welding causes an heat affected zone (HAZ), which reduces the strength of the material.

See Figure 2.10 for the hardness overview of the HAZ.

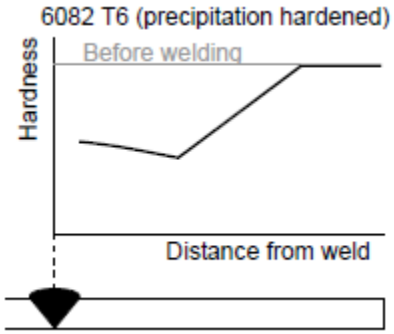

Figure 2.10 Hardness of the HAZ of alloy 6082-T6 [Maljaars et. al, 2009]

Attention should be paid to both the weld and the heat affected zone adjacent to the weld. The boundaries of the HAZ generally need to be assumed as straight lines perpendicular to the metal surface, in particular, if thin material is welded (see Figure 2.11) For a MIG weld the values of b_{haz} are as follows [EN 1999-1-1, 2007]:

$0 < t \leq 6$ mm	$b_{haz} = 20$ mm
$6 < t \leq 12$ mm	$b_{haz} = 30$ mm
$12 < t \leq 25$ mm	$b_{haz} = 35$ mm
$t > 25$ mm	$b_{haz} = 40$ mm

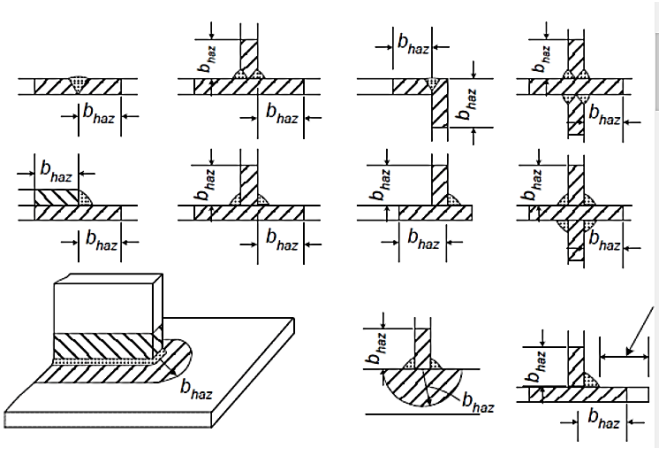

Figure 2.11 Dimensions of the heat affected zone in mm.

A heat-affected zone (HAZ) is the portion of the base metal that was not melted during welding, but whose microstructure and mechanical properties were altered by the heat. This alteration can be detrimental, causing a reduction of the strength of the base material.

As previously mentioned, stress-strain properties for ambient temperatures are representative for the temperature range -30 to 80 °C. The high temperature range concerns the behavior under fire conditions but also the heat-input as a result of welding. Aluminum alloys do suffer from that heat-input. This results in lower strength values compared to the parent metal values in the heat-affected zone (HAZ).

The temperature in the HAZ during welding is not homogeneously distributed. In [Myhr et. al, 1991 - I] an overall process model for the microstructural stability of 6082-T6 aluminum alloys with thickness of 15 mm at elevated temperatures has been developed. The model allows calculations of the hardness distribution. [Myhr et. al, 1991 - II] deals with the application of the model for prediction of strength losses in the heat affected zone (HAZ) of fusion welds. [Myhr et. al, 1991 - II] showed a minimum hardness at a distance in the range of 10 mm from the center of the weld. [Missori et. al, 2000] investigates the microstructure and mechanical characteristics of joints welded with Gas Metal Arc Welding (GMAW) procedure made of plates of 6082-T6 alloy with a thickness of 10 mm. Experimental work included also Vickers micro hardness test. The Vickers test showed a minimum hardness recorded at a distance variable in the range of 7 mm from the weld fusion line. [Myhr et. al, 2004] simulates the sequence of reactions occurring during artificial ageing, welding and post weld heat treatment of plates of Al-Mg-Si alloys with a thickness of 5 mm. The calculations reveal that the peak temperature is located 10 mm from the center of the weld.

Also [Missori et. al, 1997] conducted micro hardness tests with a Vickers hardness device, with 100 g load, along a line on the transverse section of the welded joint. A typical trend in values measured is shown in Figure 2.12. It is possible to isolate a first zone, from the fusion zone and approx. 10 mm wide, in which hardness was moderately reduced.

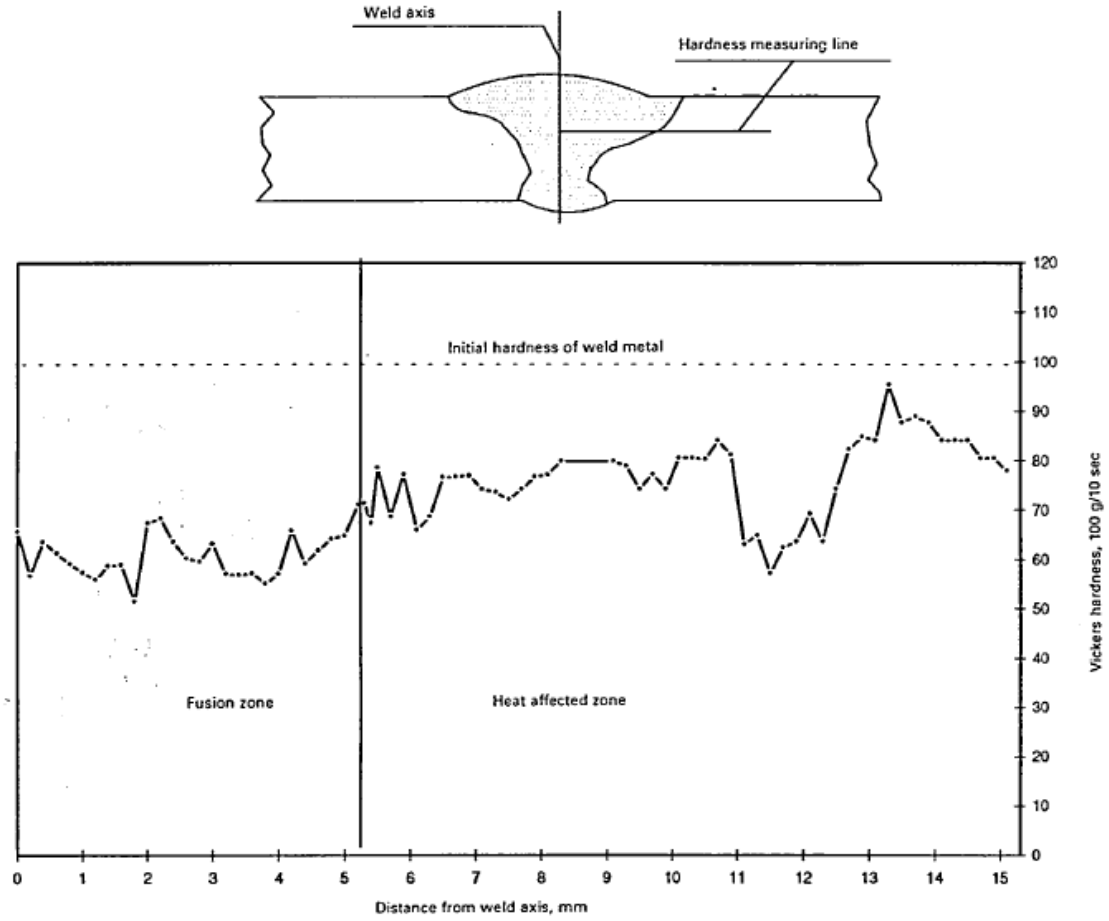

Figure 2.12 Microhardness profile of welded joint in [Missori et. al, 1997]

[Missory et. al, 1997] investigated the mechanical characteristics of MIG welded joints in 6082-T6 plate alloy by means of tensile tests. Tensile tests were carried out at 60 and 180 days from welding on test pieces taken from samples welded transverse to the welding axis. The results, shown in Table 2.1, were compared with those obtained from the material deposited.

Table 2.1 Tensile test data from base materials and welded testpieces in [Missori et. al, 1997]. Ruptures in the HAZ were observed up to a distance of 10mm from the fusion line.

No.	Type of material	Tensile strength (MPa)	Position of rupture zone*	Elongation to rupture
1	Unwelded	276	–	8.9
2		269	–	8.8
3	Welded	177	HAZ	7.0
4	(after 60	178	HAZ	6.5
5	days)	180	HAZ	5.5
6	Welded	154	HAZ	6.3
7	(after	165	FZ†	5.6
8	180 days)	158	HAZ	6.3

The welded joints undergo marked reduction in tensile strength from the initial value of ≈275 MPa to ≈178 MPa after 60 days and to ≈160 MPa after 180 days. The reduction in tensile strength and hardness are in good agreement with the values prescribed by Italian and other engineering codes, which show reduction factors around 50-60%. Rupture of welded test pieces in five cases out of six occurred in the heat affected zone, from the external surface, at a distance from the fusion line of approx. 10 mm. In the majority of cases the fracture surface occurred in the HAZ and with a 45" trend in respect of thickness. Tests on deposited material show fracture edges with a slightly more deformed appearance through lateral contraction. Compared with the characteristics of the base material of the weld, there was a reduction in percentage elongation to rupture, which gives an indication of the loss of ductility in the welded joint.

[Maljaars et. al, 2009] focuses on one of the knowledge gaps, being the strength of welds when exposed to fire.

2.4 Microstructural analyses

The strength degradation due to heat treatment is closely related to the microstructural damage inside the materials. Due to thermal exposure, internal microstructural damage may be accumulated in surviving aluminum structures after returning to ambient conditions. In addition to the grain recrystallization and precipitate evolution caused by thermal exposure, stress will cause additional damage to the microstructure during plastic deformation. The thermally-induced microstructural damage and corresponding residual (post-fire) mechanical behavior are studied in [Summers et. al, 2014] and [Matulich, 2011].

However, these researchers only studied the thermally induced damage and did not account for the stress influence on microstructural damage and post-fire response of the load-bearing aluminum structures.

The damages in aluminum are complex and may be a combination of grain growth, precipitate cracking, and cavity formation [Leckie et. al, 1974]. Permanent changes will take place in the microstructure after material exposure to fire. The microstructural evolution and precipitation sequence associated with the increase of temperature provide evidence for the thermally-induced damage in the material.

For a load-bearing aluminum structure, stress is an important factor to accelerate the microstructure damage and the residual material strength degradation. During fire exposure, the applied stress may cause large plastic deformation, grain elongation, dislocation agglomeration, precipitate cracking, and cavity formation associated with the increase of strain; collectively, these are the stress-induced damage [Martin et. al, 2009]. [Blakenship, 1996] investigated the cavitation evolution in 6061-T651 aluminum alloy during creep to study the stress-induced microstructural damage mechanism. Specimens are investigated to study the effect of stress on the cavitation nucleation and growth. Since the solely thermal exposure condition does not cause any cavity formation, no cavitation is observed in the solely thermal exposure samples. As the stress was applied, samples began to creep and large plastic deformation developed with the increase of exposure time. Samples heat treated to 400°C have higher ductility than those exposed to 300 °C, thus the 400°C strained sample obtains higher strain (58%) before fracture than the 300°C one (19%), after unloading to 20 °C. However, the cavitation displays opposite feature with ductility in the just-before-fracture states exposure at 300°C and 400°C. Although the 400°C strained sample has higher strain (58%) before fracture than the 300°C one (19%), the number of cavities in the 300°C strained sample appears more than the 400°C strained one. These differences in the stress-induced cavitation development result in distinct fracture mechanism in 300°C and 400°C creep samples. Figure 2.13 exhibits the fracture surfaces for samples creep at both temperatures. The large amount of cavitation leads to brittle fracture of the 300°C creep sample; while 400°C creep sample experience a more ductile failure due to the higher ductility and lower cavitation in the before failure stage.

Figure 2.13 Fracture surface of thermo-mechanical tested samples (a) 300°C, (b) 400°C [Blakenship, 1996].

2.5 Fire of aluminum

Temperature has a significant influence on the mechanical behavior of aluminum structural elements. As mentioned in the previous chapter, temperature can have a positive effect on the properties of aluminum. But this does not exclude that it can have also negative effects on the properties. Because of the temperature difference in a fire is not controlled, this will have a negative effect on the strength of the structure. Knowledge of the behavior of temperature progress in fire is decisive for the necessary fire protection for a building. People in the building need to be able to escape safely before the structure collapses due to the fire. Thinking and working with fire protection concepts requires insight into the development of a fire.

This chapter gives general overview of fire behavior and aluminum structures in fire design. For more detailed information reference is made to [Maljaars, 2008] Chapter 4 *Heating of aluminum members exposed to fire*.

2.5.1 Fire behavior

A major concern with the application of aluminum is the safety during extreme fire conditions. While an aluminum structure is subjected to fire, the mechanical properties of the material may be degraded and premature failure may occur with the accumulation of fire damage. Thus particular consideration must be given to the structural stability during fire exposure. Because of this, it is necessary to know the behavior of fire and what effect it has on aluminum.

The behavior of the temperature development in time in fire conditions can be described in a fire curve. The most known curve is shown in Figure 2.14 (blue line). The actual gas temperature depends on the geometry of the fire compartment and the amount and types of combustibles. In most cases nominal standard fire curves (red line) are applied for the verification of the fire resistance of a structure. These

curves are independent of the specific layout and occupancy of the fire compartment and they are a simplified representation of a real fire [Wald, 2009].

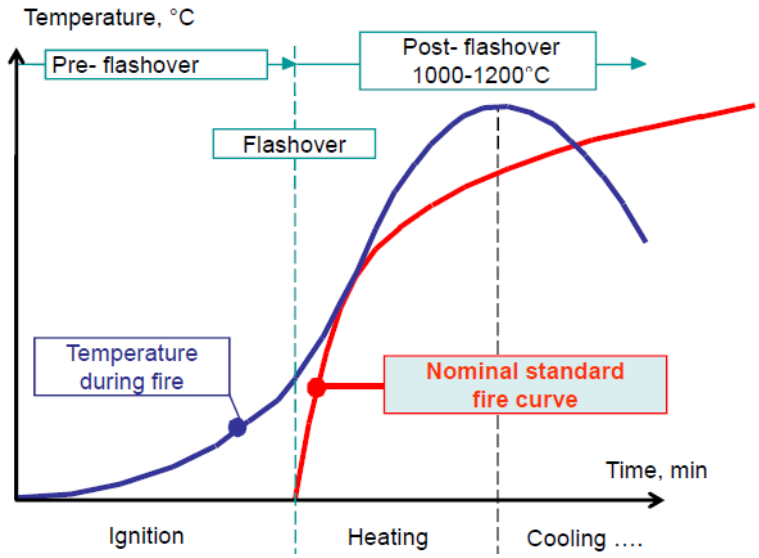

Figure 2.14 Fire modelling. Temperature during fire and nominal standard fire curve [Wald, 2009].

The standard fire curve, also referred to as the ISO834 curve is a curve used internationally for fire resistance testing of components. This allows for a direct comparison between standard fire tests of components rather than giving an indication of how long the component will survive in the fire. Equation (2.14) shows the definition of the standard fire curve as described in [EN 1991-1-2, 2002].

$$\theta_g = 20 + 345 log_{10}(8t + 1) \tag{2.14}$$

Where: θ_g = the gas temperature in compartment in °C

t = time in minutes.

Also natural fire models are specified in [EN 1991-1-2, 2002]. Simplified fire models allow for a more realistic fire scenario to be considered in design. Unlike a nominal fire curve, a natural fire model takes into account how the environment, density of combustible materials and ventilation will affect the development of the fire. Again, reference is made to [Maljaars, 2008] for more detailed information about NFSC.

In order to determine whether or not a structure complies with the fire design, the requirement on the fire resistance has to be known. For a standard fire, the requirement is given by national laws, and is commonly 30 up to 120 minutes.

2.5.2 Development of the aluminum temperature

Unprotected aluminum elements applied in a compartment

The temperature increase $\Delta\theta_{al(t)}$ of an unprotected element in a time interval Δt, with an equivalent uniform temperature distribution in the cross section, should be determined according to Equation (2.15), which is described in [EN 1999-1-2, 2007] paragraph 4.2.3.1.

$$\Delta\theta_{al(t)} = k_{sh} \cdot \frac{1}{c_{al} \cdot \rho_{al}} \cdot \frac{A_m}{V} \cdot \dot{h}_{net} \cdot \Delta t \qquad (2.15)$$

Where:

k_{sh} = correction factor for the shadow effect

$\frac{A_m}{V}$ = profile factor for unprotected elements of aluminum in m^{-1}

$\dot{h}_{net}$ = net heat flux density per unit area according to [EN 1991-1-2]

c_{al} and ρ_{al} = material constants.

The 0.2% proof stress of aluminum alloys reduces in the temperature range of 150 to 350°C. in the evaluation of the fire resistance, it is focused on this temperature range. Insulation is always requires when the fire design of aluminum members is evaluated based on the standard fire.

Aluminum elements protected with fire resistant protection applied in a compartment

As mentioned before, insulation is required in most cases. Therefore, this paragraph gives the temperature development in insulated members exposed to fire.

The temperature increase $\Delta\theta_{al(t)}$ of an protected element in a time interval Δt, with an equivalent uniform temperature distribution in the cross section, should be determined according to Equation (2.16), which is described in [EN 1999-1-2, 2007] paragraph 4.2.3.2.

$$\Delta\theta_{al(t)} = \frac{\lambda_p / d_p}{c_{al} \cdot p_{al}} \cdot \frac{A_p}{V} \left[\frac{1}{1 \cdot \frac{\phi}{3}} \right] \cdot \left(\theta_{(t)} - \theta_{al(t)}\right)\Delta t - (e^{\frac{\phi}{10}} - 1) \cdot \Delta\theta_{(t)} \qquad (2.16)$$

Where:

$\frac{A_p}{V}$ = profile factor for protected elements of aluminum in m^{-1}

$\theta_{al(t)}$ = aluminum temperature at time t in °C

$\theta_{(t)}$ = temperature of the surrounding gases at time t in °C

$\Delta\theta_{(t)}$ = increase of the temperature of the surrounding gases at time interval Δt in °C

[Maljaars, 2008] made a finite element analysis for the required amount of insulation for aluminum elements to obtain a maximum member temperature of 200 or 300°C after 30 or 120 minutes of exposure to the standard fire. The determination is made for three fictitious (but not unrealistic) insulation materials, see Table 2.2.

Table 2.2 Thermal properties of insulation materials considered in the analyze in [Maljaars, 2008]

material	ρ_p [kg/m^3]	c_p [J/kgK]	λ_p [W/mK]	symbol
p1	60	1030	$5\cdot10^{-8}\,\theta_p^2 + 2.6\cdot10^{-5}\,\theta_p + 2\cdot10^{-2}$	+
p2	240	900	$1\cdot10^{-8}\,\theta_p^2 + 2.1\cdot10^{-2}$	□
p3	240	1000	$4\cdot10^{-8}\,\theta_p^2 + 2.6\cdot10^{-5}\,\theta_p + 2.5\cdot10^{-2}$	○

Results of the finite element analyses are given in Table 2.3, Figure 2.15.

Table 2.3 Required thickness of insulation material according to analyze in [Maljaars, 2008]

A_m/V [/m]	1020				136			
Fire resistance [min]	30		120		30		120	
Temperature [°C]	200	300	200	300	200	300	200	300
Thickness p1 [mm]	51	41	144	131	13	8	79	55
Thickness p2 [mm]	30	25	78	70	12	8	52	41
Thickness p3 [mm]	22	17	58	50	7	4	32	22

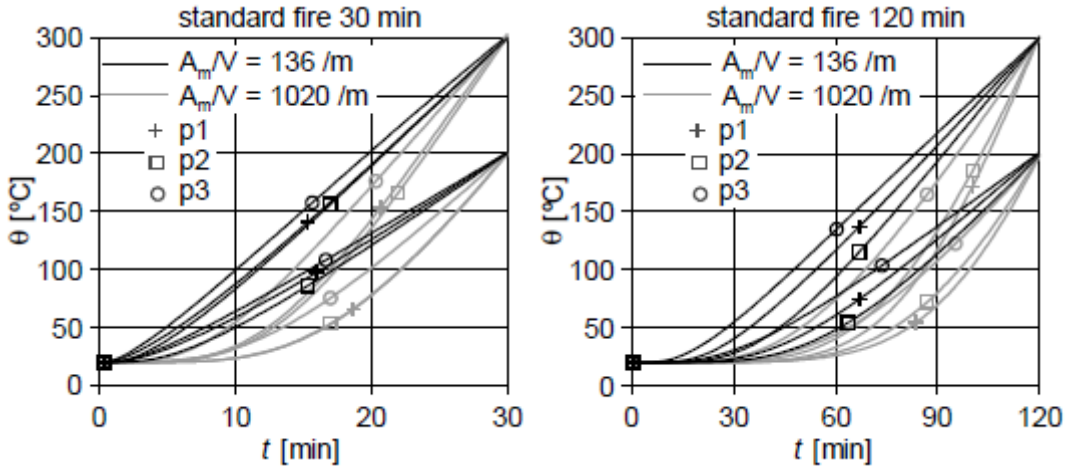

Figure 2.15 Member temperature as a function of time of insulated aluminum members exposed to the standard fire according to analyze in [Maljaars, 2008].

The temperature development in the section is similar for the different insulation materials. From a temperature of 50°C onwards, the heating rate remains approximately constant. The duration of the period before this temperature is reached varies, and depends mainly on the fire resistance requirement and the section factor.

It is known that the mechanical properties of aluminum members almost not reduce at temperatures lower than 150°C, so that the determination of the structural response in the fire design can be omitted. However, the analyze of [Maljaars, 2008] shows that considerably more insulation is requited for a maximum member temperature of 150°C than for e.g. 200 or 300°C. therefore, it may be economical to determine the structural response in fire design, in order to determine the actual critical temperature.

[Maljaars, 2008] analyzed also the temperature development in members exposed to the gas temperature-time curves that are based on the NFSC for insulation material p1. Figure 2.16 gives the temperature development as a function of the time of insulated aluminum sections exposed to a certain gas temperature-time curve, with a gas temperature of 1300°C. it can be seen that the insulation thickness has to be large (>100 mm.) in some cases. In practice, this may result in uneconomical and/or difficult to apply solutions. Besides, the advantage of relative lightweight construction is lost.

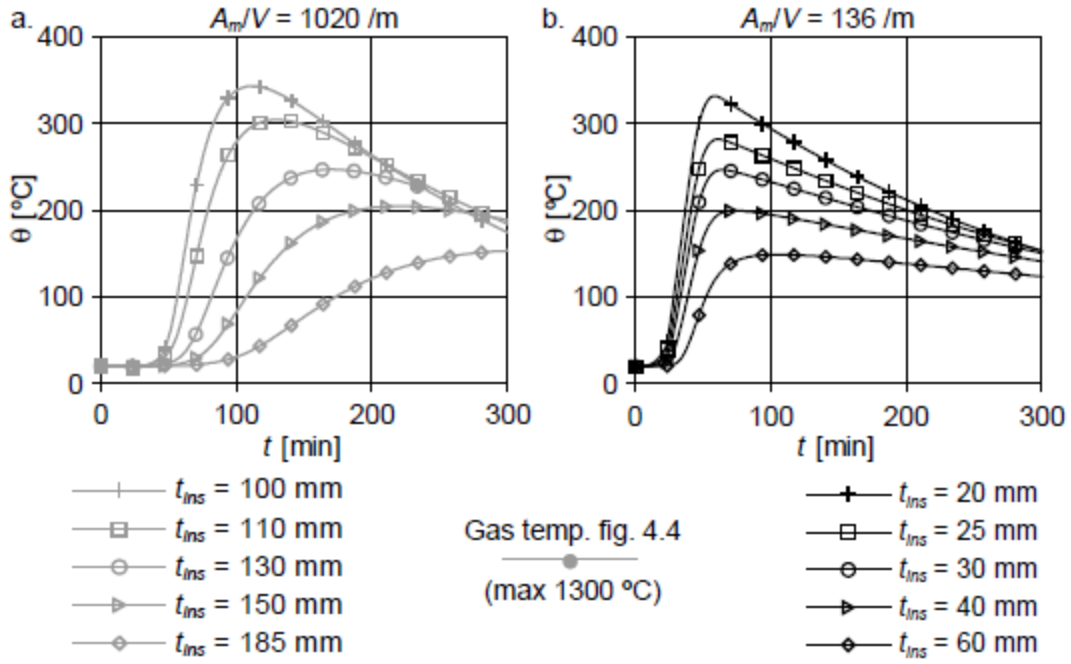

Figure 2.16 Temperature development of sections with various insulation thicknesses t_{ins} exposed to certain natural fire conditions [Maljaars, 2008].

The analyze of [Maljaars, 2008] shows that a significant amount of extra insulation is needed in order to reduce the member temperature with 50°C. This indicates that it is important to determine the critical temperature of aluminum members in fire design. Because of this, it is important to evaluate the structural response of aluminum members exposed to fire conditions in detail.

Unprotected aluminum elements applied outside a compartment

Due to the good corrosion resistance of aluminum, it is also possible to apply aluminum members outside, i.e. in the open air. According to [EN 1991-1-2, 2002] and [EN 1999-1-2, 2007] Equation (2.17) describes the basis of the method to determine the member temperature.

$$\sigma_{SB} \cdot T_m^4 + \alpha_c \cdot T_m = \sum I_z + \sum I_t + 293 \cdot \alpha_c \qquad (2.17)$$

Where: I_z = radiative heat flux from a flame

I_t = radiative heat flux from an opening

The left-hand side of Equation (2.17) considers the member and the right-hand side considers the surroundings. The method considers steady state conditions for the various parameters. [Maljaars, 2008] had performed an analyses with two types of external members; 1 column which is placed directly opposite to an opening and 1 column which is places between two openings. From its analysis it can be concluded that in case of members in between openings, the maximum member temperature is in most cases within the relevant temperature range of 150 to 350°C. For such columns it depends on the critical temperature, and thus on the structural response, whether or not insulation is required. In case of a member opposite to an opening, the temperature is only within the range of relevant temperatures for low fire load densities and large distances between the member and the opening. In other cases, such members need to be insulated.

3. Experimental work

This chapter provides an overview of the manner of implementation of the various experiments conducted for this research. In order to determine the constitutive properties at elevated temperature, three types of (uniaxial tensile) tests can be carried out. In this research creep tests are carried out to determine the parameters of the creep model. With transient state tests this model is validated. The different tests are:

- Steady state tests where the specimen is subjected to a constant, elevated temperature in time, while a certain strain rate is applied (i.e. a displacement-controlled test), see Figure 3.1. The actual test is preceded by a period with a constant temperature equal to the test temperature (the thermal exposure period).

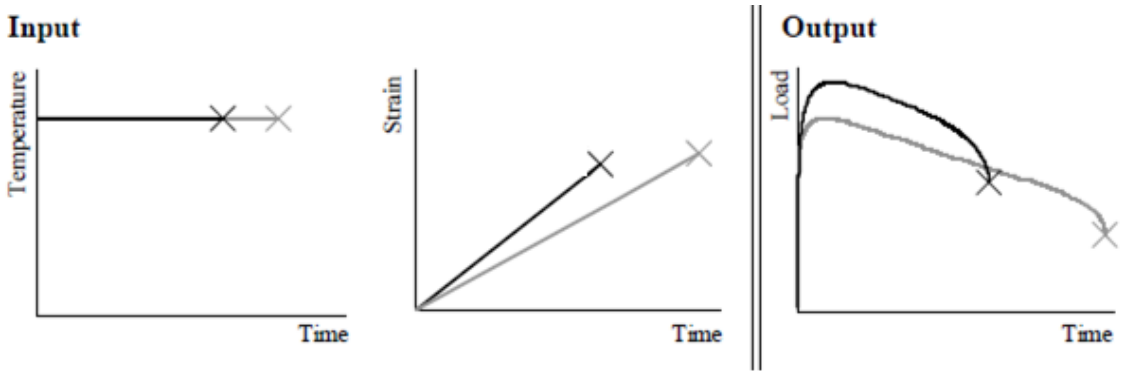

Figure 3.1 Representation of a steady state tensile test.

- Transient state tests where the test is carried out at a certain stress level and an increasing temperature in time. The deformation (strain) is monitored. Usually, a constant heating rate and a constant stress level in time are applied, see Figure 3.2.

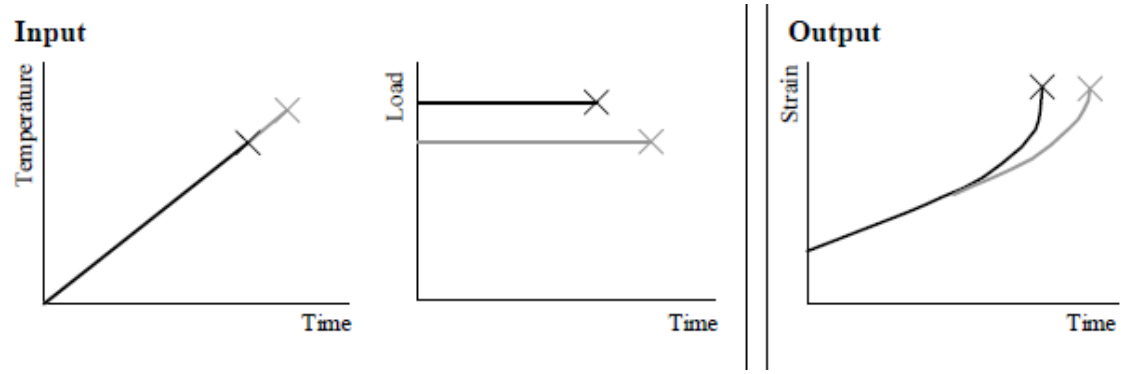

Figure 3.2 Representation of a creep test.

- Creep tests where a constant, elevated temperature and a constant load is applied at the specimen. In time, the strain will increase until rupture occurs, see Figure 3.3.

Creep tests may give the essential information for creep models, with which it may be possible to simulate transient state tests.

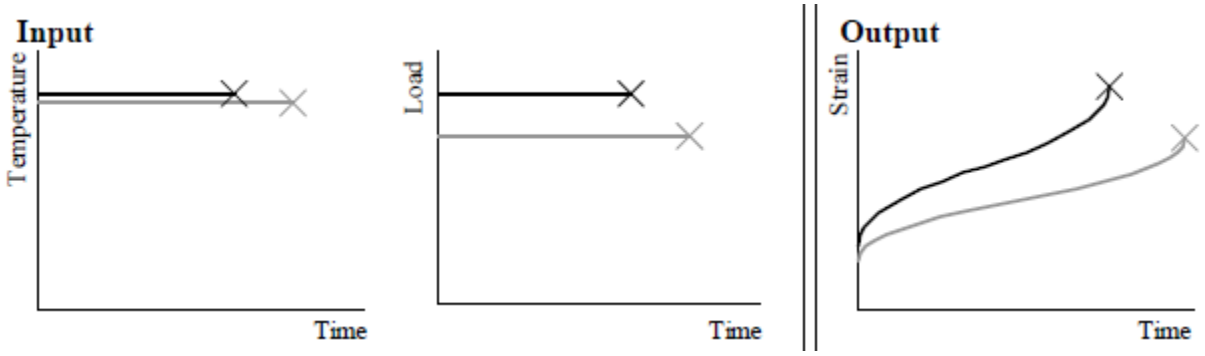

Figure 3.3 Representation of a creep test.

3.1 Chemical composition and strength of 6082-T651 alloy

Alloy 6082-T6 is used in the experimental analyses, so that it can be compared with aluminum alloy 6060-T66 from the literature of Maljaars [Maljaars, 2008]. All specimens originate from the same batch. The aluminum alloy studied and subjected to the experimental tests for this thesis have been provided by Bayards Aluminum Constructies BV.. The chemical components are tabulated in table 3.1. Annex A.1 shows the inspection certificate EN10204 – 3.1 of this alloy.

According to the manufacturer, a proof strength of 299 MPa and an ultimate tensile strength of 322 MPa is experimentally determined for this aluminum alloy (not welded).

The welds in the welded specimens are made by Bayards. The Eurocode indicated the proof strength and ultimate tensile strength as 125 Mpa and 185 Mpa respectively. The proof strength and ultimate tensile strength of the welded specimens in this research are determined with experiments as 133 Mpa and 196 Mpa, respectively.

Table 3.1 Chemical composition of the 6082-T651 alloy.

	Alloy	Si (%)	Fe (%)	Cu (%)	Mn (%)	Mg (%)	Cr (%)	Zn (%)	Ti (%)	Each (%)	Total (%)	Al (%)
Min.		0.7	-	-	0.40	0.6	-	-	-	-	-	
Max.		1.3	0.50	0.10	1.0	1.2	0.25	0.20	0.10	0.05	0.15	
	6082	1.00	0.29	0.02	0.58	0.80	0.02	0.01	0.008			97.23

3.2 Thermal expansion

Thermal expansion is the tendency of matter to change in shape, area and volume in response to a change in temperature. The coefficient of thermal expansion of alloys is affected by the nature of their constituents: the presence of silicon and copper reduces expansion while magnesium increases it.

[EN 1999-1-2, 2007] gives equation (3.1) for the relation between thermal expansion ε_{th} and the member temperature θ.

$$\varepsilon_{th} = \frac{\Delta l}{l} = 1.0 \cdot 10^{-8}\theta^2 + 22.5 \cdot 10^{-6}\theta - 4.5 \cdot 10^{-4} \qquad (0°C < \theta < 500°C) \qquad (3.1)$$

Where: l = Length at 20 °C

Δl = Expansion caused by temperature

Thermal expansion experiments are conducted to not welded and welded specimens to verify the formula given in the Eurocode. Not welded and welded specimens are exposed to temperatures rising to 350°C without addition of a force. Figure 3.4 shows the result of the thermal expansion experiment on a specimen without a weld and a specimen with a weld. Equation (3.2) and (3.3) are obtained on the basis of the least square regression method. Also the plot of Equation (3.1) is given in this figure as comparison.

$$\varepsilon_{th,not\ welded} = 2.0 \cdot 10^{-8}\theta^2 + 18 \cdot 10^{-6}\theta - 9 \cdot 10^{-4} \qquad (0°C < \theta < 350°C) \qquad (3.2)$$

$$\varepsilon_{th,welded} = 5.0 \cdot 10^{-8}\theta^2 + 1 \cdot 10^{-6}\theta - 9 \cdot 10^{-4} \qquad (0°C < \theta < 350°C) \qquad (3.3)$$

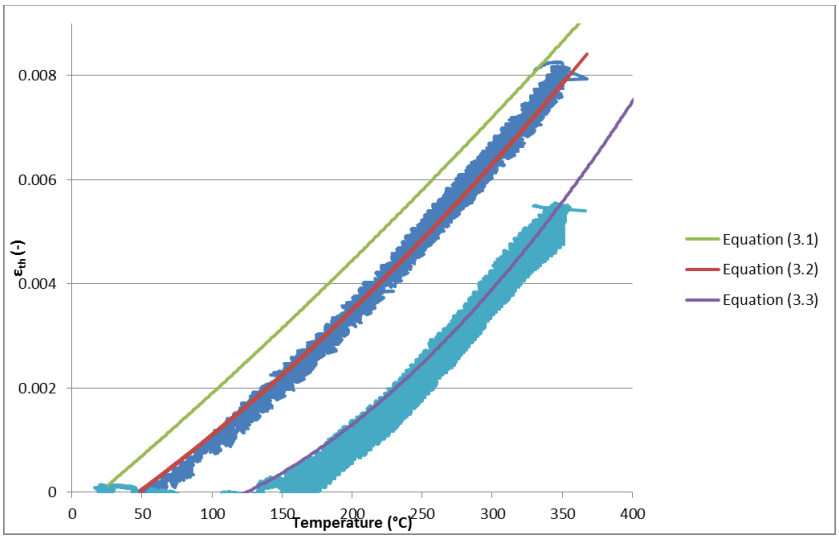

Figure 3.4 Results of the thermal expansion experiments on specimens without a weld (red line) and with a weld (purple line). Also Eurocode 9 data shown for comparison.

It can be seen that the thermal expansion curve of the not welded specimen, the welded specimen and the curve of Eurocode 9 are almost parallel with each other. This means that the thermal expansion of the graphs are almost identical. However, there can again be seen an unexplained (slip) behavior in the graph of the non-welded test pieces. However, both type of specimens show less thermal expansion with increasing temperature as compared to the Eurocode.

Also the literature study [Soyal, 2016] thermal expansion of alloy 5083 and 6060 was discussed. It was noted that the 6060 alloy showed less thermal expansion with increasing temperature as compared to the general curve of the Eurocode. On the other hand, the thermal expansion curve of alloy 5083 corresponded well with the curve given in the Eurocode.

It may be concluded that the 6xxx aluminum alloys, both welded and not welded, give almost the same thermal expansion with increasing temperature as compared to the thermal expansion data in Eurocode 9.

3.3 Creep tests

The mechanical properties of aluminum exposed to fire conditions depend on the temperature development in time and the variation of the stress level in time. The existing Dorn-Harmathy creep model is used as a basis for deriving the mechanical properties of aluminum alloys exposed to fire conditions. The goal of the creep tests is to calibrate the material parameters of the Dorn-Harmathy creep model as described in paragraph 2.2.1. The material parameters are the activation energy Q in the Arrhenius equation (2.2), parameter A, α and n in equation (2.6) for the Zener-Holloman parameter and parameters D and m in equation (2.8) for the primary creep factor ε_{t0}.

The experiments consist of two types test pieces, welded and not welded. Standard flat tensile specimens with a parallel length of 75 mm, a width of 12.5 mm and a thickness of 5 mm will be used in the creep tests, see Figure 3.5 for specimens with weld. Specimens without weld have exactly the same dimensions.

For the experiments it is essential that the hottest part of the Gleeble meets with the minimum hardness of the HAZ. Because of the fact that the temperature is not uniformly distributed in the test device (Gleeble 3800) and the hardness is not the same in the HAZ, the position of the weld is not located in the middle of the specimen, see Figure 3.5 and 3.6. The literature study showed that the minimum hardness is positioned at 10mm from the center of the weld, see also paragraph 2.3.

Therefore, the weld is placed at 10 mm from the center of the specimen, so that the center of the Gleeble joins with the weakest point of the specimen.

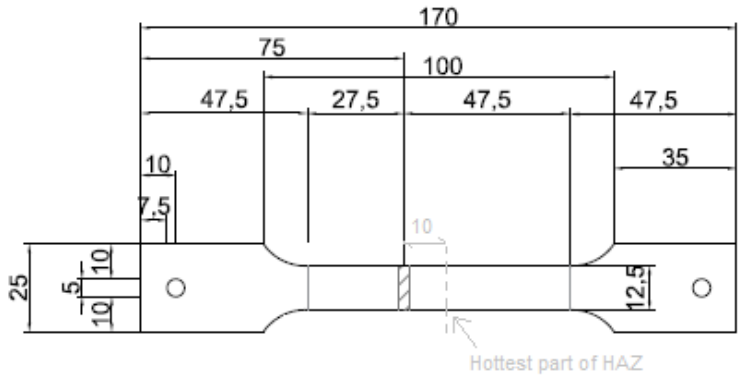

Figure 3.5 Description of the specimen used for creep tests

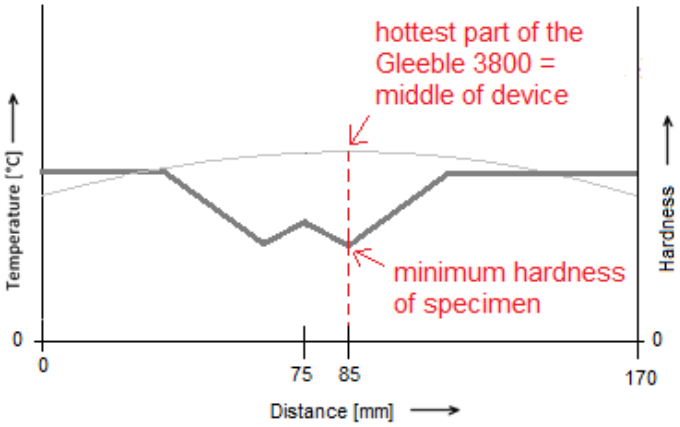

Figure 3.6 Temperature distribution in Gleeble and hardness in specimen

The creep tests have been carried out in a Gleeble 3800 thermo mechanical simulator (dual servo valve) installed with a pocket jaw, see Figure 3.7. The Gleeble contains a furnace under vacuum in order to prevent the clamps and measurement devices from oxidising. Deformations are measured with a hot zone extensometer attached to the sample, see Figure 3.8. The measuring distance applied is 20 mm for (10 mm out of the middle of the specimen at both sides).

Figure 3.7 Test device Gleeble 3800

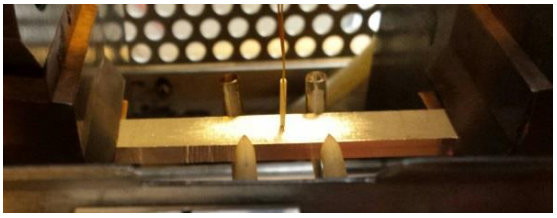

Figure 3.8 Hot zone extensometer attached to a sample

The temperature will be measured with a thermocouple spot-welded at the middle of the specimen, see Figure 3.9. The pit and the heat input introduced by spot-welding are so small that it is expected to have a negligible influence on the results of the creep tests.

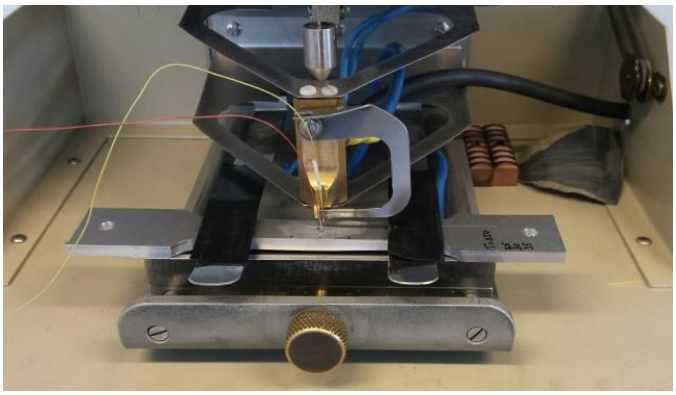

Figure 3.9 Spot welding of a thermocouple at the middle of the specimen

The specimens are heated by induction through the clamps and cooled by water flow. The thermocouple is used to control the induction current.

The load will be applied with a 200 kN actuator and measured with a 200 kN load cell. This capacity is large compared to the loads which will be applied: 1.3 to 9.4 kN. Unfortunately, the setup of the Gleeble is fixed. Therefore there will be worked with these actuator, although small forces will be carried out on the test pieces. The creep specimens will be subjected to a constant load.

The parameters of the Dorn-Harmathy creep model (see equation 3.4 to 3.7) and the model for tertiary creep in [Maljaars et. al, 2008] (see equation 3.8) will be calibrated with creep tests and validated with tensile tests subjects to an increasing temperature and a constant stress in time (so-called transient state conditions).

$$\dot{\varepsilon}_{t,II} = Z \cdot e^{\frac{-Q}{R \cdot T}} \tag{3.4}$$

$$\dot{\varepsilon}_{t,I+II} = \dot{\varepsilon}_{t,II} \cdot \coth^2\left(\frac{\varepsilon_{t,I+II}}{\varepsilon_{t0}}\right) \tag{3.5}$$

$$Z = A \cdot (\sinh(\alpha \cdot \sigma))^n \tag{3.6}$$

$$\varepsilon_{t0} = D \cdot \sigma^m \tag{3.7}$$

$$\dot{\varepsilon}_{t,III} = C \cdot \dot{\varepsilon}_{t,I+II+III} \tag{3.8}$$

Equation (3.8) is only usable if the creep strain rate in the first part of the tertiary creep stage $\dot{\varepsilon}_{t,III}$ will found to be linear proportional to the creep strain $\varepsilon_{t,I+II+III}$, where subscript III indicates the first part of the tertiary creep stage, and I+II+III indicate primary, secondary and the first part of the tertiary creep stage.

Several types of creep tests will be applied. To determine the value for Q, tests with a constant stress in time and a stepwise varied temperature will be carried out. At each step, the secondary strain rate will be determined ($\dot{\varepsilon}_{t,II,1}$ at temperature T_1 and $\dot{\varepsilon}_{t,II,2}$ at temperature T_2). Using equation 3.9, this will result the value for Q.

$$\frac{\dot{\varepsilon}_{t,II,1}}{\dot{\varepsilon}_{t,II,2}} = \frac{e^{\frac{-Q}{R \cdot T_1}}}{e^{\frac{-Q}{R \cdot T_2}}} \quad \rightarrow \quad Q = \frac{R \cdot T_1 \cdot T_2}{T_2 - T_1} \ln\left(\frac{\dot{\varepsilon}_{t,II,2}}{\dot{\varepsilon}_{t,II,1}}\right) \tag{3.9}$$

In a similar way, the Zener Holloman parameter and parameter ε_{t0} will be obtained from tests with a constant temperature and a stepwise varied stress. With aid of curve fitting these parameters will also be known.

The range of loads, temperatures and times at which the creep tests are carried out and the number of creep tests are summarized in Table 3.2.

Table 3.2 Creep test conditions

Type	Stress range (N/mm^2)	Temperature range (°C)	Duration of tests (min)	Duration of each step (min)	Number of tests
Not welded	25 - 175	150 - 350	25 - 55	5 - 30	12
Welded	25 - 125	150 - 340	25 - 55	5 - 20	11

3.3.1 Creep test results of specimens without weld

The mechanical strain in the creep tests is obtained by subtraction of the thermal strain obtained by tests, whereby no stress but only high temperature is applied at the test piece. Data of individual creep tests are given in Annex B.1 and graphs of individual creep tests are given in Annex B.2.

Figure 3.10 gives the resulting secondary strain rate as a function of the reciprocal of the temperature for the creep tests with a constant load and a stepwise varied temperature. The slopes of the lines are parallel, indicating that one value for the activation energy *Q* covers the entire test range. The value for *Q* is determined based on the slopes of the curves and is 197573 J/mol for specimens without a weld. Also (deviating) grey lines can be seen in the figure. These lines indicate that the primary stage was not yet finished, causing an deviating line which is not parallel with the other lines.

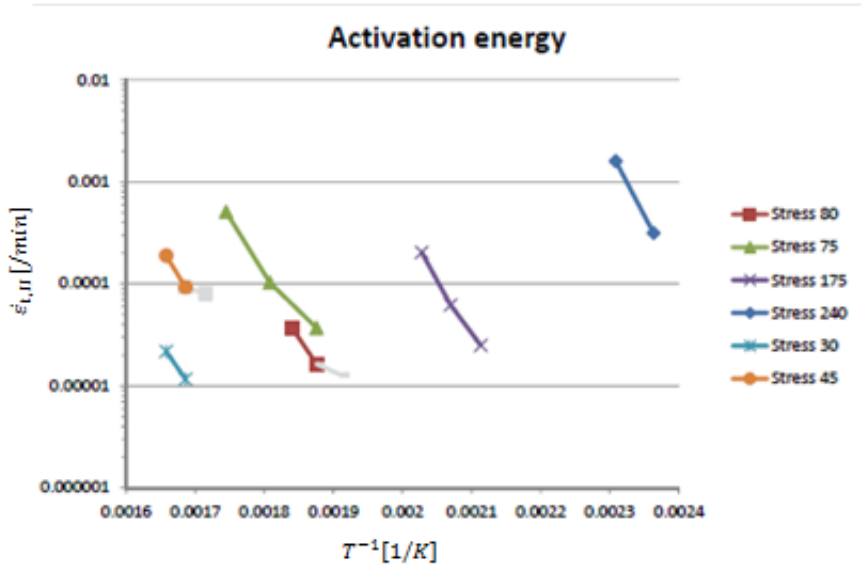

Figure 3.10 Secondary strain rate as a function of the reciprocal of the temperature for alloys without a weld

Using equation (3.4) and the values determined for the activation energy, the Zener-Holloman parameter Z is determined for each creep test. Figure 3.11 gives Z at logarithmic scale as a function of the stress. Equation (3.10) is proposed as a function for Z with Z in [1/min]. This equation is indicated with a green curve in Figure 3.11a. Because there are not much test results between the stress range of 150 – 240 N/mm^2, equation (3.11) is proposed for the function of Z for 25 N/mm^2 < σ < 125 N/mm^2, see Figure 3.11b.

$$Z = 2.1 \cdot 10^{16} \cdot \sinh(9.9 \cdot 10^{-12} \cdot \sigma^{5.07}) \qquad for\ 25\ N/mm^2 < \sigma < 240\ N/mm^2 \qquad (3.10)$$

$$Z = 5.2 \cdot 10^{12} (\sinh(0.028 \cdot \sigma))^3 \qquad for\ 25\ N/mm^2 < \sigma < 120\ N/mm^2 \qquad (3.11)$$

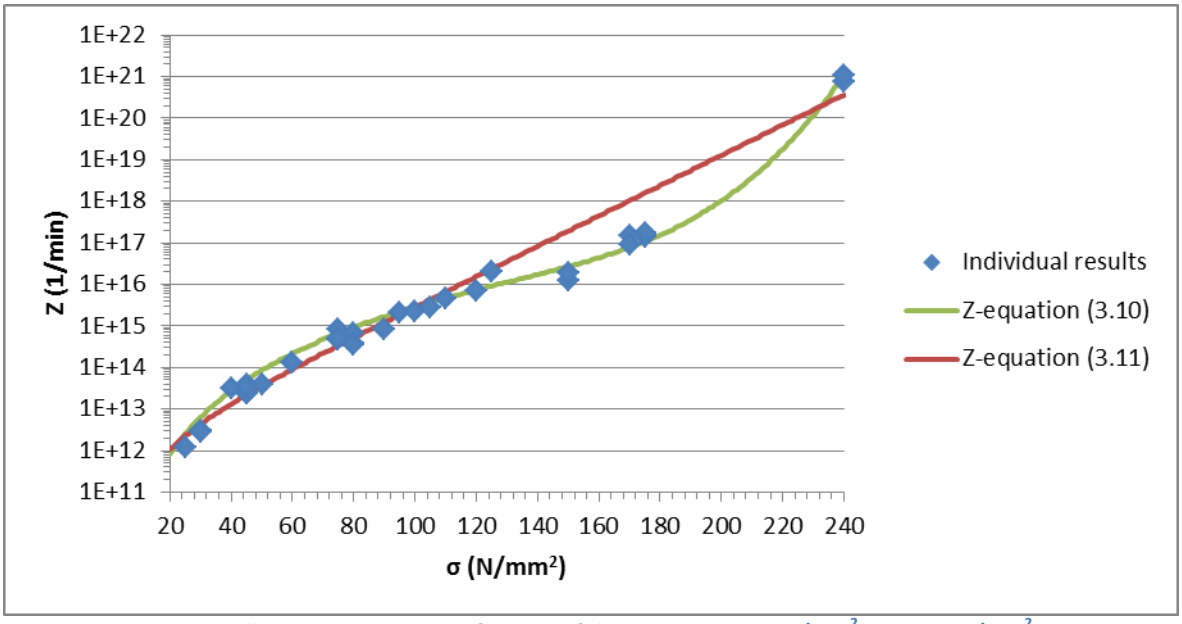

Figure 3.11a Zener-Holloman parameter as a function of the stress range 25 N/mm^2 < σ < 240 N/mm^2

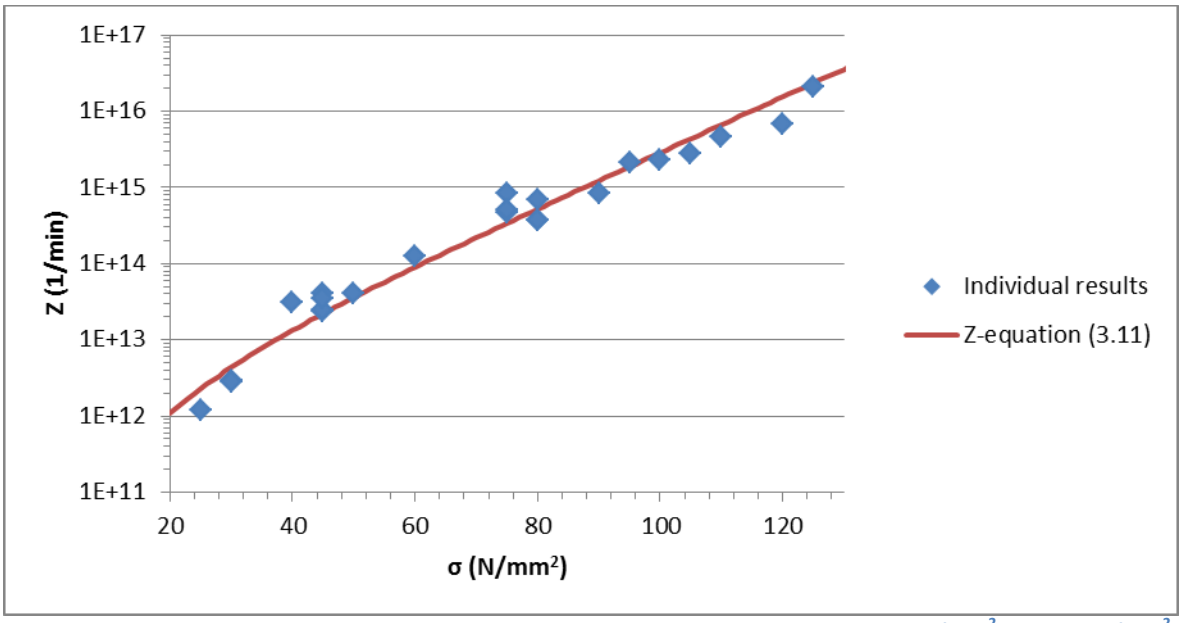

Figure 3.11b Zener-Holloman parameter as a function of the stress for the stress range 25 N/mm^2 < σ < 125 N/mm^2

Also the projection back to zero of each curve, which is data on ε_{t0}, is determined from the outcome of the tests. The individual test data are given with dots in Figure 3.12. the line in Figure 3.12 represents Equation (3.12).

$$\varepsilon_{t0} = 5.59 \cdot 10^{-5} \cdot \sigma^{0.71} \qquad (3.12)$$

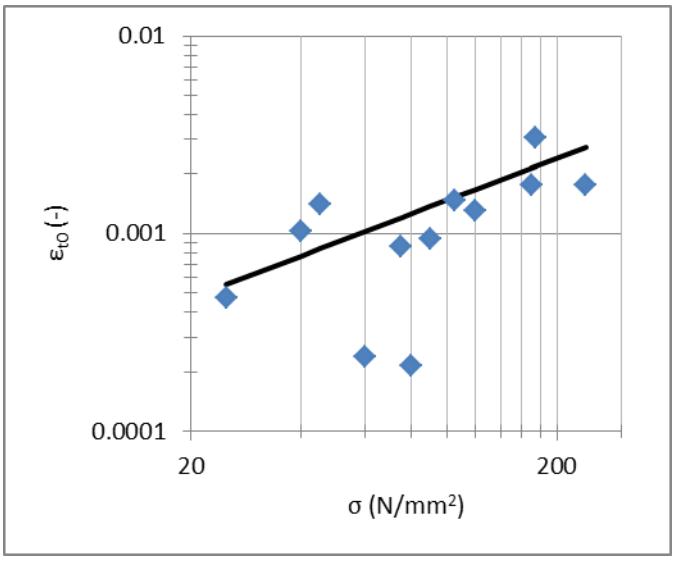

Figure 3.12 Primary creep parameter ε_{t0}

The reduction in area evolution is reflected by the failed samples shown in Figure 3.13. A notable decrease in area can be seen in the temperatures above 280 °C.

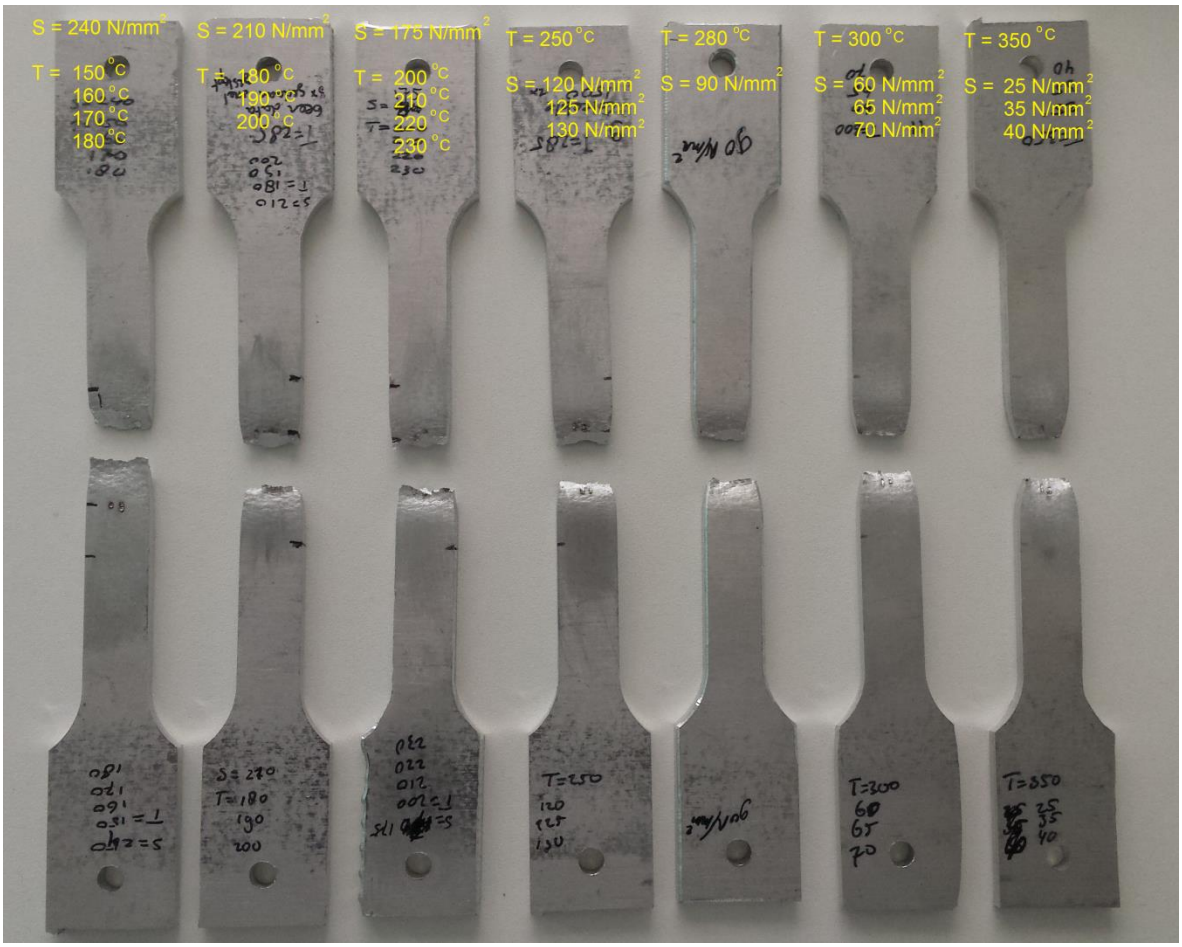

Figure 3.13 Reduction in area evolution of samples without a weld

3.3.2 Creep test results of specimens with weld

Just like the creep test results of the specimens without weld, also for the specimens with weld, the mechanical strain in the creep tests is obtained by subtraction of the thermal strain obtained by tests, whereby no stress but only high temperature is applied at the test piece. Data of individual creep tests are given in Annex B.1 and graphs of individual creep tests are given in Annex B.3.

As mentioned before, the creep tests of the welded specimens are executed with a measuring distance of the LVDT of 30 mm. When measuring distance of 20mm was chosen for the welded specimens, the LVDT slipped for some of the specimens, resulting in unusable measurement data, see Figure 3.14. Probably this was the case, because the specimen broke at the point where the LVDT touched the specimen. As the test piece was necking, slip caused dips in the test results. So the parameters of the creep curve are found with the test results which belongs to the specimens with a measuring distance of 30 mm. For specimens without a weld a measuring distance of 20 mm was applied.

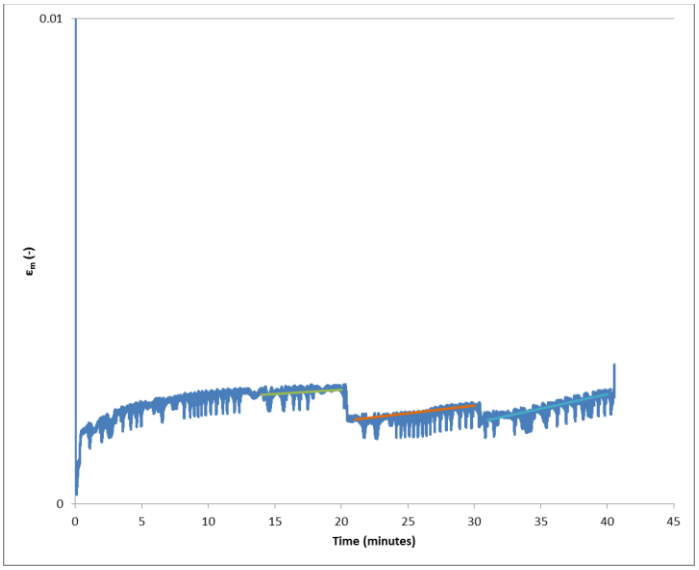

Figure 3.14 Creep test result of a specimen with weld with a constant stress of 40 N/mm^2 and a measuring distance of LVDT of 20 mm.

Figure 3.15 gives the resulting secondary strain rate as a function of the reciprocal of the temperature for the creep tests with a constant load and a stepwise varied temperature. The slopes of the lines are parallel, indicating that one value for the activation energy *Q* covers the entire test range. The value for *Q* is determined based on the slopes of the curves and is 142862 J/mol for specimens with a weld. Also (deviating) grey lines can be seen in the figure. These lines indicate that the primary stage was not yet finished, causing an deviating line which is not parallel with the other lines.

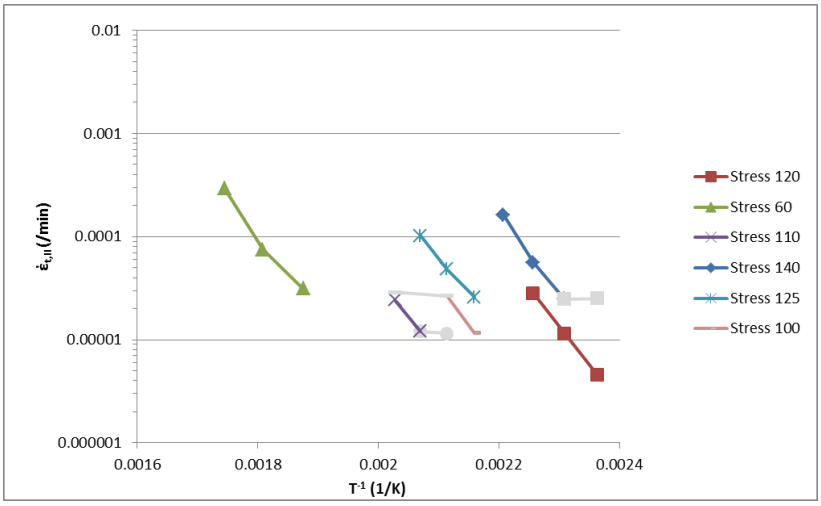

Figure 3.15 Secondary strain rate as a function of the reciprocal of the temperature for alloys with a weld

Using equation (3.4) and the values determined for the activation energy, the Zener-Holloman parameter Z is determined for each creep test. Figure 3.16 gives Z at logarithmic scale as a function of the stress. Equation (3.13) is proposed as a function for Z with Z in [1/min]. This equation is indicated with a curve in Figure 3.16.

$$Z = 1.5 \cdot 10^{8} (\sinh(0.028 \cdot \sigma))^{2.9} \tag{3.13}$$

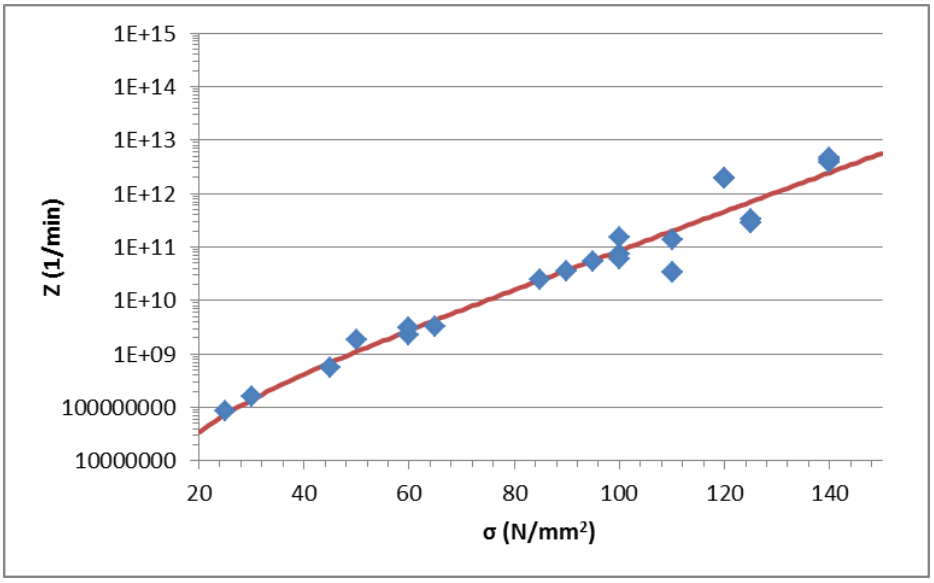

Figure 3.16 Zener-Holloman parameter as a function of the stress

Also the projection back to zero of each curve, which is data on ε_{t0}, is determined from the outcome of the tests. The individual test data are given with dots in Figure 3.17. The line in Figure 3.17 represents Equation (3.14).

$$\varepsilon_{t0} = 1.5 \cdot 10^{-6} \cdot \sigma^{1.8} \tag{3.14}$$

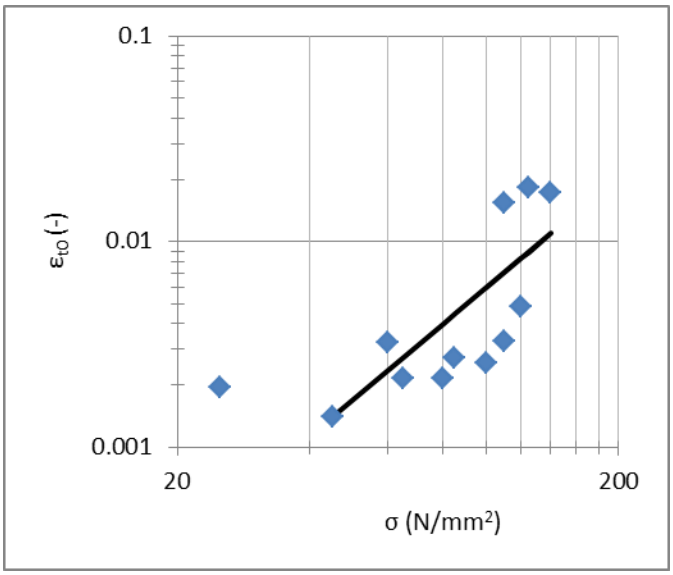

Figure 3.17 Primary creep parameter ε_{t0}

The reduction in area evolution is reflected by the failed samples shown in Figure 3.18. A notable decrease in area can be seen in the temperatures above 300 °C. As expected It can also be noticed that the specimens are broken at the hottest location of the HAZ.

Figure 3.18 Reduction in area evolution of samples with a weld

3.3.3 Creep test results of 6060-T66 and 5083-H111 alloys in [Maljaars, 2008]

Because the results of the different aluminum alloys will be compared with each other, the results of the alloys 6060-T66 and 5083-H111, which are discussed in [Maljaars, 2008], are shown in this section. For the tests on alloy 6060-T66 two batches are used, denoted as batch '05 and batch '06.

Figure 3.19 gives the resulting secondary strain rate as a function of the reciprocal of the temperature for the creep tests with a constant load and a stepwise varied temperature. The values for Q are determined based on the slopes of the curves and are 15000 J/mol for alloy 5083-H111 ($20 < \sigma < 110$ N/mm^2) and 195000 J/mol for alloy 6060-T66 ($30 < \sigma < 150$ N/mm^2 for both batches).

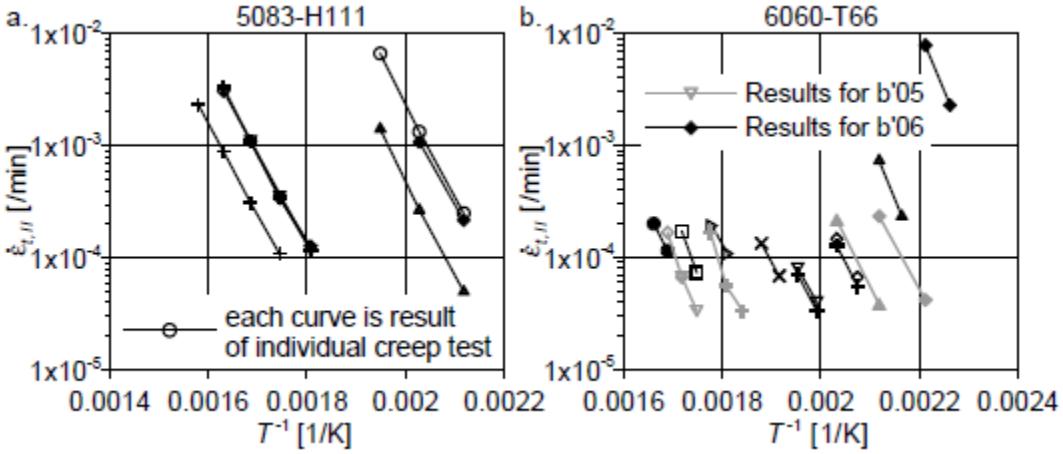

Figure 3.19 Secondary strain rate as a function of the reciprocal of the temperature (a. Alloy 5083-H111; b. Alloy 6060-T66)

Also the Zener-Holloman parameter Z is determined for each creep test. Figure 3.20 gives Z at logarithmic scale as a function of the stress. The test results for alloy 6060-T66 b'05 and b'06 are different. Equations (3.15), (3.16) and (3.17) are proposed by Maljaars for alloys 5083-H111, 6060-T66 b'05 and 6060-T66 b'06, respectively as a function for Z with Z in [1/min]. The equation are indicated with curves in Figure 3.20.

$$Z = 6.7 \cdot 10^{10} (\sinh(0.025 \cdot \sigma))^3 \qquad for\ 20\ N/mm^2 < \sigma < 120\ N/mm^2 \qquad (3.15)$$

$$Z = 7.0 \cdot 10^{12} (\sinh(0.04 \cdot \sigma))^3 \qquad for\ 30\ N/mm^2 < \sigma < 150\ N/mm^2 \qquad (3.16)$$

$$Z = 2.0 \cdot 10^{14} (\sinh(0.019 \cdot \sigma))^4 \qquad for\ 25\ N/mm^2 < \sigma < 120\ N/mm^2 \qquad (3.17)$$

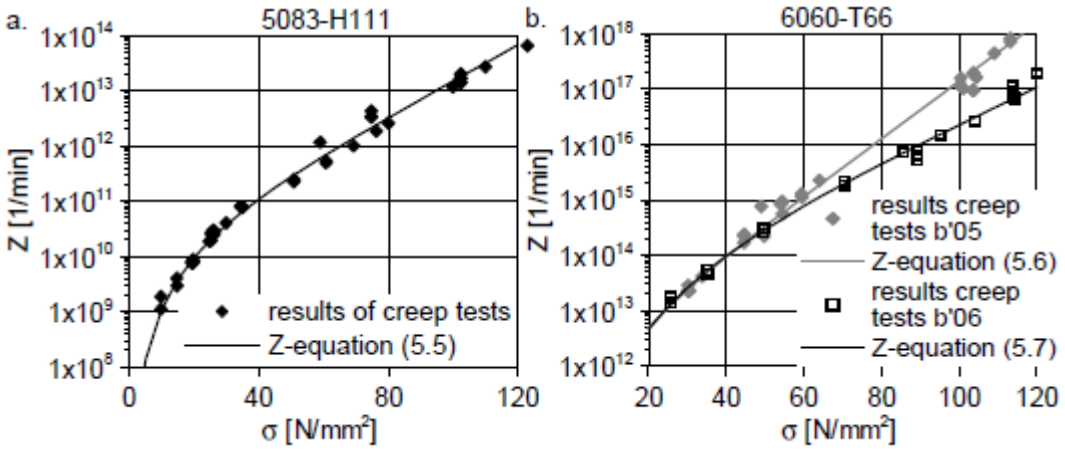

Figure 3.20 Zener-Holloman parameters as a function of the stress (a. Alloy 5083-H111; b. Alloy 6060-T66)

Also the projection back to zero of each curve, which is data on ε_{t0}, is determined by Maljaars from the outcome of the tests. Due to slip between the clamps of the extensometer and the specimen at the start of loading, the projection back to zero time of the secondary strain curve was not accurately determined in case of alloys 5083-H111 and 6060-T66 b'05. Instead data of ε_{t0} found in literature were used in the model. The individual test data are given with dots in Figure 3.21. the lines in Figure 3.21 represents Equation (3.18) and (3.19) for alloys 5083-H111 and 6060-T66, respectively.

$$\varepsilon_{t0} = 4 \cdot 10^{-10} \cdot \sigma^{3.4} \tag{3.18}$$

$$\varepsilon_{t0} = 2 \cdot 10^{-18} \cdot \sigma^{7.45} \tag{3.19}$$

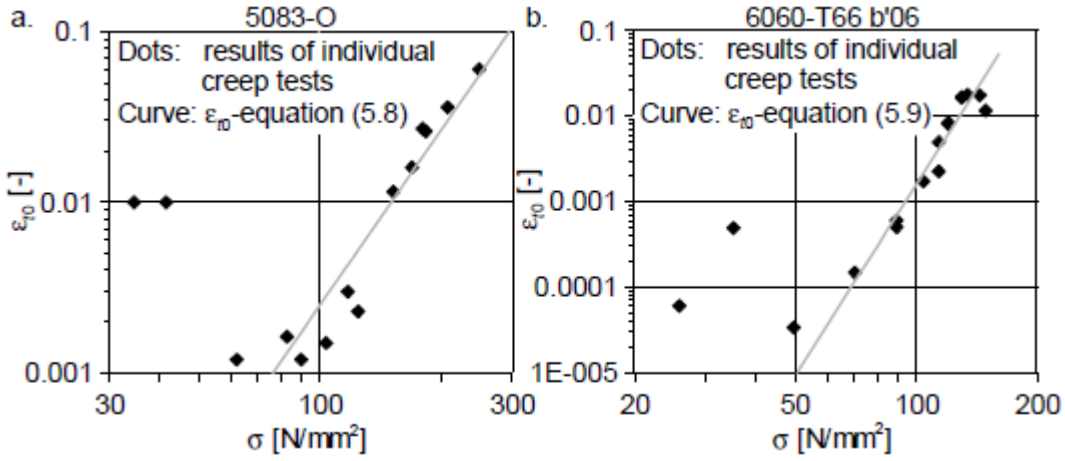

Figure 3.21 Primary creep parameter ε_{t0} (a. Data on alloy 5083-O according to literature; b. Data on alloy 6060-T66 b'06)

3.4 Discussion of the creep test results

Table 3.3 gives an overview of all material parameters determined in the creep tests and which have to be applied in equations (3.4) – (3.7).

The average value for all tests of the ratio between the simulated secondary creep strain rate according to the model and the measured secondary creep strain rate $\dot{\varepsilon}_{t,II,model}/\dot{\varepsilon}_{t,II,test}$ is equal to 1.0. The average value for all tests of the ratio between the simulated value for ε_{t0} according to the model and the measured ε_{t0} value, $\varepsilon_{t0,model}/\varepsilon_{t0,test}$, is equal to 0.9 for not welded specimens and 1.5 for welded specimens. This difference in the value of ε_{t0} can be attributed to the found scatter in the test results.

Table 3.3 Material dependent parameters in equations (3.1) – (2.8)

Parameter	Alloy 6082-T6 not welded	Alloy 6082-T6 welded	Alloy 5083-H111	6060-T66 b'05	6060-T66 b'06
Q (J/mol)	$1{,}98 \cdot 10^{5}$	$1.43 \cdot 10^{5}$	$1.52 \cdot 10^{5}$	$1.95 \cdot 10^{5}$	$1.95 \cdot 10^{5}$
A (/min)	$5.2 \cdot 10^{12}$	$1.5 \cdot 10^{8}$	$6.7 \cdot 10^{10}$	$7.0 \cdot 10^{12}$	$2.0 \cdot 10^{14}$
α	$2.8 \cdot 10^{-2}$	$2.8 \cdot 10^{-2}$	$2.5 \cdot 10^{-2}$	$4.0 \cdot 10^{-2}$	$1.9 \cdot 10^{-2}$
n	3.0	1.8	3.0	3.0	3.0
D	$5.59 \cdot 10^{-5}$	$1.5 \cdot 10^{-6}$	$4.0 \cdot 10^{-10}$	$2.0 \cdot 10^{-18}$	$2.0 \cdot 10^{-18}$
m	0.71	2.9	3.40	7.45	7.45

The parameters of the Zener Holloman equation and the primary creep equation are determined with curve fit.

It can be seen that the activation energy of not welded alloy 6082-T6 and alloy 6060-T66 are reasonably close on each other. Also the activation energy of the welded specimens of alloy 6082-T6 and alloy 5083-H111 are reasonably close on each other. The value for Q is equal for the entire stress range investigated, indicating that one creep process is dominant in this entire stress range. The standard deviations of the tested activation energy of both types (welded and not welded) are given in Table 3.4.

Table 3.3 Standard deviations of the activation energy of not welded and welded specimens.

Type of specimen	Not welded	Welded
Standard deviation	0.16	0.18

The tertiary creep stage with increasing strain rate started after a relatively short period and after a small creep strain for specimens without a weld. A linear relation between the creep strain rate and the creep strain in the tertiary creep stage was found, at least for strains up to approximately 1.5%, see Figure 3.22. This relation is present in all tests with a tertiary stage (see Annex C.1 for some of the results).

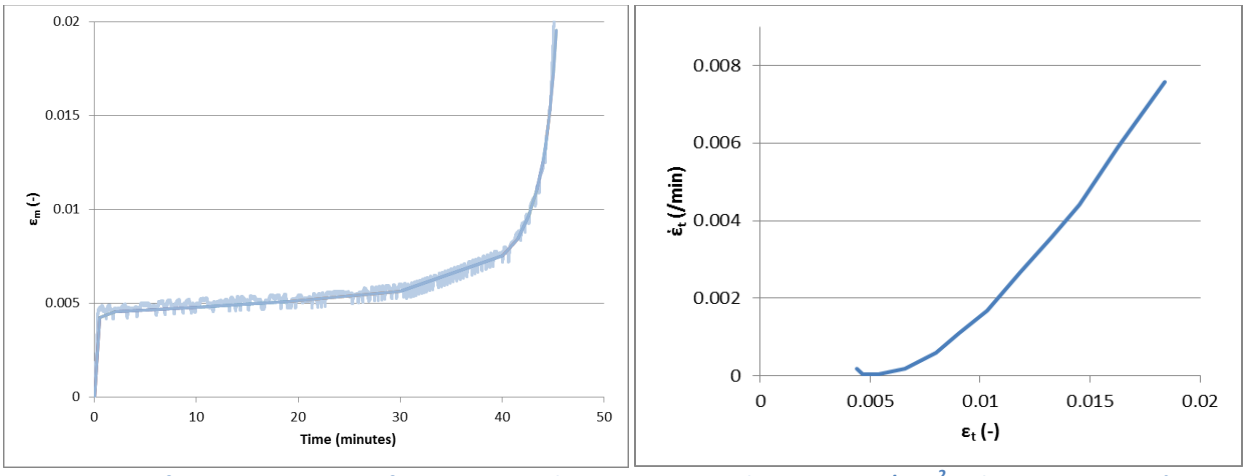

Figure 3.22 Left: Strain versus time of a creep test with tertiary creep with stress 175 N/mm^2 and temperature 200°C, 210°C and 220°C on specimen without weld. Right: Strain rate as function of strain.

Also for the welded specimens, the tertiary creep stage with increasing strain rate started after a relatively short period and after a small creep strain. A linear relation between the creep strain rate and the creep strain in the tertiary creep stage has also been found for welded specimens, at least for strains up to approximately 1.5%, see Figure 3.23. This relation is present in all tests with a tertiary stage (see Annex C.2 for some of the results)..

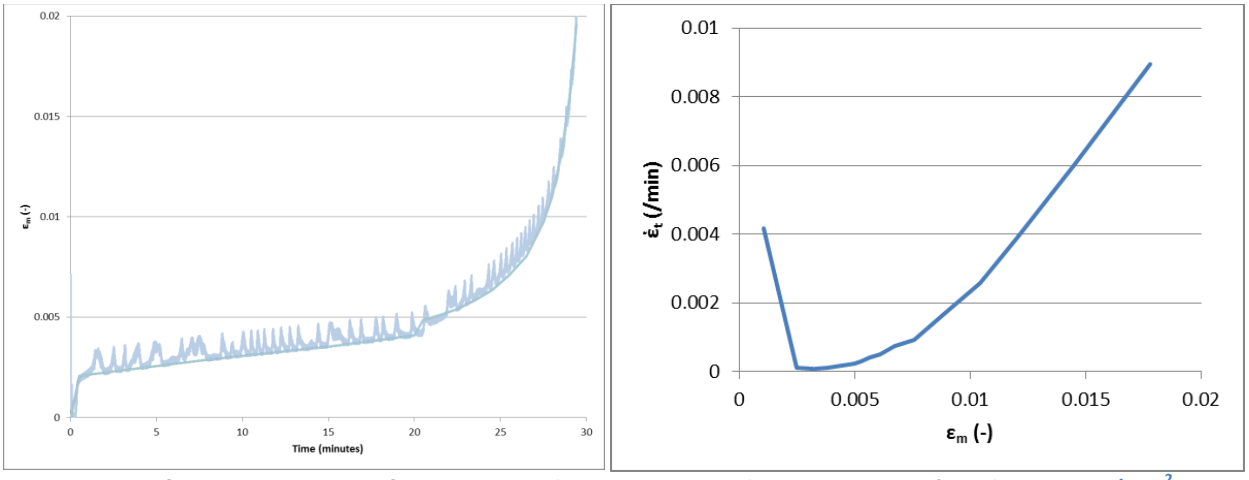

Figure 3.23 Left: Strain versus time of a creep test with tertiary creep with temperature 280°C and stress 65 N/mm^2, 70 N/mm^2, 75 N/mm^2 on welded specimen. Right: Strain rate as function of strain.

Also alloy 6060-T66, which is investigated in [Maljaars, 2008], a linear relation exists between the creep strain rate and creep strain in the tertiary creep stage. Experiments with different gauge lengths of the LVDT showed that the tertiary creep strain development in time appeared to be independent of the gauge length of the LVDT. Unfortunately, there are no test results with different gauge lengths for alloy 6082-T6.

3.5 Model validation with transient state tests

The total strain at a certain time, according to the constitutive model, is equal to the summation of the thermal strain, the elastic strain and the creep strain rate integrated over time, see Equation (3.20).

$$\varepsilon = \varepsilon_{th} + \varepsilon_{el} + \varepsilon_t = \int_0^t \alpha_{th}\dot{T}\,dt + \frac{\sigma}{E_\theta} + \int_0^t \dot{\varepsilon}_t\,dt \tag{3.20}$$

Uniaxial transient state tests are carried out to validate the constitutive model for fire conditions. The same test set-up and type of specimens are used as for the creep tests. The ranges of loads and heating rates applied in the transient state tests and the number of tests are summarized in Table 3.3. In all of the tests the stress level is constant during the tests.

Table 3.3 Transient state test conditions

Type	Stress range (N/mm^2)	Heating rates (°C/min)	Number of tests
Not welded	40 - 125	2.9 to 11.7	4
Welded	40 -100	1.9 to 11.0	4

The creep strain rate in the first part of the tertiary creep stage $\dot{\varepsilon}_{t,III}$ is found to be linear proportional to the creep strain $\varepsilon_{t,I+II+III}$. This means that Equation (3.8) can be used for the validation of the experiments. The creep strain at the start of the tertiary stage is denoted with symbol ε_{lim}. The constitutive model including the first part of the tertiary creep is described with Equation (3.21).

$$\varepsilon_{t,I+II+III} \leq \varepsilon_{lim}: \quad \varepsilon = \frac{\sigma}{E} + \int_0^t \dot{\varepsilon}_{t,I+II}\,dt \tag{3.21 a}$$

$$\varepsilon_{t,I+II+III} \geq \varepsilon_{lim}: \quad \varepsilon = \frac{\sigma}{E} + \int_0^t \dot{\varepsilon}_{t,I+II} \, \frac{\varepsilon_{t,I+II+III}}{\varepsilon_{lim}} \, dt \tag{3.21 b}$$

The start of the tertiary stage ε_{lim} varied between the creep tests. The parameter is temperature and stress dependent. The average value of the creep tests is used as ε_{lim}. The average value of ε_{lim} for the not welded specimens is $\varepsilon_{lim} = 0.0045$ and for specimens with a weld $\varepsilon_{lim} = 0.0085$.

3.5.1 Transient state test results of specimens without weld

The simulation results of the transient state tests carried out with the model in Equation (3.20), using the modified creep model are simulated. Figure 3.24a shows the result of the transient state test with a constant stress of 40 N/mm^2 and a constant heating rate of 2.9 °C/min and 11.7 °C/min. The test results are the blue and purple lines and the simulations are the green and red lines. It can be seen that the strain at begin differs between the experiments and the simulations. Slip in the Gleeble or the LVDT can be the reason for this. To eliminate these faults, the graphs are shifted, see Figure 3.24b. Also the individual results of the transient state tests with a heating rate of 2.9 (°C/min) and 11.7 (°C/min) can be seen in Figures 3.24c and 3.24d respectively.

Figure 3.25a shows the result of the transient state test with a constant stress of 100 N/mm^2 and a constant heating rate of 9 °C/min, where the blue line indicates the test and the red line indicates the simulation. Also here the graph of the test result is shifted to eliminate the fault of the test devices, see Figure 3.25b.

Figure 3.26 shows the result of the transient state test with a constant stress of 125 N/mm^2 and a constant heating rate of 8 °C/min where the blue line indicates the test and the red line indicates the simulation.

The curves in the Figures show a small strain increase up to approximately 50-75°C before failure, which is followed by an accelerated increase of the strain.

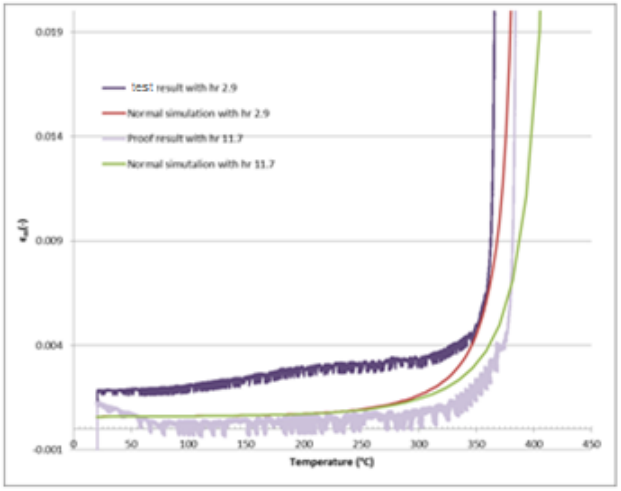

Figure 3.24a Strain as function of temperature of transient state tests with a constant stress of 40 N/mm^2 and simulations with heating rate 2.9 °C/min and 11.7 °C/min

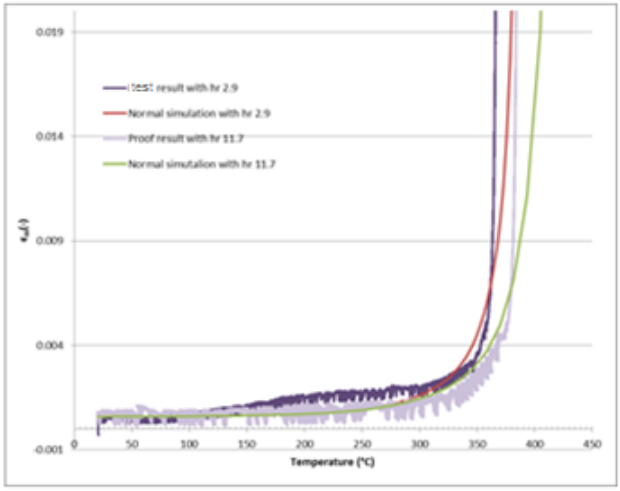

Figure 3.24b Shifted strain as function of temperature of transient state tests with a constant stress of 40 N/mm^2 and simulations with heating rate 2.9 °C/min and 11.7 °C/min

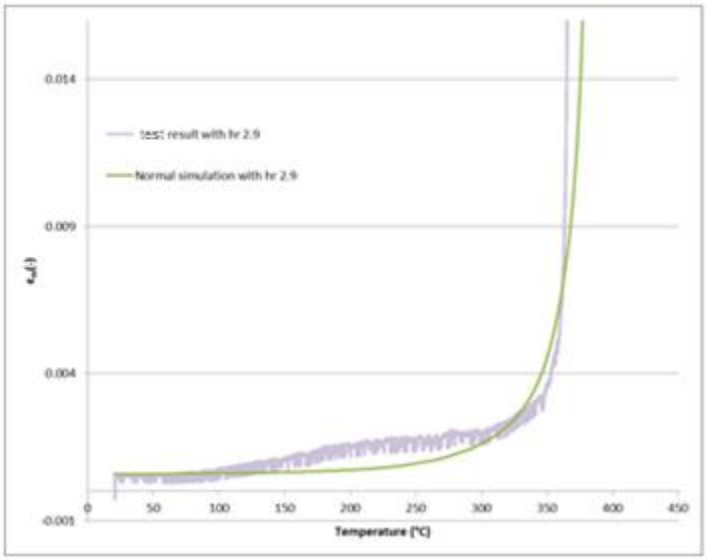

Figure 3.24c Shifted strain as function of temperature of transient state tests with a constant stress of 40 N/mm^2 and simulations with heating rate of 2.9 °C/min

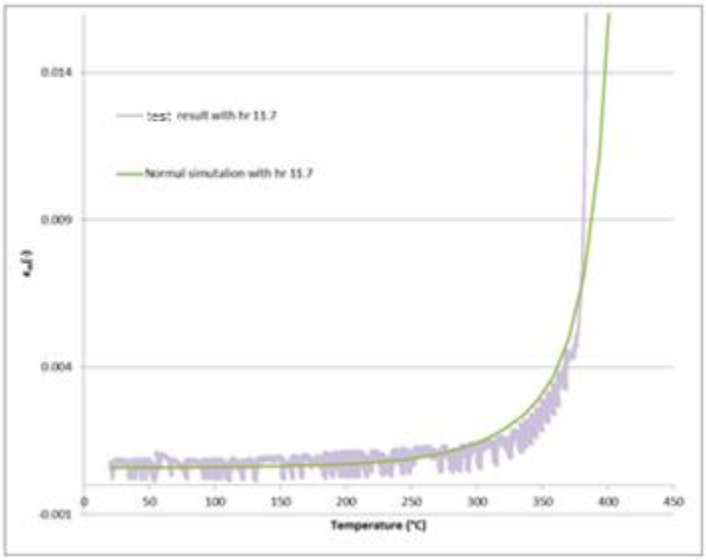

Figure 3.24d Shifted strain as function of temperature of transient state tests with a constant stress of 40 N/mm^2 and simulations with heating rate of 11.7 °C/min

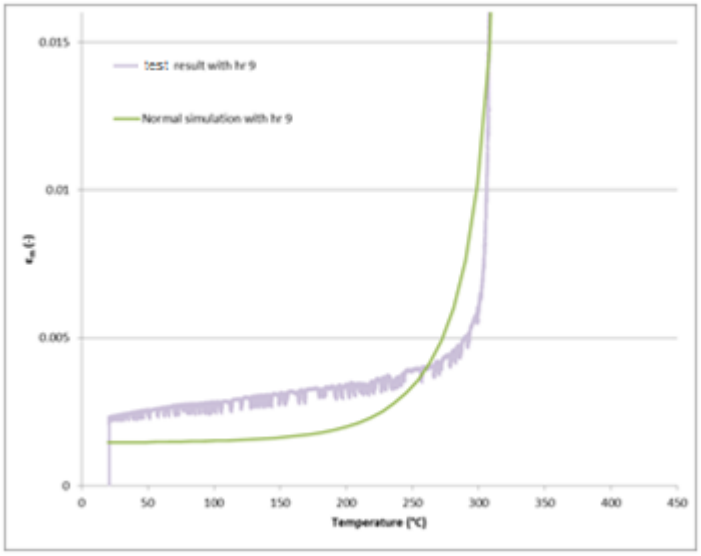

Figure 3.25a Strain as function of temperature of transient state test with a constant stress of 100 N/mm^2 and simulations with heating rate of 9 °C/min

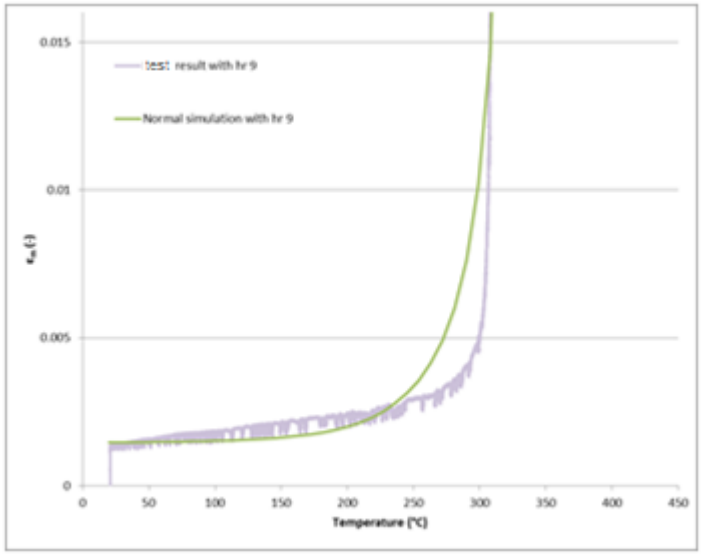

Figure 3.25b Shifted strain as function of temperature of transient state test with a constant stress of 100 N/mm^2 and simulations with heating rate of 9 °C/min

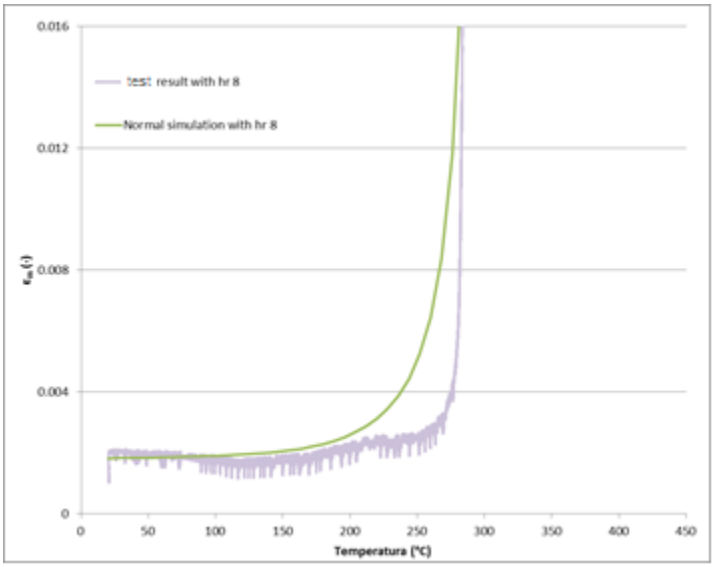

Figure 3.26 Strain as function of temperature of transient state test with a constant stress of 125 N/mm^2 and simulations with heating rate of 8 °C/min

3.5.2 Transient state test results of specimens with weld

Figure 3.27a shows the result of the transient state test with a constant stress of 100 N/mm^2 and a constant heating rate of 7.6 °C/min. The test results are the blue and purple lines and the simulation is the red line. Also in this experiment, it can be seen that the strain at begin differs between the experiments and the simulations. To eliminate this difference, the graphs are shifted, see Figure 3.27b.

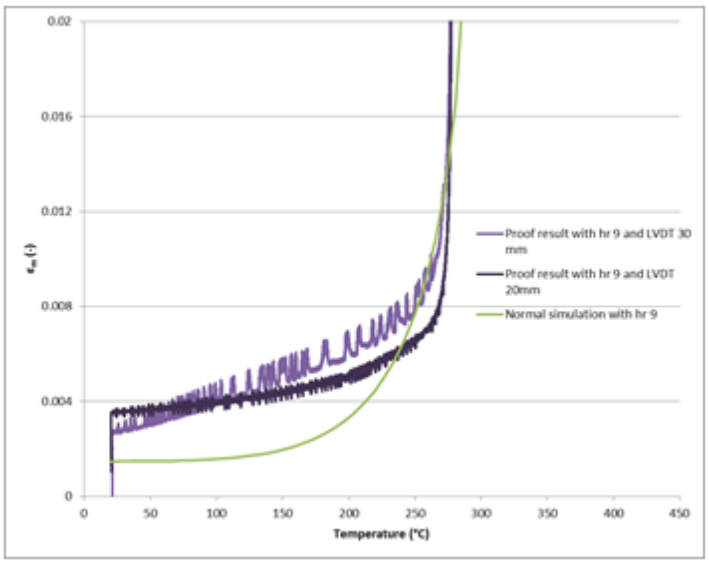

Figure 3.25a Strain as function of temperature of transient state test with a constant stress of 100 N/mm^2 and simulations with heating rate of 7.6 °C/min with LVDT distance of 20mm and 30mm.

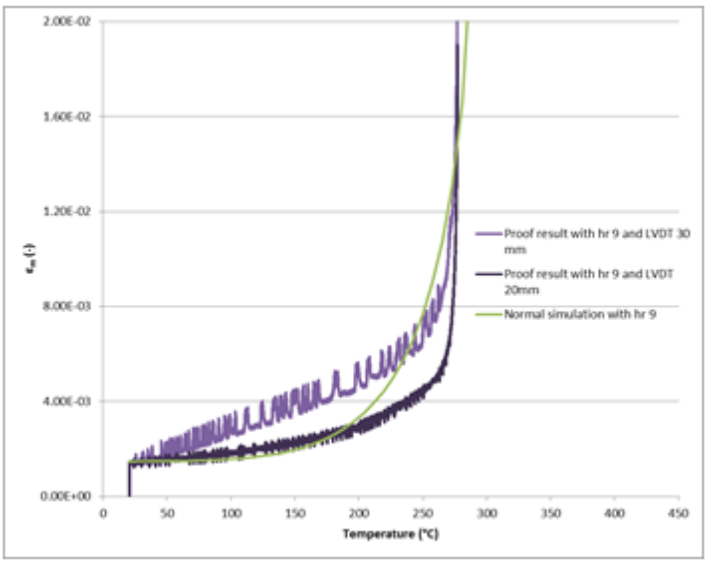

Figure 3.25b Shifted strain as function of temperature of transient state test with a constant stress of 100 N/mm^2 and simulations with heating rate of 7.6 °C/min with LVDT distance of 20mm and 30mm.

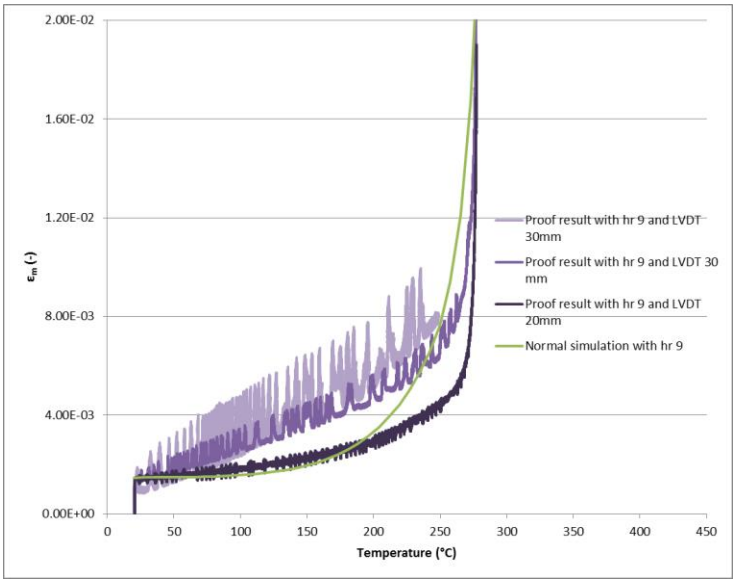

Figure 3.27c Strain as function of temperature of transient state test with a constant stress of 100 N/mm^2 and simulations with heating rate of 7.6 °C/min with LVDT distance of 20mm and two times 30mm.

The transient state test with a constant stress of 100 N/mm^2 and a heating rate of 7.6 °C/min has been performed two times with different measuring distances. The purple line in Figure 3.27 belongs to the test data with a measuring distance of the LVDT of 30 mm and the blue line belongs to the test data with a measuring distance of the LVDT of 20 mm. As discussed in section 3.2.2, the creep test data of the welded specimens are found with results which belong to a measuring distance of the LVDT of 30 mm. So the transient state simulation (red line in Figure 3.27) is simulated with the data which belongs to the measuring distance of 30 mm. In contrast to this, it is remarkable that the blue line, which belongs to the 20 mm measuring distance data, is more in line with the simulation (which is calculated with de data of the creep parameters with a measuring distance of 30 mm). Figure 3.27c shows an additional green curve, which is also an measurement with an LVDT distance of 30mm. Because the thermocouples detached during the execution of the experiment, this curve is not finished and is executed twice. So the green and the purple lines are both measurements with an LVDT distance of 30mm, it can be seen that the green curve is quit in line with the purple curve. Also, it is remarkable that creep starts already at 20°C, while it is shown in literature that creep has a large influence after temperatures of 150°C. Most probably slip ensured for this difference. If the rapid increase in creep at the start of the purple curve is taking out of consideration, it is seen that the purple curve and the blue curve are largely in line.

It is assumed that there are no large differences between the measurements of the experiments with an LVDT distance of 20 mm and LVDT distance of 30 mm. In the sequel, the transient state tests of the welded specimens are performed with an LVDT distance of 20 mm. This is done so, so to compare the results of the experiments with each other, because the not welded specimens are also performed with an LVDT distance of 20 mm. Also it is seen in the Eurocode that the HAZ has a size of 20 mm at both sides of the weld. When the transient state tests will be carried out with an LVDT distance of 20 mm, we will have the results of the transient state tests in which only the HAZ is considered.

Figure 3.28a shows the result of the transient state test with a constant stress of 60 N/mm^2 and a constant heating rate of 9.3 °C/min. Also here the graph of the test result is shifted to eliminate the fault of the test devices, see Figure 3.28b.

Figure 3.29a shows the result of the transient state test with a constant stress of 40 N/mm^2 and a constant heating rate of 2.7 °C/min and 11.3 °C/min. The test results are the green and blue lines and the simulations are the purple and red lines. The graphs are shifted in Figure 3.29b. Also the individual results of the transient state tests with a heating rate of 11.3°C/min and 2.7°C/min can be seen in Figures 3.29c and 3.29d respectively.

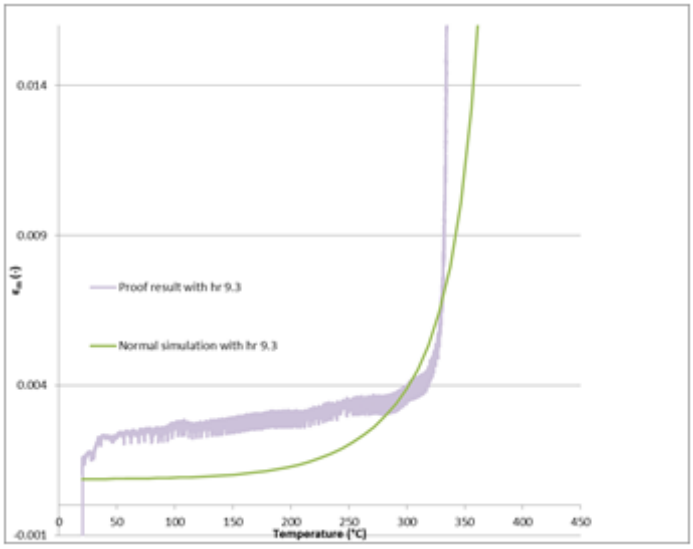

Figure 3.28a Strain as function of temperature of transient state test with a constant stress of 60 N/mm^2 and simulations with heating rate of 9.3 °C/min.

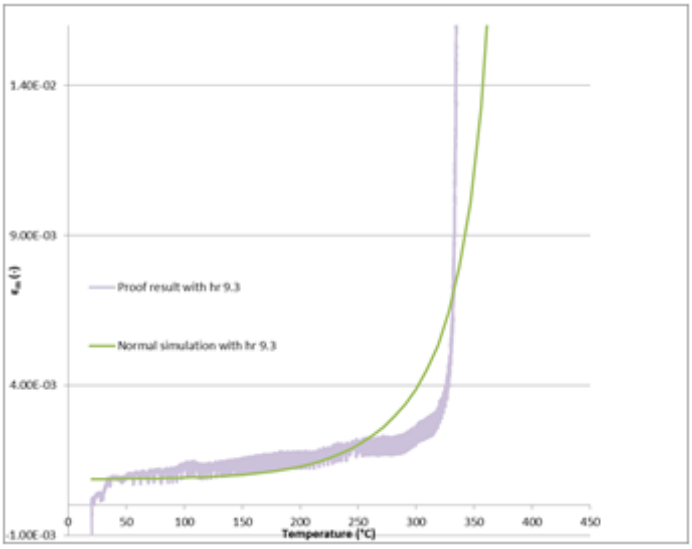

Figure 3.28b Shifted strain as function of temperature of transient state test with a constant stress of 60 N/mm^2 and simulations with heating rate of 9.3 °C/min.

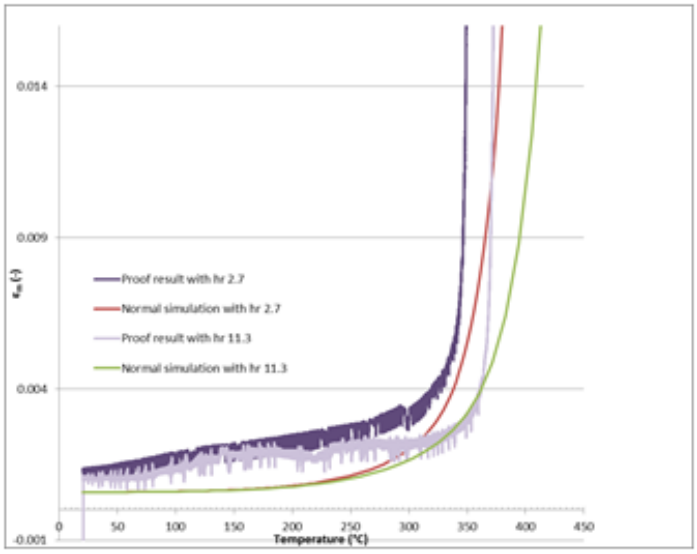

Figure 3.29a Strain as function of temperature of transient state tests with a constant stress of 40 N/mm^2 and simulations with heating rate 2.7 °C/min and 11.3 °C/min

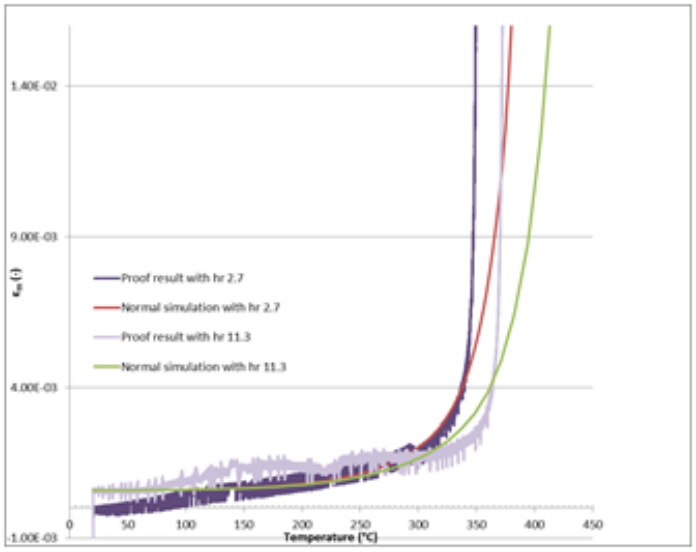

Figure 3.29b Shifted strain as function of temperature of transient state tests with a constant stress of 40 N/mm^2 and simulations with heating rate 2.7 °C/min and 11.3 °C/min.

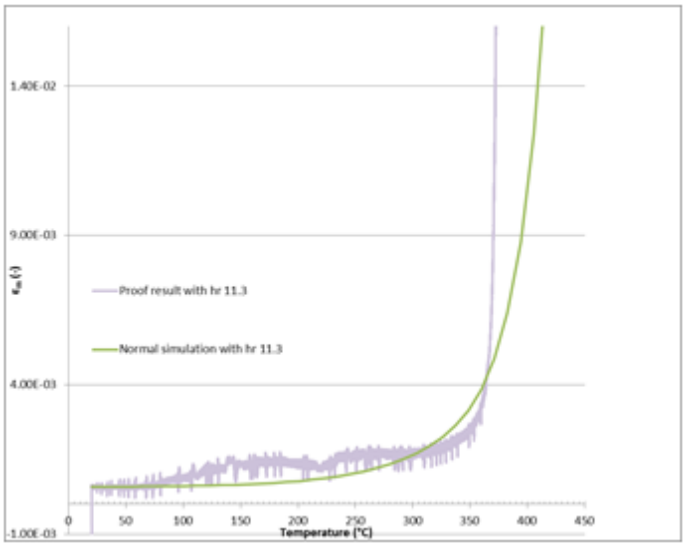

Figure 3.29c Shifted strain as function of temperature of transient state tests with a constant stress of 40 N/mm^2 and simulations with heating rate of 11.3 °C/min

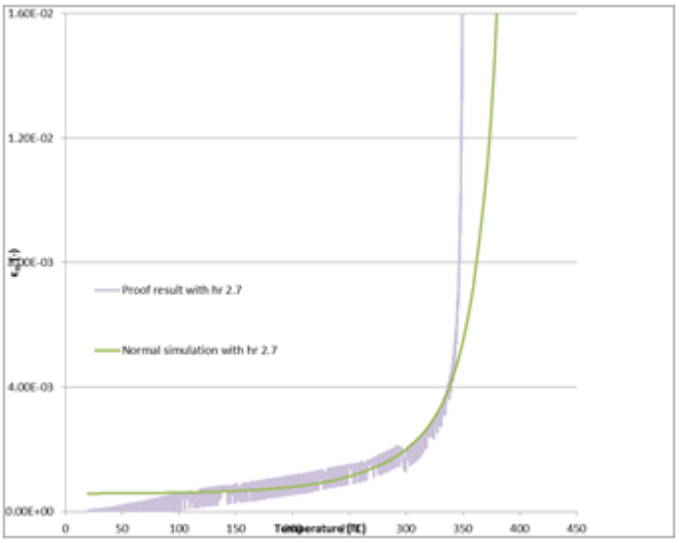

Figure 3.29d Shifted strain as function of temperature of transient state tests with a constant stress of 40 N/mm^2 and simulations with heating rate of 2.7 °C/min

3.5.3 Transient state test results of 6060-T66 and 5083-H111 alloys in [Maljaars, 2008]

Also here, for the reason of comparison, the transient state test results of the alloys 6060-T66 and 5083-H111, which are discussed in [Maljaars, 2008], are shown in this section.

Figure 3.30, Figure 3.31 and Figure 3.32 show the results of the transient state tests with constant heating rate and a constant stress on alloy 5083-H111, 6060-T66 b´05 and 6060-T66 b'06, respectively. The test results are indicated with black curves and the simulations are indicated with grey curves.

The curves in the figures show a small strain increase up to approximately 50 °C before failure. This is followed by an exponential increase of the strain.

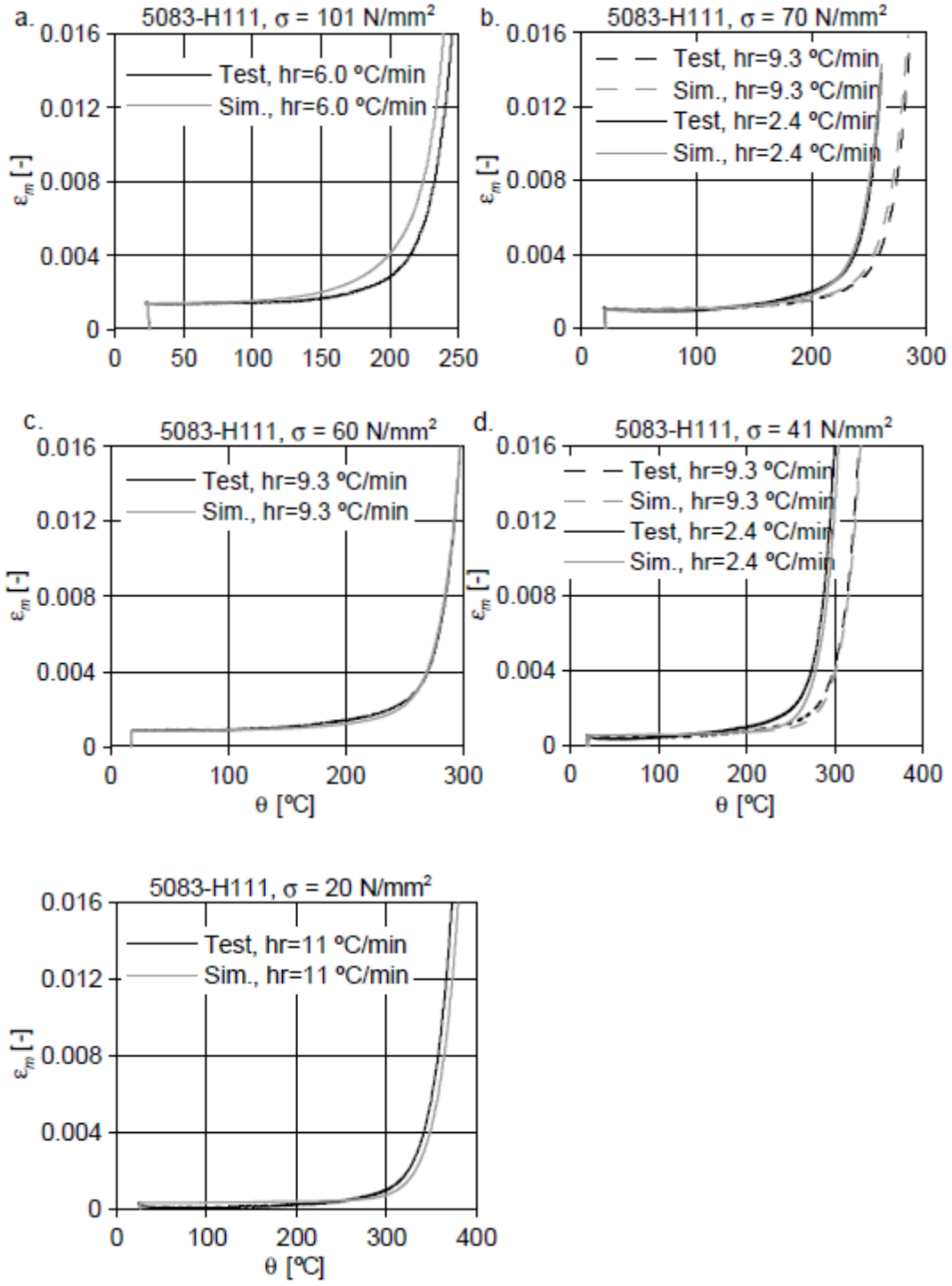

Figure 3.30 Strain as function of temperature of transient state tests and simulations on alloy 5083-H111 (a. Constant stress of 101 N/mm^2; b. Constant stress of 70 N/mm^2; c. Constant stress of 60 N/mm^2; d. Constant stress of 41 N/mm^2); e. Constant stress of 20 N/mm^2.

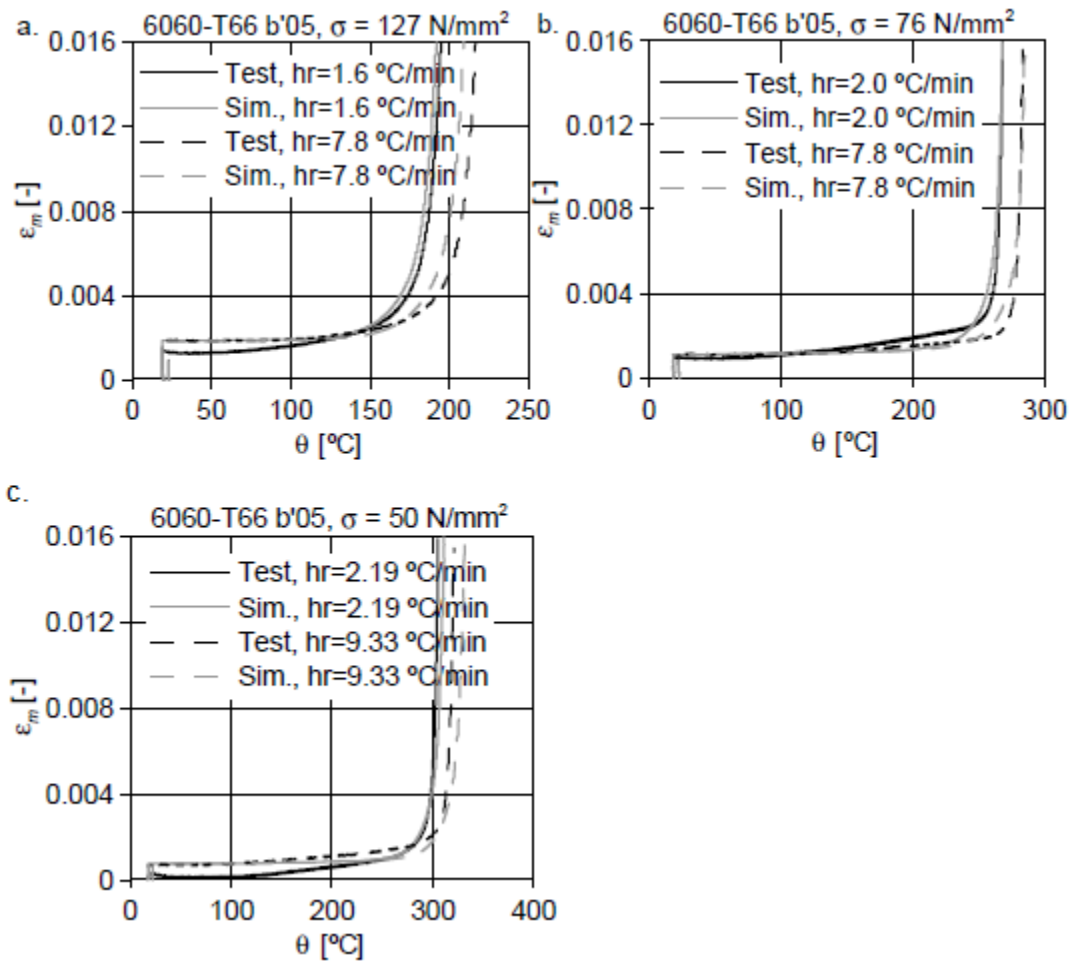

Figure 3.31 Strain as function of temperature of transient state tests and simulations on alloy 6060-T66 b´05 (a. Constant stress of 127 N/mm^2; b. Constant stress of 76 N/mm^2; c. Constant stress of 50 N/mm^2)

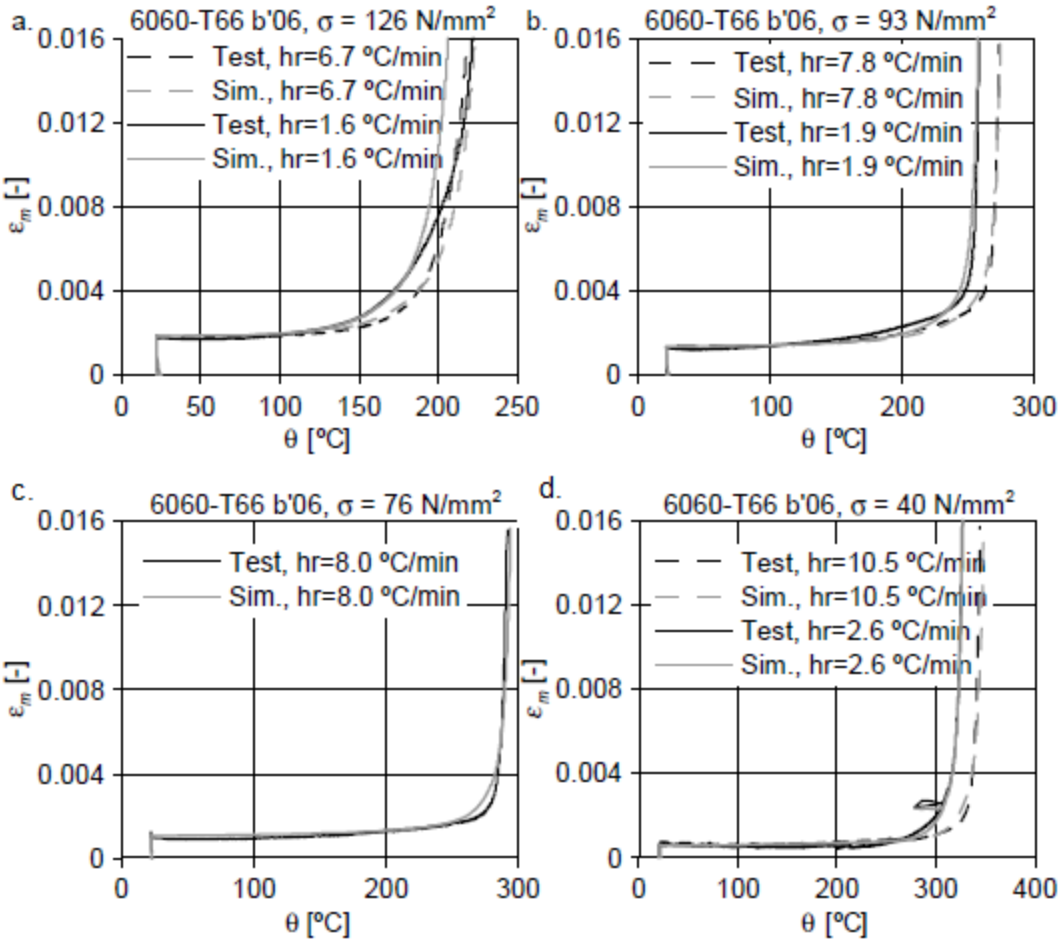

Figure 3.32 Strain as function of temperature of transient state tests and simulations on alloy 6060-T66 b´06 (a. Constant stress of 126 N/mm^2; b. Constant stress of 93 N/mm^2; c. Constant stress of 76 N/mm^2; d. Constant stress of 40 N/mm^2)

3.5.4 Discussion of the transient state test and simulation results

The transient state tests are simulated with the modified Dorn-Harmathy model. The Dorn-Harmathy model is applicable only for temperatures higher than 0.5 times the absolute melting temperature, which is approximately 150°C for most 6xxx series alloys, while in case of transient state tests, the constitutive model has to be used also for temperatures between ambient temperature and 150°C. this is justified because the creep strain developed at such low temperatures is negligible for the stress levels relevant for fire design. The results of the simulations can be seen in paragraph 3.5.1 for not welded specimens and 3.5.2 for welded specimens.

Unfortunately, the agreement between the test results and the simulations of the not welded and welded specimens are not as good as the agreement between the test results and simulations of the 6060-T66 alloy. A larger deviation can be seen at welded specimens.

A large deviation can be seen at temperature of rupture. This deviation is larger for specimens with weld. The largest difference in temperature of rupture for welded specimens is about 40°C. For specimens without a weld this value is about 10°C.

Also a large deviation can be seen at the transition to fracture. The primary creep parameter ε_{t0}, where large deviations can be seen in Figures 3.12 and 3.17, can be the reason for the large difference between simulation and test result. This parameter has a greater influence at higher stresses.

Figure 3.33a gives the results of the tests and the simulations of the temperature at which a plastic strain of 0.4% or 2% is detected for specimens without a weld (top graphs) and for specimens with a weld (bottom graphs) of aluminum alloy 6082-T6. The average difference and standard deviation of the difference in temperature between tests and simulations at a plastic strain of 0.4% and 2% for aluminum alloy 6082-T6 are given in Table 3.4. Also the deviations of the model based on the creep test results are determined for the Zener Holloman parameter and ε_{t0} (see Annex D.1 and D.2). The black lines in the figures are indicating the scatter band for the transient state tests. These scatter bands are determined as one standard deviations away from the mean. The red lines in the graph indicate a deviation between the test temperature and the temperature of the simulations of -5%, 0% and +5%. Also these graphs show that the results of the welded specimens deviate more with the simulations. Figure 3.33b shows the results of the tests and the simulations of the temperature at which a plastic strain of 0.2% or 1% is detected for specimens of aluminum alloy 6060-T66 from [Maljaars, 2008]. Also in this figure lines are plotted indicating a deviation between the test temperature and the temperature of the simulations of

-5%, 0% and +5%. The average difference and standard deviation of the difference in temperature between tests and simulations at a plastic strain of 0.2% for alloy 6060-T66 is given in Table 3.5.

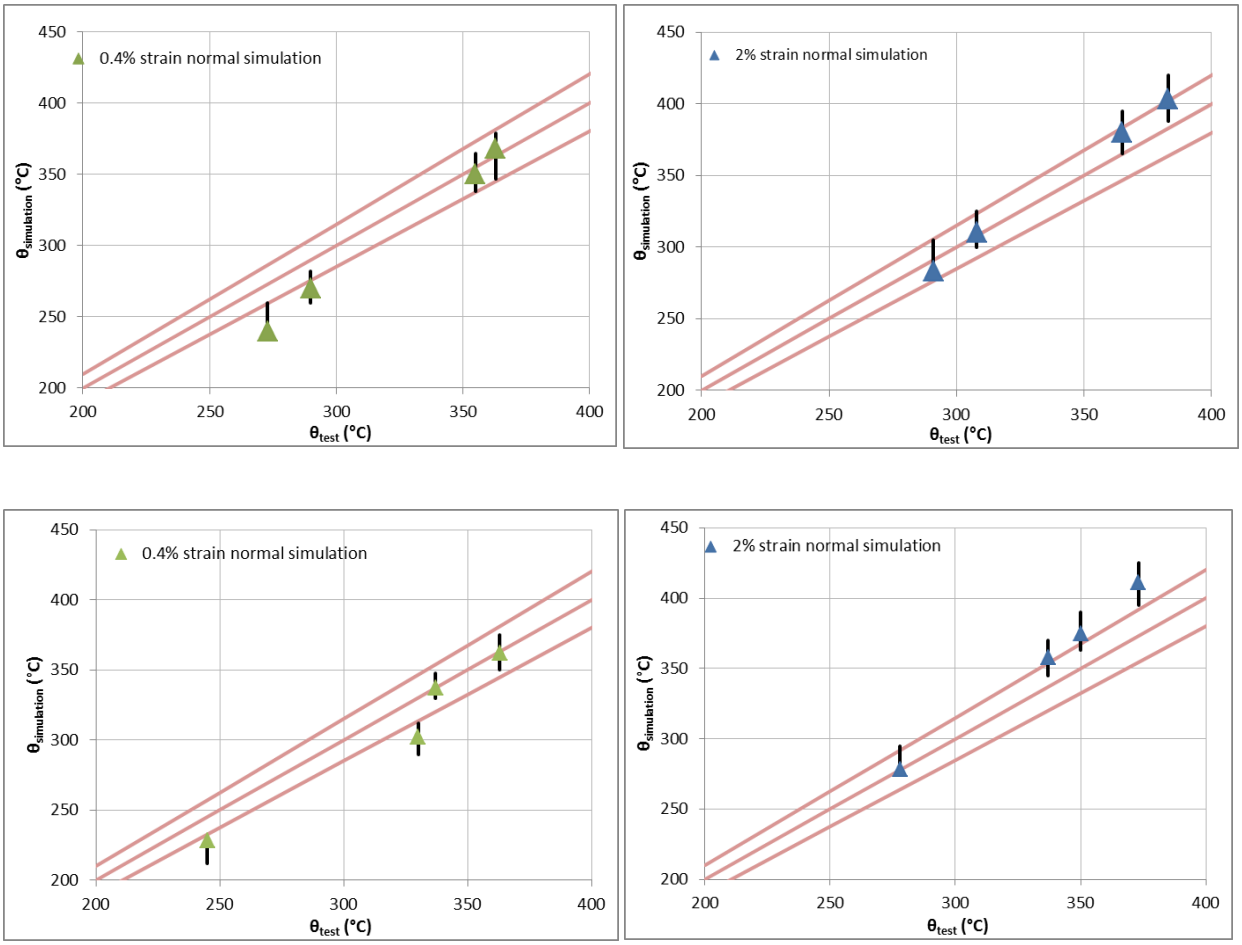

Figure 3.33a Relation between simulation temperature and test temperature at plastic strains of 0.4% and 2%. Top graphs: Not welded specimens. Bottom graphs: Welded specimens.

Table 3.4 Average value and standard deviation of the difference in temperature between simulations and test at a plastic strain of 0.2% for aluminum alloy 6082-T6

	6082-T6 not welded	6082-T6 welded
Average difference at 0.4% strain (°C)	-13.3	-11.5
Standard dev. Difference at 0.4% strain (°C)	14.5	11.7
Average difference at 2% strain (°C)	7.3	21
Standard dev. Difference at 2% strain (°C)	11	13.7

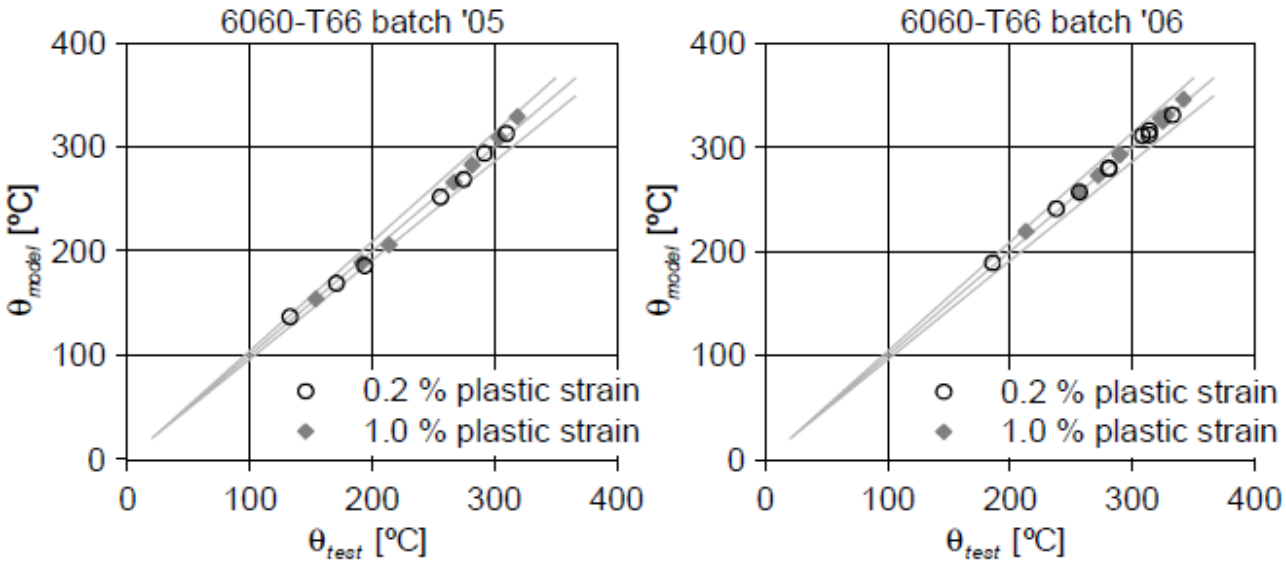

Figure 3.33b Relation between simulation temperature and test temperature at plastic strains of 0.2% and 1% from [Maljaars, 2008].

Table 3.5 Average value and standard deviation of the difference in temperature between simulations and test at a plastic strain of 0.2% for aluminum alloy 6060-T66 [Maljaars, 2008].

	6060-T66 b'05	6060-T66 b'06
Average difference (°C)	2	0
Standard dev. Difference (°C)	5	2

It can be clearly seen that there is a small difference between the temperature of tests and simulations for alloy 6060-T66. But compared to alloy 6060-T66, this difference is large for alloy 6082-T6.

Unfortunately, the deviations are too large to conclude that the model suits well with the experiments. Also the scatter bands are showing that the simulations are not meeting the "perfect situation line". Large deviations can be seen in the temperature of rupture and the transition to fracture. The leading parameter for the temperature of rupture is the ε_{lim} and for the part to transition to fracture is ε_{t0}. Both of these parameters are determined from the test graphs. A small error or slip in the LVDT will cause a different value for the parameters. Due to the slip in the LVDT large deviations could be seen in Figures 3.12 and 3.17, which is used for the determination of the ε_{t0} parameter. Also large differences at welded specimens could be seen in the values of the ε_{lim}. Due to this, the large difference in the transient state test results and simulation is probably related to the error and slip in the LVDT.

3.5.5 Change of the parameters

In the previous paragraph it is seen that the parameters ε_{lim} and ε_{t0} are the leading parameters for the large deviations between the simulations and the transient state test result. To achieve a more suitable model it is chosen to change these parameters. The test results of the transient state tests showed a more sharp transition to fracture in comparison with the simulations. This means that the ε_{t0} parameter will be closer at the value of 0. From the results of the simulations it can also be seen that the value of ε_{lim} needs to be smaller than the value which is determined from the creep test results.

For the simulations of the model in paragraph 3.5.3, Equation (3.11) was used for the specimens without a weld. Because there were not much test results between the stress range of 150 – 240 N/mm^2, equation (3.11) was proposed for the function of Z for 25 N/mm^2 < σ < 125 N/mm^2. But the fact that there are not much test results between the stress range of 150 – 240 N/mm^2 does not mean that Equation (3.10) is more suitable for the simulations. Also the impact of the different Zener-Holloman equations of the not welded specimens (Equation (3.10) and (3.11)) are investigated.

Because of the fact that there is a sharp transition to fracture in the transient state test graphs, which means that the ε_{t0} parameter is close to 0, it is chosen to change the ε_{t0} parameter to 0. In this way this parameter is excluded. [Allen, 2012] has conducted creep tests at 6061-T651 alloy specimens. Figure 2.10 shows the creep behavior data of 6061-T651 alloy. The absence of a primary creep region is noticeable. If a primary region is present it is so small that it cannot be identified from the data. So the primary creep parameter could also be excluded in the data of the 6061-T651 alloy.

ε_{lim} is changed in a value whereby the simulation is in good agreement with the transient state test graph.

By changing the various parameters, respectively the graphs of transient state tests in Figure 3.34–3.37 and 3.38–3.41 are obtained for specimens without weld and specimens with weld. The meaning of the various designations given in the legend are given in Table 3.6 for specimens without weld and Table 3.7 for welded specimens.

Table 3.6 Designations given in the legend of Figures 3.34 – 3.37.

Normal simulation	**ε_{t0} excluded**	**ε_{lim} = 0.00045**	**Zener-Holloman Eq.(3.10)**
$\varepsilon_{t0} = 5.59 \cdot 10^{-5} \cdot \sigma^{0.71}$ Z = Equation (3.11) $\varepsilon_{lim} = 0.0045$	$\varepsilon_{t0} = 0$ Z = Equation (3.11) $\varepsilon_{lim} = 0.0045$	$\varepsilon_{t0} = 0$ Z = Equation (3.11) $\varepsilon_{lim} = 0.00045$	$\varepsilon_{t0} = 0$ Z = Equation (3.10) $\varepsilon_{lim} = 0.0045$

Table 3.7 Designations given in the legend of Figures 3.38 – 3.41.

Normal simulation	**ε_{t0} excluded**	**ε_{lim} = 0.0004**
$\varepsilon_{t0} = 1.5 \cdot 10^{-6} \cdot \sigma^{1.8}$ $\varepsilon_{lim} = 0.0085$	$\varepsilon_{t0} = 0$ $\varepsilon_{lim} = 0.0085$	$\varepsilon_{t0} = 0$ $\varepsilon_{lim} = 0.0004$

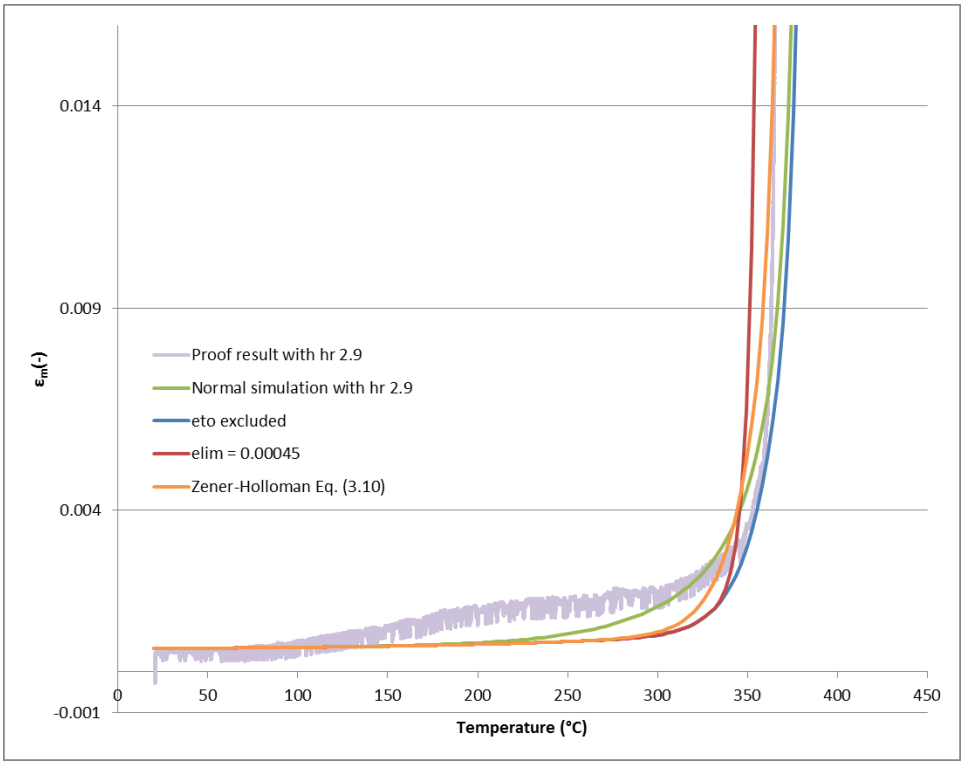

Figure 3.34 Strain as function of temperature of transient state tests with a constant stress of 40 N/mm^2 and heating rate of 2.9 °C/min with various simulations for not welded specimen.

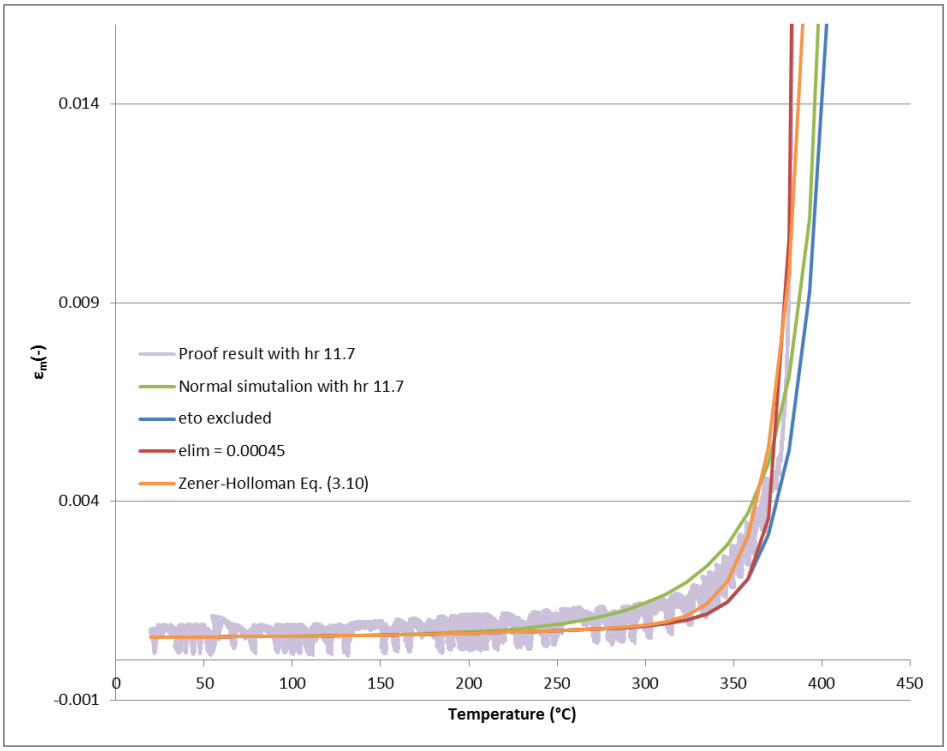

Figure 3.35 Strain as function of temperature of transient state tests with a constant stress of 40 N/mm^2 and heating rate of 11.7 °C/min with various simulations for not welded specimen.

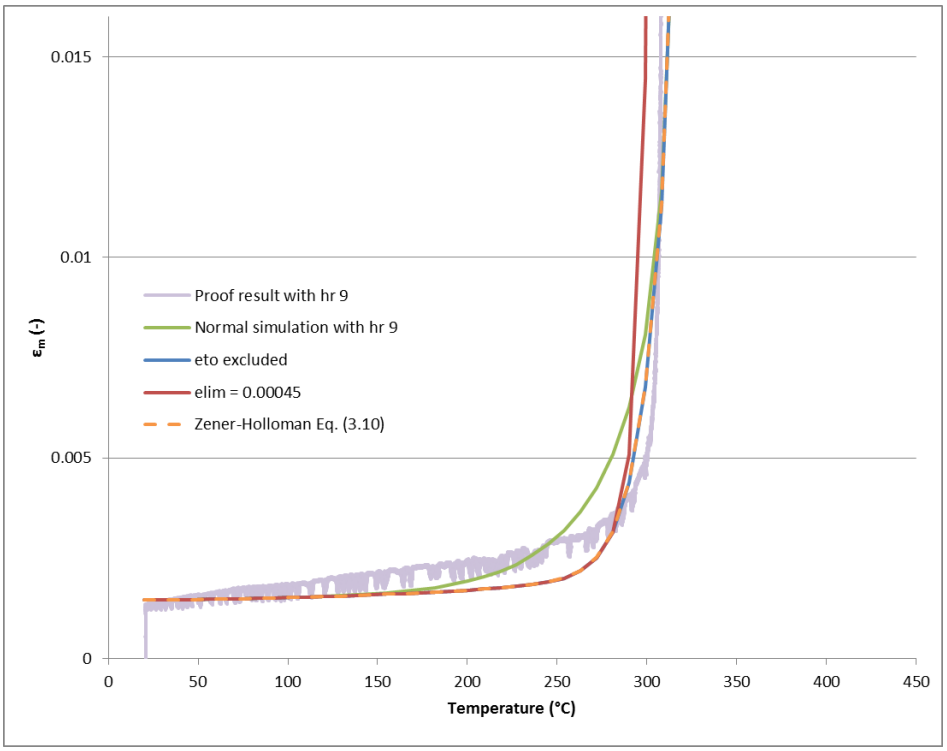

Figure 3.36 Strain as function of temperature of transient state tests with a constant stress of 100 N/mm^2 and heating rate of 9 °C/min with various simulations for not welded specimen.

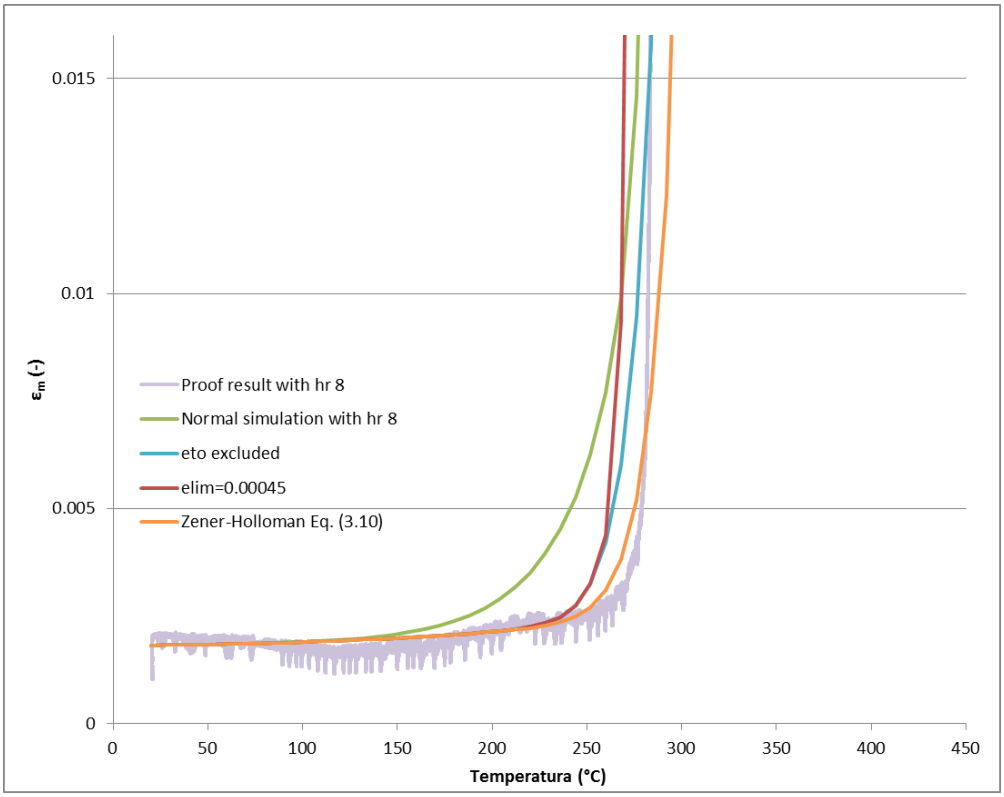

Figure 3.37 Strain as function of temperature of transient state tests with a constant stress of 125 N/mm^2 and heating rate of 8 °C/min with various simulations for not welded specimen.

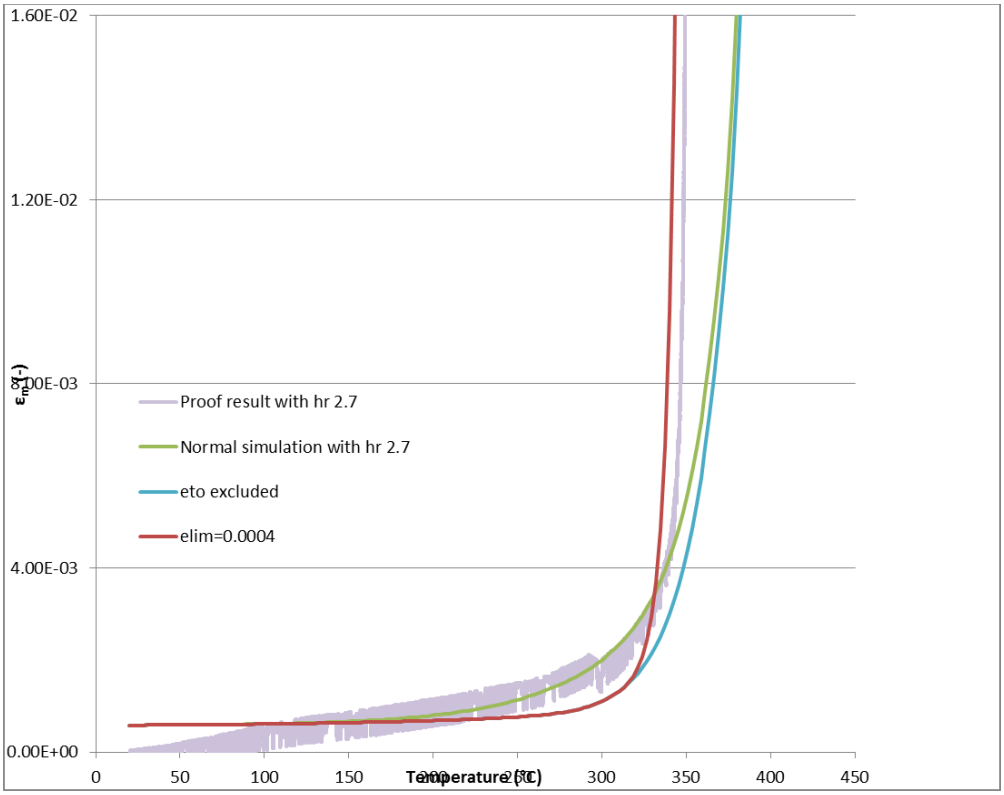

Figure 3.38 Strain as function of temperature of transient state tests with a constant stress of 40 N/mm^2 and heating rate of 2.7 °C/min with various simulations for welded specimen.

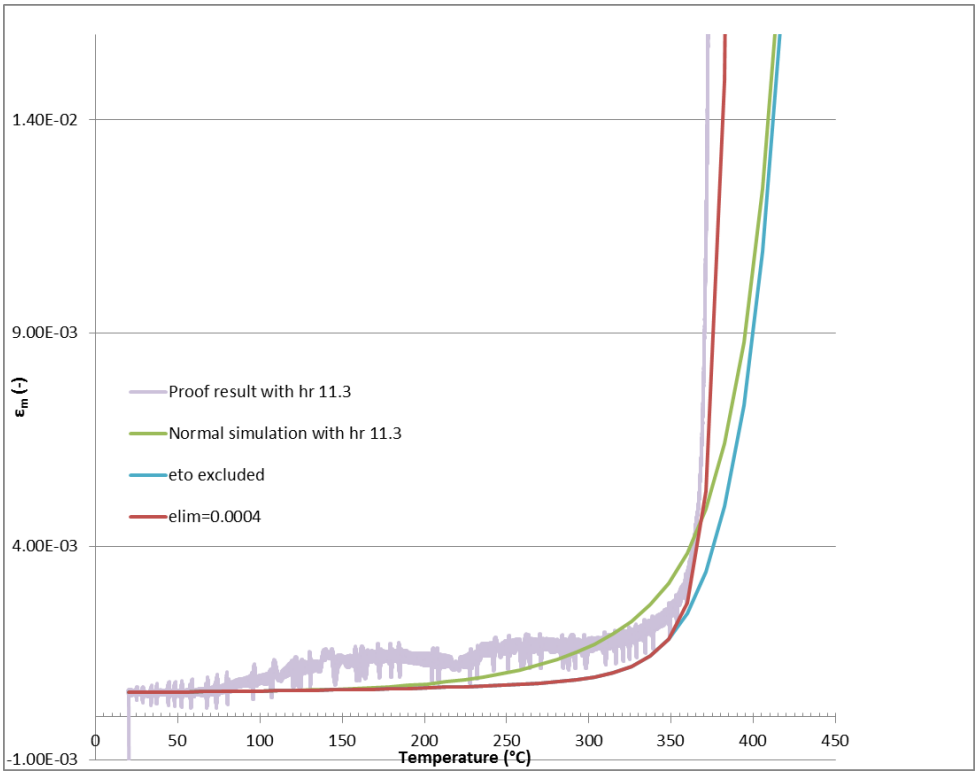

Figure 3.39 Strain as function of temperature of transient state tests with a constant stress of 40 N/mm^2 and heating rate of 11.3 °C/min with various simulations for welded specimen.

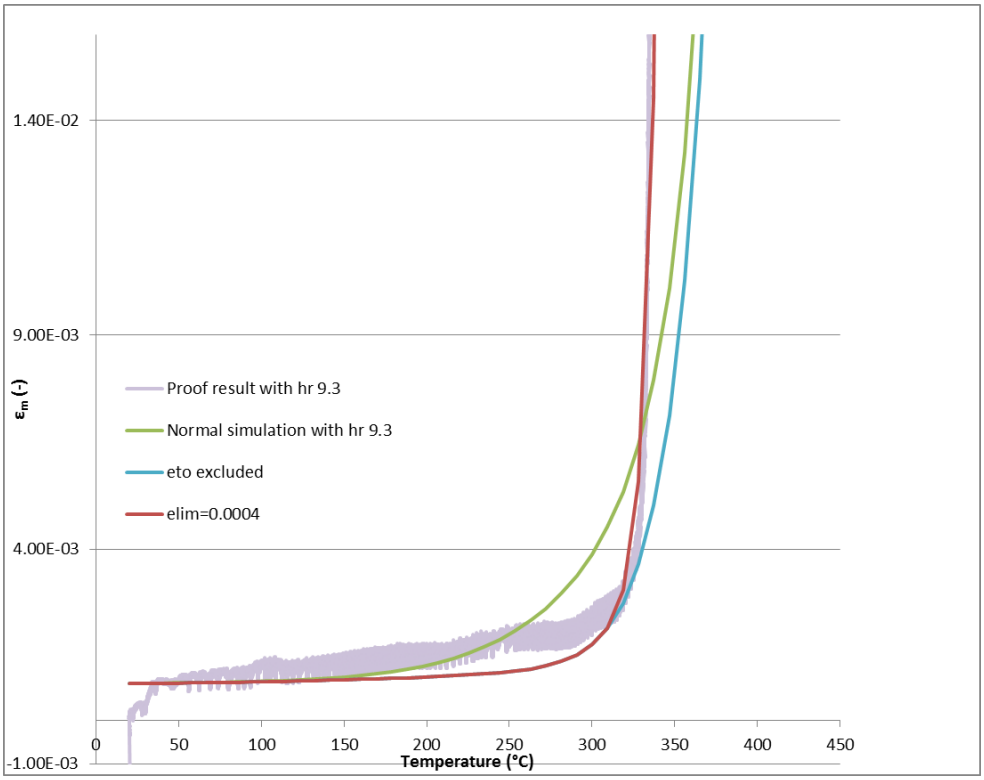

Figure 3.40 Strain as function of temperature of transient state tests with a constant stress of 60 N/mm^2 and heating rate of 9.3 °C/min with various simulations for welded specimen.

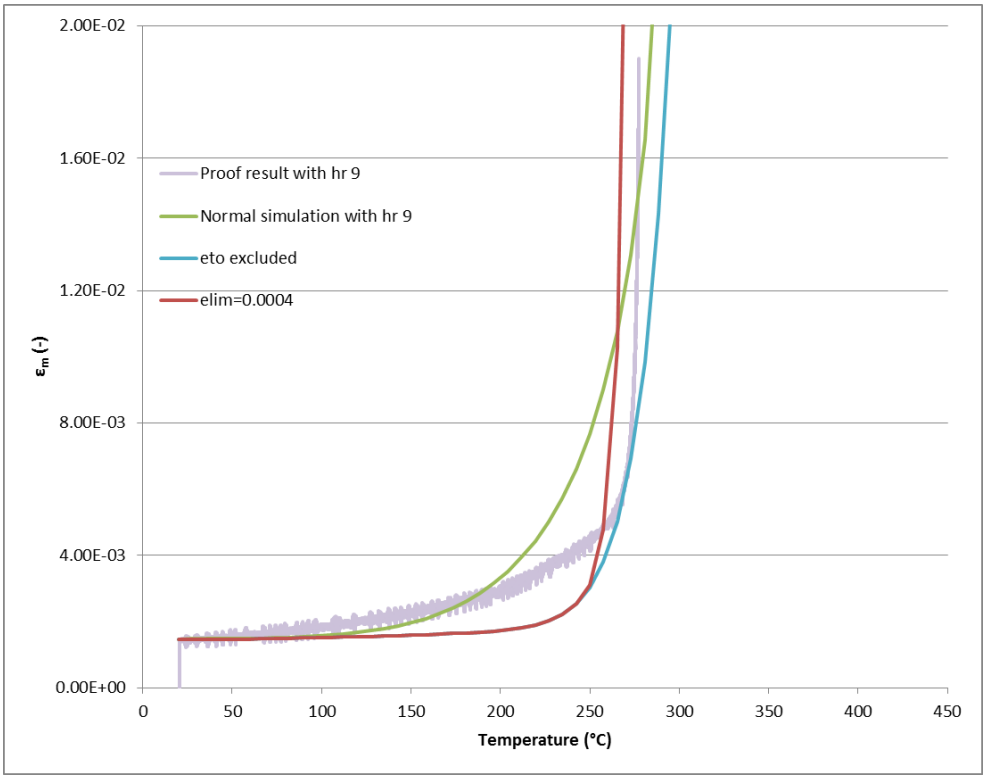

Figure 3.41 Strain as function of temperature of transient state tests with a constant stress of 100 N/mm^2 and heating rate of 9 °C/min with various simulations for welded specimen.

Figures 3.34–3.37 for not welded specimens and Figures 3.38–3.41 for welded specimens show that a change in the parameters have a significant influence on the simulation of the transient state tests. In the first instance it seems to have been the right choice to exclude the ε_{t0} parameter for both types of specimens. This makes sense, because the sharp transition to fracture relates to a ε_{t0} parameter which is near by the value of 0. Because the primary creep parameter ε_{t0} relates to very small strains, slip in the LVDT at the beginning of the creep test, will cause very large deviations in the results to determine the ε_{t0} parameter. This is probably the reason of the error in the Equations (3.12) and (3.17). Considering the standard deviation of the ε_{t0} values obtained from the creep curves resulting from the not welded specimen tests is 0.0009 with a mean of 0.0010. The value of 0 is 1.1 standard deviations away from the mean of 0.0010. Considering the standard deviation of the ε_{t0} values obtained from the creep curves resulting from the welded specimen tests is 0.0063 with a mean of 0.0063. The value of 0 is 1.0 standard deviations away from the mean of 0.0010.

For specimens without a weld, it can be seen that either the change of the ε_{lim} factor to 0.00045 and the change of the Zener-Holloman equation to Eq. (3.10), will give good agreement with the measured and simulated strain development. However, the standard deviation of ε_{lim} values obtained from the creep curves resulting from the tests is 0.0019 with a mean of 0.0045. The value of 0.00045 is 2.13

standard deviations away from the mean of 0.0045. This result shows that it is very likely that the used Zener-Holloman Equation (3.11) in the simulation of the curves in paragraph 3.5.1, caused for the deviations in the results. The use of Equation (3.10) will give good agreement between the measured and simulated strain development.

For welded specimens it is clearly visible that the change of the values of ε_{t0} and ε_{lim} has ensured that the simulation are better in agreement to the test results. The large deviations in the determined ε_{lim} values from the creep curves of the welded specimens have caused the differences between the measured and simulated strain development. Considering the standard deviation of the ε_{lim} values obtained from the creep curves resulting from the tests is 0.0071 with a mean of 0.0085. The value of 0.0004 is 1.1 standard deviations away from the mean of 0.0085. This result shows that it is likely to assume that the value of ε_{lim} is determined wrong and needed to be approximately 0.0004.

Figure 3.42 and 3.43 gives respectively the results of the tests and the simulations of the temperature at which a plastic strain of 0.4% or 2% is detected for specimens without a weld and for specimens with a weld for all the simulation models. The lines in the graph indicate a deviation between the test temperature and the temperature of the simulations of -5%, 0% and +5%.

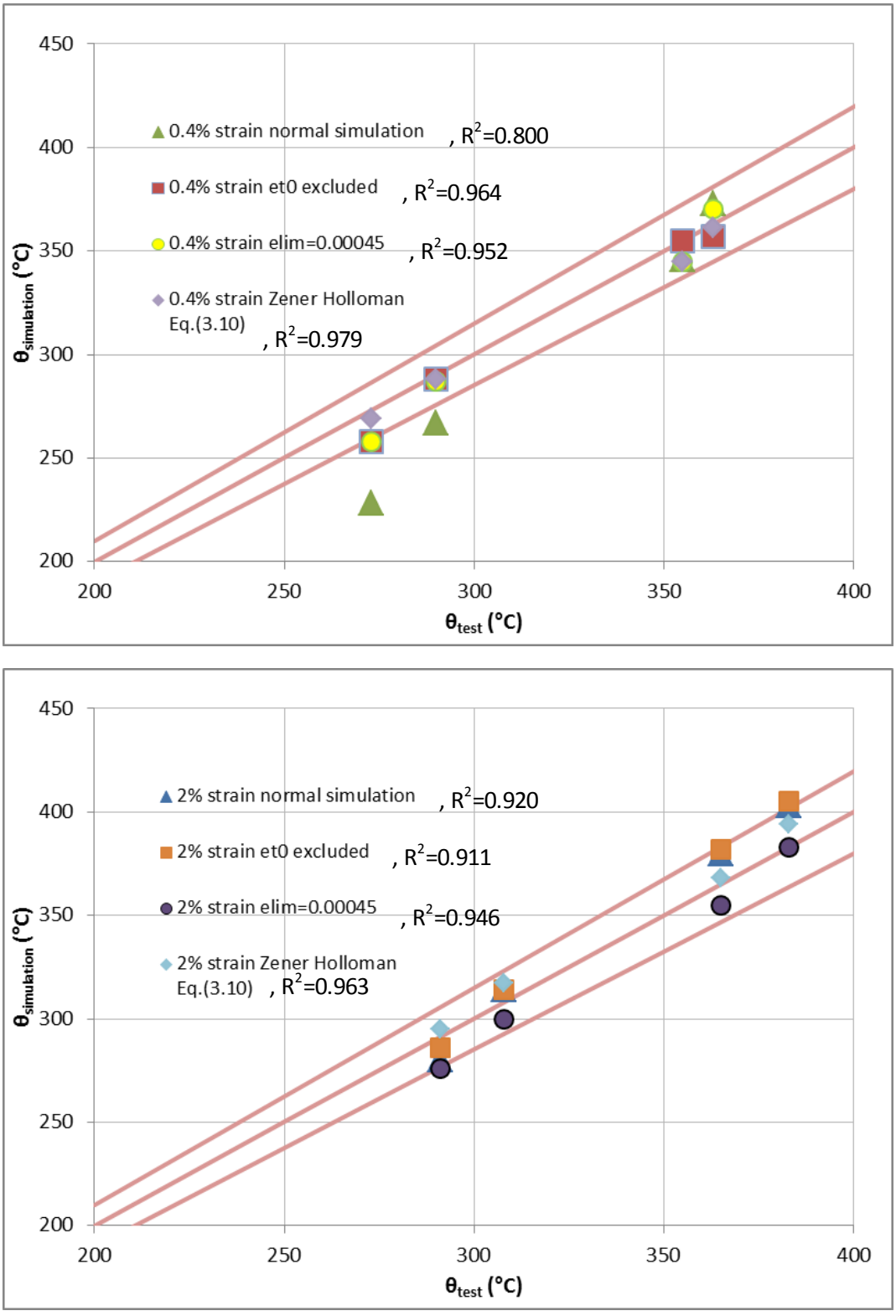

Figure 3.42 Relation between simulation temperature and test temperature at plastic strains of 0.4% and 2% for all investigated models for specimens without weld.

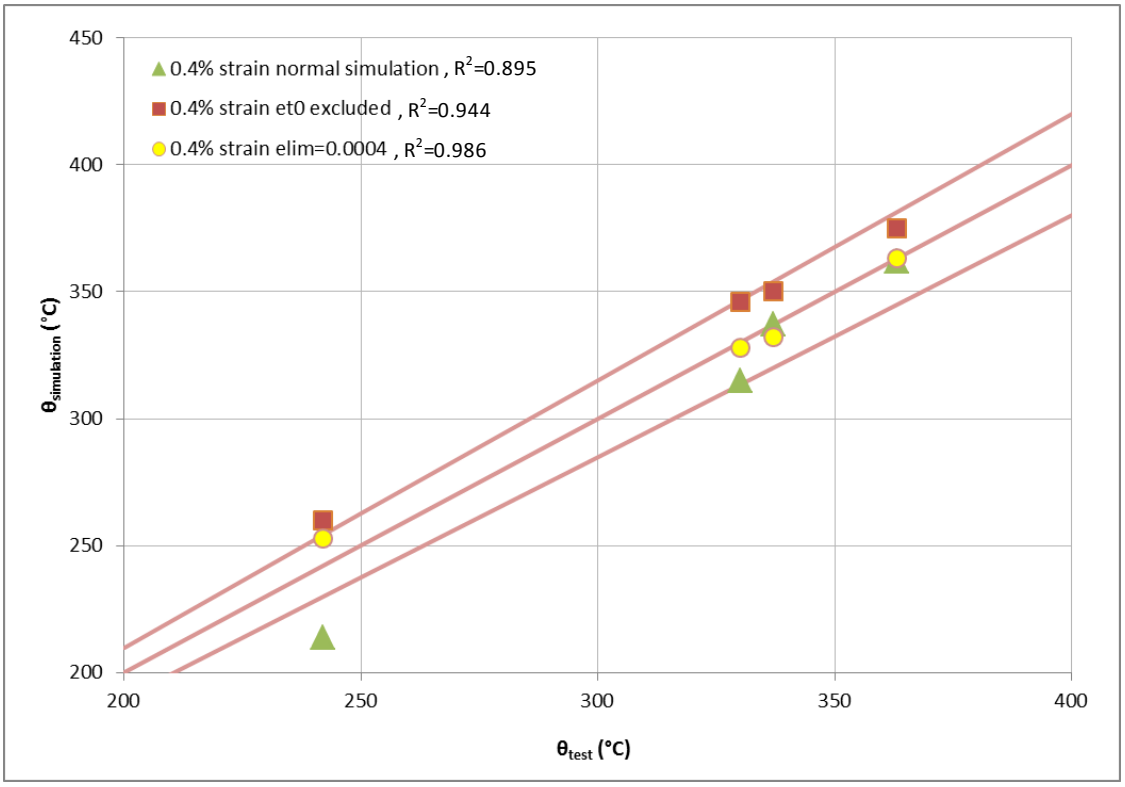

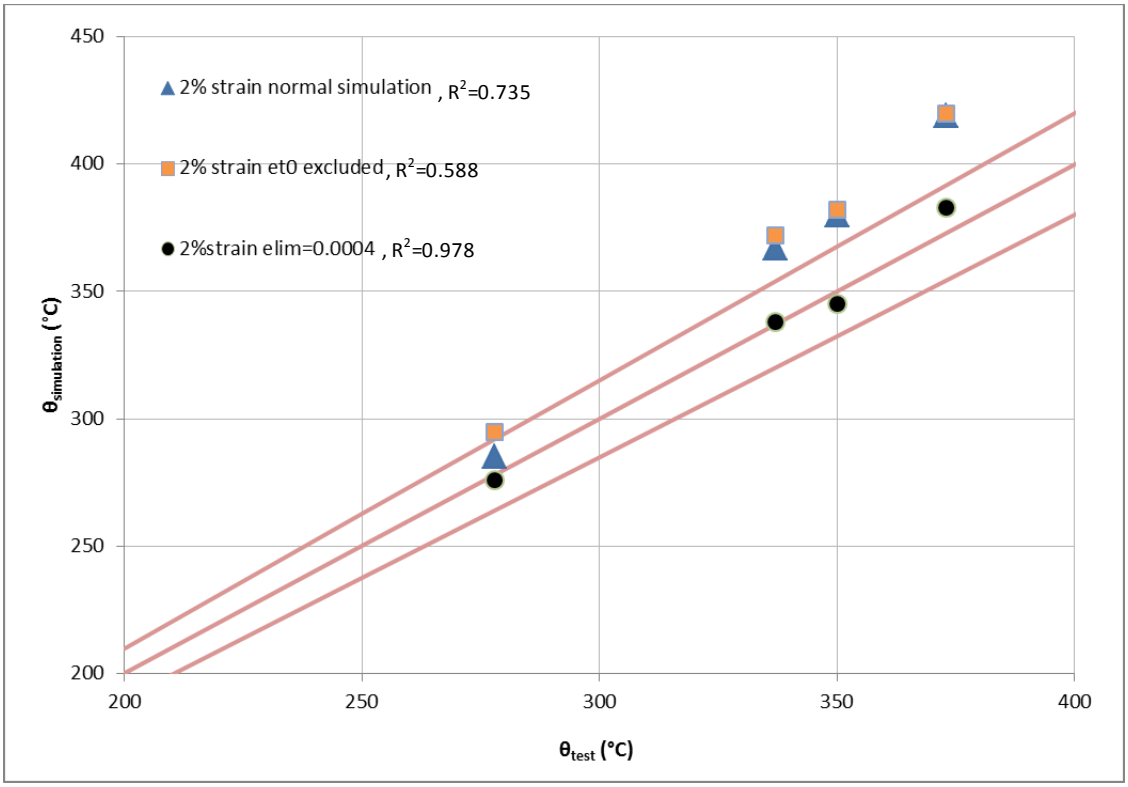

Figure 3.43 Relation between simulation temperature an test temperature at plastic strains of 0.4% and 2% for all investigated models for welded specimens.

Figure 3.42 shows that the simulations with the Zener-Holloman Equation (3.10) suits the best with the transient state results, such as it is was discussed before. From Figure 3.43, it can be clearly seen that the simulation with ε_{lim}=0.0004 suits the best with the results of the transient state tests. Table 3.8 shows the coefficient of determination of the simulations and the line in "perfect situation".

Table 3.8 Coefficient of determination of the simulations and the line in perfect situation.

R^2	**Not welded specimens 0.4% strain**	**Not welded specimens 2% strain**
Normal simulation	0.800	0.920
ε_{t0} **excluded**	0.964	0.911
ε_{lim} **= 0.00045**	0.952	0.946
Zener-Holloman Eq.(3.10)	0.979	0.963
R^2	**Welded specimens 0.4% strain**	**Welded specimens 2% strain**
Normal simulation	0.895	0.735
ε_{t0} **excluded**	0.944	0.588
ε_{lim} **= 0.0004**	0.986	0.978

3.6 Stress-strain relations

Calculations for transient state conditions are carried out with various constant stress levels, while keeping the heating rate constant. Each calculation results in a certain strain at a certain temperature. Varying the stress level gives stress-strain points in function of the temperature and the heating rate. Combining these points at the same temperature and heating rate leads to a stress-strain relation. This stress-strain relation is valid for the heating rate and exposure period considered. The stress-strain curves are based on calculations with the simulated constitutive models.

Figure 3.44 and 3.45 shows respectively the stress-strain diagrams for the not welded and welded specimens for the best suited simulations which are determined in paragraph 3.5.5. Annex E.1 and E.2 shows the stress-strain diagrams for all simulation models as described in paragraph 3.5.5. It can be clearly seen that changing a parameter will cause a large difference in the stress-strain curves. The heating rates applied are such as to give the indicated temperature after approximately 30 and 120

minutes. It is shown that the mechanical properties of aluminum exposed to fire conditions not only depend on the temperature, but also on the exposure time.

Annex E.1 and E.2 will also give the temperatures at which a plastic strain of 0.2% and 2% is measured in the simulated stress-strain curves, i.e. the figure gives the 0.2% proof stress and the 2% stress for transient state conditions as a function of the temperature.

The stress-strain curves are also approximated by the Ramberg-Osgood relationship, which can be seen in Annex F.1 and F.2, using three material parameters to describe each curve: $f_{0.2,\theta}$, E_θ and n_θ. The values for n_θ are selected such as to give good agreement between the Ramberg-Osgood stress-strain curves and the original stress-strain curves. Also the stress-strain curves determined with the Ramberg-Osgood equation at room temperature are indicated as reference. The stress-strain curves also show that the transient state stress–strain curves at elevated temperatures are significantly more curved than at room temperature. This corresponds with very low values for parameter n for fire exposure. At welded specimens it can be seen that the stress-strain curve at room temperature meets with the stress-strain curve at 200°C. This is due to the $f_{0.2}$ at ambient temperature. This may indicate that creep affects after 200°C at welded specimens.

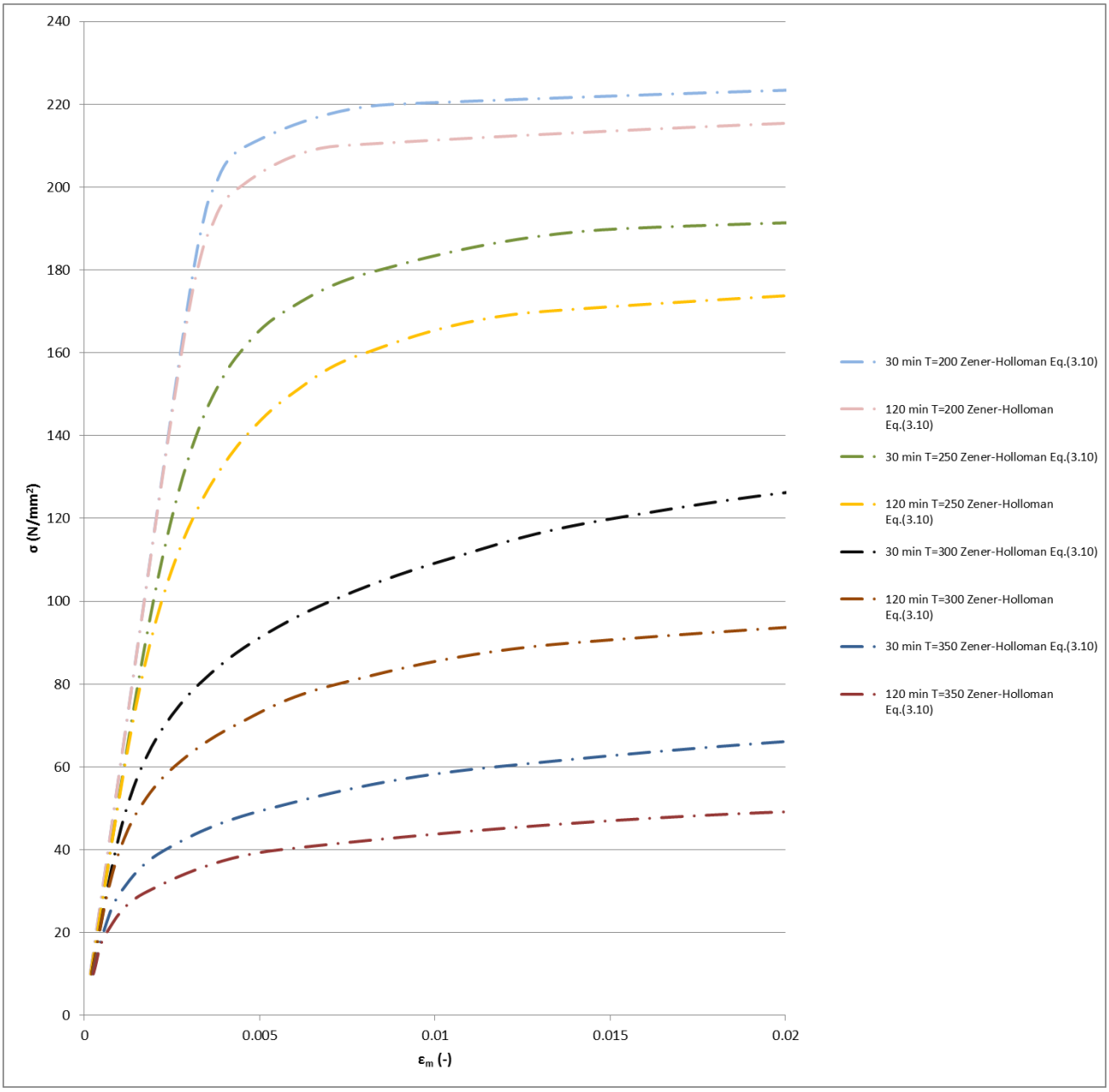

Figure 3.44 Stress strain curves for fire design derived for a constant heating rate and a constant stress in time for the best suited simulation model determined in paragraph 3.5.5 for specimens without a weld.

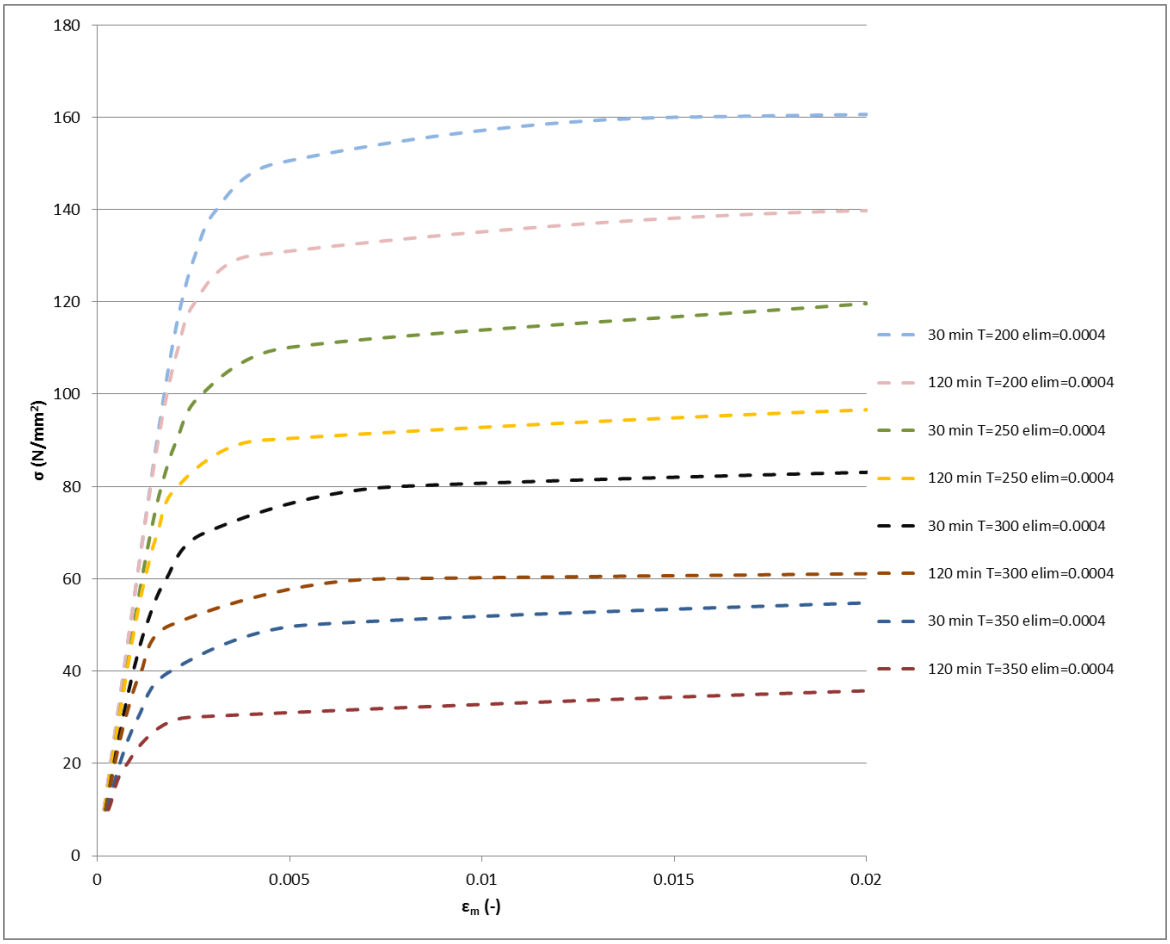

Figure 3.45 Stress strain curves for fire design derives for a constant heating rate and a constant stress in time for the best suited simulation model determined in paragraph 3.5.5 for welded specimens.

The relative values $f_{0.2,\theta}/f_{0.2,room}$ in [EN 1999-1-2, 2007] are based on steady state tests. Respectively, Figure 3.46 and 3.47 give a comparison between $f_{0.2,\theta}$ according to the standard, and $f_{0.2,\theta}$ for transient state conditions as based on simulation with the most suitable constitutive models for specimens without a weld and specimens with a weld (also $f_{2,\theta}$ for transient state conditions are indicated in this figure). In Figures 3.46 – 3.50 "Eurocode 9-1-2 (f0 eurocode)" refers to data obtained from the multiplication of the $f_{0.2}$ value, which is obtained from the [EN 1999-1-1, 2007], with relative values from [EN 1999-1-2, 2007]. "Eurocode 9-1-2 (f0 test)" refers to data obtained from the multiplication of the $f_{0.2}$ value, which is obtained from tensile tests, with relative values from [EN 1999-1-2, 2007]. Annex F.1 and F.2 shows the stress versus temperature graphs of the other simulation models. The values of the standard are obtained by multiplying the relative values $f_{0.2,\theta}/f_{0.2}$ in [EN 1999-1-2, 2007] with $f_{0.2}$ in [EN 1999-1-1, 2007]. For both types of specimens, not welded and welded, the values for $f_{0.2,\theta}$ in the standard are conservative compared to the values determined in the transient state simulations.

Annex F.1 and F.2 shows also $f_{0.2,\theta}/f_{0.2}$ graphs. Just like the stress/strain curves, also here it can be seen that the $f_{0.2,\theta}/f_{0.2}$ value at 200°C is above the value 1. This is not logic because $f_{0.2}$ is determined at room temperature. As mentioned earlier, this might mean that creep occurs above 200°C for specimens with a weld.

Figure 3.46 and 3.47 shows that the curves for the different heating rates are close together. The maximum influence of the heating rate on the fire resistance is about 17%, when assuming that $f_{0.2,\theta}$ is the governing parameter for the resistance.

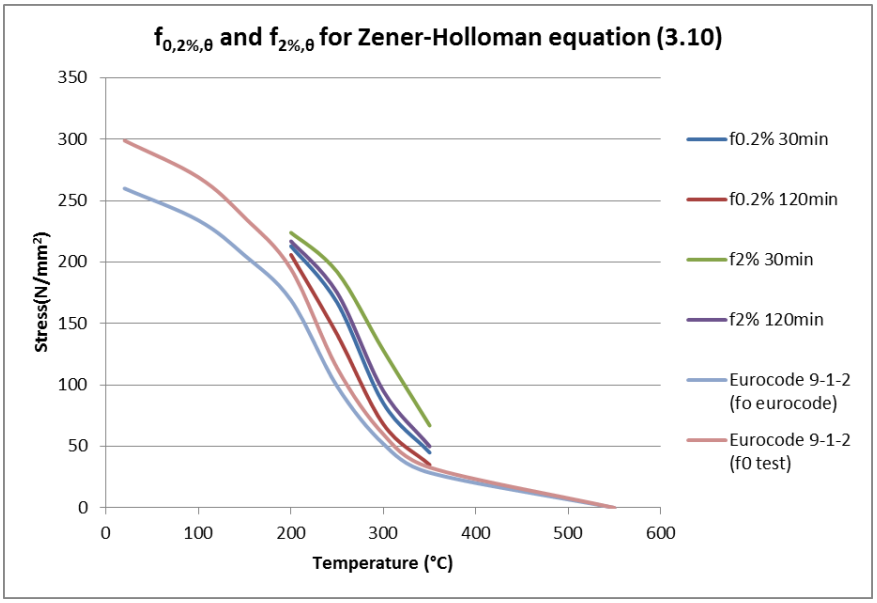

Figure 3.46 Relation between 0.2% proof stress and 2% stress and temperature for specimens without a weld. Also data of 0.2% proof stress according to the Eurocode [EN 1999-1-2, 2007] for not welded specimens is shown for comparison.

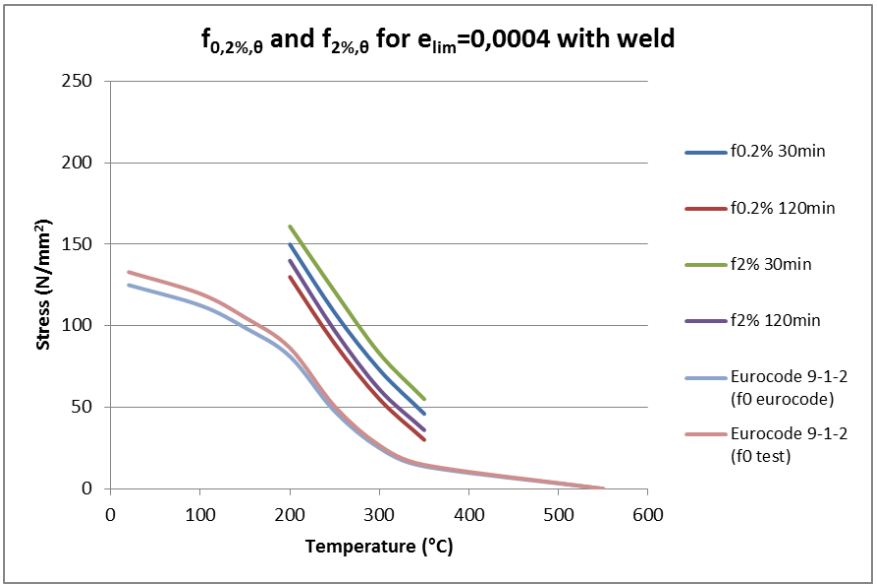

Figure 3.47 Relation between 0.2% proof stress and 2% stress and temperature for welded specimens. Also data of 0.2% proof stress according to the Eurocode [EN 1999-1-2, 2007] for welded specimens is shown for comparison.

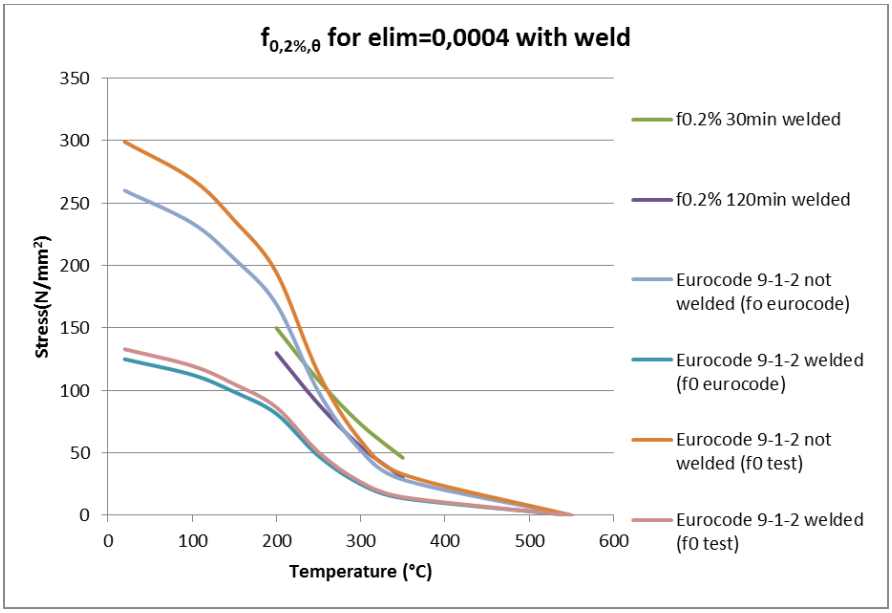

Figure 3.48 Relation between 0.2% proof stress and temperature for welded specimens. Also data of 0.2% proof stress according to the Eurocode [EN 1999-1-2, 2007] for welded and not welded specimens is shown for comparison.

Figure 3.47 showed that [EN 1999-1-2, 2007] is conservative for welded specimens. Figure 3.48 gives a comparison between $f_{0.2,\theta}$ for not welded specimens and welded specimens according to the standard, and $f_{0.2,\theta}$ for transient state conditions as based on simulation with the most suitable constitutive model for specimens with a weld. It can be seen that the standard for not welded specimens is unsafe for the tested specimens with a weld between 200°C - 250°C. But when we look at higher temperatures, it can be seen that the standard for not welded specimens is also safe for the tested specimens with a weld.

Figure 3.49 gives a comparison between $f_{0.2,\theta}$ for not welded specimens and welded specimens according to the standard, and $f_{0.2,\theta}$ for transient state conditions as based on simulation with the most suitable constitutive model for specimens without and with a weld. The tests carried out at elevated temperature show that the difference in strength between the HAZ and the parent metal decreases with increasing temperature. At a temperature of approximately 300°C the 0.2% proof stress of the not welded and welded specimens meet each other. This is due to the fact that the favorable metal structure obtained by a treatment is already destroyed by the heat input at welding. Consequently, heating by a fire has a smaller impact on the strength of the HAZ than on the strength of the treated parent metal.

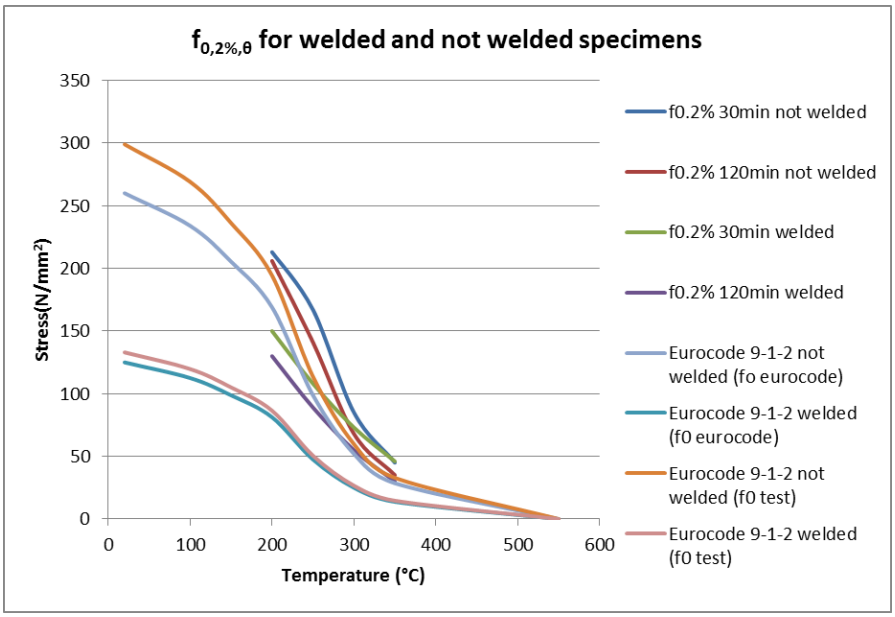

Figure 3.49 Relation between 0.2% proof stress and temperature for not welded and welded specimens. Also data of 0.2% proof stress according to the Eurocode [EN 1999-1-2, 2007] for welded and not welded specimens is shown for comparison.

Figure 3.50 gives a comparison between $f_{0.2,\theta}$ for 6060-T66 from [Maljaars, 2008] and 6082-T6 alloys according to the standard, and $f_{0.2,\theta}$ for transient state conditions as based on simulation. Also here it can be seen that the difference in strength between the two aluminum alloys decrease with increasing temperature. At a temperature of approximately 300°C the 0.2% proof stress of the alloys meet each other. At temperatures of such a height, the treatment has not much impact and the strength of the alloys meat each other.

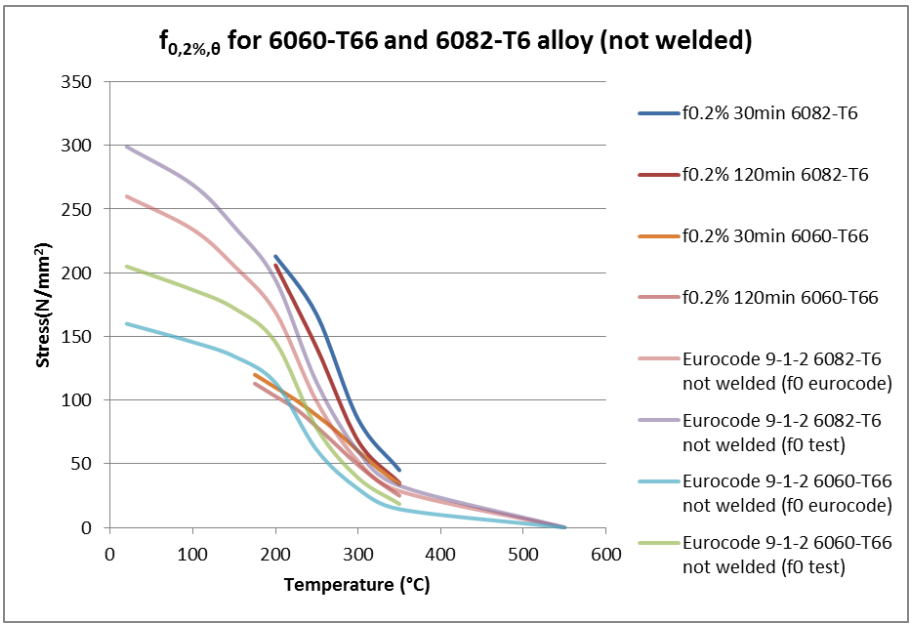

Figure 3.50 Relation between 0.2% proof stress and temperature for 6060-T66 and 6082-T6 alloy. Also data of 0.2% proof stress according to the Eurocode [EN 1999-1-2, 2007] for each alloy is shown for comparison.

According to data in [Kaufmann, 1999] the strength of different alloys in the same series and with the same temper shows an approximately equal decrease. Figure 3.51 shows the 0,2% proof stress (left picture) and the relative 0,2% proof stress (proof stress relative to that at room temperature, right picture) of alloys in series 6xxx and temper T6. The relative 0,2% proof stress corresponds reasonable for different alloys in the 6xxx series, with T6 temper. Also [EN 1999-1-2, 2007] assumes that the relative values $f_{0.2,\theta}/f_{0.2}$ for alloys in the same series with the same temper are reasonably equal to each other, see Figure 3.52. In this figure it can be seen that de relative values of alloys 6063-T6 and 6060-T6 are the same and the relative values of alloy 6082-T6 is reasonably equal to the other two plotted alloys. These results are based on steady state tests.

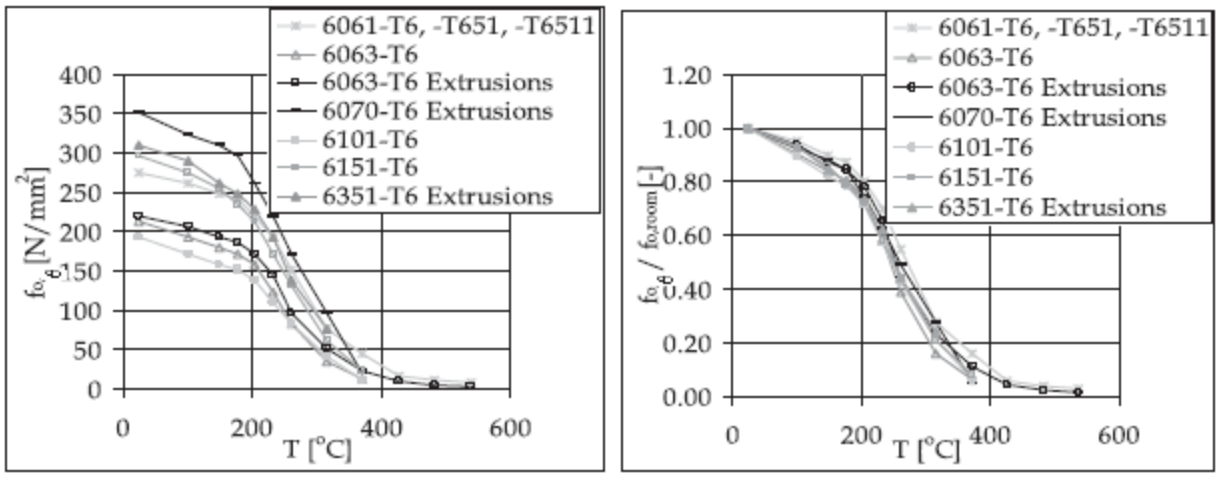

Figure 3.51 0.2% proof stress (left picture) and relative 0.2% proof stress for alloy series 6xxx with temper T6.

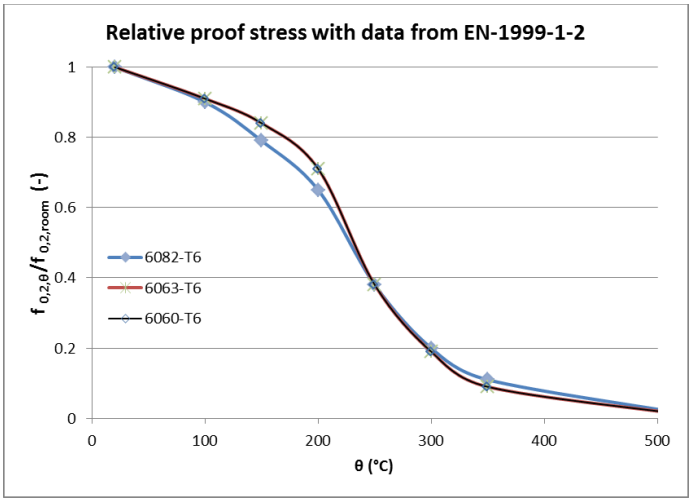

Figure 3.52 Relative 0.2% proof stress for alloy series 6xxx with temper T6 of data from [EN 1999-1-2, 2007].

Figure 3.53 shows the relative values $f_{0.2,\theta}/f_{0.2,room}$ based on transient state tests of the welded and not welded 6082-T6 alloys and alloy 6060-T66 from [Maljaars, 2008]. The relative value in the left-hand figure is determined with $f_{0.2,room}$ from the conducted tensile tests on the specimens. The relative value in the right-hand figure is determined with $f_{0.2,room}$ from [EN 1999-1-1]. It can be seen that the relative values of the different types differ from each other for the left-hand side figure, although they are from the same alloy and temper. For the right-hand side figure the relative values of the not welded specimens are reaching each other, but the relative value of the welded specimen differs from the not welded specimens.

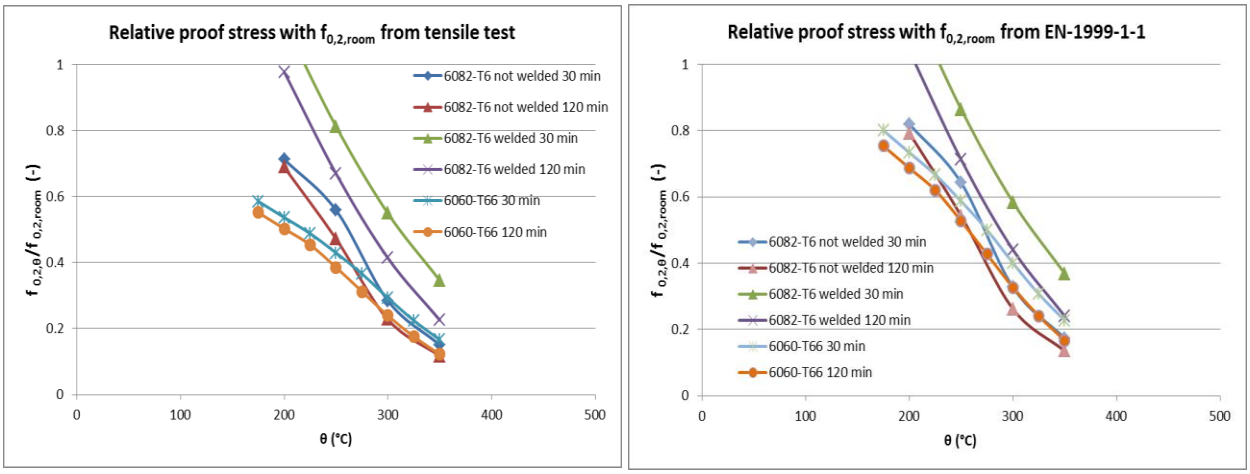

Figure 3.53 Relative 0.2% proof stress for welded and not welded 6082-T6 alloy and 6060-T66 alloy.

The difference can be attributed to the fact that Figure 3.51 is based on steady state tests and Figure 3.53 (left-hand figure) is based on transient state tests.

3.7 Chapter conclusions

The material parameters of the Dorn-Harmathy creep model have been determined in creep tests. The parameters are determined based on tests with a stepwise increasing temperature or stress level. Unfortunately, due to the error and slip in the LVDT not very consistent results are found for some of the parameters which are determined from the creep curves. Due to this, modifications in the parameters was needed for a better curve fit of the simulations. The transient state test results needed to be shifted down, to meet with the simulation of the transient state model. This error and slip in the LVDT could also be the reason for the high values for ε_{t0} and ε_{lim}. Also the impact of the different Zener-Holloman equations of the not welded specimens (Equation (3.10) and (3.11)) are investigated. Because of the fact that there is a sharp transition to fracture in the transient state test graphs, which means that the ε_{t0} parameter is close to 0, this parameter is excluded. In the first instance it seems to have been the right choice to exclude the ε_{t0} parameter for both types of specimens. This makes sense, because the sharp transition to fracture relates to a ε_{t0} parameter which is near by the value of 0. Because the primary creep parameter ε_{t0} relates to very small strains, slip in the LVDT at the beginning of the creep test, will cause very large deviations in the results to determine the ε_{t0} parameter. Considering the standard deviation of the ε_{t0} values obtained from the creep curves resulting from the not welded specimen tests is 0.0009 with a mean of 0.0010. The value of 0 is 1.1 standard deviations away from the mean of 0.0010. Considering the standard deviation of the ε_{t0} values obtained from the creep curves resulting from the welded specimen tests is 0.0063 with a mean of 0.0063. The value of 0 is 1.0 standard deviations away from the mean of 0.0010.

For specimens without a weld, it can be seen that either the change of the ε_{lim} factor to 0.00045 and the change of the Zener-Holloman equation to Eq. (3.10), will give good agreement with the measured and simulated strain development. However, the standard deviation of ε_{lim} values obtained from the creep curves resulting from the tests is 0.0019 with a mean of 0.0045. The value of 0.00045 is 2.13 standard deviations away from the mean of 0.0045. This result shows that it is very likely that the used Zener-Holloman Equation (3.11) in the simulation of the curves in paragraph 3.5.1, caused for the deviations in the results. The use of Equation (3.10), without the change of the measured ε_{lim} (0.0045) value from the test graphs, will give good agreement between the measured and simulated strain development.

For welded specimens it is clearly visible that the change of the values of ε_{t0} and ε_{lim} has ensured that the simulation are better in agreement to the test results. The large deviations in the determined ε_{lim} values from the creep curves of the welded specimens have caused the differences between the measured and simulated strain development. Considering the standard deviation of the ε_{lim} values obtained from the creep curves resulting from the tests is 0.0071 with a mean of 0.0085. The value of 0.0004 is 1.1 standard deviations away from the mean of 0.0085. This result shows that it is likely to assume that the value of ε_{lim} is determined wrong and needed to be approximately 0.0004.

Also from the coefficient of determination it is clearly visible that the simulations with the Zener-Holloman Equation (3.10) suits the best with the transient state results of the not welded specimens and that the simulation with ε_{lim}=0.0004 suits the best with the results of the transient state tests of the welded specimens. Table 3.9 shows the coefficient of determination of the simulations and the line in "perfect situation".

Table 3.9 Coefficient of determination of the simulations and the line in perfect situation.

R^2	Not welded specimens 0.4% strain	Not welded specimens 2% strain
Normal simulation	0.800	0.920
ε_{t0} excluded	0.964	0.911
ε_{lim} = 0.00045	0.952	0.946
Zener-Holloman Eq.(3.10)	0.979	0.963
R^2	**Welded specimens 0.4% strain**	**Welded specimens 2% strain**
Normal simulation	0.895	0.735
ε_{t0} excluded	0.944	0.588
ε_{lim} = 0.0004	0.986	0.978

Such like alloy 6060-T66 in [Maljaars, 2008], tertiary creep already started at low strains. In this first part of the tertiary creep stage (approximately up to 1.5%), there appears to be a linear relation between the strain and the strain rate. For larger strains, a distinct necking is developed. Due to the linear behavior between the strain rate and strain in the first part of the tertiary creep, the modified model of the Dorn-Harmathy model in [Maljaars, 2008] could also be used in this research. The same assumptions which are made in [Maljaars, 2008] are also made in this research.

With the adjustments of the parameters, the modified model showed good agreement with transient state tests. The difference in the temperature at $f_{0.2}$ between the model and tests of specimens without a weld is on average 4.5°C and the standard deviation is 3°C. The difference in the temperature at $f_{0.2}$ between the model and tests of welded specimens is on average also 4.5°C and the standard deviation is 4°C.

Stress-strain relations for aluminum alloys exposed to fire conditions are determined that can easily be used in fire design in practice. Small differences in the constitutive model parameters, made large differences in the stress-strain diagram. These differences where less seen in the curves of the $f_{0.2},\theta$ and f_2,θ. Comparing the results of the $f_{0.2},\theta$ values, obtained from the stress-strain curves of the experiments, with the data in [EN 1999-1-2, 2007], showed that the relative values $f_{0.2,\theta}/f_{0.2}$ of alloy 6082 (for welded and not welded specimens) in the standard are safe. This was also the case for alloy

6060-T66 in [Maljaars, 2008]. As an alternative, there can be chosen to use the standard of not welded specimens for the welded specimens. Till 250°C this will be an unsafe alternative, but after 250°C it can be seen that this will be a safe alternative.

The tests carried out at elevated temperature show that the difference in strength between the HAZ and the parent metal decreases with increasing temperature. At a temperature of approximately 300°C the 0.2% proof stress of the not welded and welded specimens meet each other, HAZ strength is equal to the strength of the parent metal at temperatures of 300 ºC and higher. This is due to the fact that the favorable metal structure obtained by a treatment is already destroyed by the heat input at welding. Consequently, heating by a fire has a smaller impact on the strength of the HAZ than on the strength of the treated parent metal. Also the difference between the strength of 6060-T66 and 6082-T6 alloys decreased with increasing strength. It is also seen that the relative values $f_{0.2,\theta}/f_{0.2,room}$ of the different types of specimens differ from each other, although they are from the same series and temper. Such a major difference is not seen in the data of [EN 1999-1-2, 2007] and [Kaufmann, 1999] between the alloys in the same series with the same temper. The difference can be attributed to the fact that data in [EN 1999-1-2, 2007] is based on steady state tests and provided in this research is based on transient state tests.

4. Microstructural analyses: difference of microstructure at elevated temperatures

In the previous chapter it has been shown that aluminum exhibit significant strength degradation at elevated temperature exposure. Microstructural damage could be the reason for this strength degradation. It has been found that the strength of the different type of specimens (welded and not welded) clearly differ from each other at low temperatures, but this difference in strength decreases with increasing temperatures. At temperatures around 300°C there is substantially no difference between the strength of the different types of specimens (welded and not welded).

This chapter will focus on the grain structure of the different type of specimens. Grain sizes of the different type of specimens will be investigated.

4.1 Experimental work

Grain sizes of welded and not welded specimens will be investigated. Specimens which are conducted to creep tests in the previous chapter are investigated. Also specimens which are only conducted to elevated temperature without a stress are investigated. Table 4.1 shows the selected test pieces to study the influence of grain structure. There has been a period of 7 months between the creep tests and microscopic tests. After the creep tests the specimens where immediately cooled by water flow. Also the specimens which are only conducted to elevated temperature are immediately cooled by water flow.

Table 4.1 Investigated specimens for grain size.

Specimen number	Welded
1W	Original specimen (without exposition of stress or heat. Only heat exposition during welding)
2W	Thermal exposed to 350°C in 30 minutes with heating rate of 11°C/min.
3W	Conducted to 300°C and 45 N/mm^2, 50 N/mm^2 and 55 N/mm^2 in steps.
	Not welded
1NW	Original specimen without exposition of stress of heat.
2NW	Thermal exposed to 350°C in 30 minutes with heating rate of 11°C/min.
3NW	Conducted to 300°C and 60 N/mm^2, 65 N/mm^2 and 70 N/mm^2 in steps.

Table 4.2 shows the steps which are followed during the experiments. Red lines in Figure 4.1 indicates where the specimens are cut.

Table 4.2 Followed steps for the microstructural analyze.

Step 1	Embedding of the test pieces. 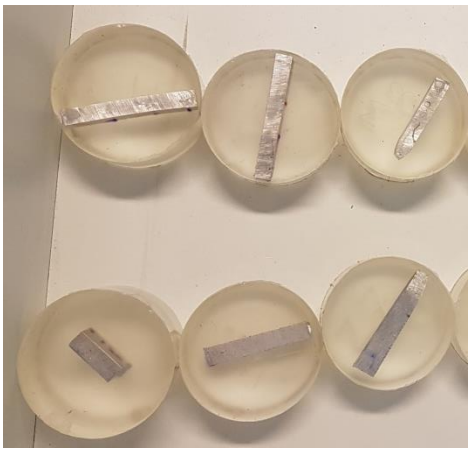
Step 2	Sanding of the test pieces. Sand from coarsest to finest grainsize. (P80 → P180 → P320 → P800 → P1200 → P 2000) 
Step 3	Polishing of the test pieces. After sanding the next step is polishing with polishing liquid in the following steps: 3µ → 1µ → 0.5µ. 
Step 4	Etching of the test pieces with a mixture of 3ml HF, 3ml HNO_3, 5ml HCl and 5ml H_2O.

	
Step 5	Investigation with microscope.  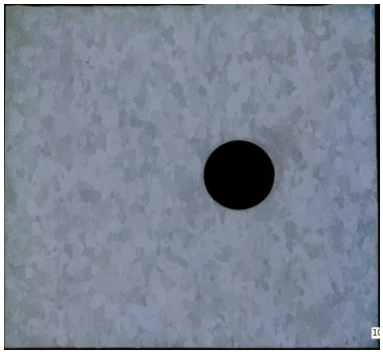

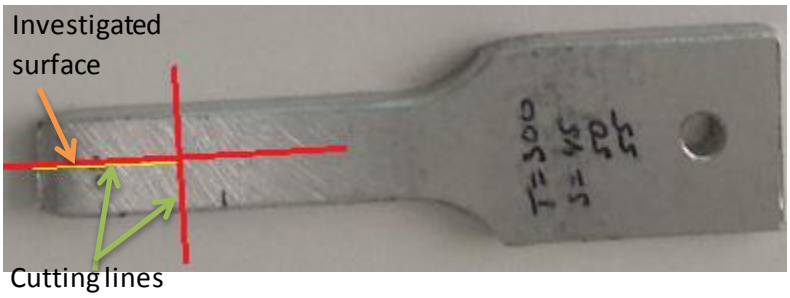

Figure 4.1 Red lines indicating where the specimens has been cut.

4.2 Discussion of the results

Figure 4.2 shows the grain structure of not affected base material of the not welded specimens. It can be noted that there is a large scatter in grain sizes. As the temperature increases to 350°C, the grain structure and size are still nearly equal to each other, see Figure 4.3. Table 4.3 shows the average grain area and standard deviation of the specimens showed in Figure 4.2 and 4.3. The areas in Table 4.3 are not measured with high precision, but are global approaches. It can be seen that there are more deviations in grain area in Figure 4.2. Exposure to 350°C without a force will not cause significantly changes in the average grain area. Figure 4.4 shows the grain structure of a not welded specimen exposed to 300°C and stresses of 60-65-70N/mm^2. It can be seen that the grains are stretched (in horizontal direction) in comparison of the not stressed specimens. The stretching is in the same direction as the applied loading direction.

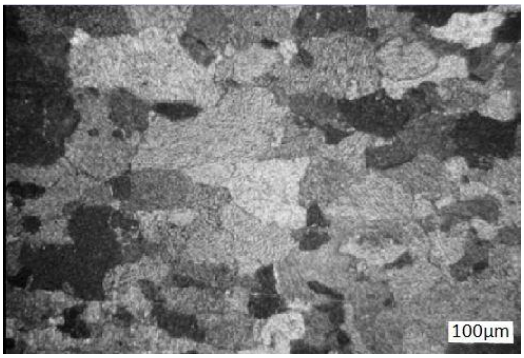

Figure 4.2 Grain structure not affected base material of a not welded specimen.

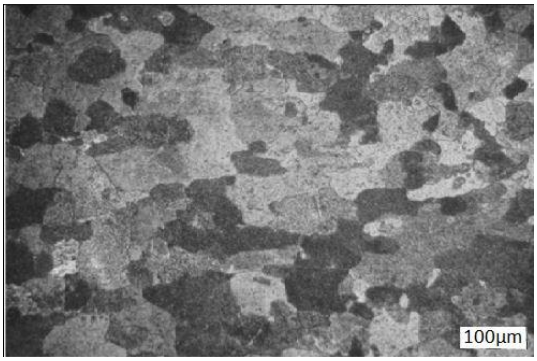

Figure 4.3 Grain structure of a not welded specimen conducted to 350°C .

Figure 4.4 Grain structure of a not welded specimen conducted to 300°C and 60 – 65 – 70 N/mm^2.

Table 4.3 Average grain area and standard deviation of grains in Figures 4.2 and 4.3.

	Average area of the grains	Standard deviation of the grain area	σ/µ
Specimen in Figure 4.2	77 µm^2	65 µm^2	0.84
Specimen in Figure 4.3	66 µm^2	32 µm^2	0.48

Figure 4.5 shows the grain structure of the original specimen (without exposition of stress or heat. Only heat exposition during welding) with a weld. The left hand side of the figure indicates the HAZ and the right hand side indicates the weld in the material. It can be noted that the grain size in the HAZ is smaller than the grain size in the weld. This is most likely caused by the heat during welding, which has ensured that the grains are reduces in size in the HAZ. Figure 4.6 shows the grain structure of a specimen conducted to a temperature of 350°C. Such as the not welded specimens, also in this figure there is not much difference in the grain sizes in comparison with the grains of the original specimen. Table 4.4 shows the average grain area and standard deviation of the specimens showed in Figure 4.5 and 4.6. The areas in Table 4.4 are not measured with high precision, but are global approaches. It seems like the grains in the weld have a small reduction in size. Figure 4.7 shows the grain structure of a welded specimen exposed to 300°C and stresses of 45-50-55N/mm^2. It can be seen that the grain sizes in the weld are reduced in size in comparison with Figures 4.5 and 4.6. Also stretched grains are visible which was also the case for the not welded specimens.

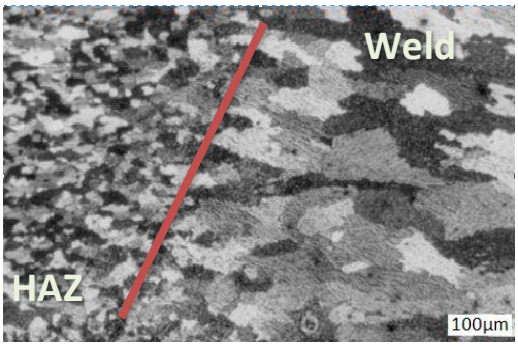

Figure 4.5 Grain structure not affected material of a welded specimen.

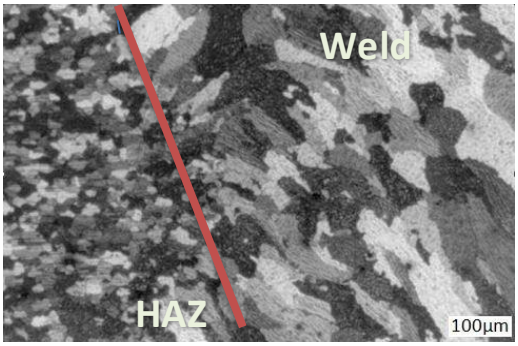

Figure 4.6 Grain structure of a welded specimen conducted to 350°C .

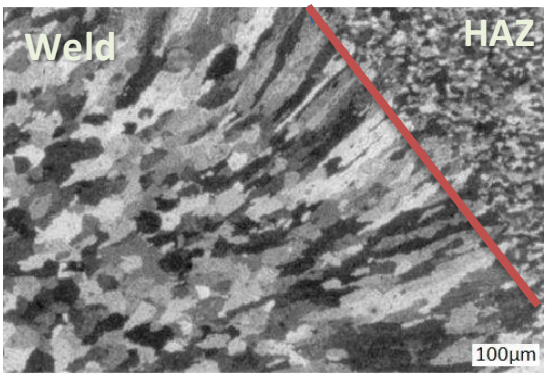

Figure 4.7 Grain structure of a welded specimen conducted to 300°C and 45 – 50 – 55 N/mm^2.

Table 4.4 Average grain area and standard deviation of grains in Figures 4.5 and 4.6.

	Average area of the grains in weld	Standard deviation of the grain area in weld	σ_{weld}/μ_{weld}	Average area of the grains in HAZ	Standard deviation of the grain area in HAZ	σ_{HAZ}/μ_{HAZ}
Specimen in Figure 4.5	68 μm^2	43 μm^2	0.63	3.9 μm^2	3.4 μm^2	0.87
Specimen in Figure 4.6	59 μm^2	35 μm^2	0.59	2.1 μm^2	1.6 μm^2	0.76

4.3 Chapter conclusions

This chapter shows the microstructural analyses of the welded and not welded specimens. The focus is on the grain size of the specimens. Unfortunately, a clear similarity between the grain size of the welded and not welded specimens is not seen on the investigated specimens. The similarity in strength at 300°C, does not mean that the grain structure will also be the same at this temperature. The only similarity is stretching of the grains when the specimens are conducted to stresses. In comparison with the grain sizes in the weld, the grain sizes in the HAZ are considerably smaller. This is probably caused by the heat during welding, which has ensured that the grains are reduces in size in the HAZ.

5. Practical case: design example of a column in compression

This chapter contains a practical case, where the material properties obtained in chapter 3 are used to determine the resistance of a column in compression. Flexural buckling of a column in compression will be determined.

5.1 Introduction

The Euler formula for the elastic critical buckling load of a slender column is the earliest engineering design formula that is still in use today. The history of this formula, together with its modifications by Engesser and Shanley for inelastic behavior, provides the basis for a verification method that has continuity over the past 239 years [Johnston, 2011]. In the case of structural steel, the stress-strain relationship is assumed to be linear up to the yield stress level, after which the material (on average) deforms plastically without change in stress until a strain is reached that is several times that of the elastic range. It is assumed the stress-strain relationships in tension and compression are identical and without variation throughout the member. If the column is made of a material with no sharply defined yield point, such as structural aluminum alloys, it is assumed that the stress is linearly related to strain up to a proportional limit and that for greater stress the strain increases at a continuously increasing strain rate with respect to stress.

The strength of a compression member (column) depends on its geometry (slenderness ratio L_{eff} / r) and its material properties (stiffness and strength).

The Euler buckling formula, Equation (5.1) describes the critical load for elastic buckling. The buckling force of a straight, centrally compressed, prismatic column in the elastic range is obtained from Euler's buckling formula.

$$F_{cr} = \frac{\mu \cdot E \cdot I \cdot \pi^2}{{l_{buc}}^2} \tag{5.1}$$

Where E denotes the modulus of elasticity, I the smallest moment of inertia of the cross-section and l_{buc} the buckling length of the column. μ is the coefficient of restraint depending on the manner in which the ends of the column are fixed. The value of this coefficient varies within the ranges $\frac{1}{4} \leq \mu \leq 4$. Figure 5.1 presents the value of μ in some modes of restraint. The case 2 of a column with hinged ends is very often encountered in practical applications.

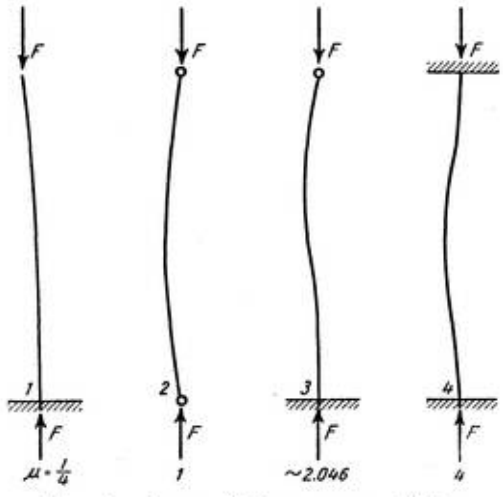

Figure 5.1 Some fixing cases of the ends of the column.

Expressing in Equation (4.1) the moment of inertia I by the radius of gyration i and the area A of the cross section in the form $I = i^2 A$, the formula may be written in the form of Equation (5.2) for the buckling stress.

$$\frac{F_{cr}}{A} = \sigma_{cr} = \frac{\mu \cdot E \cdot \pi^2}{\left(\frac{l_{buc}}{i}\right)^2} \tag{5.2}$$

With $\frac{l_{buc}}{i}$ the slenderness ratio of the column.

Euler's formulas in Equation (5.1) and (5.2) are valid only as far as the compressive stress $\sigma_{cr} < \sigma_p$.

Buckling occurring after the stress in the column exceeds the proportional limit of the column material and before the stress reaches the ultimate strength, is called inelastic buckling. Some buckling theories appropriate for inelastic material behavior are the tangent modulus theory, the Secant modulus theory and the theory of Shanley.

Suppose that the critical stress σ_{cr} in an intermediate column exceeds the proportional limit of the material σ_{pl}, the Young's modulus at that particular stress-strain point is no longer E. Instead, the Young's modulus decreases to the local tangent value, E_t. Replacing the Young's modulus E in the Euler's formula with the tangent modulus E_t, the critical load becomes Equation (5.3).

The Secant Modulus theory defines a Secant Young's modulus E_s to compensate for the underestimation given by the tangent-modulus theory.

Tangent-modulus assumed the material to be perfectly elastic even beyond the proportional limit and thus had not taken into consideration the effect of permanent deformations. In fact, when the compressive stress in Figure 5.2 has increased up to point C above the proportional limit σ_{pl} and the column bends, the decreasing stress on the convex side of the column does not under actual conditions follow the same curve CBO along which the stress has increased, but decreases from point C along the straight line C E. According to the secant modulus theory, the effect of permanent deformations in the inelastic buckling phenomenon can be taken into consideration by replacing the tangent modulus in formulas by the so-called "secant modulus".

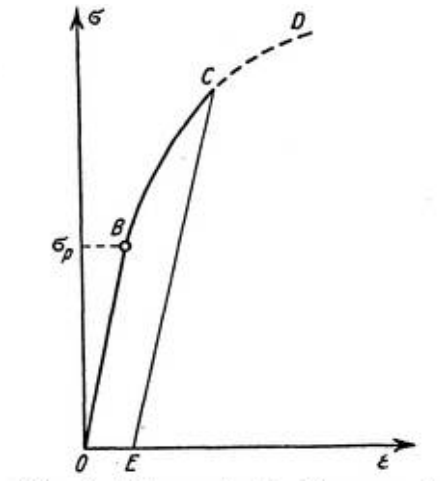

Figure 5.2 Stress-strain diagram for increase and decrease of load.

In the elastic range E_s equals E, while in the inelastic range E_s is variable and depends on $\sigma_s = \frac{F_s}{A}$ and on the shape of the cross section. In the inelastic range E_s is always greater than E_t and, consequently, the buckling stress will be slightly higher according to the secant modulus theory than according to the tangent modulus theory. The definition of the tangential modulus of elasticity E_t and the secant modulus of elasticity E_s is given in Figure 5.3. The figure shows that the value of E_t depends on the strain ε.

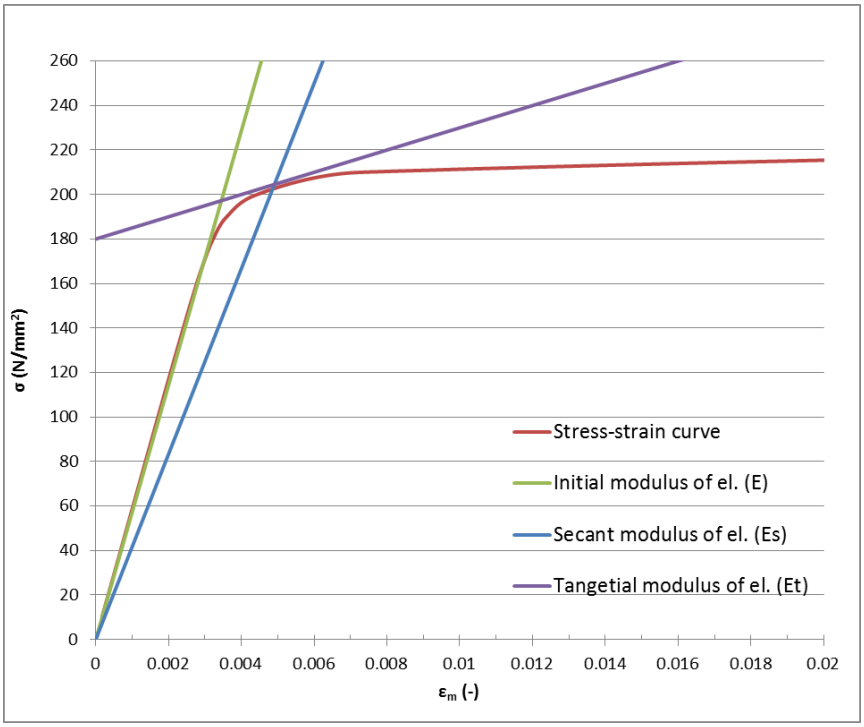

Figure 5.3 Definition of the tangential modulus of elasticity E_t and the secant modulus of elasticity E_s.

Both tangent-modulus theory and secant-modulus theory were accepted theories of inelastic buckling until Shanley [Shanley, 1946] published his logically correct paper in 1946. The critical load of inelastic buckling is in fact a function of the transverse displacement w.

Shanley showed that in case of inelastic material, the modulus of elasticity in Equation (5.1) should be replaced by the tangential modulus of elasticity E_t. In an iterative process, the value of F_{cr} should be found for which the stress at buckling corresponds to the strain at E_t. In [Maljaars et. al, 2009b], the model of Shanley is used as a basis of a design model for the ultimate buckling resistance of fire exposed aluminum columns subjected to flexural buckling.

5.2 Design model in Eurocode [EN 1999-1-1, 2007] and [EN 1999-1-2, 2007]

Eurocode 9 gives design models for load bearing structures of aluminium, to be used by designers and engineers. Part 1-1 of this code, [EN 1999-1-1, 2007], gives general rules. Part 1-2, [EN 1999-1-2, 2007] gives rules for structural fire design. To evaluate the structural response to fire exposure, [EN 1999-1-2, 2007] provides the possibility to divide the structure into individual members and to verify each member, for which simple calculation models are provided.

In the simple calculation models in [EN 1999-1-1] the elastic critical buckling load is applied. At room temperature, the design model consists of two steps. First, the relative slenderness is determined according to Equation (5.3). Subsequently, the relative buckling resistance χ is determined using a buckling curve. χ depends not only on the value of λ_{rel}, but also on the curvature of the stress–strain relationship. In order to account for this, the alloys in EN 1999-1-1 are divided into two classes, and different buckling curves are provided for these classes.

Buckling curves defined in the Eurocode for aluminum give the ultimate buckling resistance as a function of a parameter called the relative slenderness, see Figure 5.4 with the relative slenderness on the horizontal axes and the buckling factor on the vertical axes. In order to obtain the ultimate buckling resistance, the buckling factor should be multiplied with the cross-sectional resistance. Curve 1 in Figure 5.1 should be applied for alloys in material class A and with material characteristics approaching an elastic-perfectly plastic behavior, while curve 2 should be applied for alloys in material class B for which the proportional limit is considerably lower than the 0.2% proof stress.

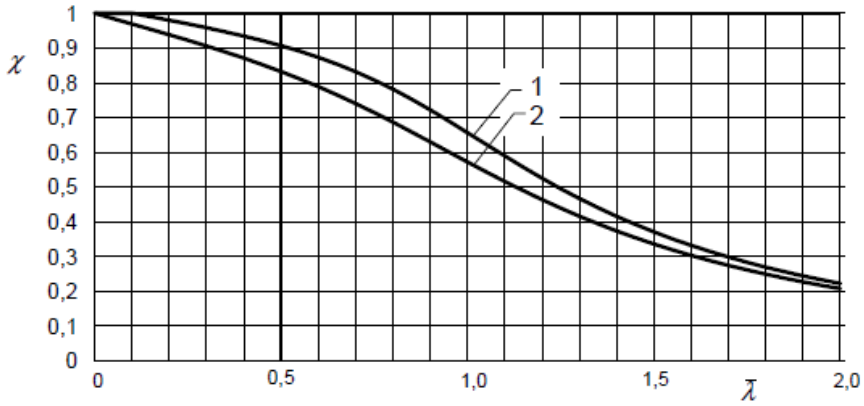

Figure 5.4 Buckling curves defined in[EN 1999-1-1].

The relative slenderness can be determined using Equation (5.3) and the elastic critical buckling load follow from Equation (5.4).

$$\lambda_{rel} = \sqrt{\frac{N_{pl}}{F_{cr}}} = \sqrt{\frac{Af_{0.2}}{F_{cr}}} = \sqrt{\frac{A \cdot {L_k}^2}{\pi^2 \cdot I_y}} \cdot \sqrt{\frac{f_{0.2}}{E}} \tag{5.3}$$

$$F_{cr} = \frac{\mu \cdot E \cdot I \cdot \pi^2}{{l_{buc}}^2} \tag{5.4}$$

Equation (5.3) shows that the relative slenderness depends on the ratio between the 0.2% proof stress $f_{0.2}$ and the modulus of elasticity E. A large value of this relative slenderness, corresponding to a slender column, indicates that the column is sensitive to buckling, while a small value, corresponding to a stocky column, indicates that failure is dominated by reaching the plastic capacity.

[EN 1999-1-2] gives a simple calculation model for flexural buckling of fire exposed aluminum columns. Due to limited research into fire exposed aluminum structures, some of the design models in [EN 1999-1-2] are based on conservative approximations. In this model, χ_θ is taken equal as χ at room temperature. This follows from the approximations that λ_θ equals λ at room temperature and that the buckling curves at room temperature are also applicable at elevated temperature. In particular, the design model for flexural buckling of columns is based on the assumption that the reduction as a function of temperature of the modulus of elasticity E_θ/E is equal to the reduction of the 0.2% proof stress $f_{0.2,\theta}/f_{0.2,20°C}$ in case of aluminum alloys. A direct consequence of this assumption is that the relative slenderness at elevated temperature equals the relative slenderness at room temperature: $\lambda_{rel,\theta} = \lambda_{rel,20°C}$.

The ratio between the reduction coefficient of the modulus of elasticity and the relative value of the 0.2% proof stress of the alloys listed in [EN 1999-1-2] generally increases at increasing temperature. Consequently, the calculation model overestimates the value for the relative slenderness at elevated temperature. This may lead to conservative ultimate buckling resistance at elevated temperatures.

In order to take creep into account in the verification rules for columns, [EN 1999-1-2] specifies a factor with which the design value of the load should be multiplied. The value for this factor is specified at 1.2, independent of the elevated temperature and the time of exposure to this temperature. The value for this creep factor is not based on experimental or numerical data. The ultimate buckling resistance in fire $F_{u,\theta}$ is subsequently determined with Equation (5.5).

$$F_{u,\theta} = \frac{\chi_{20°C} \cdot A \cdot f_{0.2,\theta}}{1.2 \cdot \gamma_{fi}} \tag{5.5}$$

The recommended value for the partial factor γ_{fi} is equal to 1.0.

Thus in case of global buckling phenomena, [EN 1999-1-2] provides simple calculation models. These are however validated with tests. The application of a creep factor of 1.2 and the determination of the relative slenderness in [EN1999-1-2] are subject of discussion.

5.3 The method proposed by Maljaars, Soetens and Twilt [Maljaars et. al, 2009b]

A more refined calculation model is developed allowing for the above points [Maljaars et. al, 2009b]. The influence of creep is implicitly taken into account in the derivation of the transient-state stress-strain curves. The new calculation model is based on these stress-strain curves, meaning that an explicit creep factor in the model is not required.

As mentioned before Shanley [Shanley, 1946] proposed an analytical model to determine the critical buckling load of columns with a curved stress–strain relationship. This so-called inelastic critical buckling load $F_{cr,inel,\theta}$ is represented by Equation (5.6), whereby the tangential stiffness $E_{T,\theta}$ in Equation (5.7) is used.

$$F_{cr,inel,\theta} = \frac{E_{T,\theta} \cdot I \cdot \pi^2}{{l_{buc}}^2} \tag{5.6}$$

$$E_{T,\theta} = \frac{d\sigma}{d\varepsilon} \tag{5.7}$$

Equations (5.6) and (5.7) are used as a basis of a design model for the ultimate buckling resistance of fire exposed aluminum columns subjected to flexural buckling.

The tangential stiffness can be described using the parameters of the Ramberg-Osgood relationship in Equation (2.1), see Equation (5.8).

$$E_{t,\theta} = \frac{E_\theta}{1 + \left(\frac{E_\theta 0.002 n_\theta}{f_{0.2,\theta}}\right)\left(\frac{\sigma}{f_{0.2,\theta}}\right)^{n_\theta - 1}} \tag{5.8}$$

Applying Equation (5.8) into Equation (5.6), and applying the substitution of $\sigma = \frac{F_{cr,inelastic}}{A}$, gives Equation (5.9).

$$\frac{F_{cr,inelastic,\theta}}{A} + E_\theta 0.002 n_\theta \left(\frac{F_{cr,inelastic,\theta}}{A f_{0.2,\theta}}\right)^{n_\theta} = \frac{E_\theta I \cdot \pi^2}{A\, {l_{buc}}^2} \tag{5.9}$$

Knowing the parameters of the Ramberg-Osgood relationship and the geometrical properties I and A, Equation (5.9) allows the determination of $F_{cr,inelastic,\theta}$.

Further, the inelastic relative slenderness $\lambda_{rel,inelastic,\theta}$ is determined in Equation (5.10).

$$\lambda_{rel,inelastic,\theta} = \sqrt{\frac{Af_{0.2,\theta}}{F_{cr,inel,\theta}}} \tag{5.10}$$

The relative buckling resistance χ_θ plotted as a function of $\lambda_{rel,inelastic,\theta}$ determined in the research is shown in Figure 5.5.

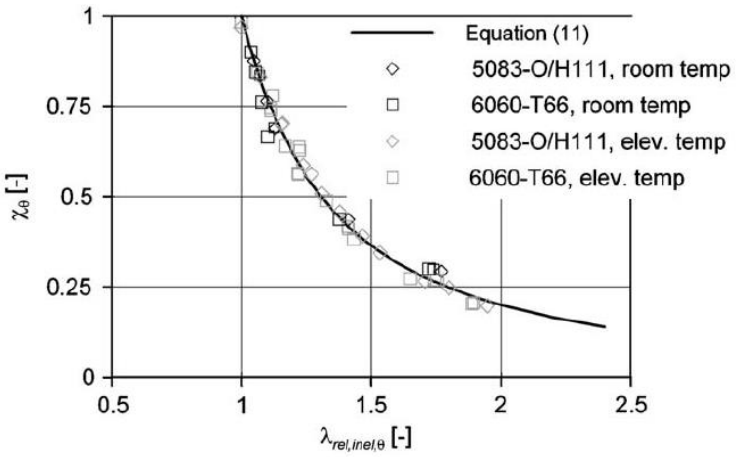

Figure 5.5 Buckling curve defined in [Maljaars et. al, 2009b].

Equation (5.11) shows the function of the determined buckling curve.

$$\chi_\theta = \frac{1}{\lambda^2_{rel,inel,\theta}} - \frac{0.8}{\lambda^3_{rel,inel,\theta}} + \frac{0.8}{\lambda^4_{rel,inel,\theta}} \tag{5.11}$$

The ultimate buckling resistance then arises as in Equation (5.12).

$$F_{u,\theta} = \chi_\theta \cdot A \cdot f_{0.2,\theta} \tag{5.12}$$

Because of the influence of creep is already incorporated in the proposed stress-strain curves based on transient state experiments, it is not necessary to take creep explicitly into account in the equations.

A prerequisite for the application of the new design model is the availability of transient state stress–strain relationships for aluminum alloys.

5.4 Hand calculation column in compression

The two calculation models discussed in the previous chapters (4.2 and 4.3) will be used to calculate the column in compression for flexural buckling. On the basis of this calculation, the two methods will be compared with each other.

5.4.1 Material properties, dimensions and loads on the column

The statically determined column in Figure 5.6 will be used in the calculations.

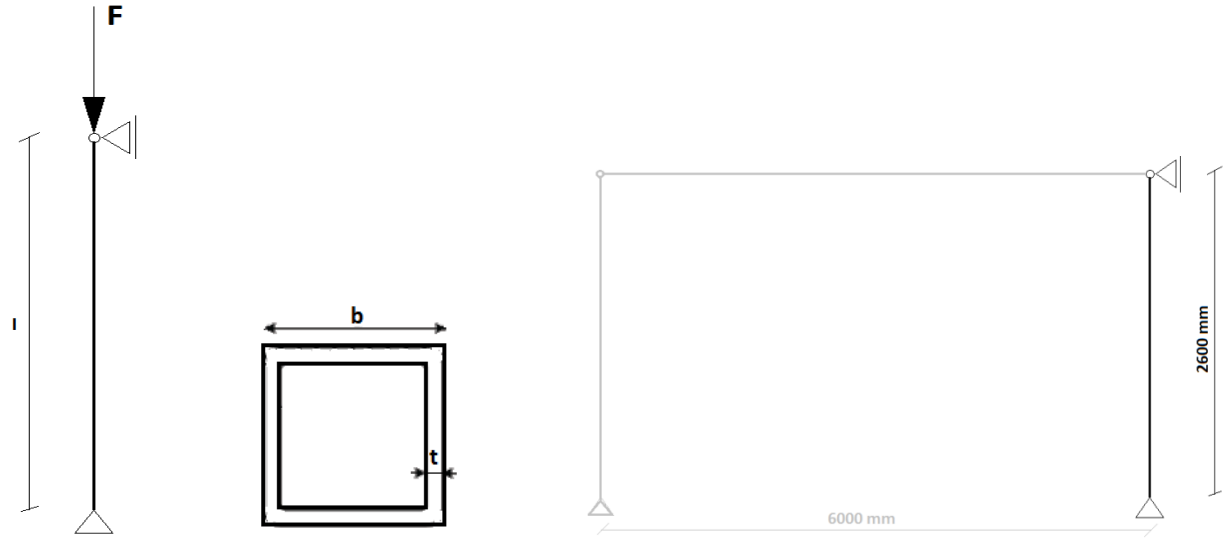

Figure 5.6 Column which will be calculated in the hand calculation and a schematization of the floor against the column.

The column is a square hollow section profile with a length of 2600mm and b=100mm and t=5.5mm. The governing failure mechanism of the column will be global buckling. The shapes and dimensions of the beam do not reflect an optimal design. The reason to apply these dimensions is to give some examples of the application of the design model. A uniform temperature distribution is assumed.

In a real frame, the connections between the beam and the columns will generate eccentricity by the load application in the columns. This load eccentricity is not considered in this example. In real design, this eccentricity will reduce the load bearing capacity, and may not be neglected.

All members are composed of alloy 6082-T6, with the mechanical properties in this research. The mechanical properties in fire are according to the derived stress-strain curves in Annex F.1.

For the calculation of the column, it is assumed that there is a floor against the column, see Figure 4.6. So there will also forces from the floor to the column. Table 5.1 shows the material properties, dimensions and loads which are used in the hand calculation.

The required fire resistance period is 30 minutes. The heating rate of the member is 9.3°C/min and the temperature after 30 minutes is 300°C.

Table 5.1 Material properties, dimensions and loads which are used in the hand calculation.

Material properties	
Measured 0.2 % proof stress	$f_{0.2,20℃} = 299\ N/mm^2$
Modulus of elasticity ambient temperature	$E = 65000\ N/mm^2$
0.2 % proof stress in fire of 30 minutes	$f_{0.2,\theta} = \left(212 - 45 \cdot \frac{\theta - 200}{50}\right) N/mm^2\ if\ 200℃ \leq \theta \leq 250℃$ $f_{0.2,\theta} = \left(167 - 82 \cdot \frac{\theta - 250}{50}\right) N/mm^2\ if\ 250℃ < \theta \leq 300℃$ $f_{0.2,\theta} = \left(85 - 40 \cdot \frac{\theta - 300}{50}\right) N/mm^2\ if\ 300℃ < \theta \leq 350℃$
Modulus of elasticity in fire	$E_\theta(\theta) = 65000 - 10 \cdot \theta - 0.21 \cdot \theta^2 N/mm^2$
Parameter n_θ in Ramberg-Osgood equation	$n_{200℃} = 40$ $n_{250℃} = 11$ $n_{300℃} = 6$ $n_{350℃} = 6$
Dimensions	
Width of the column *b*	80 mm
Thickness of the column *t*	5 mm
Height of the column	2600 mm
Width of the floor	6000 mm
Distance between columns	4500 mm
Loads	
Floor	$q_{rep,floor} = 3.5\ kN/mm^2$ $g_{rep,floor} = 3.0\ kN/mm^2$
Normal force on column, ambient temperature	$F_{Sd} = \left(\left(\gamma_Q \cdot 3.0 + \gamma_G \cdot 3.5\right) \cdot 4.5 \cdot \left(\frac{1}{2} \cdot 6.0\right)\right)$ $= \left((1.5 \cdot 3.0 + 1.2 \cdot 3.5) \cdot 4.5 \cdot (0.5 \cdot 6.0)\right)$ $= 117.45\ kN$
Normal force on column, fire	$F_{Sd,\theta} = \left(\left(3.0 + 3.5 \cdot \psi_{floor}\right) \cdot 4.5 \cdot \left(\frac{1}{2} \cdot 6.0\right)\right)$ $= \left((3.0 + 3.5 \cdot 0.5) \cdot 4.5 \cdot (0.5 \cdot 6.0)\right) = 64.13\ kN$

5.4.2 Calculation at ambient temperature

Table 5.2 shows the steps which should be followed for the hand calculation for flexural buckling of columns at ambient temperature. The hand calculation is proposed with [EN 1999-1-1, 2007] and material properties from the uniaxial tensile test at ambient temperature is used. Also the load bearing capacity obtained with the use of the steady state material properties from [EN 1999-1-1, 2007] can be seen in parenthesis at step 4.

Table 5.2 Steps in the hand calculation in [EN 1999-1-1] at ambient temperature.

Step	What to do?	Equation	
1	Determine the elastic critical load for flexural buckling	$F_{cr} = \frac{\pi^2 \cdot E \cdot I}{{l_{buc}}^2}$	$l_{buc} = 2600\ mm.$ $I = \frac{80^4 - (80 - 2 \cdot 5)^4}{12}$ $= 1.41 \cdot 10^6\ mm^4$ $F_{cr} = \frac{\pi^2 \cdot 65000 \cdot 1.41 \cdot 10^6}{2600^2}$ $= 134\ kN$
2	Determine the relative slenderness for flexural buckling	$\lambda_{rel} = \sqrt{\frac{A \cdot f_{0.2}}{F_{cr}}}$	$A = 90^2 - (90 - 2 \cdot 5)^2$ $= 1.5 \cdot 10^3\ mm^2$ $\lambda_{rel} = \sqrt{\frac{1.5 \cdot 10^3 \cdot 299}{134 \cdot 10^3}}$ $= 1.83$
3	Determine the relative resistance χ of the column. Using the parameters $\alpha = 0.2$ and $\bar{\lambda}_0 = 0.1$ of class A alloys.	$\chi = \frac{1}{\phi + \sqrt{\phi^2 - \lambda^2}}$ $\phi = 0.5(1 + \alpha(\lambda - \lambda_0) + \lambda^2)$	$\phi = 0.5(1 + 0.2(1.83 - 0.1) + 1.83^2)$ $= 2.35$ $\chi = \frac{1}{2.35 + \sqrt{2.35^2 - 1.83^2}}$ $= 0.26$
4	Determine the load bearing capacity of the column with $\gamma_{fi} = 1.0$	$F_u = \chi \cdot A \cdot f_{0.2}$	$F_u = 0.26 \cdot 1.5 \cdot 10^3 \cdot 299$ $= 117.6\ kN\ (114.7\ kN)$

5.4.3 Calculations at elevated temperature

Table 5.3 shows the steps which should be followed for the hand calculation for flexural buckling of columns at elevated temperature. The hand calculation in Table 5.3 is proposed with [EN 1999-1-2, 2007] and material properties from the transient state tests is used. The results at $\theta = 300℃$ are showed in this table. Also the load bearing capacity obtained with the use of the steady state material properties from [EN 1999-1-2, 2007] can be seen in parenthesis at step 4.

Table 5.3 Steps in the hand calculation in [EN 1999-1-2] at elevated temperature.

Step	What to do?	Equation	
1	Determine the elastic critical load for flexural buckling at $300℃$.	$F_{cr} = \frac{\pi^2 \cdot E \cdot I}{l_{buc}{}^2}$	$l_{buc} = 2600\ mm.$ $I = \frac{80^4 - (80 - 2 \cdot 5)^4}{12}$ $= 1.41 \cdot 10^6\ mm^4$ $F_{cr} = \frac{\pi^2 \cdot 65000 \cdot 1.41 \cdot 10^6}{2600^2}$ $= 134\ kN$
2	Determine the relative slenderness for flexural buckling	$\lambda_{rel} = \sqrt{\frac{A \cdot f_{0.2}}{F_{cr}}}$	$A = 80^2 - (80 - 2 \cdot 5)^2$ $= 1.5 \cdot 10^3 mm^2$ $\lambda_{rel} = \sqrt{\frac{1.5 \cdot 10^3 \cdot 299}{134 \cdot 10^3}}$ $= 1.83$
3	Determine the relative resistance χ of the column. Using the parameters $\alpha = 0.2$ and $\bar{\lambda}_0 = 0.1$ of class A alloys.	$\chi = \frac{1}{\phi + \sqrt{\phi^2 - \lambda^2}}$ $\phi = 0.5(1 + \alpha(\lambda - \lambda_0) + \lambda^2)$	$\phi = 0.5(1 + 0.2(1.83 - 0.1) + 1.83^2)$ $= 2.35$ $\chi = \frac{1}{2.35 + \sqrt{2.35^2 - 1.83^2}}$ $= 0.26$
4	Determine the load bearing capacity of the column with $\gamma_{fi} = 1.0$	$F_{u,300℃} = \frac{\chi_{20℃} \cdot A \cdot f_{0.2,300℃}}{1.2 \cdot \gamma_{fi}}$	$F_{u,300℃} = \frac{0.36 \cdot 5 \cdot 85}{1.2 \cdot 1.0}$ $= 27.85\ kN \quad (17.04\ kN)$

In the calculation in Table 5.3, the relative slenderness and relative resistance for flexural buckling are determined with the material properties at room temperature. The obtained resistance is subsequently divided by a creep factor of 1.2. Because it is not known whether the creep factor of 1.2 is conservative or not, also a calculation with the design model in [EN 1999-1-1, 2007] with the obtained material

properties from transient state tests at the temperature considered is applied. While in Table 5.3 the material properties considered with transient state tests at the temperature considered was only used at step 4, in Table 5.4 the obtained material properties will be applied from the beginning of the calculation. So ultimately it is not necessary to apply the creep factor of 1.2, because creep is already incorporated in the material properties at elevated temperature. This calculation can be seen in Table 5.4.

Table 5.4 Hand calculation with [EN 1999-1-1] with material properties at elevated temperature.

Step	What to do?	Equation	
1	Determine the elastic critical load for flexural buckling at $300℃$.	$F_{cr,300℃} = \frac{\pi^2 \cdot E_{300℃} \cdot I}{l_{buc}{}^2}$	$l_{buc} = 2600\ mm.$ $I = \frac{80^4 - (80 - 2 \cdot 5)^4}{12}$ $= 1.41 \cdot 10^6\ mm^4$ $E_\theta(\theta) = 65000 - 10 \cdot 300 - 0.21 \cdot 300^2$ $= 43100 N/mm^2$ $F_{cr} = \frac{\pi^2 \cdot 43100 \cdot 1.41 \cdot 10^6}{2600^2}$ $= 88.89\ kN$
2	Determine the relative slenderness for flexural buckling	$\lambda_{rel,300℃} = \sqrt{\frac{A \cdot f_{0.2,300℃}}{F_{cr,300℃}}}$	$A = 80^2 - (80 - 2 \cdot 5)^2$ $= 1.5 \cdot 10^3\ mm^2$ $\lambda_{rel} = \sqrt{\frac{1.5 \cdot 10^3 \cdot 85}{88.89 \cdot 10^3}}$ $= 1.2$
3	Determine the relative resistance χ of the column. Using the parameters $\alpha = 0.32$ and $\bar{\lambda}_0 = 0$ of class B alloys.	$\chi_{300℃} = \frac{1}{\phi + \sqrt{\phi^2 - \lambda^2}}$ $\phi = 0.5(1 + \alpha(\lambda - \lambda_0) + \lambda^2)$	$\phi = 0.5(1 + 0.32(1.2 - 0) + 1.2^2)$ $= 1.41$ $\chi_{300℃} = \frac{1}{1.41 + \sqrt{1.41^2 - 1.2^2}}$ $= 0.46$
4	Determine the load bearing capacity of the column with $\gamma_{fi} = 1.0$	$F_{u,300℃} = \chi_{300℃} \cdot A \cdot f_{0.2,300℃}$	$F_{u,350℃} = 0.46 \cdot 1500 \cdot 85$ $= 59.3\ kN$

Table 5.5 shows also the steps which should be followed for the hand calculation for flexural buckling of columns at elevated temperature. The hand calculation in Table 5.5 is proposed with [Maljaars et. al, 2009b]. The results at $\theta = 300℃$ are showed in this table.

Table 5.5 Steps in the hand calculation in [Maljaars et. al, 2009b] at elevated temperature.

Step	What to do?	Equation	
1	Determine the inelastic critical load $F_{cr,inelastic,\theta}$ for flexural buckling with iterative process.	$\frac{F_{cr,inelastic,\theta}}{A} + E_\theta 0.002 n_\theta (\frac{F_{cr,inelastic,\theta}}{A f_{0.2,\theta}})^{n_\theta} = \frac{E_\theta I \cdot \pi^2}{A\ l_{buc}{}^2}$	$A = 90^2 - (90 - 2\cdot 5)^2 = 1.7 \cdot 10^3\ mm^2$ $I = \frac{80^4 - (80 - 2\cdot 5)^4}{12} = 1.41 \cdot 10^6\ mm^4$ $\frac{F_{cr,inelastic,300℃}}{1700} + 43100 \cdot 0.002 \cdot 6(\frac{F_{cr,inelastic,300℃}}{1700 \cdot 85})^6 = \frac{43100 \cdot 2.054 \cdot 10^6 \cdot \pi^2}{1700\ 2600^2}$ ➔ $F_{cr,inelastic,300℃} = 69.15$ kN
2	Determine the inelastic slenderness $\lambda_{rel,inelastic,\theta}$ for flexural buckling	$\lambda_{rel,inelastic,\theta} = \sqrt{\frac{A f_{0.2,\theta}}{F_{cr,inel,\theta}}}$	$\lambda_{rel,inelastic,300℃} = \sqrt{\frac{1500 \cdot 85}{69.15 \cdot 10^3}} = 1.36$
3	Determine the inelastic resistance χ_θ of the column.	$\chi_\theta = \frac{1}{\lambda^2_{rel,inel,\theta}} - \frac{0.8}{\lambda^3_{rel,inel,\theta}} + \frac{0.8}{\lambda^4_{rel,inel,\theta}}$	$\chi_{300℃} = \frac{1}{1.36^2} - \frac{0.8}{1.36^3} + \frac{0.8}{1.36^4} = 0.46$
4	Determine the load bearing capacity of the column with	$F_{u,\theta} = \chi_\theta \cdot A \cdot f_{0.2,\theta}$	$F_{u,300℃} = 0.46 \cdot 1500 \cdot 85 = 58.41\ kN$

5.5 Chapter conclusions

This chapter shows the application of different design models for flexural buckling of a column. The different ultimate resistances at different elevated temperatures are calculated and compared with each other.

Table 5.6 shows the ultimate resistance for flexural buckling of the calculated column for different temperatures. The design model in [Maljaars et. al, 2009b] is named as the new model. Also the values of the unity check are shown in this table. Table 5.7 shows which property is used for the calculation of the F_u.

Figure 5.7 shows the ultimate resistance, calculated with the different design models, as a function of the temperature. Figure 5.8 shows the relative resistance of the different design models. It can clearly be seen that the design model in [EN 1999-1-2, 2007] is conservative in comparison with the design model in [Maljaars et. al, 2009b]. The maximum difference in relative ultimate resistance $F_{u,\theta}/F_{u,room}$ between [EN 1999-1-2, 2007] and [Maljaars et. al, 2009b] is 0.26 (31 kN) at a temperature of 300°C. A smaller difference can be seen between the ultimate resistance calculated with the model in [1999-1-1, 2007] (with the determined properties for elevated temperatures) and the model in [Maljaars et. al, 2009b]. The maximum difference in relative ultimate resistance $F_{u,\theta}/F_{u,room}$ between [EN 1999-1-1, 2007] and [Maljaars et. al, 2009b] is 0.04 (4.43 kN) at a temperature of 200°C.

Figure 5.9 shows the unity check, calculated with the different design models, as a function of the temperature. Also here it is clearly visible that the design model in [EN 1999-1-2, 2007] is very conservative in comparison with the other two design models. So it can be concluded that it is more appropriate to determine the material slenderness with the material properties at elevated temperature.

Table 5.6 Ultimate resistance for flexural buckling of the column at different temperatures.

θ	EN 1999-1-1	EN1999-1-2	New model	EN 1999-1-2 Steady state	Unity check Fsd/ EN 1999-1-1	Unity check Fsd/ EN 1999-1-2	Unity check Fsd/ New model	Unity check Fsd/ EN 1999-1-2 steady state
20 °C	117.58 kN			115.85 kN	1.0			1.01
200 °C	89.05 kN	69.47 kN	90.89 kN	62.75 kN	0.72	0.92	0.71	1.02
250 °C	78.50 kN	54.72 kN	82.93 kN	36.69 kN	0.82	1.17	0.77	1.75
300 °C	59.28 kN	27.85 kN	58.41 kN	17.04 kN	1.08	2.30	1.10	3.76
350 °C	40.31 kN	14.75 kN	35.44 kN	10.62 kN	1.59	4.35	1.81	6.04

Table 5.8 shows the critical temperature and fire resistance in minutes determined from Figure 5.9. The required fire resistance period is 30 minutes. The heating rate of the member is 9.3℃/min and the temperature after 30 minutes is 300℃.

Table 5.7 Use of different models for the calculation of ultimate resistance load F_u.

Calculation of F_u with design model:	Used $f_{0.2,20℃}$ from	k_0 value from
1999-1-1	Transient state test	Transient state
1999-1-2	Transient state test	Transient state
New model	Transient state test	Transient state
1999-1-2 steady state	EN 1999-1-1	EN 1999-1-2

Table 5.8 Critical temperature and fire resistance in minutes of different models.

	Critical temperature θ_{cr} in °C	Fire resistance in minutes
EN 1999-1-1	290	31
EN1999-1-2	225	24
New model	290	31

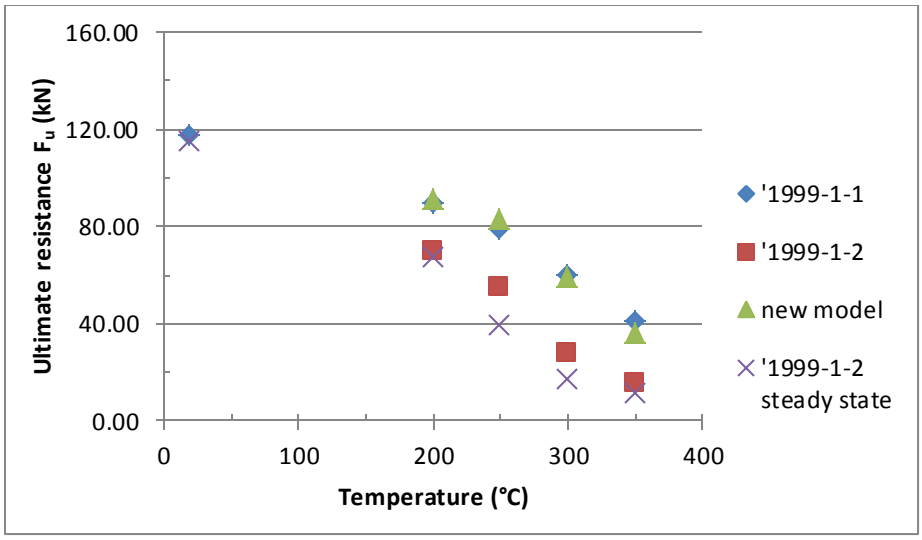

Figure 5.7 Ultimate resistance as a function of the temperature for different design models.

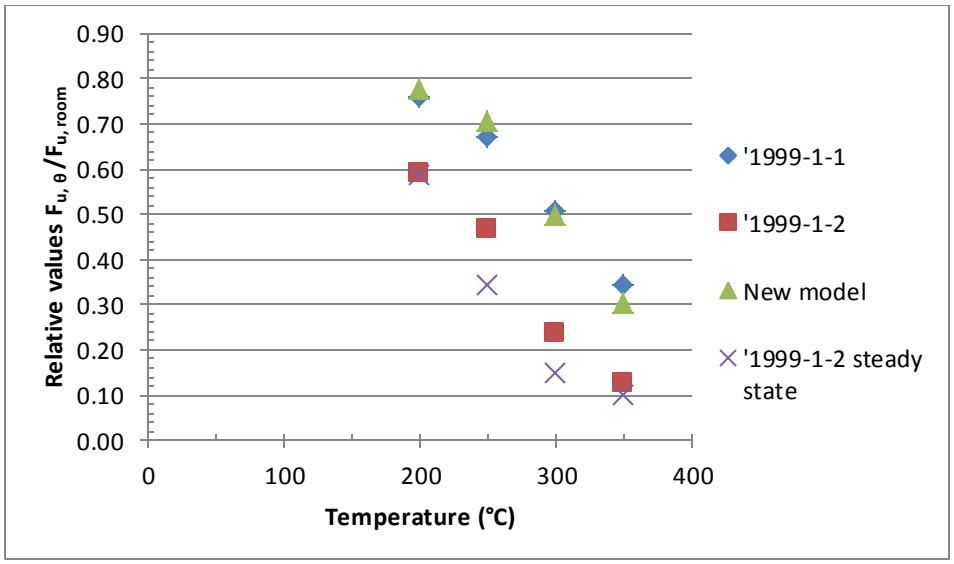

Figure 5.8 Relative values $F_{u,\theta}/F_{u,room}$ for different design models.

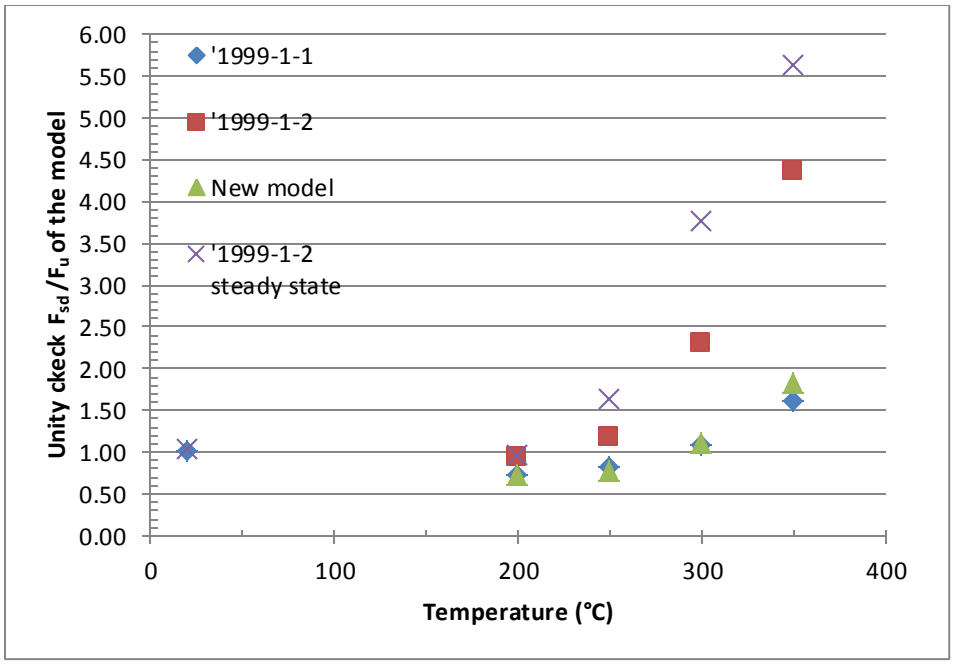

Figure 5.9 Unity check as a function of the temperature for different design models.

[EN 1999-1-2, 2007] is conservative because the relative buckling resistance is taken equal to the value at room temperature $\chi_\theta = \chi_{20℃}$. This is based on the assumption that the reduction as a function of temperature of the modulus of elasticity $E_\theta/E_{20℃}$ is equal to the reduction of the 0.2% proof stress $f_{0.2,\theta}/f_{0.2,20℃}$. A consequence of this is that the relative slenderness at elevated temperature equals the relative slenderness at ambient temperature $\lambda_{rel,\theta} = \lambda_{rel,20℃}$. However, [Kaufman, 1999] documented steady state tensile test results of 158 different alloys and tempers at various elevated temperatures and shows that $E_\theta/E_{20℃}$ reduces less fast as compared to $f_{0.2,\theta}/f_{0.2,20℃}$ for most alloys and tempers. This also proves that the assumption that $\lambda_{rel,\theta} = \lambda_{rel,20℃}$ is a conservative approximation.

6. Conclusions and recommendations

In this research specimens with and without a weld are investigated on creep at elevated temperatures. Based on uniaxial creep tests at elevated temperatures and transient state tests, stress-strain relationships are obtained. With the aid of the resulting stress-strain relationships, comparisons have been made with the Eurocode. It is checked if there is a relationship between the grains and the strength at elevated temperature between the welded and not welded specimens. Also, with the obtained results from the transient state tests, calculations of the flexural buckling of a column have been conducted with different design models. In this chapter the main conclusions of the research can be reed. For more detailed conclusions about one of the indicated subjects, reference is made to the individual chapter conclusions.

6.1 Conclusions

The material parameters of the Dorn-Harmathy creep model with extension of Maljaars have been determined in creep tests and validated with transient state tests.

Based on simulations with the creep model, stress-strain relationships for aluminum alloys exposed to fire conditions are determined. Small differences in the constitutive model parameters made large differences in the stress-strain diagram. These differences where less evident in the curves of $f_{0.2},\theta$ and f_2,θ versus the temperature. Comparing the results of the $f_{0.2},\theta$ values, obtained from the stress-strain curves of the experiments, with the data in [EN 1999-1-2, 2007], showed that the relative values $f_{0.2,\theta}/f_{0.2}$ of alloy 6082 (for welded and not welded specimens) in the standard are safe. This was also the case for alloy 6060-T66 in [Maljaars, 2008]. The most conservative results were seen for specimens with a weld. As an alternative for the conservative standard of the welded specimens, there can be chosen to use the standard of not welded specimens for the welded specimens. Till 250°C this will be an unsafe alternative, but after 250°C it can be seen that this will be a safe alternative. Below the 250°C maybe a factor can be determined to multiply the curve in the standard for not welded specimens.

The tests carried out at elevated temperature show that the difference in strength between the HAZ and the parent metal decreases with increasing temperature. At a temperature of approximately 300°C the 0.2% proof stress of the not welded and welded specimens meet each other, HAZ strength is equal to the strength of the parent metal at temperatures of 300 °C and higher. This is due to the fact that the favorable metal structure obtained by a treatment is already destroyed by the heat input at welding. Consequently, heating by a fire has a smaller impact on the strength of the HAZ than on the strength of

the treated parent metal. Also the difference between the strength of 6060-T66 and 6082-T6 alloys decreased with increasing temperature. It is also seen that the relative values $f_{0.2,\theta}/f_{0.2,room}$ of 6082-T6 and 6060-T66 alloys differ from each other, although they are from the same series and temper. Such a major difference is not seen in the data of [EN 1999-1-2, 2007] and in literature [Kaufmann, 1999] between the alloys in the same series with the same temper. The difference can be attributed to the fact that data in [EN 1999-1-2, 2007] is based on steady state tests and data provided in this research are based on transient state tests.

The Dorn-Harmathy model with the extension of Maljaars is suited for 6082-T6 alloy after the change of parameters, which showed large deviations in the individual experiment results. Because there were large deviations, which are caused by the measuring accuracy of the test device, these changes of the parameters are permitted.

It is showed that the difference in strength between the not welded and welded specimens degraded with increasing temperature. Unfortunately, a clear relation between the grain size and the decrease of strength with increasing temperature between the welded and not welded specimens is not seen. The similarity in strength at 300°C, does not mean that the grain structure will also be the same at this temperature. The only similarity is stretching of the grains when the specimens are conducted to stresses. In comparison with the grain sizes in the weld, the grain sizes close to the weld are considerably smaller. This is probably caused by the heat during welding, which has ensured that the grains are reduced in size in the HAZ. It is also seen that the grain sizes of both welded and not welded are nearly the same for the original specimens which are not conducted to any thermal or mechanical exposure and the specimens which are conducted to a thermal exposure of 350°C in 30 minutes.

Calculations have been made for flexural buckling with the obtained stress-strain relations from creep tests. On the basis of different design models for flexural buckling of a column, it can clearly be seen that the design model in [EN 1999-1-2, 2007] is conservative in comparison with the design model in [Maljaars et. al, 2009b]. The maximum difference in relative ultimate resistance $F_{u,\theta}/F_{u,room}$ between [EN 1999-1-2, 2007] and [Maljaars et. al, 2009b] is found at a temperature of 300°C. The relative ultimate resistance $F_{u,\theta}/F_{u,room}$ for design model in [EN 1999-1-2, 2007] is 0.24 at 300°C. The relative ultimate resistance $F_{u,\theta}/F_{u,room}$ for design model in [Maljaars et. al, 2009b] is 0.50 at 300°C. A smaller difference can be seen between the ultimate resistance calculated with the model in [1999-1-1, 2007] (with the determined properties for elevated temperatures) and the model in [Maljaars et. al, 2009b]. A

difference of fire resistance of 7 minutes is found between the calculation with the design model in [EN 1999-1-2, 2007] and [Maljaars et. al, 2009b]. This difference in fire resistance has one more time shown that the design model in [EN 1999-1-2, 2007] will give conservative results.

Also from the unity check it is clearly visible that the design model in [EN 1999-1-2, 2007] is very conservative in comparison with the other two design models. So it can be concluded that it is more appropriate to determine the material slenderness with the material properties at elevated temperature.

[EN 1999-1-2, 2007] is conservative because the relative buckling resistance is taken equal to the value at room temperature $\chi_\theta = \chi_{20°C}$. This is based on the assumption that the reduction as a function of temperature of the modulus of elasticity $E_\theta / E_{20°C}$ is equal to the reduction of the 0.2% proof stress $f_{0.2,\theta} / f_{0.2,20°C}$. A consequence of this is that the relative slenderness at elevated temperature equals the relative slenderness at ambient temperature $\lambda_{rel,\theta} = \lambda_{rel,20°C}$. However, [Kaufman, 1999] documented steady state tensile test results of 158 different alloys and tempers at various elevated temperatures and shows that $E_\theta / E_{20°C}$ reduces less fast as compared to $f_{0.2,\theta} / f_{0.2,20°C}$ for most alloys and tempers. This also proves that the assumption that $\lambda_{rel,\theta} = \lambda_{rel,20°C}$ is a conservative approximation.

6.2 Recommendations

It has been found that the accuracy of the test results is very important for the validation of transient state tests. A minimal adjustment of a parameter will cause a marked change in the simulation of the model and the stress-strain curves. Unfortunately, the measuring accuracy of the strain in this research was not as high as desired. It is recommended to apply a different system in which the measuring device of the strain will give accurate results.

It is seen that the ε_{t0} parameter is temperature and stress dependent. In the Dorn-Harmathy model, this is not taking into account. [Kandare et. al, 2009] describes a way to calculate the primary creep in which they are taking into account the temperature and stress dependency of the primary creep. Due to a lack of data, this research could not determine the value of the primary creep as described in [Kandare et. al, 2009]. For the further research it is recommended to determine the primary creep in the way described in [Kandare et. al, 2009] and compare it with the results which come out of the Dorn-Harmathy method.

Alloy 6082-T6 is the second alloy in the 6xxx series which is investigated for this research. It is seen that the relative values $f_{0.2,\theta} / f_{0.2,room}$ of the alloys 6082-T6 and 6060-T66 differ from each other, although

they are from the same alloy and temper. Such a major difference is not seen in the data of [EN 1999-1-2, 2007]. Unfortunately, tests at two alloys are not enough to get a proper conclusion about the validated model. More tests on specimens in the 6xxx series will ensure that there can be drawn confident conclusions.

Grain structure is not the only influencing factor for the strength of the specimens. During fire exposure, the applied stress may cause large plastic deformation, grain elongation, precipitate cracking, and cavity formation associated with the increase of strain. In this research only the grain structure is investigated. To draw better conclusions, it is recommended to investigate all these influences on the microstructure of the material. After comparing all the microstructural influences, maybe there can be drawn a proper conclusion between the decrease of the strength of the different types of specimens with increasing temperature.

7. References

[Aluminum Association, 2005] *Aluminum Association (2005). Aluminum Design manual. Specifications & and guidelines for aluminum structures*. 1525 Wilson Boulevard, Suite 600, Arlington, VA 22209.

[Allen, 2012] Allen, B., (2012). *Creep and elevated temperature mechanical properties of 5083 and 6061 aluminum*. Thesis, Virginia Polytechnic Institute & State University.

[Božič et. al.] Božič, S., Šircelj, D. *Measuring of stress-strain behaviour of steel 1.0718 and aluminium alloy at different temperature range.* Higher vocational school, Slovenia.

[Blakenship, 1996] Blakenship, C. B., (1996). *Microstructure and Properties of Materials.* (Volume 1) ISBN: 978-981-02-2403-5

[Courtney, 2000] Courtney, C. H., (2000). *Mechanical behavior of materials*. McGraw-Hill, New York.

[Davis, 1993] Davis, J. R., (1993). *Aluminum and Aluminum Alloys.* ASM Specialty Handbook, ASM International.

https://books.google.nl/books?hl=nl&lr=&id=Lskj5k3PSIcC&oi=fnd&pg=PA3&dq=thermal+properties+aluminum+alloy&ots=Fuz-cg8DeT&sig=qfyX7dPaJ6EPv9uPohWtd93a9-Y#v=onepage&q=thermal%20properties%20aluminum%20alloy&f=false

[Doherty et. al, 1997] Doherty, R.D., Hughes, D.A., Humphreys, F.J., Jonas, J.J., Juul Jensen, D., Kassner, M.E., King g, W.E., McNelley, T.R., McQueen, H.J., Rollett, A.D., (1997). *Current issues in recrystallization: a review.* Materials Science and Engineering A238 (1997) 219–274.

[Dorn, 1954] Dorn, J. E. (1954). *Some fundamental experiments on high temperature creep*. Journal of the mechanical physics of solids, vol. 3, pp. 85-116.

[Edwards et. al, 1998] Edwards, G. A., Stiller, K., Dunlop, G. L., Couper, M. J., (1998). *The precipitation sequence in Al-Mg-Si Alloys.* Published by Elsevier Science Ltd. Vol. 46, No. 11, pp. 3893±3904.

[El-Danaf et. al, 2008] El-Danaf, E. A., AlMajid, A. A., Soliman, M. S., (2008). *Hot deformation of AA6082-T4 aluminum alloy.* J Mater Sci (2008) 43:6324–6330.

[EN 1999-1-1, 2007] Eurocode 9: Design of aluminum structures – Part 1-1, General rules.

[EN 1999-1-2, 2007] Eurocode 9: Design of aluminum structures – Part 1-1, General rules – structural fire design.

[EN 1991-1-2, 2002] Eurocode 1: Actions on structures – Part 1-2, General actions – Actions on structures exposed to fire.

[Gupta et. al, 2000] Gupta, A.K., Lloyd, D. J., Court, S. A., (2000). *Precipitation hardening processes in an Al–0.4%Mg–1.3%Si–0.25%Fe aluminum alloy.* Materials Science and Engineering A301 (2001) 140–146.

[Harmathy, 1967] Harmathy, T.Z., (1967). Journal basic engineering, vol. 89, pp. 496-502.

[Harun et. al, 1978] Harun, H.J., McCormick, P. G., (1978). *Effect of precipitation hardening on strain are sensitivity and yield behaviour in an Al-Mg-Si alloy.* Acta metallurgica vol. 27 pp. 155-159. University of western Australia.

[Hénaff et. al, 2011] Hénaff, G., Odemer, G., Journet, B., (2011). *Creep and creep fatigue crack growth in aluminium Alloys.* Aluminium Alloys, Theory and Applications, pp. 259-282. France.

[Holdsworth et. al, 2008] Holdsworth, S. R., Askins, M., Baker, A., Gariboldi, E., Holmstrom, S., Klenk, A., Ringel, M., Merckling, G., Sandstrom, R., Schwienheer, M., Spigarelli, S., (on behalf of Working Group 1 of the European Creep Collaborative Committee), (2008). *Factors influencing creep model equation selection.* International Journal of Pressure Vessels and Piping 85 (2008) 80–88

[Johnston, 2011] Johnston, B. G., (1983). *Column buckling theory: hystoric highlightss.* J. Struct. Eng., 1983, 109(9): 2086-2096.

[Kachanov, 1958] Kachanov, L.M., (1958). Izv. AKd. Nauk. S.S.S.R., Otd. Teck. Nauk. No. 8, 26-31.

[Kandare et. al, 2009] Kandare, E., Feih, S., Kootsookos, A., Mathys, Z., Lattimer, B.Y., Mouritz, A.P., (2009). *Creep-based life prediction modelling of aluminium in fire*. Materials Science and Engineering A 527 p.1185–1193.

[Kandare et. al, 2010] Kandare, E., Feih, S., Z., Lattimer, B.Y., Mouritz, A.P., (2010). Larson–Miller Failure Modeling of Aluminum in Fire. The Minerals, Metals & Materials Society and ASM International 2010. DOI: 10.1007/s11661-010-0369-1

[Kassner et. al, 2002] Kassner, M.E., Hayes, T.A., (2003). Creep cavitation in metals. International Journal of Plasticity 19 p1715–1748.

[Kaufmann, 1999] Kaufman, J.G., (1999). *Properties of Aluminum Alloys: Tensile, Creep, and Fatigue Data at High and Low Temperatures.* The Aluminium Association.

https://books.google.nl/books?hl=nl&lr=&id=3U_eQdnmzmwC&oi=fnd&pg=PA1&dq=creep+rupture+data+for+aluminium+alloys&ots=1i0Nao-PQe&sig=cFoR73hQ-FjsXRzFiUK7aYODeAg#v=onepage&q=creep%20rupture%20data%20for%20aluminium%20alloys&f=false

[Kumar et. al., 1999] Kumar, D.R., Swaminathan, K., (1999). *Tensile deformation behaviour of two aluminium alloys at elevated temperatures.* Materials at High Temperatures, Vol. 16.

[Langhelle et. al, 2001] Langhelle, N.K., Amdahl, J., (2001). In: Proc 11th int offshore polar eng conf. p. 406–13.

[Leckie et. al, 1974] Leckie, F. A., Hayhurst, D. R., (1974). *Creep Rupture of Structures*. Proc. R. Soc. Lond. A, pp. 323-347. Leicester, Grait Britain.

[Maljaars, 2008] Maljaars, J. (2008). *Local buckling of slender aluminum sections expose to fire*, Strategic Research Programme of the Netherlands Institute for Metals Research, Phd thesis.

[Maljaars et. al, 2008] Maljaars, J., Soetens, F., Katgerman, L. (2008). *Constitutive Model for Aluminum Alloys Exposed to Fire Conditions,* The Minerals, Metals & Materials Society and ASM International.

[Maljaars et. al, 2009] Maljaars, J., Soetens, F., (2009). *Strength of MIG welded connections in fire exposed aluminium structures.* Advanced steel construction Vol. 5, No. 2, pp. 136-150.

[Maljaars et. al, 2009b] Maljaars, J., Soetens, F., Twilt, L., (2009). *Flexural buckling of fire exposed aluminium columns*. Fire Safety Journal 44, pp. 711-717.

[Martin et. al, 2009] Vlacha, M., Smolaa, B., Stulíkováa, I., Očenášekb, V. (2009). *Microstructure and mechanical properties of the AA6082 aluminium alloy with small additions of Sc and Zr.* International Journal of Materials Research: Vol. 100, No. 3, pp. 420-423.

[Matulich, 2011] Matulich, R. D., (2011). *Post-fire Mechanical Properties of Aluminum Alloys and Aluminum Welds.* Thesis submitted to the faculty of the Virginia Polytechnic Institute and State University. Blacksburg, VA.

[Mazzolani, 1995] Mazzolani, F., (1995). *Aluminium Alloy Structures, Second Edition.* E&FN Spon, London, UK.

https://books.google.nl/books?hl=nl&lr=&id=GzkKQXU-HOcC&oi=fnd&pg=PR7&dq=stress+strain+aluminum+mazzolani&ots=BZeS0vTMBo&sig=cP9y9FTSjwYQrwRMR-kW-CyWwPg#v=onepage&q=stress%20strain%20aluminum%20mazzolani&f=false

[McQueen et. al, 1971] McQueen, H.J., Jonas, J.J., (1971). In metal forming, *Interrelation between theory and practice*. Edited by A.L. Hoffmanner, Plenum Publ. Corp., New York, NY, page 393-428.

[Missori et. al, 1997] Missori, s., Pezzuti, E., (1997). *Microstructural and mechanical characteristics of welded joints in type 6082-T6 aluminium alloy.* Welding International, 11 (6), 468-474.

[Missori et. al, 2000] Missori, S., Sili, A. (2000). *Mechanical behaviour of 6082-T6 aliminium alloy welds*, Metallurgical Science and Technology, Vol. 18 (1).

[Mondolfo, 1976] Mondolfo, L. F., (1976). *Aluminum Alloys: Structure and Properties.* Butterworth & Co, London.

https://books.google.nl/books?hl=nl&lr=&id=Xf4kBQAAQBAJ&oi=fnd&pg=PP1&dq=thermal+properties+aluminum+alloy&ots=Q40v-pIArf&sig=c-LnABen3khw_5pxVhgYVPtC4Gg#v=onepage&q=thermal%20properties%20aluminum%20alloy&f=false

[Myhr et. al, 1991 - I] Myhr, O. R., Grong, O. (1991). *Process modelling applied to 6082-T6 aluminium weldments – I. Reaction kinetics,* Department of Metallurgy, The Norwegian Institute of Technology, N-7034 Trondheim, Norway.

[Myhr et. al, 1991 - II] Myhr, O. R., Grong, O. (1991). *Process modelling applied to 6082-T6 aluminium weldments – I. Applications of model,* Department of Metallurgy, The Norwegian Institute of Technology, N-7034 Trondheim, Norway.

[Myhr et. al, 2004] Myhr, O. R., Grong, O., Fjaer, H. G., Marioara, C. D. (2004). *Modelling of the microstructure and strength evolution in Al–Mg–Si alloys during multistage thermal processing*, Acta Materialia 52 (2004) 4997–5008.

[Ozturk et. al., 2008] Ozturk, F., Toros, S., Kilic, S., (2008). *Evaluation of tensile properties of 5052 type aluminum-magnesium alloy at warm temperatures.* Department of Mechanical Engineering, Nigde University, Nigde, Turkey.

[Preftitsi et. al.] Preftitsi, F. G., Thomopoulos, K. A.. *Creep in aluminium structures.* Research Associate of TEI of Serres and TEI of West Macedonia. Institute of Metal Structures, Aristotle University of Thessaloniki, Greece.

[Ramberg et. al, 1943] Ramberg, W., Osgood, W.R., (1943). *Description of stress-strain curves by three parameters*, Technical note 902, NACA.

[Semb, 2013] Semb, E., (2013). *Behavior of aluminum at elevated strain rates and temperatures.* Civil and Environmental Engineering, Norwegian University of Science and Technology, Master Thesis Department of Structural Engineering.

[Shanley, 1946] Shanley, F. R., (1946). *Inelastic column theory.* Journal of Aeronautical Science, Vol. 14 No. 5.

[Sinha et. al, 2011] Sinha, K. N., Sinha, S., (2011). *High-temperature yield strength and its dependence on primary creep and recovery.* Materials Science and Engineering A 528 (2011) 5366–5378.

[Soetens et. al, 2013] Soetens, F., Hove, B.W.E.M. van, (2013). *Bouwen met aluminium*. The Netherlands, Eindhoven University of Technology, structural design and construction technology, dictaat bij het college 7P880 Aluminiumconstructies.

[Soyal, 2016] Soyal, Z., (2016). Literature study "Creep of aluminum alloys exposed to fire conditions". Eindhoven University of Technology, Structural Design.

[Stewart, 2008] Stewart, C. M., (2008). *Tertiary creep damage modeling of a transversely isotropic Ni-based superalloy.* B.S. University of Central Florida, Graduation Thesis, Orlando, Florida.

[Summers et. al., 2014] Summers, P. T., Case S. W., Lattimer B. Y., (2014). *Residual Mechanical Properties of AA5083-H116 and AA6061-T651 after Fire*. Engineering Structures, vol. 76, pp. 49-61.

[Summers et. al., 2015] Summers, P. T., Chen, Y., Rippe, C. M., Allen, B., Mouritz, A. P., Case, S. W., Lattimer, B. Y., (2015). *Overview of aluminum alloy mechanical properties during and after fires.* Fire Science Reviews, a Springer Open Journal. 4:3, DOI 10.1186/s40038-015-0007-5.

[TALAT 1501, 1994] Cobden, R., Alcan, Banbury (1994). *Aluminium: Physical Properties, Characteristics and Alloys.* TALAT Lecture 1501, European Aluminium Association.

[Wald, 2009] Wald, F., (2009). *9-2. Fire behavior and thermal response.* Lecture 9-1, V001. Czech Technical University in Prague.

[Zener et al, 1944] Zener, C., Holloman, H.H., (1944). *Effect of strain rate on the plastic flow of steel*. Journal of applied physics, Vol. 15, p.22.

.

Annex A.1 Inspection certificate EN10204 – 3.1

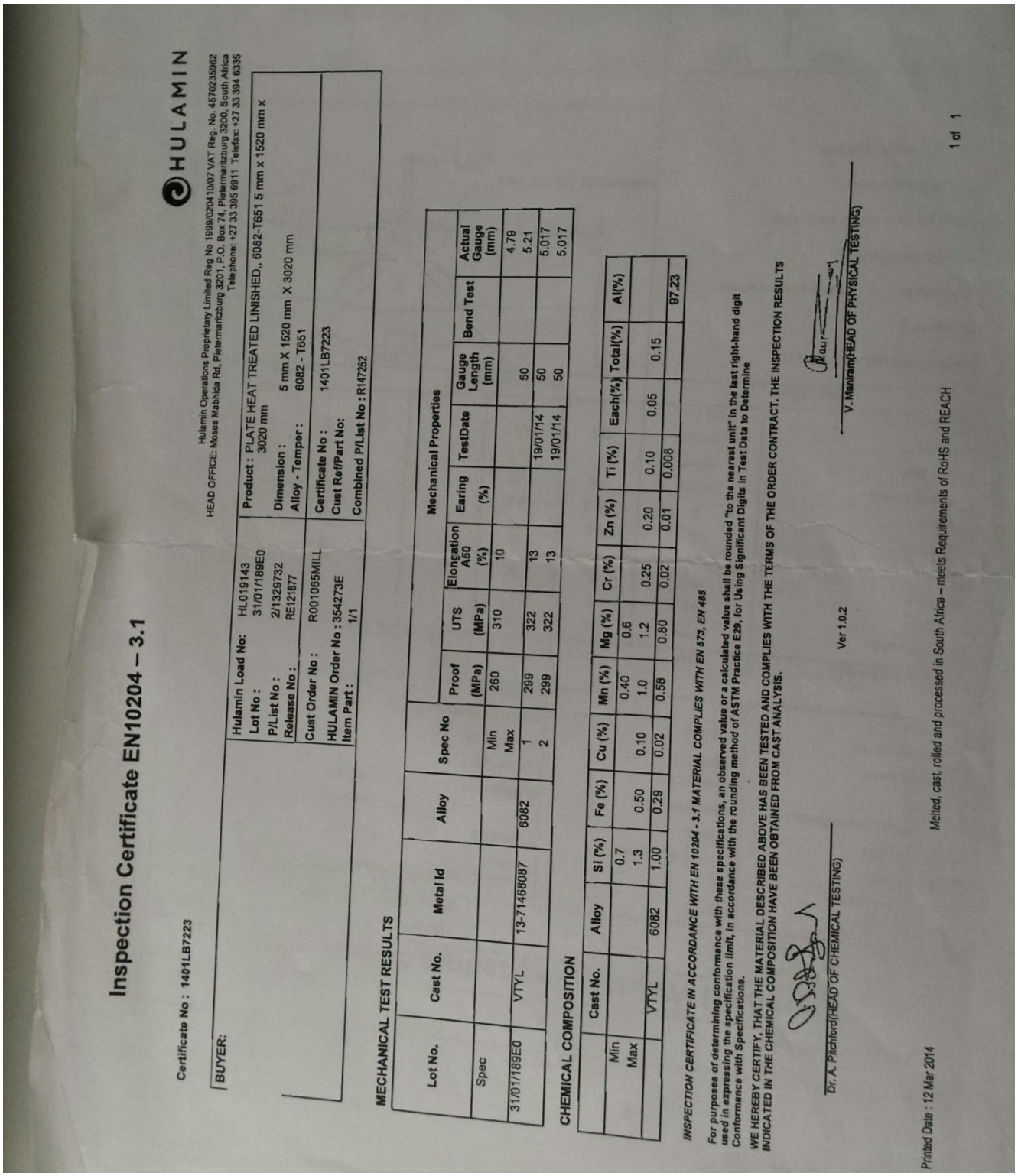

Inspection Certificate EN10204 – 3.1

HULAMIN

Hulamin Operations Proprietary Limited Reg No 1999/020410/07 VAT Reg. No. 4570235962
HEAD OFFICE: Moses Mabhida Rd, Pietermaritzburg 3201, P.O. Box 74, Pietermaritzburg 3200, South Africa
Telephone: +27 33 395 6911 Telefax: +27 33 394 6335

Certificate No : 1401LB7223

BUYER:

Hulamin Load No: HL019143	Product : PLATE HEAT TREATED LINISHED., 6082-T651 5 mm x 1520 mm x 3020 mm
Lot No : 31/01/189E0	
P/List No : 2/1329732	Dimension : 5 mm X 1520 mm X 3020 mm
Release No : RE121877	Alloy - Temper : 6082 - T651
Cust Order No : R001065MILL	Certificate No : 1401LB7223
HULAMIN Order No : 354273E	Cust Ref/Part No:
Item Part : 1/1	Combined P/List No : R147252

MECHANICAL TEST RESULTS

Lot No.	Cast No.	Metal Id	Alloy	Spec No	Mechanical Properties								
					Proof (MPa)	UTS (MPa)	Elongation A50 (%)	Earing (%)	TestDate	Gauge Length (mm)	Bend Test	Actual Gauge (mm)
Spec				Min	260	310	10					4.79
				Max								5.21
31/01/189E0	VTYL	13-71468087	6082	1	299	322	13		19/01/14	50		5.017
				2	299	322	13		19/01/14	50		5.017

CHEMICAL COMPOSITION

	Cast No.	Alloy	Si (%)	Fe (%)	Cu (%)	Mn (%)	Mg (%)	Cr (%)	Zn (%)	Ti (%)	Each(%)	Total(%)	Al(%)
Min			0.7			0.40	0.6						
Max			1.3	0.50	0.10	1.0	1.2	0.25	0.20	0.10	0.05	0.15	
	VTYL	6082	1.00	0.29	0.02	0.58	0.80	0.02	0.01	0.008			97.23

INSPECTION CERTIFICATE IN ACCORDANCE WITH EN 10204 - 3.1 MATERIAL COMPLIES WITH EN 573, EN 485

For purposes of determining conformance with these specifications, an observed value or a calculated value shall be rounded "to the nearest unit" in the last right-hand digit used in expressing the specification limit, in accordance with the rounding method of ASTM Practice E29, for Using Significant Digits in Test Data to Determine Conformance with Specifications.

WE HEREBY CERTIFY, THAT THE MATERIAL DESCRIBED ABOVE HAS BEEN TESTED AND COMPLIES WITH THE TERMS OF THE ORDER CONTRACT. THE INSPECTION RESULTS INDICATED IN THE CHEMICAL COMPOSITION HAVE BEEN OBTAINED FROM CAST ANALYSIS.

Dr. A. Pitchford(HEAD OF CHEMICAL TESTING)

V. Maniram(HEAD OF PHYSICAL TESTING)

Printed Date : 12 Mar 2014

Melted, cast, rolled and processed in South Africa – meets Requirements of RoHS and REACH

Ver 1.0.2

1 of 1

Figure A.1.1 Inspection certificate of alloy 6082-T6

Annex B.1 Creep tests data

Table B.1.1 Creep tests data on not welded specimens.

Test	Step	$\theta\ [°C]$	$\sigma\ [N/mm^2]$	$t\ [min]$	$\dot{\varepsilon}_{II}[/min]$
No 1	1	310	31	30	-
	2	320	31	20	$1.17 \cdot 10^{-5}$
	3	330	31	15	$2.17 \cdot 10^{-5}$
No 2	1	310	45	10	$8.03 \cdot 10^{-5}$
	2	320	45	5	$9.26 \cdot 10^{-5}$
	3	330	45	5	$1.89 \cdot 10^{-4}$
No 3	1	260	76	20	$3.70 \cdot 10^{-5}$
	2	280	76	10	$1.03 \cdot 10^{-4}$
	3	300	76	5	$5.06 \cdot 10^{-4}$
No 4	1	250	81	30	$1.27 \cdot 10^{-5}$
	2	260	81	20	$1.64 \cdot 10^{-5}$
	3	270	81	10	$3.63 \cdot 10^{-5}$
No 5	1	200	175	20	$2.49 \cdot 10^{-5}$
	2	210	175	10	$6.19 \cdot 10^{-5}$
	3	220	176	10	$2.03 \cdot 10^{-4}$
	4	230	176	5	-
No 6	1	150	241	20	$3.15 \cdot 10^{-4}$
	2	160	242	10	$1.59 \cdot 10^{-3}$
No 7	1	280	91	25	$1.86 \cdot 10^{-4}$
No 8	1	250	95	15	$4.02 \cdot 10^{-5}$
	2	250	101	10	$4.30 \cdot 10^{-5}$
	3	250	106	10	$5.11 \cdot 10^{-5}$
	4	250	111	5	$8.63 \cdot 10^{-5}$
No 9	1	250	121	15	$1.45 \cdot 10^{-4}$
	2	250	126	10	$4.28 \cdot 10^{-4}$
No 10	1	300	40	30	$2.83 \cdot 10^{-5}$
	2	300	45	15	$4.09 \cdot 10^{-5}$
	3	300	50	10	$6.19 \cdot 10^{-5}$
No 11	1	300	61	30	$1.25 \cdot 10^{-4}$
	2	300	67	10	$9.74 \cdot 10^{-4}$
No 12	1	350	26	30	$4.40 \cdot 10^{-5}$
	2	350	36	10	-

Table B.1.2 Creep tests data on welded specimens.

Test	Step	$\theta\ [°C]$	$\sigma\ [N/mm^2]$	$t\ [min]$	$\dot{\varepsilon}_{II}[/min]$
No 1	1	260	61	20	$3.12 \cdot 10^{-5}$
	2	280	61	10	$7.46 \cdot 10^{-5}$
	3	300	61	8	$2.95 \cdot 10^{-4}$
No 2	1	190	101	15	$1.16 \cdot 10^{-5}$
	2	200	101	10	$2.67 \cdot 10^{-5}$
	3	220	101	10	$2.88 \cdot 10^{-4}$
No 3	1	190	111	20	-
	2	200	111	15	-
	3	210	111	10	$1.20 \cdot 10^{-4}$
	4	220	111	5	$2.44 \cdot 10^{-4}$
No 4	1	230	110	16	$1.98 \cdot 10^{-4}$
No 5	1	150	120	15	$4.54 \cdot 10^{-6}$
	2	160	120	10	$1.15 \cdot 10^{-5}$
	3	170	120	10	$2.83 \cdot 10^{-5}$
No 6	1	190	125	20	$2.58 \cdot 10^{-5}$
	2	200	125	10	$4.81 \cdot 10^{-5}$
	3	210	125	10	$1.01 \cdot 10^{-4}$
No 7	1	150	144	20	$2.51 \cdot 10^{-5}$
	2	160	144	15	$2.47 \cdot 10^{-5}$
	3	170	144	10	$5.60 \cdot 10^{-5}$
	4	180	144	10	$1.62 \cdot 10^{-4}$
No 8	1	220	85	20	$2.47 \cdot 10^{-5}$
	2	220	90	10	$4.00 \cdot 10^{-5}$
	3	220	95	5	$5.89 \cdot 10^{-5}$
	4	220	100	5	$6.91 \cdot 10^{-5}$
No 9	1	280	66	20	$1.05 \cdot 10^{-4}$
	2	280	71	10	$5.18 \cdot 10^{-4}$
No 10	1	300	45	30	$5.38 \cdot 10^{-5}$
	2	300	50	15	$1.72 \cdot 10^{-4}$
	3	300	55	2	-
No 11	1	340	26	20	$5.68 \cdot 10^{-5}$
	2	340	31	10	$1.09 \cdot 10^{-4}$
	3	340	36	10	-

Annex B.2 Graphs of individual creep tests at specimens without weld

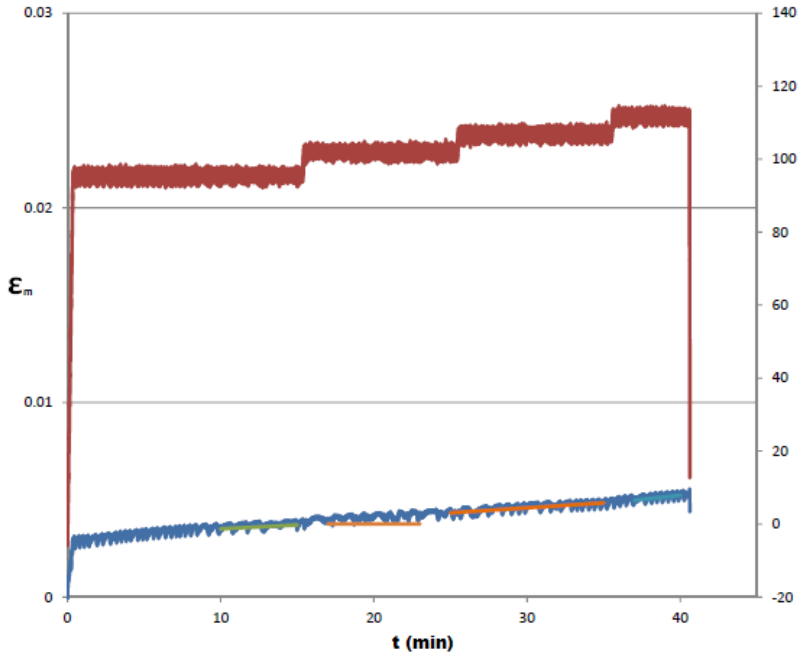

T = 250°C, σ=95N/mm^2, 100N/mm^2, 105N/mm^2, 110N/mm^2

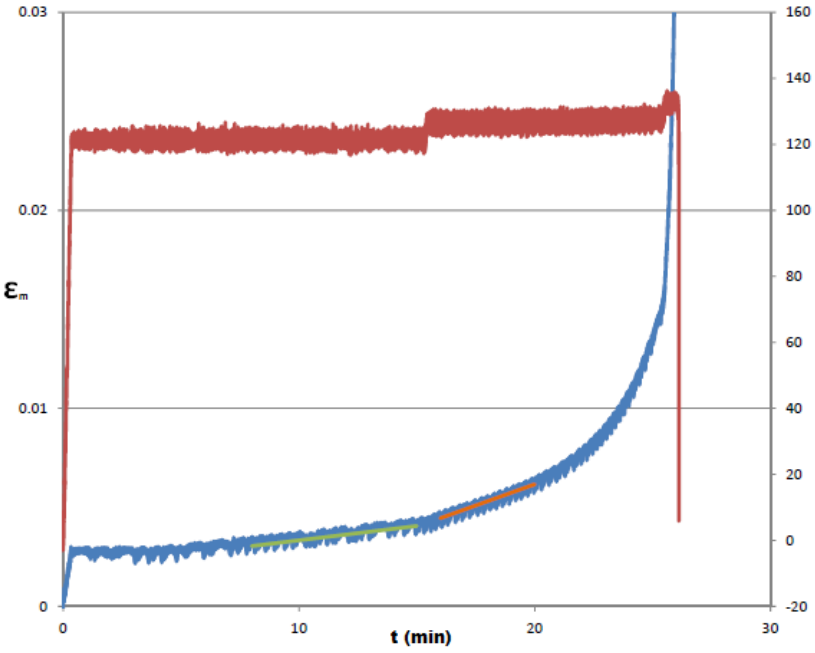

T = 250°C, σ=120N/mm^2, 125N/mm^2, 130N/mm^2

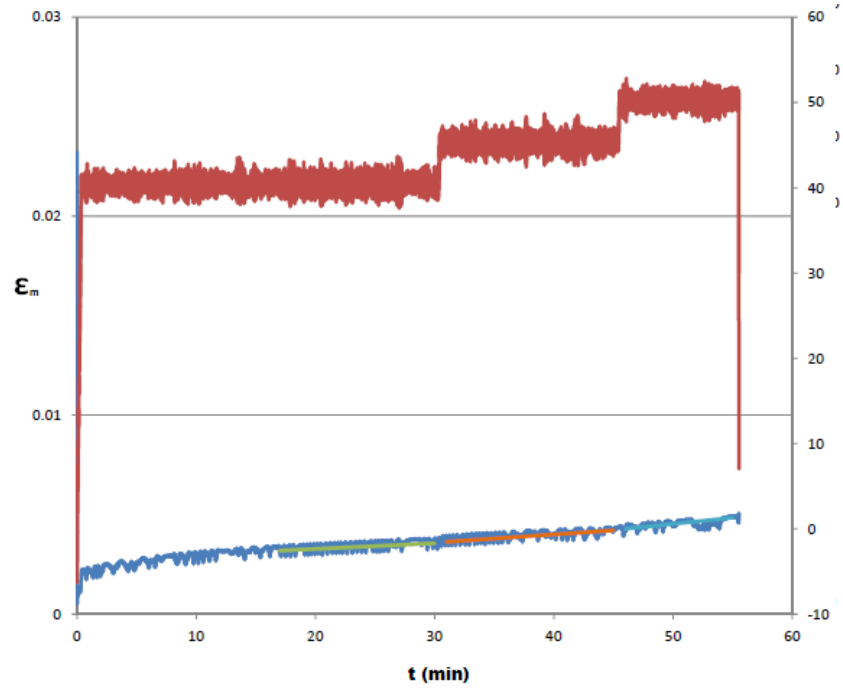

T = 300°C, σ=40N/mm^2, 45N/mm^2, 50N/mm^2

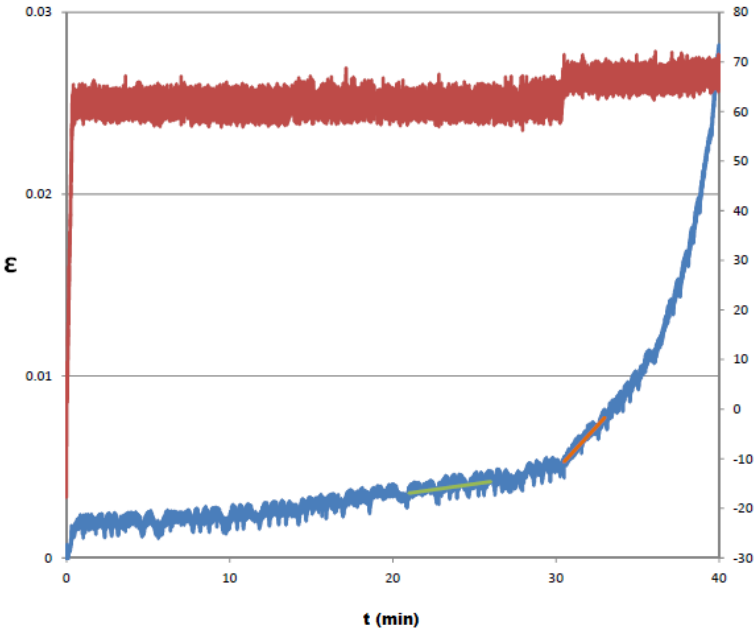

T = 300°C, σ=60N/mm^2, 65N/mm^2, 70N/mm^2

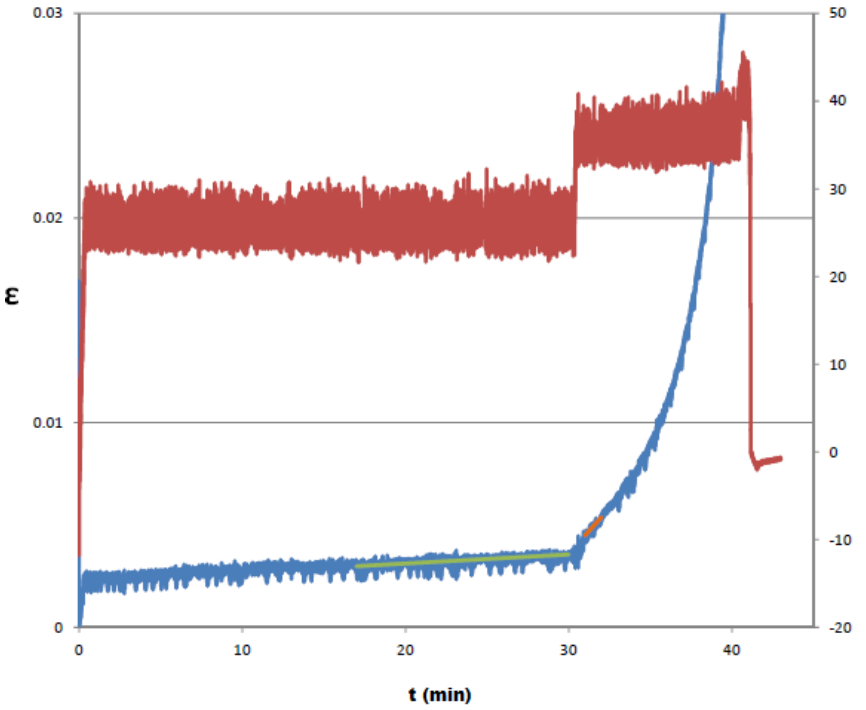

T = 350°C, σ=40N/mm^2, 45N/mm^2, 50N/mm^2

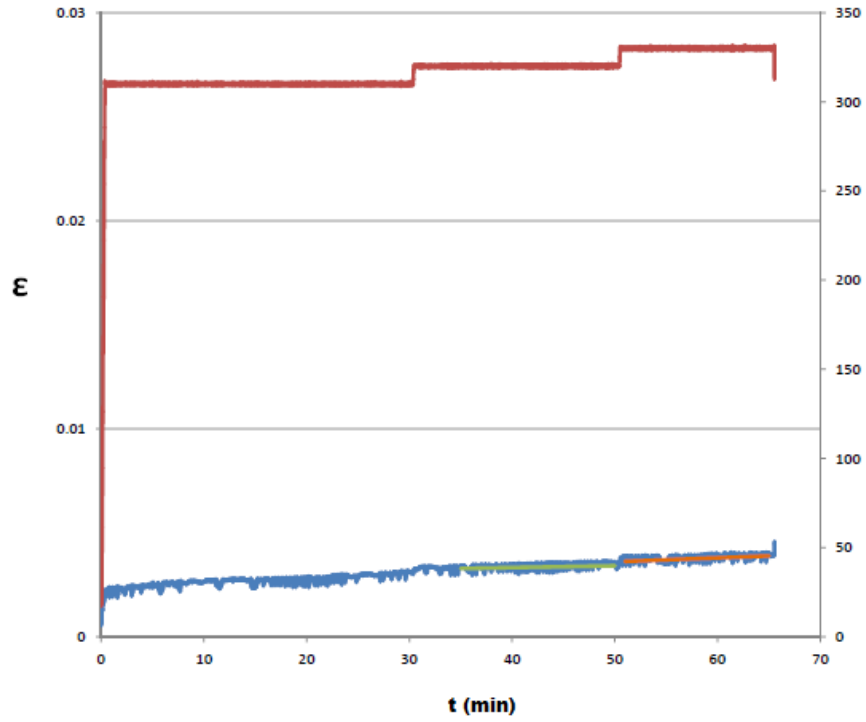

σ=30N/mm^2, T = 310°C, T = 320°C, T = 330°C

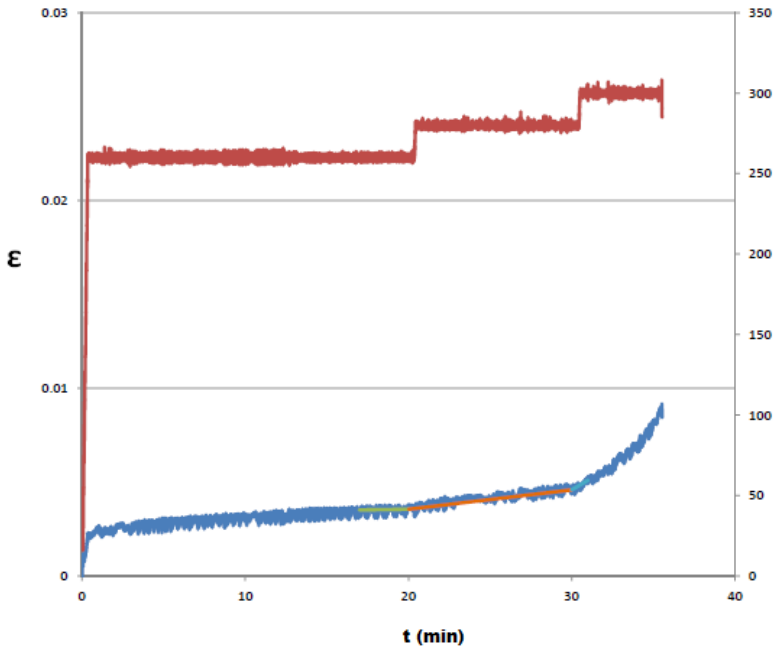

σ=75N/mm^2, T = 260°C, T = 280°C, T = 300°C

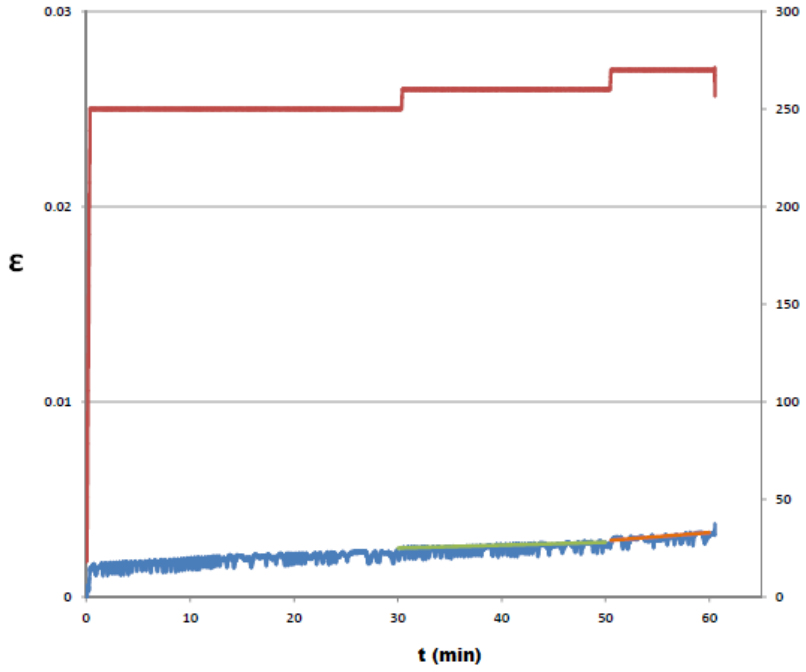

σ=80N/mm^2, T = 250°C, T = 260°C, T = 270°C

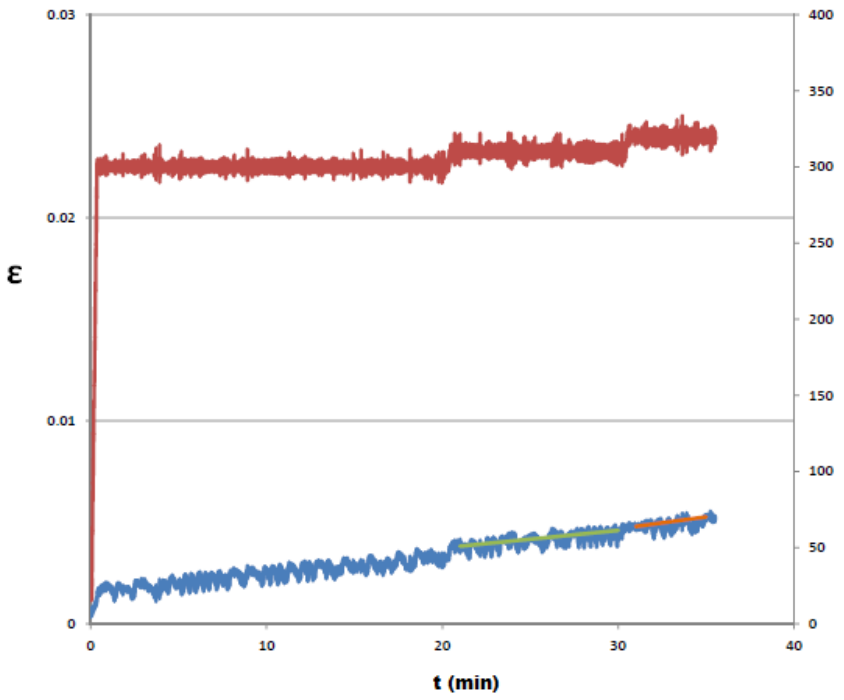

σ=45N/mm^2, T = 300°C, T = 310°C, T = 320°C

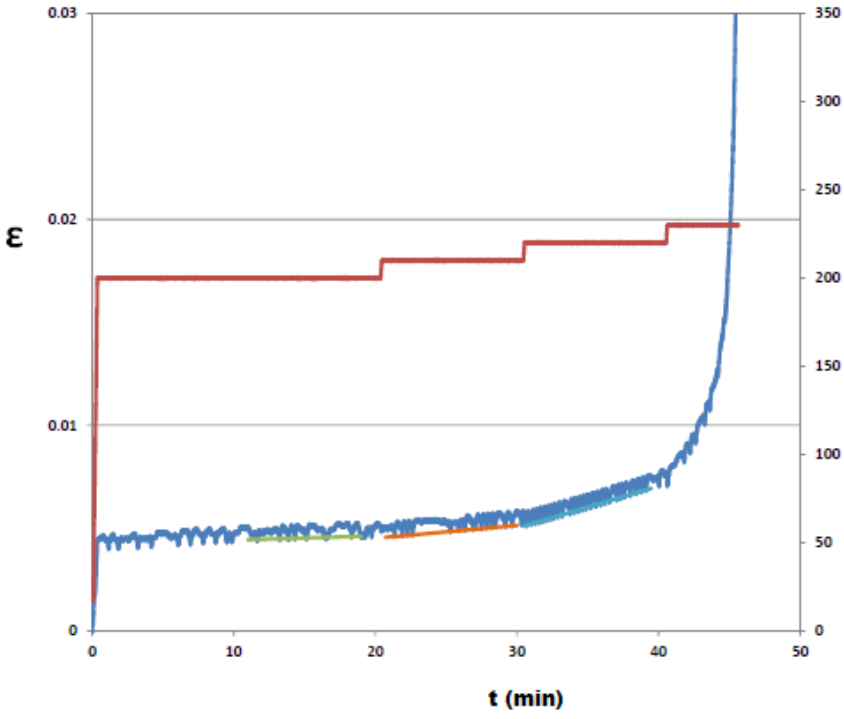

σ=175N/mm^2, T = 200°C, T = 210°C, T = 220°C, T = 230°C

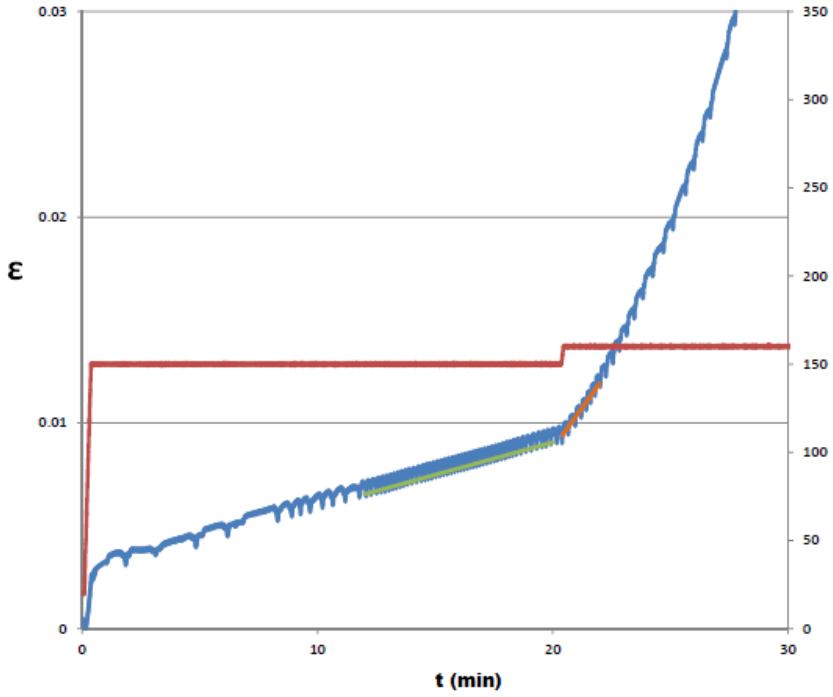

σ=175N/mm^2, T = 150°C, T = 160°C

Annex B.3 Graphs of individual creep tests at specimens with weld

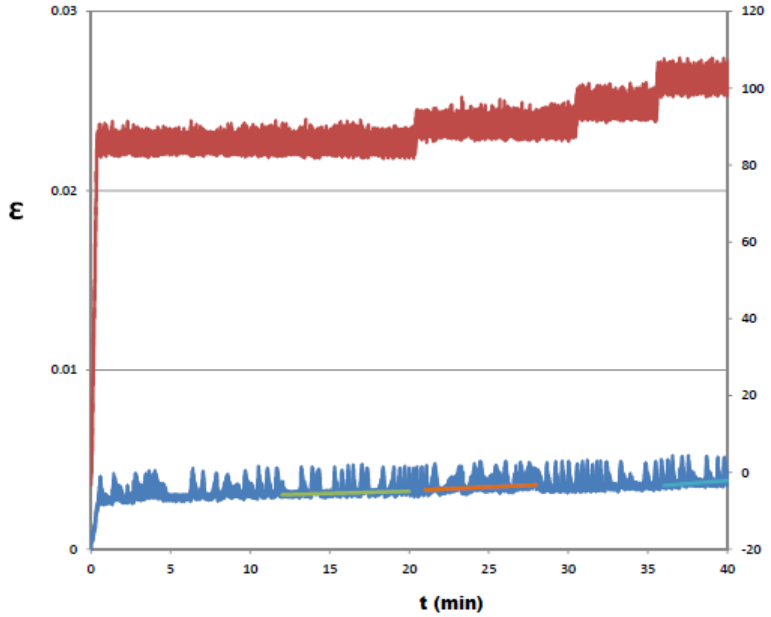

T = 220°C, σ=85N/mm^2, 90N/mm^2, 95N/mm^2, 100N/mm^2

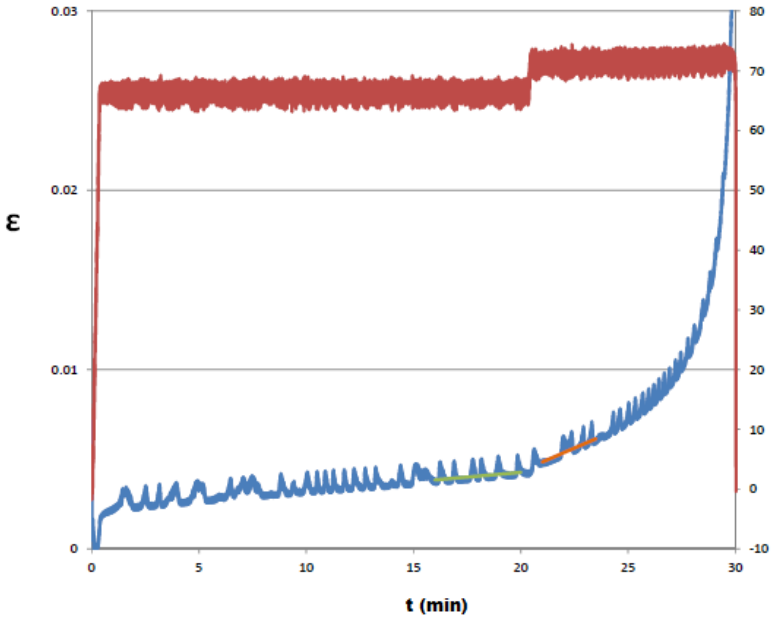

T = 280°C, σ=65N/mm^2, 70N/mm^2

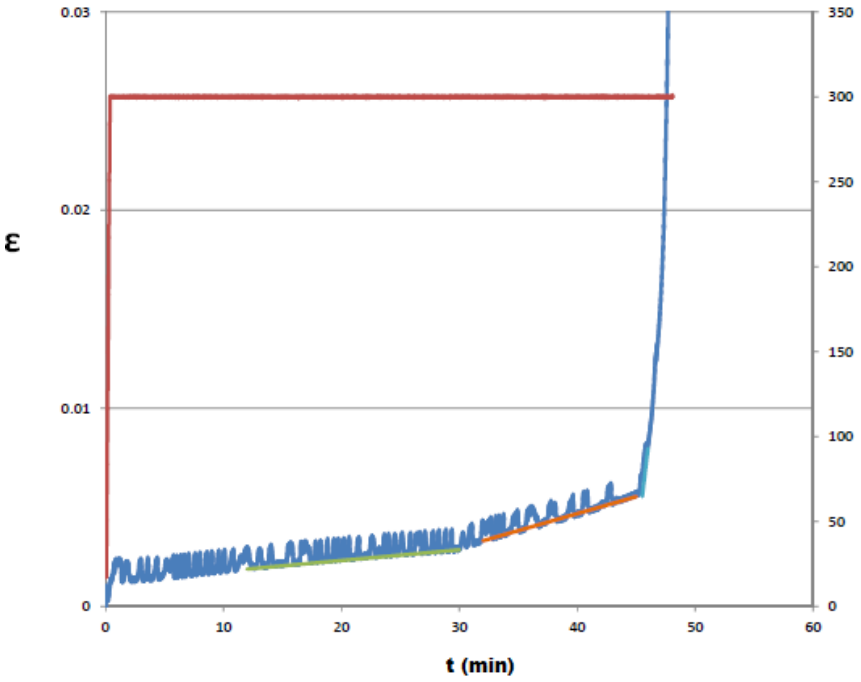

T = 300°C, σ=45N/mm^2, 50N/mm^2, 55N/mm^2

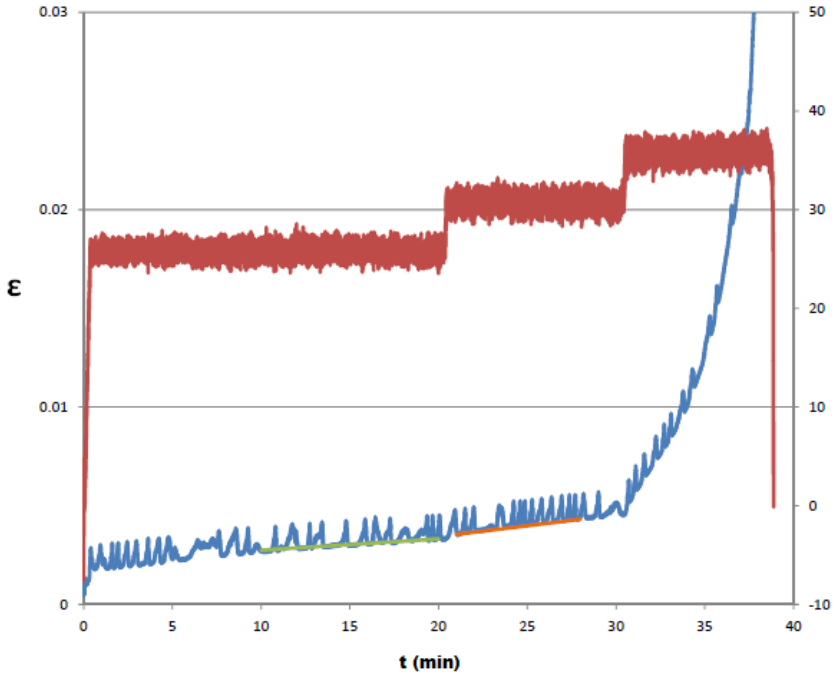

T = 340°C, σ=25N/mm^2, 30N/mm^2, 35N/mm^2

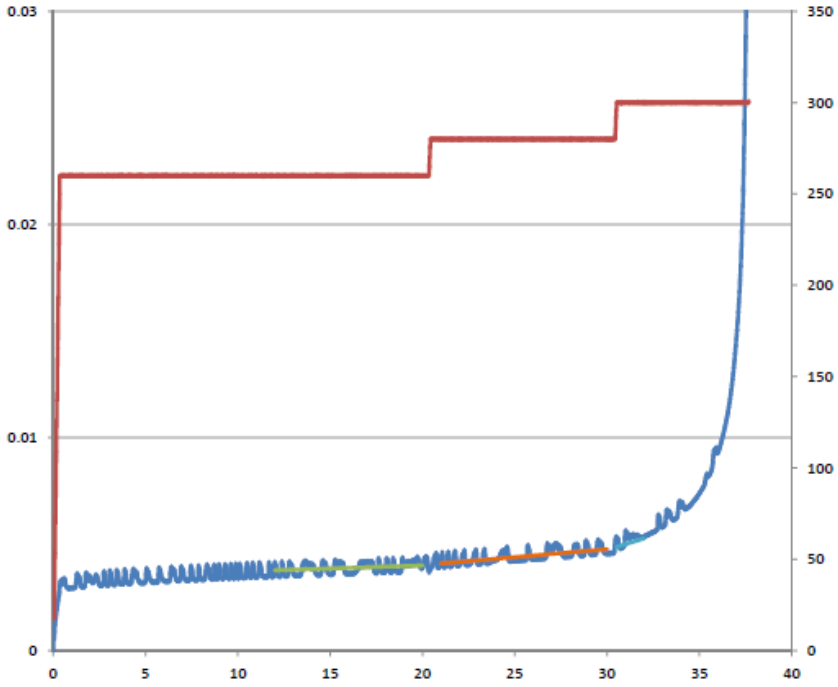

σ=60N/mm^2, T = 260°C, T = 280°C, T = 300°C

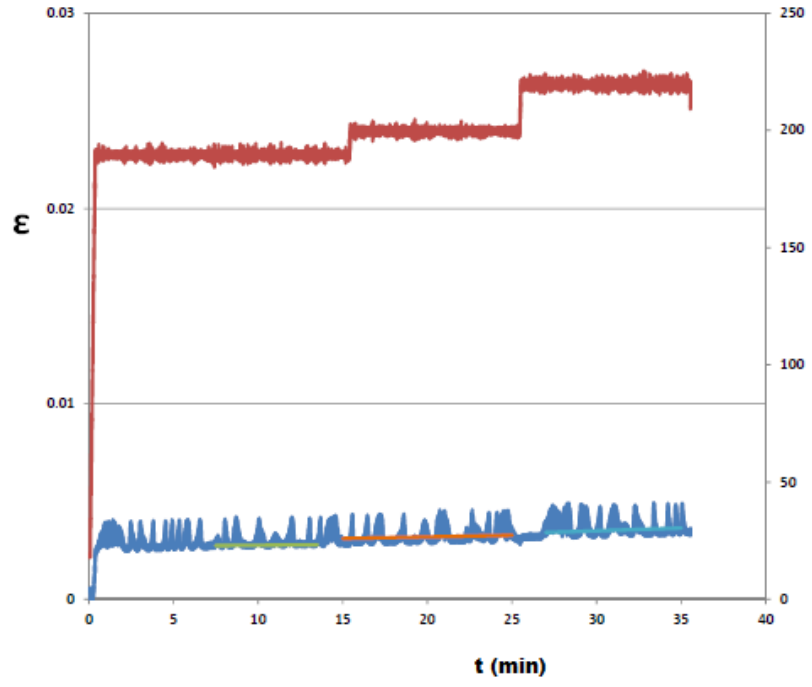

σ=100N/mm^2, T = 190°C, T = 200°C, T = 220°C

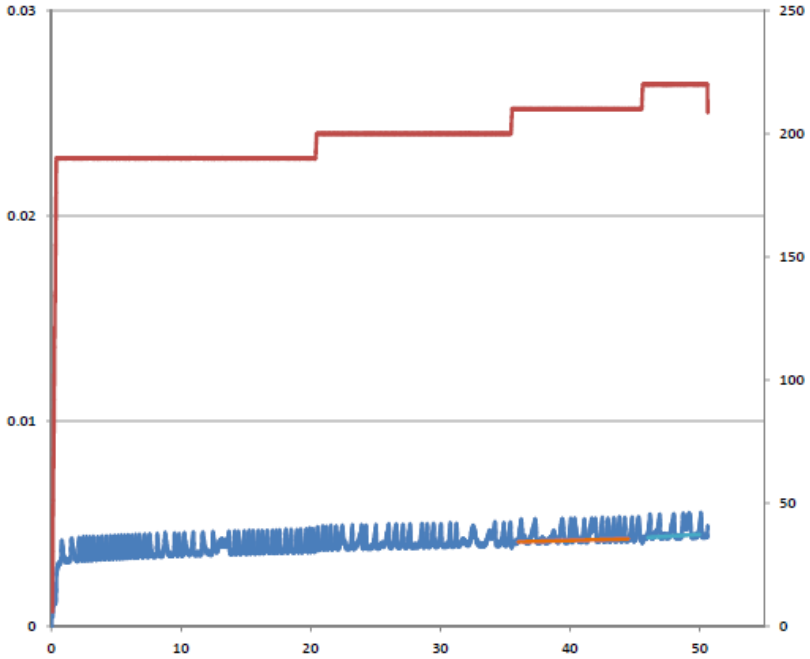

σ=110N/mm^2, T = 190°C, T = 200°C, T = 210°C

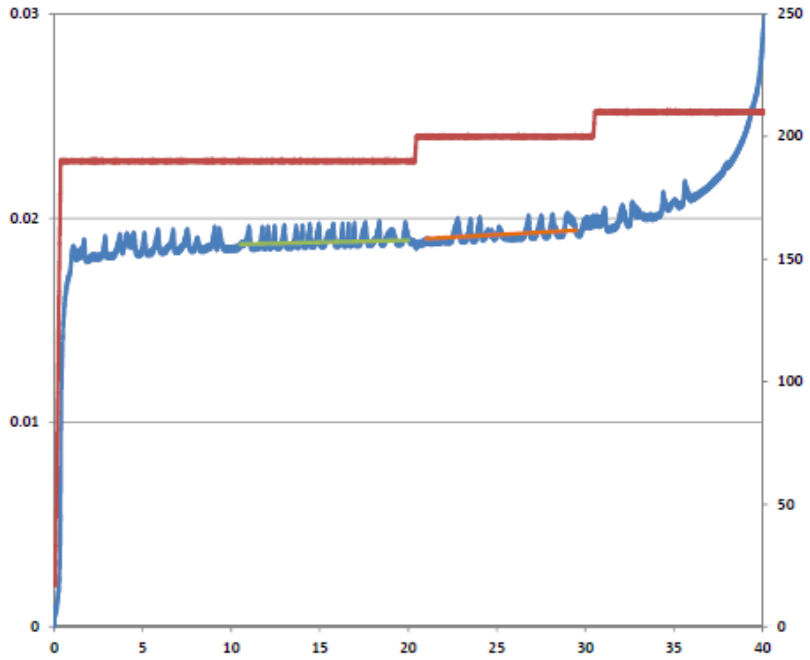

σ=125N/mm^2, T = 190°C, T = 200°C, T = 210°C

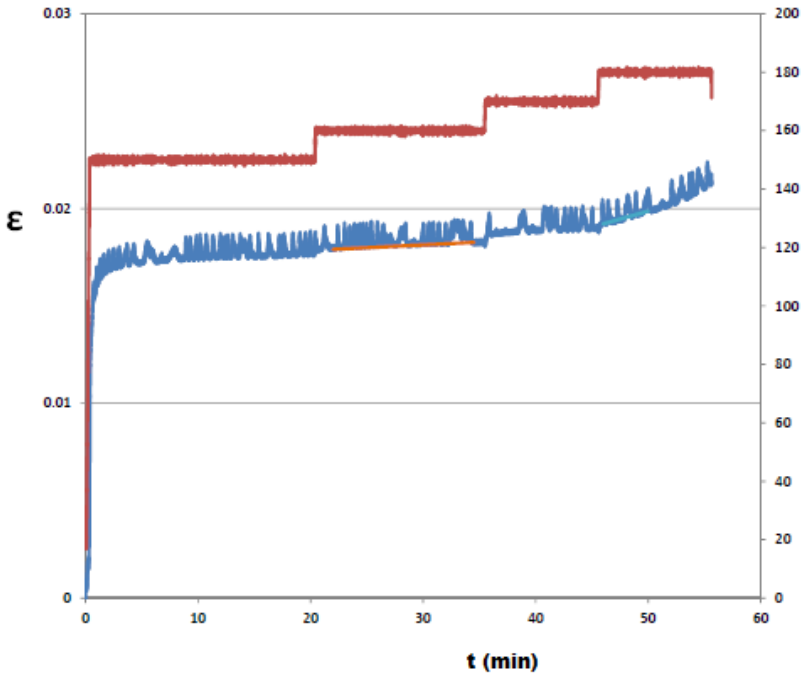

σ=140N/mm^2, T = 150°C, T = 160°C, T = 170°C, T = 180°C

Annex C.1 Creep strain rate versus creep strain graphs for not welded specimens

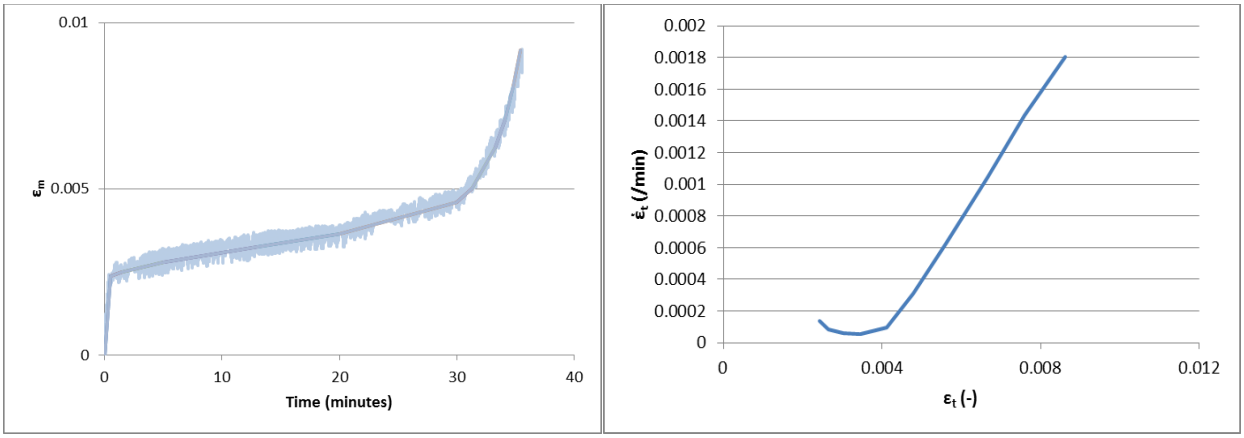

Figure C.1.1 Left: Strain versus time of a creep test with tertiary creep with stress 75 N/mm^2 and temperature 260°C, 280°C and 300°C on specimen without weld. Right: Strain rate as function of strain.

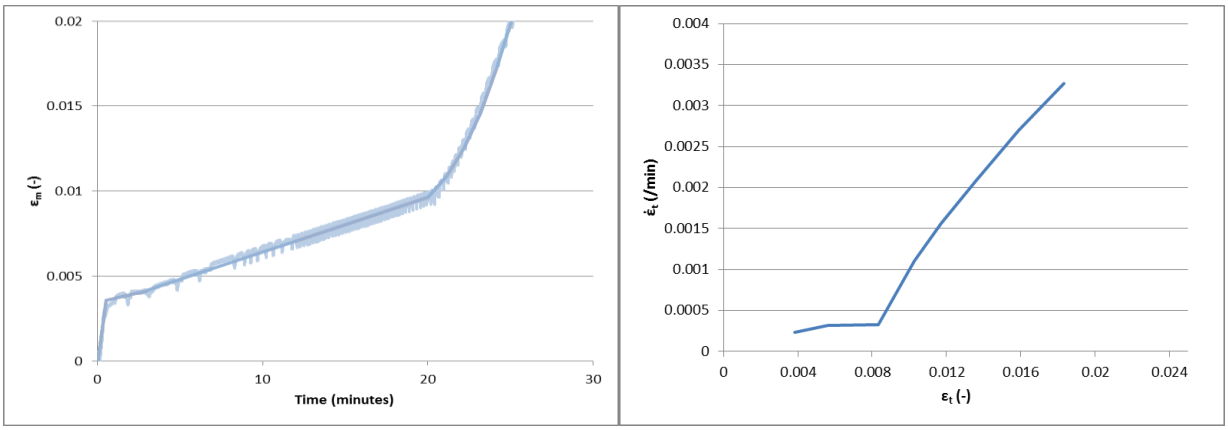

Figure C.1.2 Left: Strain versus time of a creep test with tertiary creep with stress 240 N/mm^2 and temperature 150°C and 160°C on specimen without weld. Right: Strain rate as function of strain.

Annex C.2 Creep strain rate versus creep strain graphs for welded specimens

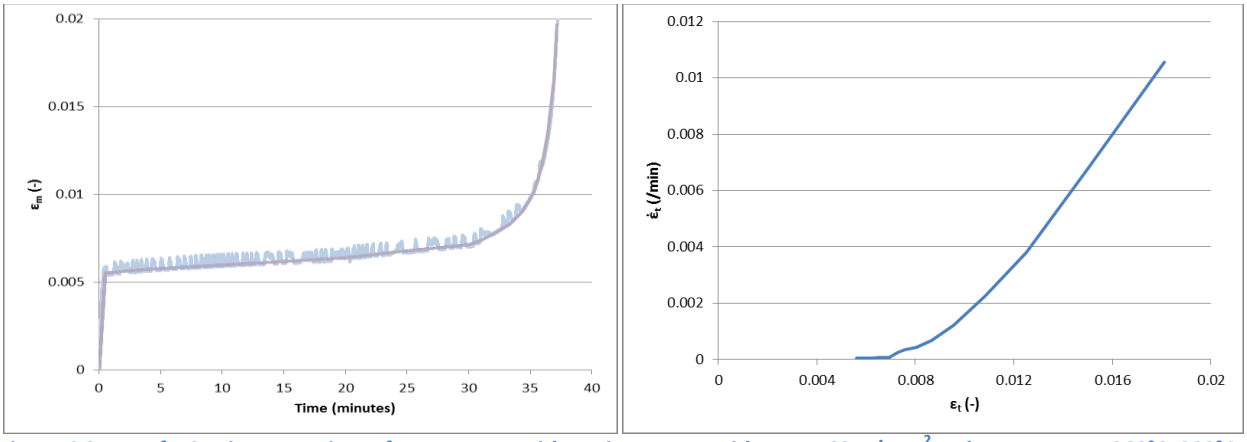

Figure C.2.1 Left: Strain versus time of a creep test with tertiary creep with stress 60 N/mm^2 and temperature 260°C, 280°C and 300°C on specimen with weld. Right: Strain rate as function of strain.

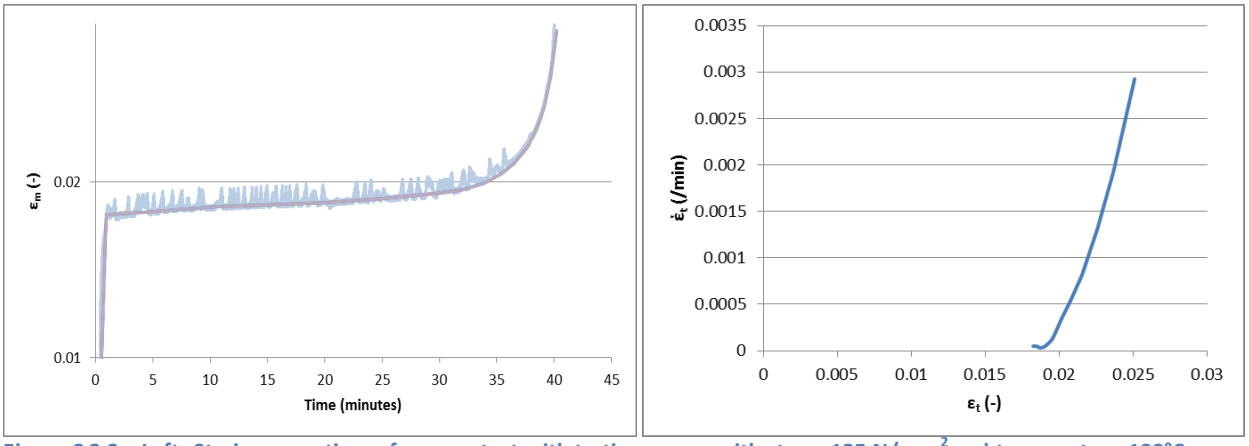

Figure C.2.2 Left: Strain versus time of a creep test with tertiary creep with stress 125 N/mm^2 and temperature 190°C, 200°C and 210°C on specimen with weld. Right: Strain rate as function of strain.

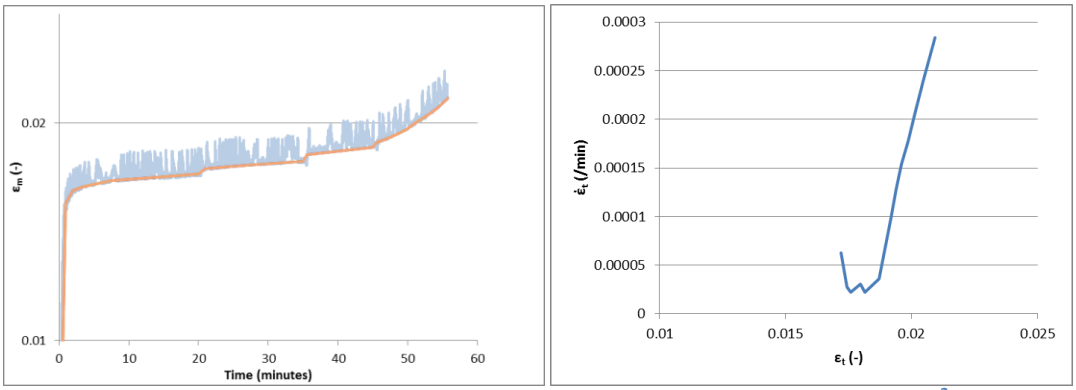

Figure C.2.3 Left: Strain versus time of a creep test with tertiary creep with stress 140 N/mm^2 and temperature 150°C, 160°C, 170°C and 180°C on specimen with weld. Right: Strain rate as function of strain.

Annex D.1 Deviations of the model based on the creep test results for not welded specimens

$$Z_{model} = 5.2 \cdot 10^{12}(\sinh(0.028 \cdot \sigma))^3$$

$$Z_{model} + \sigma = 1.32 \cdot 10^{13}(\sinh(0.028 \cdot \sigma))^3$$

$$Z_{model} - \sigma = 2.0 \cdot 10^{12}(\sinh(0.028 \cdot \sigma))^3$$

$$Z_{model} + 0.7 \cdot \sigma = 1.02 \cdot 10^{13}(\sinh(0.028 \cdot \sigma))^3$$

$$Z_{model} - 0.7 \cdot \sigma = 2.6 \cdot 10^{13}(\sinh(0.028 \cdot \sigma))^3$$

$$\varepsilon_{t0,model} = 5.59 \cdot 10^{-5} \cdot \sigma^{0.71}$$

$$\varepsilon_{t0,model} + \sigma = 6.39 \cdot 10^{-5} \cdot \sigma^{0.71}$$

$$\varepsilon_{t0,model} - \sigma = 4.88 \cdot 10^{-5} \cdot \sigma^{0.71}$$

$$\varepsilon_{t0,model} + 0.7 \cdot \sigma = 6.15 \cdot 10^{-5} \cdot \sigma^{0.71}$$

$$\varepsilon_{t0,model} - 0.7 \cdot \sigma = 5.09 \cdot 10^{-5} \cdot \sigma^{0.71}$$

TableD.1.1 Relation between simulation temperature and test temperature at plastic strain of 0.4% for not welded specimens.

0.4% strain						
Test	Z=-1σ, εt0=0 σ	Z=+1 σ, εt0=0 σ	Z=0σ, εt0=-1σ	Z=0σ, εt0=+1σ	Z=-0.7σ, εt0=-0.7σ	Z=-0.7σ, εt0=-0.7σ
363	379	347	365	361	375	351
355	365	338	352	350	362	340
290	282	260	275	268	280	260
273	260	240	250	246	258	240

Table D.1.2 Relation between simulation temperature and test temperature at plastic strain of 2% for unwelded specimens.

Test	Z=-1σ, εt0=0 σ	Z=+1 σ, εt0=0 σ	Z=0σ, εt0=-1σ	Z=0σ, εt0=+1σ	Z=-0.7σ, εt0=-0.7σ	Z=-0.7σ, εt0=-0.7σ
383	420	388	405	400	415	390
365	395	365	380	380	390	365
308	325	300	315	310	320	305
291	305	280	293	290	300	285

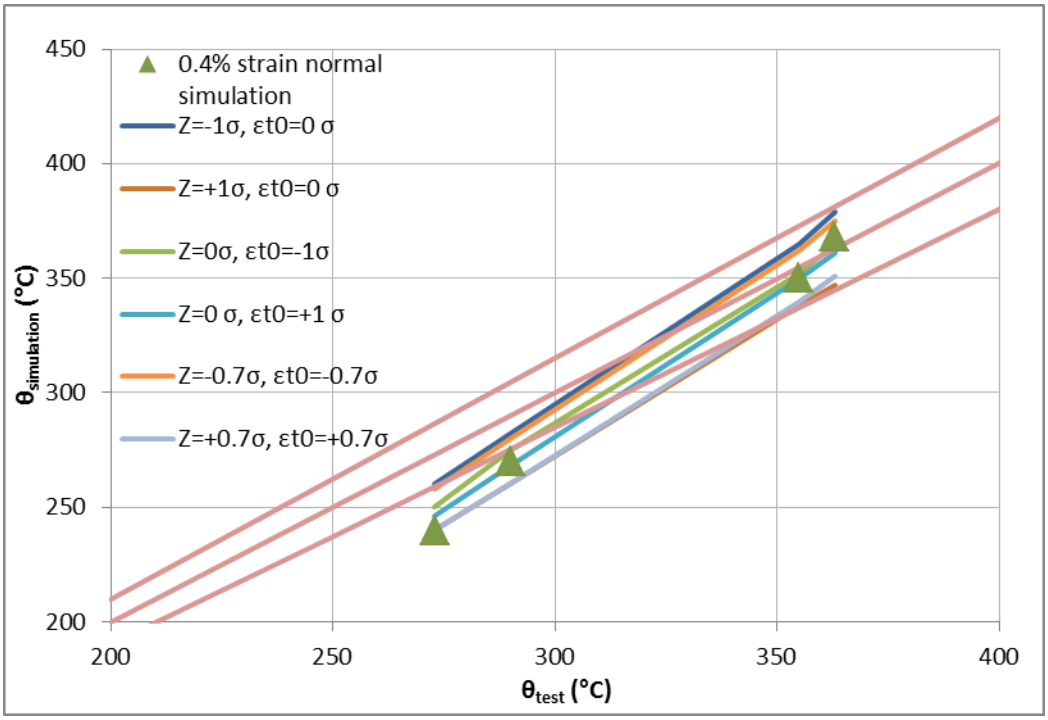

Figure D.1.1 Relation between simulation temperature and test temperature at plastic strain of 0.4% for not welded specimens.

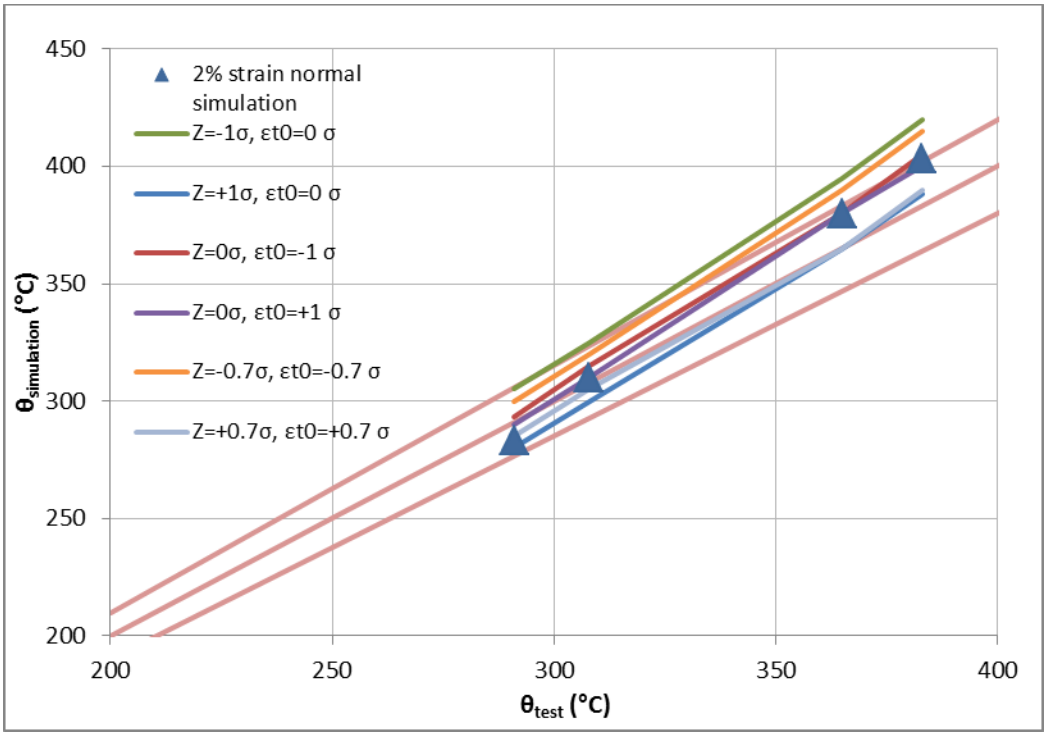

Figure D.1.2 Relation between simulation temperature and test temperature at plastic strain of 2% for not welded specimens.

Annex D.2 Deviations of the model based on the creep test results for welded specimens

$$Z_{model} = 1.5 \cdot 10^{8} (\sinh(0.028 \cdot \sigma))^{2.9}$$

$$Z_{model} + \sigma = 2.6 \cdot 10^{8} (\sinh(0.028 \cdot \sigma))^{2.9}$$

$$Z_{model} - \sigma = 8.3 \cdot 10^{7} (\sinh(0.028 \cdot \sigma))^{2.9}$$

$$Z_{model} + 0.7 \cdot \sigma = 2.2 \cdot 10^{8} (\sinh(0.028 \cdot \sigma))^{2.9}$$

$$Z_{model} - 0.7 \cdot \sigma = 1.0 \cdot 10^{8} (\sinh(0.028 \cdot \sigma))^{2.9}$$

$$\varepsilon_{t0,model} = 1.5 \cdot 10^{-6} \cdot \sigma^{1.8}$$

$$\varepsilon_{t0,model} + \sigma = 1.92 \cdot 10^{-6} \cdot \sigma^{1.8}$$

$$\varepsilon_{t0,model} - \sigma = 1.17 \cdot 10^{-6} \cdot \sigma^{1.8}$$

$$\varepsilon_{t0,model} + 0.7 \cdot \sigma = 1.79 \cdot 10^{-6} \cdot \sigma^{1.8}$$

$$\varepsilon_{t0,model} - 0.7 \cdot \sigma = 1.26 \cdot 10^{-6} \cdot \sigma^{1.8}$$

Table D.2.1 Relation between simulation temperature and test temperature at plastic strain of 0.4% for welded specimens.

Test	Z=-1σ, εt0=0 σ	Z=+1 σ, εt0=0 σ	Z=0σ, εt0=-1σ	Z=0σ, εt0=+1σ	Z=-0.7σ, εt0=-0.7σ	Z=-0.7σ, εt0=-0.7σ
373	425	395	410	410	420	400
350	390	363	375	375	385	365
337	370	345	360	355	370	350
278	295	275	285	280	290	275

Table D.2.2 Relation between simulation temperature and test temperature at plastic strain of 2% for welded specimens.

Test	Z=-1σ, εt0=0 σ	Z=+1 σ, εt0=0 σ	Z=0σ, εt0=-1σ	Z=0σ, εt0=+1σ	Z=-0.7σ, εt0=-0.7σ	Z=-0.7σ, εt0=-0.7σ
363	375	350	365	360	375	350
337	350	328	340	335	348	330
330	312	293	307	295	312	290
245	228	215	228	215	230	212

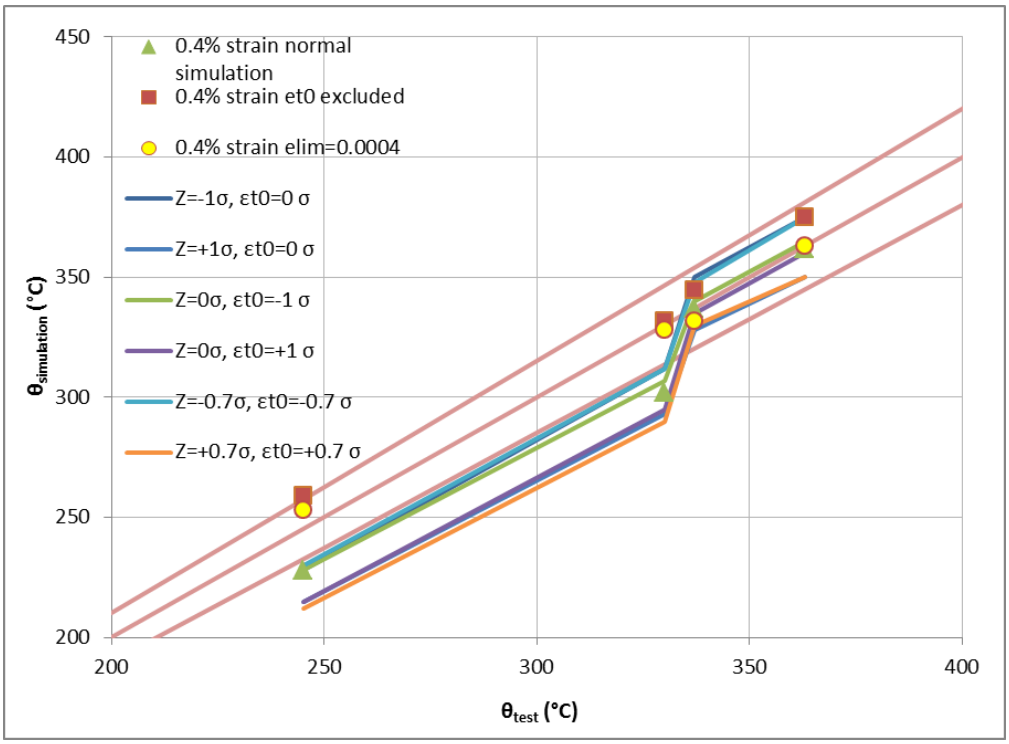

Figure D.2.1 Relation between simulation temperature and test temperature at plastic strain of 0.4% for welded specimens.

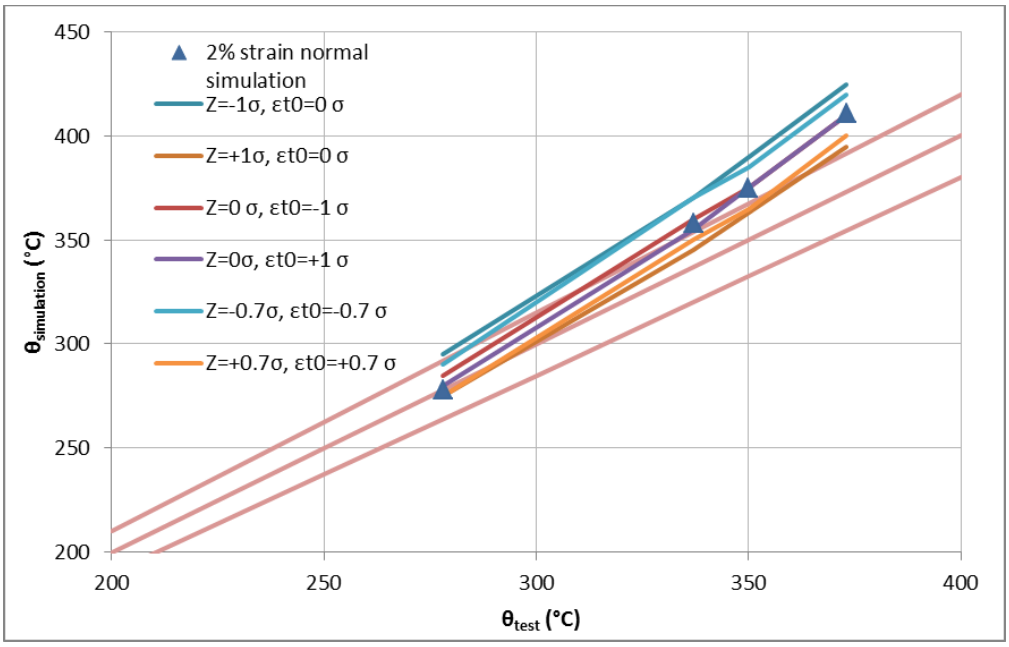

Figure D.2.2 Relation between simulation temperature and test temperature at plastic strain of 2% for welded specimens

Annex E.1 Simulation results for not welded specimens

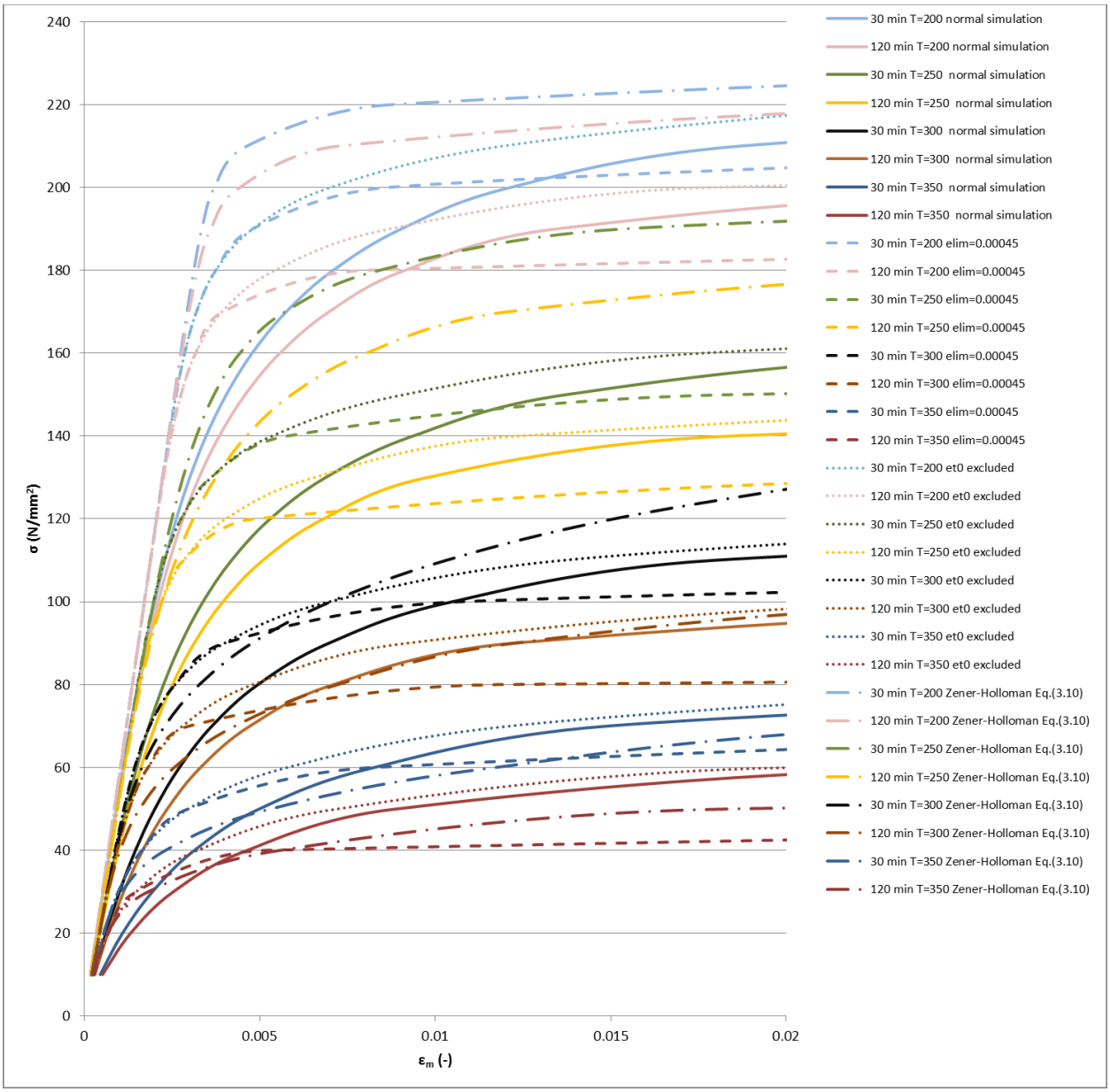

Figure E.1.1 Stress strain curves for fire design derived for a constant heating rate and a constant stress in time for all simulation models for specimens without a weld.

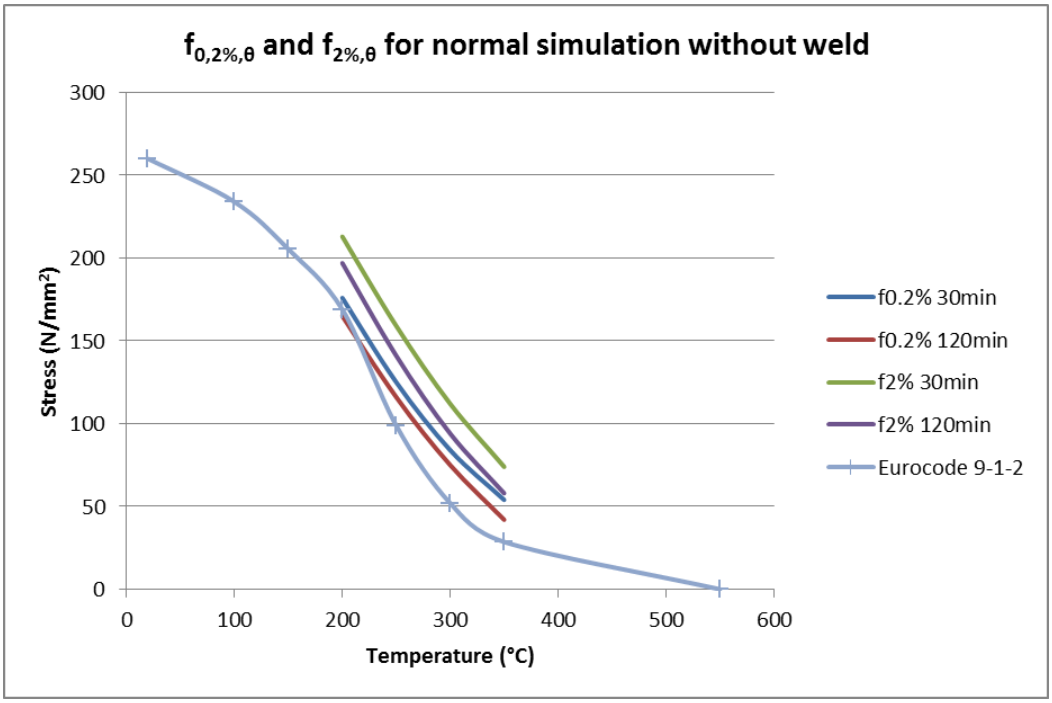

Figure E.1.2 Relation between 0.2% proof stress and 2% stress and temperature for specimens without a weld for normal simulation. Also data of 0.2% proof stress according to the Eurocode [EN 1999-1-2, 2007] for not welded specimens is shown for comparison.

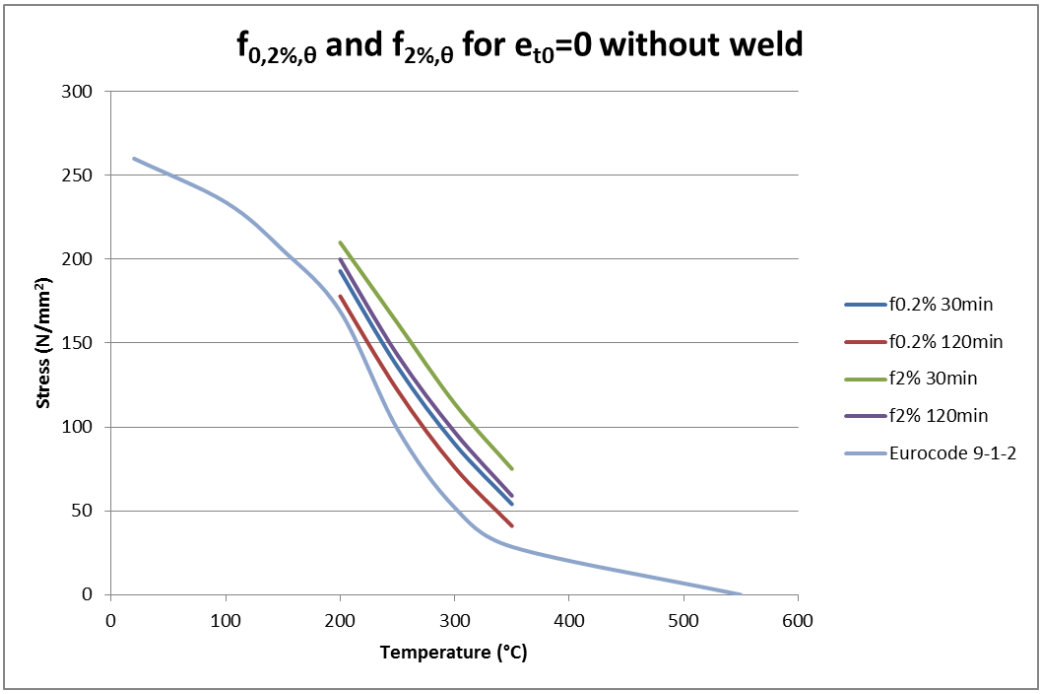

Figure E.1.3 Relation between 0.2% proof stress and 2% stress and temperature for specimens without a weld for ε_{t0}=0. Also data of 0.2% proof stress according to the Eurocode [EN 1999-1-2, 2007] for not welded specimens is shown for comparison.

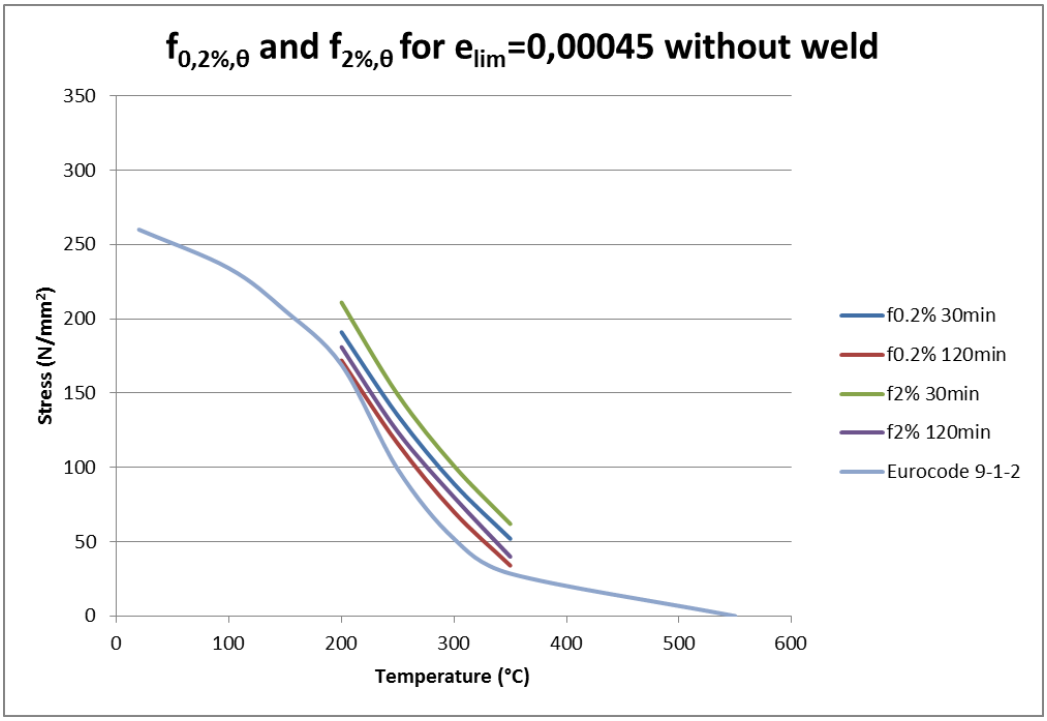

Figure E.1.4 Relation between 0.2% proof stress and 2% stress and temperature for specimens without a weld for ε_{lim}=0.00045. Also data of 0.2% proof stress according to the Eurocode [EN 1999-1-2, 2007] for not welded specimens is shown for comparison.

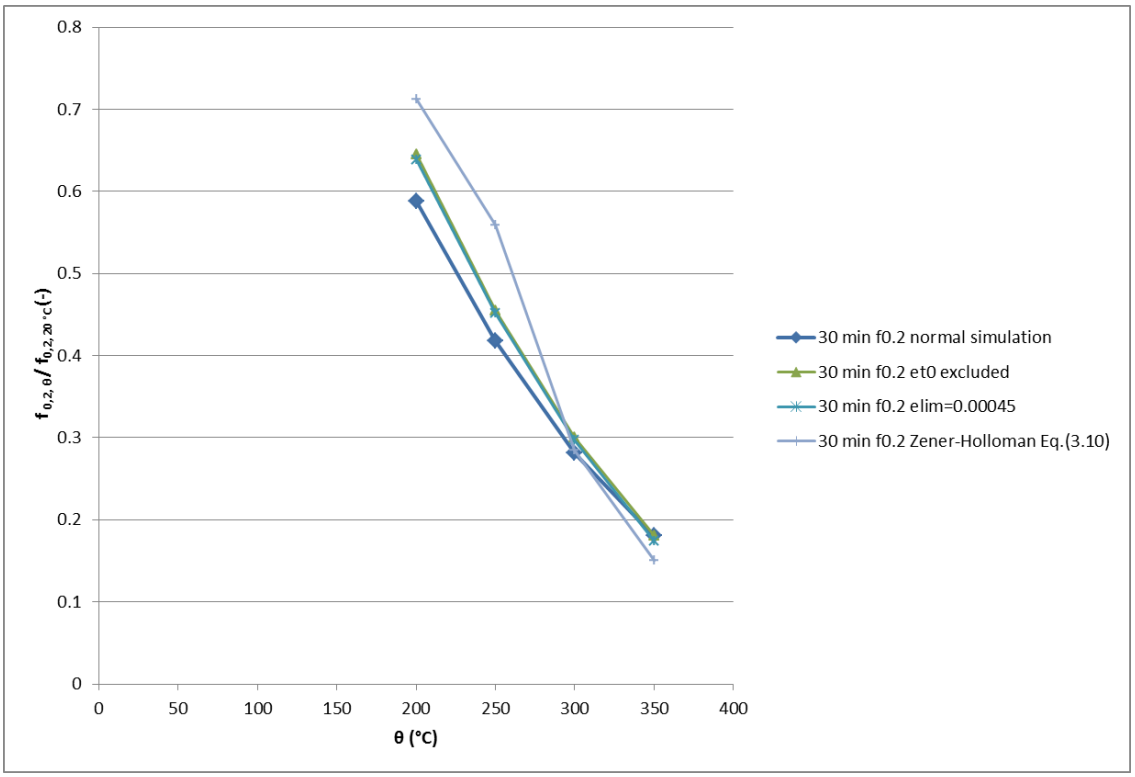

Figure E.1.5 Relative 0.2% proof stress for not welded specimens with different simulation parameters and 30 min.

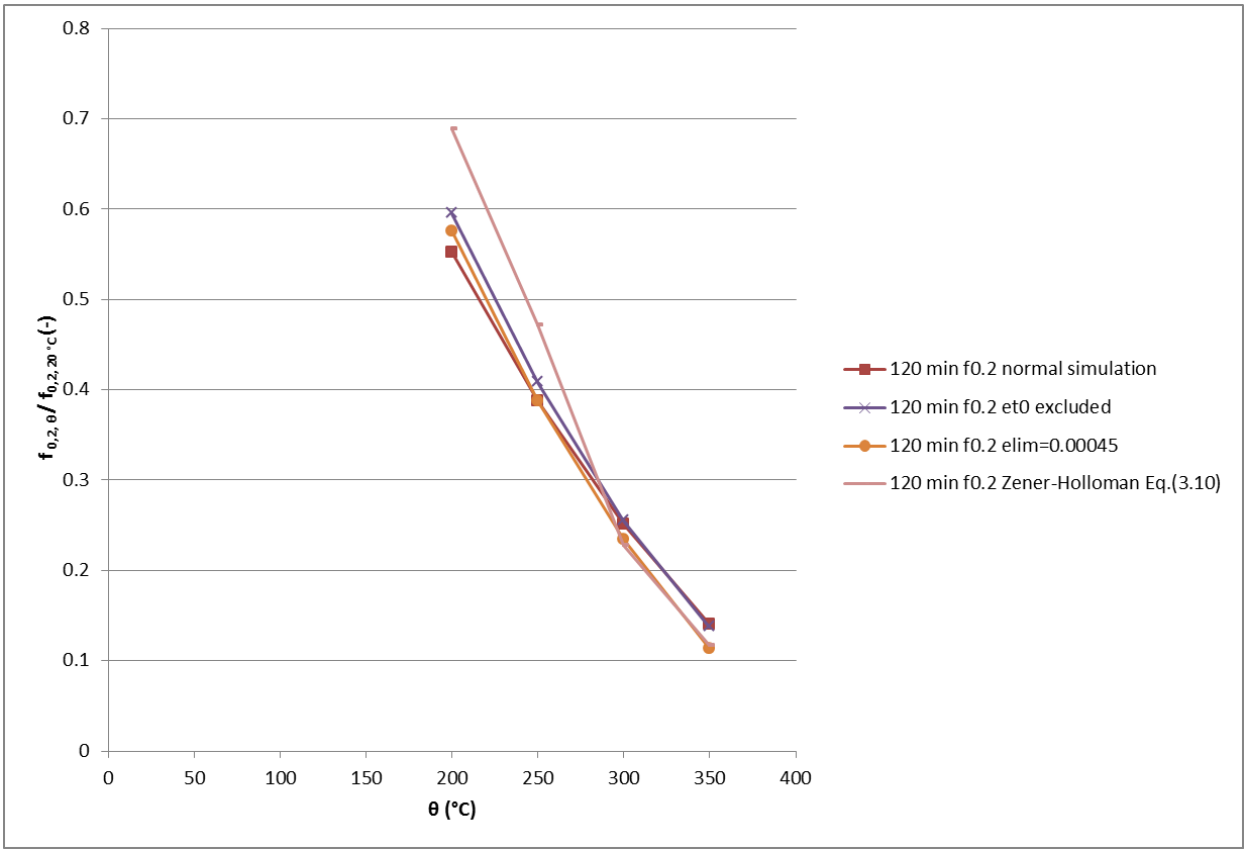

Figure E.1.6 Relative 0.2% proof stress for not welded specimens with different simulation parameters and 120 min.

Annex E.2 Simulation results for welded specimens

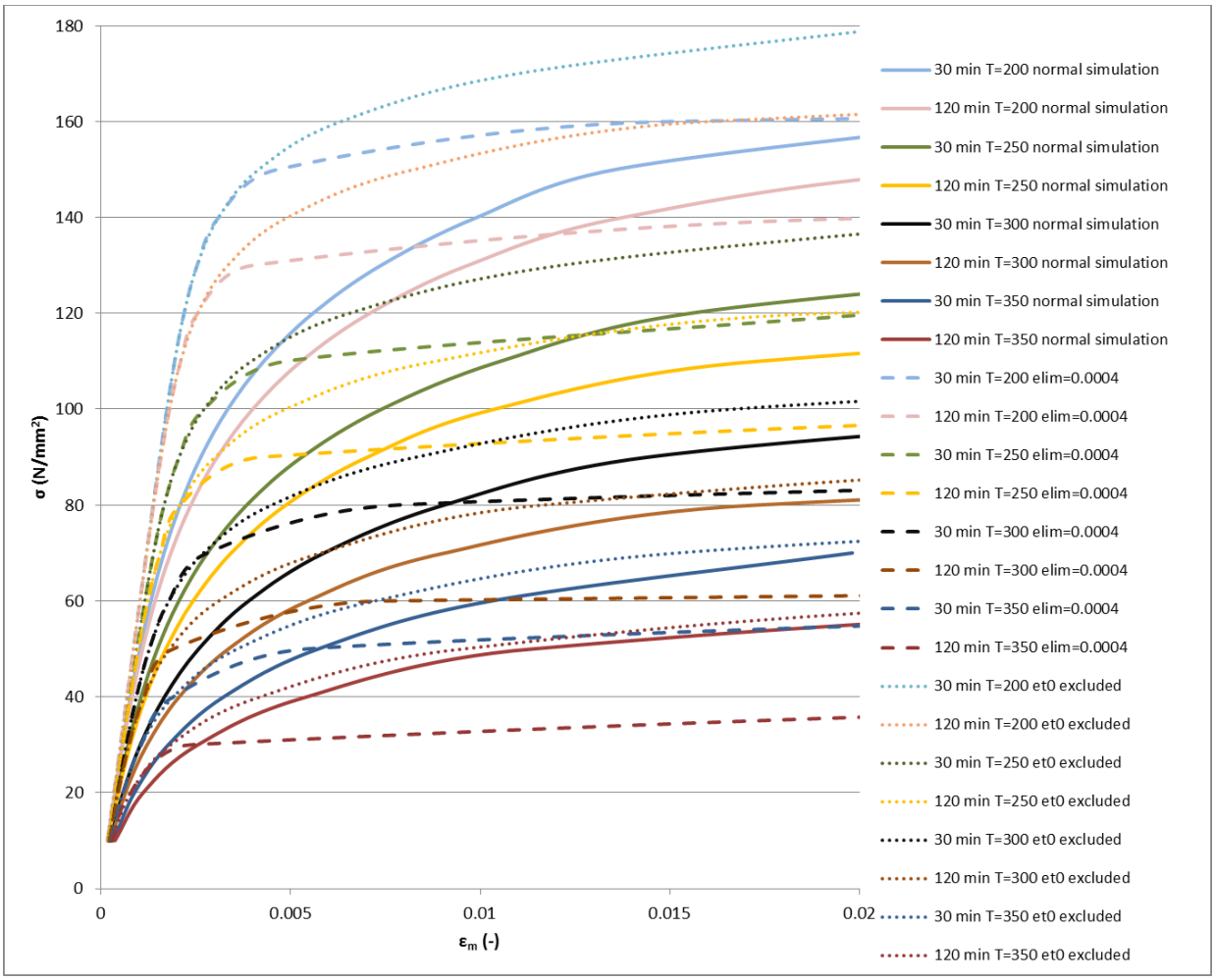

Figure E.2.1 Stress strain curves for fire design derived for a constant heating rate and a constant stress in time for all simulation models for specimens with a weld.

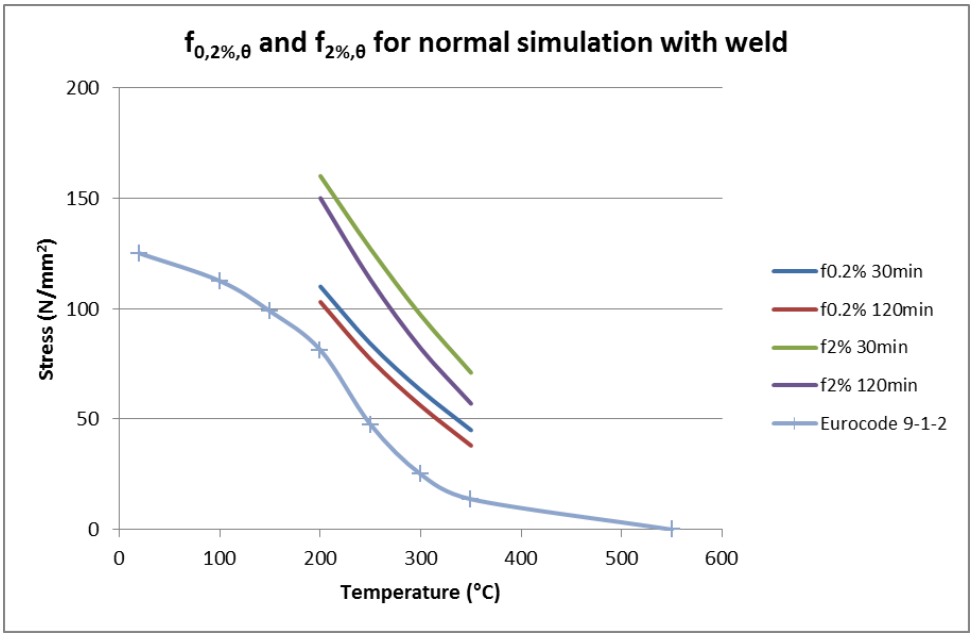

Figure E.2.2 Relation between 0.2% proof stress and 2% stress and temperature for specimens with a weld for normal simulation. Also data of 0.2% proof stress according to the Eurocode [EN 1999-1-2, 2007] for not welded specimens is shown for comparison.

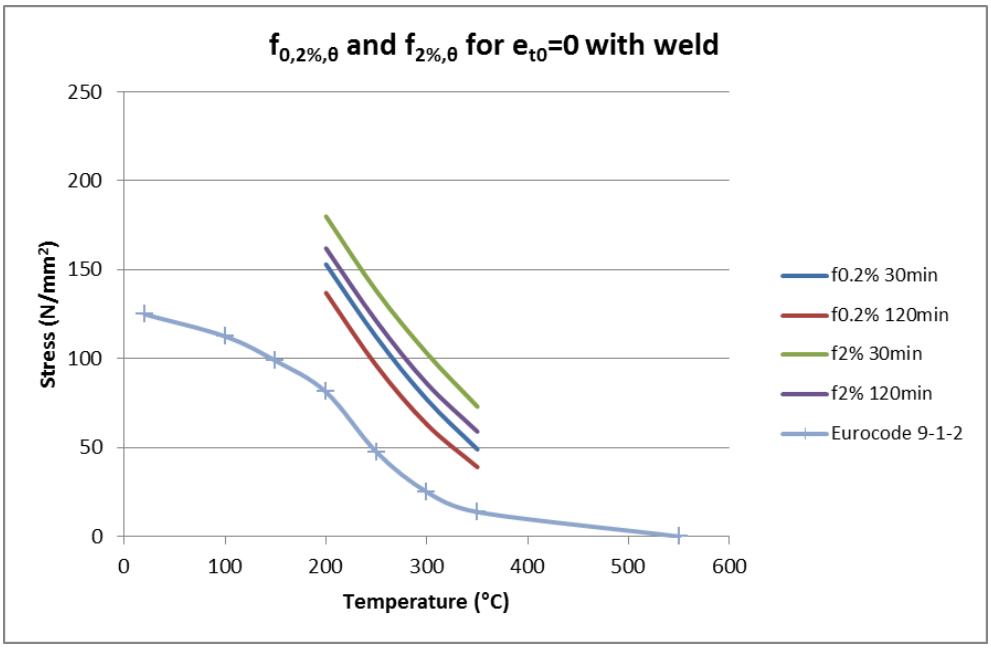

Figure E.2.3 Relation between 0.2% proof stress and 2% stress and temperature for specimens with a weld for ε_{t0}=0. Also data of 0.2% proof stress according to the Eurocode [EN 1999-1-2, 2007] for not welded specimens is shown for comparison.

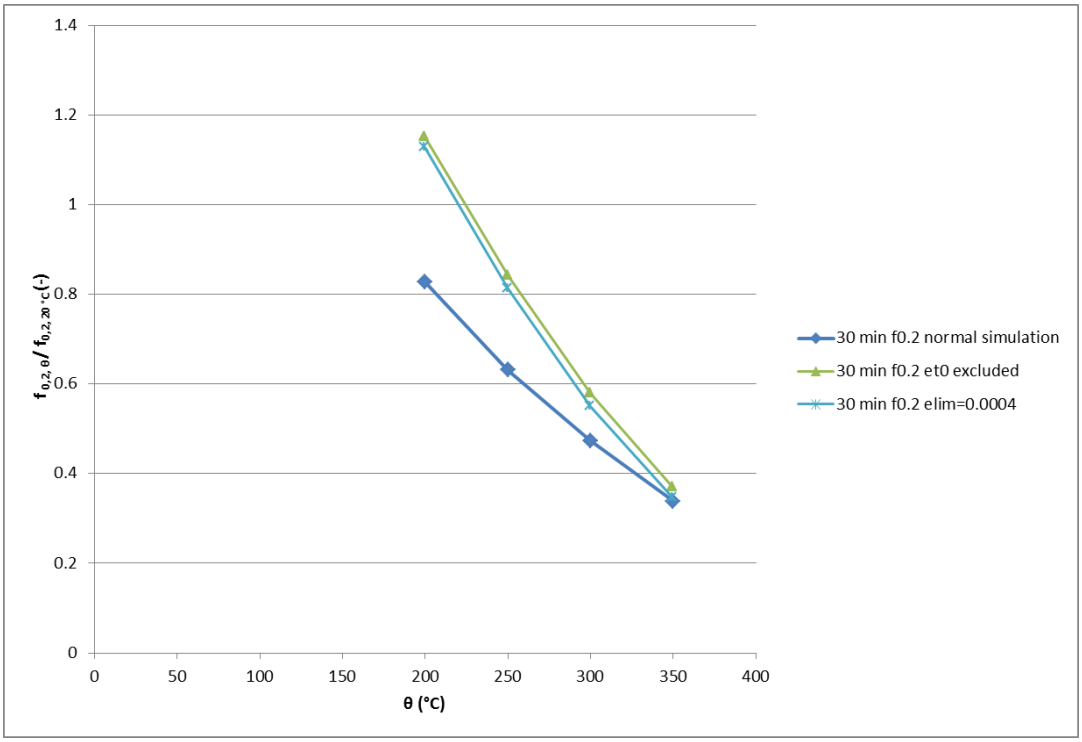

Figure E.2.4 Relative 0.2% proof stress for not welded specimens with different simulation parameters and 30 min.

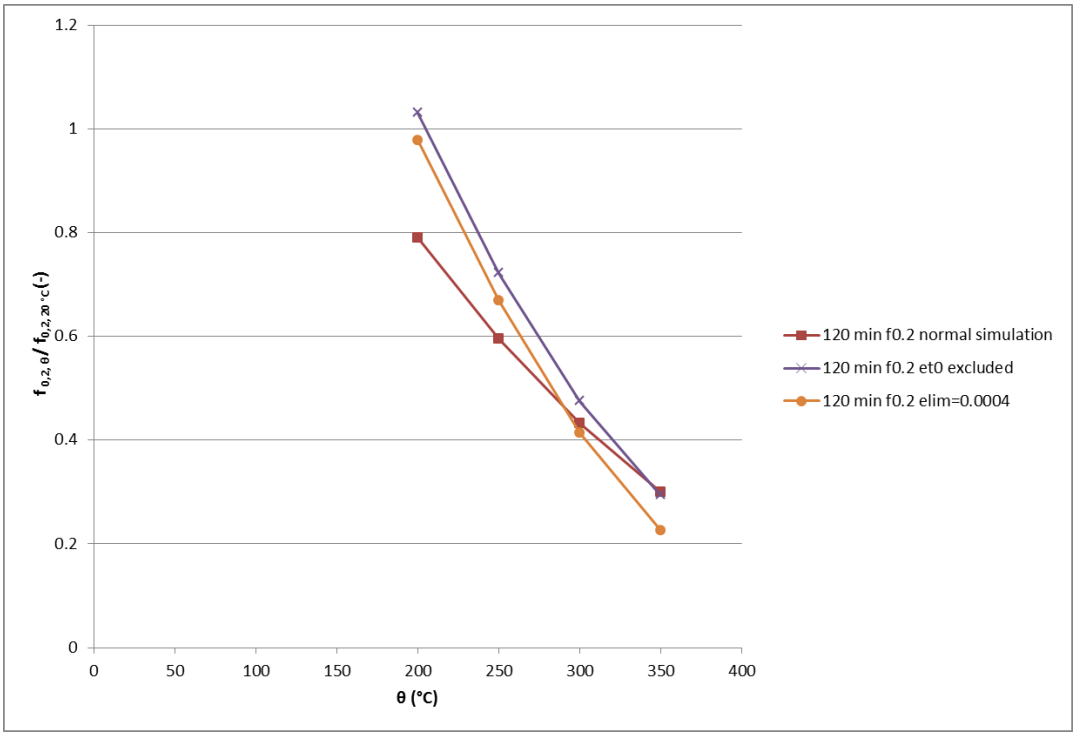

Figure E.2.5 Relative 0.2% proof stress for not welded specimens with different simulation parameters and 30 min.

Annex F.1 Ramberg-Osgood simulation not welded specimens

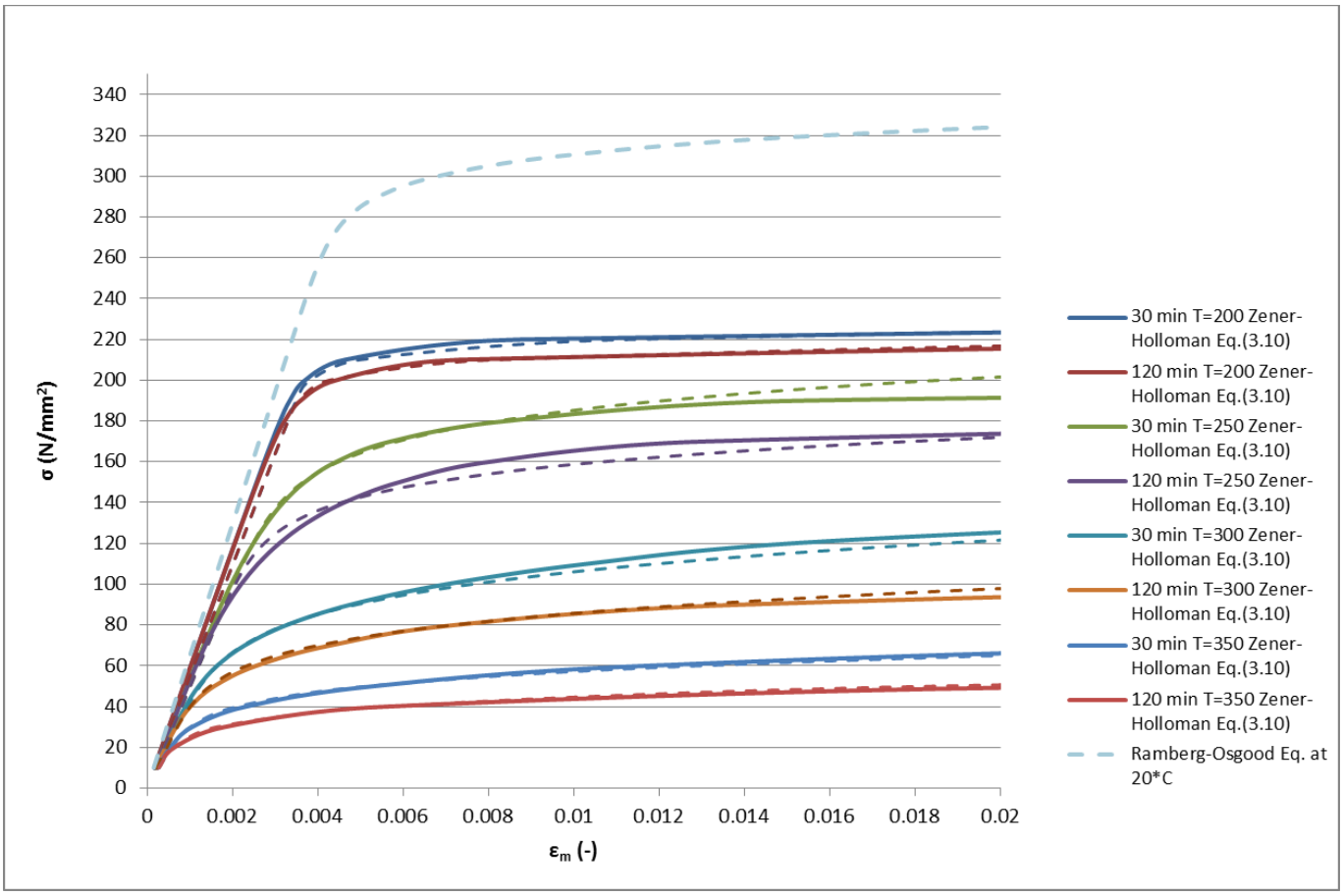

Figure F.1.1 Ramberg-Osgood simulations for not welded specimens.

Table F.1.1 Parameter n in Ramberg-Osgood equation.

θ °C	200	250	300	350
n	40	11	6	6

$$E_\theta = 65000 - 10 \cdot \theta - 0.21 \cdot \theta^2$$

Table F.1.2 $f_{0.2,\theta}$ in N/mm^2 for not welded specimens for used simulation Zener-Holloman Eq.(3.10)

θ °C	200	250	300	350
t=30 min	213	167	85	45
t=120 min	206	142	68	35

Annex F.2 Ramberg-Osgood simulation welded specimens

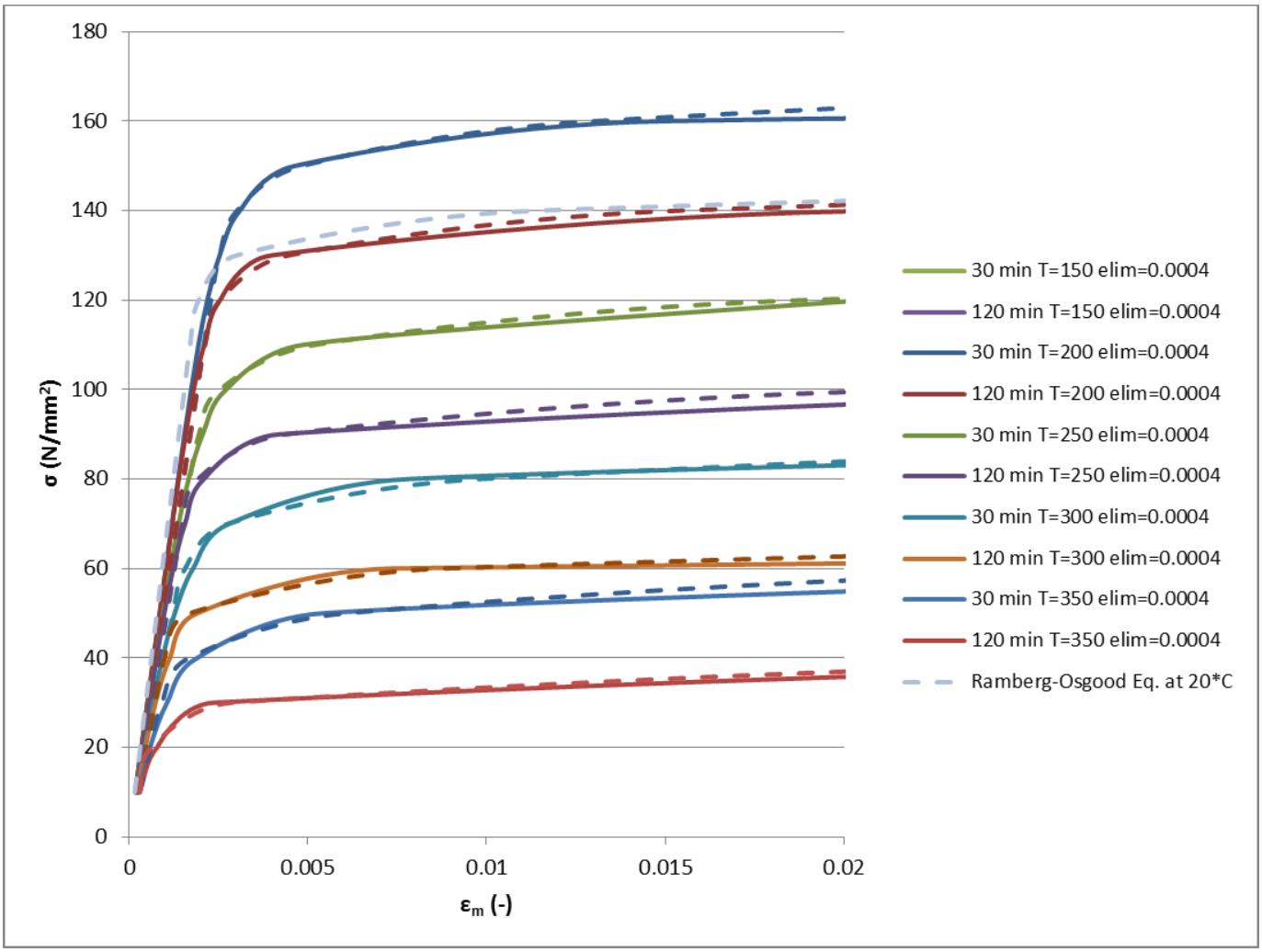

Figure F.2.1 Ramberg-Osgood simulations for welded specimens.

$$n_\theta = 45 - 0.1 \cdot \theta \qquad for\ 200°C \leq \theta \leq 350°C$$

$$E_\theta = 63000 - 10 \cdot \theta - 0.21 \cdot \theta^2$$

Table F.2.1 $f_{0.2,\theta}$ in N/mm^2 for welded specimens for used simulation e_{lim}=0.0004

θ °C	200	250	300	350
t=30 min	150	108	73	46
t=120 min	130	89	55	30